

Hierarchical model predictive control of temperature in building zones.

Martinčević, Anita

Doctoral thesis / Disertacija

2020

Degree Grantor / Ustanova koja je dodijelila akademski / stručni stupanj: **University of Zagreb, Faculty of Electrical Engineering and Computing / Sveučilište u Zagrebu, Fakultet elektrotehnike i računarstva**

Permanent link / Trajna poveznica: <https://urn.nsk.hr/urn:nbn:hr:168:049605>

Rights / Prava: [In copyright / Zaštićeno autorskim pravom.](#)

Download date / Datum preuzimanja: **2025-03-14**



Repository / Repozitorij:

[FER Repository - University of Zagreb Faculty of Electrical Engineering and Computing repository](#)





University of Zagreb

FACULTY OF ELECTRICAL ENGINEERING AND COMPUTING

Anita Martinčević

Hierarchical model predictive control of temperature in building zones

DOCTORAL THESIS

Zagreb, 2020



University of Zagreb

FACULTY OF ELECTRICAL ENGINEERING AND COMPUTING

Anita Martinčević

Hierarchical model predictive control of temperature in building zones

DOCTORAL THESIS

Supervisor: Professor Mario Vašak, PhD

Zagreb, 2020



Sveučilište u Zagrebu
FAKULTET ELEKTROTEHNIKE I RAČUNARSTVA

Anita Martinčević

Hijerarhijsko modelsko prediktivno upravljanje temperaturom u zonama zgrade

DOKTORSKI RAD

Mentor: Prof. dr. sc. Mario Vašak

Zagreb, 2020.

Doctoral thesis is made at the University of Zagreb Faculty of Electrical Engineering and Computing, Department of Control and Computer Engineering

Mentor: Professor Mario Vašak, PhD

Doctoral thesis contains 274 pages

Thesis no.:

*Mojoj obitelji,
za njihovu bezuvjetnu ljubav i podršku.*

ABOUT THE SUPERVISOR

Mario Vašak was born in Bjelovar in 1980. He received his BSc and PhD degrees in electrical engineering from University of Zagreb Faculty of Electrical Engineering and Computing (UNIZGFER), Croatia, in 2003 and 2007, respectively.

He is currently a full professor at the Department of Control and Computer Engineering, UNIZGFER and he is heading its Laboratory for Renewable Energy Systems (LARES). His research interests are in the domain of dynamic systems predictive control with applications to systems from the low-carbon energy sector: wind turbines, energy-efficient buildings, microgrids, water distribution systems and electrified railway transport. He is the main inventor of the US patent for fault-tolerant control of wind turbine generators. He designed the concept of hierarchical and modular energy management in buildings with integrated microgrids for enabling their economically optimal interoperation. He had a leading or collaborator role on several research projects funded by the European Union or Croatian national funds related to implementation of this concept and its verification from the level of consumption control in individual buildings to the level of coordination of infrastructure and buildings in the smart city environment (Interreg Danube 3Smart, ERDF PC-ATE Buildings, ERDF ENHEMS-Buildings, HRZZ 3CON, FP7 UrbanWater, FP7 DYMASOS, ERDF FER-KIET). He is the author or co-author of more than 20 papers in international scientific journals and overall of more than 100 internationally reviewed papers.

Prof. Vašak is a member of professional associations IEEE and the Croatian Society for Communications, Computing, Electronics, Measurements and Control (KoREMA). He has received more than 10 different acknowledgements and awards for his scientific and professional achievements. The following ones are highlighted: 2019 Prize for Science of UNIZGFER, 2008 Croatian annual prize for young scientists in the field of technical sciences, Vera Johanides Award of the Croatian Academy of Engineering, Josip Lončar Silver Plaque of UNIZGFER, Končar Award for Doctoral Thesis with application in industry, and Top Scholarship for Top Students 2002.

O MENTORU

Mario Vašak rođen je u Bjelovaru 1980. godine. Diplomirao je i doktorirao u polju elektrotehnike na Sveučilištu u Zagrebu Fakultetu elektrotehnike i računarstva (FER), 2003. odnosno 2007. godine.

Trenutno je redoviti profesor na Zavodu za automatiku i računalno inženjerstvo na FERu gdje vodi Laboratorij za sustave obnovljivih izvora energije (LARES). Njegovi istraživački interesi su u domeni prediktivnog upravljanja dinamičkim sustavima s primjenama na sustave iz niskougličnog energetskeg sektora: vjetroagregate, energetske učinkovite zgrade, mikromreže, vodoopskrbne sustave i elektrificirani željeznički promet. Glavni je izumitelj US patenta za upravljanje vjetroagregatima otporno na kvarove generatora. Osmislio je koncept hijerarhijskog i modularnog gospodarenja energijom u zgradama s integriranim mikromrežama za omogućavanje njihova ekonomski optimalnog međudjelovanja. Vodio je ili surađivao na nekoliko istraživačkih projekata financiranih sredstvima Europske unije ili nacionalnim sredstvima vezanih uz implementaciju navedenog koncepta te njegovu provjeru od razine upravljanja potrošnjom u pojedinim zgradama do razine koordinacije sustava distribucije električne energije i vode u okruženju naprednog (pametnog) grada (Interreg Danube 3Smart, EFRR PC-ATE Buildings, EFRR ENHEMS-Buildings, HRZZ 3CON, FP7 UrbanWater, FP7 DYMASOS, EFRR FER-KIET). Autor je više od 20 radova u međunarodnim znanstvenim časopisima te ukupno više od 100 međunarodno recenziranih radova.

Prof. Vašak član je stručnih udruga IEEE i Hrvatskog društva za komunikacije, računarstvo, elektroniku, mjerenja i upravljanje (KoREMA). Primio je više od 10 različitih priznanja i nagrada za svoj znanstveni i stručni rad. Među ostalima ističu se: Nagrada za znanost FERa za 2019. godinu, 2008. godišnja državna nagrada znanstvenim novacima u području tehničkih znanosti, Vera Johanides nagrada Akademije tehničkih znanosti Hrvatske, srebrna plaketa "Josip Lončar" FERa, nagrada koncerna Končar za doktorsku disertaciju s primjenom u industriji te Top stipendija za top studente 2002.

ZAHVALA

Na prvom mjestu želim zahvaliti svojim roditeljima, mami Bernardi i tati Andriji, koji su me cijeli život podržavali u svakom smislu. Hvala im što su i u najtežim trenucima vjerovali u mene. Posebno im zahvaljujem na nesebičnom ulaganju vremena i što mi nikad nisu zamjerali kada je s moje strane istog nedostajalo. Jedno veliko hvala stricu Danku i sestri Andreji koji su uvijek bili tu za mene. Hvala i ostatku obitelji, ujaku Marijanu, baki Đurđici, tetama Dragici i Đurđici, Vladimiru, Davoru, Ivani, Sanji, Danijeli i malom Marku, Renatiju i svima ostalima koji su uskakali svaki put kad bi zatrebalo. Jedno veliko hvala Verici i baki Marici, koje su vjerovale u mene od samog početka mog doktorskog studija usprkos tome što put nije uvijek bio najlakši. Hvala Dajani, Marku, Nikolini, Marijanu, teti Ani, Ivanki, svim prijateljima i svima koji su me pratili na ovom putu.

Posebna zahvala i veliko hvala na iznimnoj prijateljskoj i stručnoj potpori mom mentoru profesoru Mariju Vašaku koji mi je još tijekom studentskih dana usadio želju za istraživačkim radom, pružio priliku da se pridružim njegovom istraživačkom timu i doktoriram na ovako uzbudljivoj temi. Beskrajno Vam hvala na vašoj posvećenost i predanost, na svom izdvojenom vremenu, strpljenju i brojim stranicama ispisanim jednadžbama i objašnjenjima. Bila mi je i dalje mi je velika čast i privilegija što imam priliku raditi s Vama.

Zahvalila bi i kolegama iz Državnog hidrometeorološki zavoda, posebno Kristijanu Horvatu, koji su velikim dijelom omogućili ostvarivanje ove disertacije i uvijek bili spremni odgovoriti na sva moja pitanja. Puno hvala svima koji su svojom podrškom u kompliciranoj infrastrukturi koja je temelj ove disertacije pomogli njezinom ostvarivanju: Elma Kurtalj d.o.o., SBT d.o.o., služba održavanja FERa, Klimaoprema d.d., Ekorre Digital d.o.o.. Kroz sve probleme s kojima smo se zajedno susretali imala sam priliku puno toga naučiti.

Posebno se zahvaljujem svojim kolegama i prijateljima iz Laboratorija za sustave obnovljivih izvora energije. Jedno ogromno hvala Hrvoju na prijateljskoj potpori i brojnim diskusijama koje su uvijek izrodile nečim konstruktivnim, Mateji što se uvijek trudila biti pozitivna i saslušati me svaki put kada bi se suočila s nekim problemom, Vinku koji je

uvijek bio tu za sve nas i svojim iskustvom nam svima davao potporu i primjer kako da budemo bolji ljudi i znanstvenici, Nikoli na neizmjernom strpljenju u našem zajedničkom dijelu istraživanja i pozitivnom stavu uz koji ni jedna prepreka na koju smo naišli nije predstavljala problem. Hvala i svima ostalima, Filipu, Danku, Branimiru B., Branimiru N., Marku, Vici, Tamari i Goranu, koji su svatko na svoj način doprinijeli stvaranju pozitivne i produktivne radne atmosfere.

Zahvaljujem se svim bivšim i sadašnjim kolegama sa Zavoda za automatiku i računalno inženjerstvo. Tijekom doktorata upozнала sam ne samo sjajne kolege, već i vrlo dobre prijatelje. Hvala Goranu, Mladenu, Josipu, Kruni, Antoniju, Robiju i Edinu s kojima sam započela svoje prve korake na doktorskom studiju. Hvala Kristini i Igoru – koji mi uvijek poprave dan svojom vedrinom. Hvala Mirjani i teti Blanki koje su mi uvijek pomogle da se ne izgubim u svim tim silnim papirima. Jedno veliko hvala profesoru Nedjeljku Periću, koji mi je omogućio da postanem dio vizije Inovacijskog centra Nikola Tesla. Također, dugujem veliku zahvalnost profesorima Mati Baotiću i Jadranku Matušku za njihove savjete i podršku. Hvala Pauli, Tomislavu i Ani, svim sadašnjim i prošlim kolegama koji nisu ovdje spomenuti a doprinijeli su ostvarivanju produktivne i kreativne atmosfere zbog koje mi je dolazak na posao uvijek bio zadovoljstvo.

Na kraju najviše hvala mom Igoru, što je uvijek bio uz mene i bez čije ljubavi ovo ne bi bilo moguće. U mnogo toga bio je moja nadopuna i inspiracija. Hvala mu na bezuvjetnoj podršci i svemu onome što se ne može ni iskazati riječima.

U Zagrebu, 15. svibnja 2020. godine

Hierarchical model predictive control of temperature in building zones

Buildings belong to the large energy consumers class and account for 40% of worldwide primary energy consumption. The systems with the largest potential for improvement of buildings sector energy efficiency, with estimated nearly 60% of overall energy consumption in buildings, are systems for maintaining thermal comfort. Motivated by this, application of advanced control, fault detection and diagnosis algorithms in buildings has been intensively investigated with the aim to improve their energy efficiency and bring the buildings sector into the smart city arena. Hindering the trend, hysteresis and proportional-integral-derivative controllers are still a common practice. Introduction of more sophisticated model-based controllers, which proved to be the promising solution for improving the energy efficiency of the buildings sector, requires a cost-effective approach for identification of suitable mathematical models. In the thesis, the control-oriented, replicable, robust and simple methodologies for identification of suitable mathematical models consolidating the advantages of physical modelling and identification are presented and validated. Driven by the decreasing hardware cost and advances in computational power and information communication technology, buildings are becoming suitable for application of sophisticated energy management approaches to increase their energy efficiency and possibly turn them into active energy market participants. In the thesis, a general methodology for minimizing thermal energy consumption using current energy sources and minimal retrofitting through the use of advanced control techniques is presented. The control on zone level, as the level in charge for shaping the thermal energy consumption, is developed to have the possibility of modular coordination with the higher building hierarchy levels, such as central heating/cooling medium conditioning system, microgrid or smart grid. Such an approach enables the synchronization of all building subsystems and near-optimal behaviour of the whole building. The proposed modelling, identification and control algorithms are validated via simulation studies and on-line implementation of the model predictive control for zone temperature control on a real

248-zones skyscraper building. The developed frameworks pave the way to fast deployment of model-based energy management strategies in buildings and unleash significant energy and cost-saving potentials of a smart building in a smart city.

Keywords: building energy management system, zone comfort control, model predictive control, mathematical modelling, identification, energy efficiency, comfort-savings trade-off, building thermal model, constrained unscented Kalman filter, semi-physical modelling, control-oriented fan coil unit model, hydraulic and thermodynamic modelling, multi-parametric model predictive control, hierarchical coordination.

Hijerarhijsko modelsko prediktivno upravljanje temperaturom u zonama zgrade

Povećanje energetske učinkovitosti u zgradarstvu jedan je od ključnih uvjeta za smanjenje ukupne potrošnje energije u svijetu. S ukupno 40% svjetske potrošnje energije, zgrade uz promet i industriju spadaju među najveće potrošače energije [1, 2]. Potaknuto time, donesene su brojne strategije promicanja energetske učinkovitosti u zgradama. Konačni cilj Europske unije je klimatski neutralna Europa do 2050. godine, a jedan od čimbenika koji tome doprinosi je izgradnja zgrada gotovo nulte energije. Iako takve mjere predstavljaju važan čimbenik u smanjenju potrošnje energije u zgradama novijeg datuma, značajan utjecaj na ukupnu potrošnju sektora izostaje uslijed velikog udjela starijih zgrada izrazito lošeg energetskog razreda. Energetska obnova toplinske ovojnice takvih zgrada često zahtijeva značajna ulaganja [3]. Nasuprot tome, povećanje energetske učinkovitosti sustava upravljanja komforom, odgovornim za 60% ukupne potrošnje energije u zgradama, prepoznato je kao održivo rješenje za ostvarivanje značajnih ušteda energije [2].

Tehnološki napredak na području zgradarstva često je popraćen pojmovima kao što su pametne zgrade, internet stvari ili tehnologija velikih podataka. Zajednički korijen svih navedenih pojmova je upotreba digitalnih podataka iz same zgrade. Značajan napredak na polju informacijskih i komunikacijskih tehnologija u posljednjih je nekoliko godina uvelike doprinio povećanju komfora, energetske učinkovitosti i pouzdanosti sustava za automatizaciju u zgradarstvu. Veliki udio komercijalnih zgrada je sukladno tome opremljen barem nekom vrstom sustava za nadgledanje i gospodarene energijom u zgradama. Digitalni podatci na kojima se takvi sustavi temelje predstavljaju značajnu vrijednost, kako za vlasnika, tako i za distributera energije prema zgradi. Takvi podatci ključni su za digitalnu transformaciju zgrada i predstavljaju temelj za izgradnju boljih modela, predviđanje ponašanja zgrade u budućnosti i optimizaciju energetskih tokova u zgradama. Napredak na području modelskog prediktivnog upravljanja omogućio je prilagođavanje potrošnje promjenjivim cijenama na tržištu energije premještanjem tereta u intervale s nižim cijenama, korištenjem spremnika energije ili kombinacijom oba

pristupa. Napredni sustavi za automatizaciju u zgradama pružaju mogućnosti dodatnog smanjenja potrošnje energije u zgradama sudjelovanjem zgrada na tržištu energije kao entiteta koji pružaju pomoćne usluge mreži [4]. Dekarbonizacija energije, povećanje udjela obnovljivih izvora energije, važnost odgovora potražnje i rast cijena energije očigledno mijenjaju paradigme u energetici i ulogu zgrada u mreži.

Gospodarenje energijom u zgradama temeljeno na modelskom prediktivnom upravljanju (MPCu) prepoznato je kao jedno od najprimjenjivijih rješenja za poboljšanje energetske učinkovitosti u zgradarstvu. Estimirane uštede energije u simulacijskom okruženju dosežu visokih 70% u pojedinim sveobuhvatnim studijama [5, 6, 7, 8, 9, 10, 11, 12, 13] dok se eksperimentalno potvrđene uštede nalaze u intervalu 15-63% [14, 15, 16, 17, 18, 19, 20, 21, 22, 23]. Usprkos jasno izraženim prednostima i značajnim uštedama energije, implementacija MPCa za upravljanje komforom u zonama zgrade još je uvijek na samom početku. Glavni razlozi za to su računalna zahtjevnost samog algoritma te značajna ulaganja u informacijsku i komunikacijsku infrastrukturu zgrade neophodnu za sakupljanje, spremanje i analizu digitalnih podataka iz zgrade. Dodatno, svojstvene karakteristike svake zgrade, kao što su kompleksnost, neodređenost, vremenski promjenjiva dinamika i nemjerljivi poremećaji, predstavljaju velike izazove za dizajn i implementaciju sustava upravljanja.

Iskustva u implementaciji MPCa pokazuju da je vremenski najzahtjevniji dio sinteze i implementacije, koji generira i do 70% troškova inženjerskog rada [21, 24], identifikacija primjenjivog matematičkog modela zgrade. Detaljni matematički modeli zgrade temeljeni na fizikalnim zakonima najčešće se koriste u programskim alatima za simuliranje dinamičkog ponašanja zgrade [25, 26, 27]. Usprkos svojoj točnosti, zbog nelinearnosti, dimenzije i strukture, u pravilu nisu primjenjivi za upravljanje u stvarnom vremenu. Najčešći pristup modeliranju termodinamičkih procesa u zgradama, primjenjiv za sintezu sustava upravljanja, temelji se na analogiji s električnim krugovima na način da se svaki element u zgradi modelira pomoću konačnog broja otpora i kapaciteta [28, 29, 30]. Parametri takvog modela proračunavaju se analitički na temelju poznatih informacija o konstrukciji i fizikalnim svojstvima građevinskih elemenata zgrade koje su često teško dohvatljive, posebno za starije zgrade. Kao rješenje nameće se polu-fizikalni pristup kojim se osigurava model niskog reda i zadovoljavajuće točnosti na način da se struktura modela odredi unaprijed, na temelju fizike zgrade, dok se parametri modela identificiraju na temelju dostupnih digitalnih podataka iz zgrade [31, 32, 33, 34, 35, 36, 37].

Sigurnost i komfor u zgradama osigurani su kompleksnim međudjelovanjem podsustava koji su sastavni dio zgrade. To su podsustavi poput digitalne kontrole temperature u zonama zgrade, uređaja za pripremu medija za grijanje/hlađenje, mikromreže s integriranom proizvodnjom i spremnicima energije, upravljivim ili pasivnim električnim teretom, itd. Standardna operacija sustava za gospodarenje energijom u zgradama često je orijentirana lokalno na specifični podsustav, zanemarujući pritom kompleksnu spregu prema ostalim podsustavima. Posljedično, ostvaruje se nekoordinirano i neop-

timalno ponašanje zgrade kao cjeline. Koordinirani rad svih podsustava zgrade, od onih zaslužnih za oblikovanje potrošnje toplinske energije u zonama zgrade do onih na razini pametne mreže zaduženih za balansiranje tržišta energije, ključ je za značajno smanjenje operativnih troškova rada zgrade kao cjeline. Identificirani podsustavi zgrade okarakterizirani su različitim prioritetima, dinamikom, načinima rada, kao i protokolima, zahtjevima za održavanjem, energetske veze, itd. Stoga se kao prirodna alternativa objedinjenom kompleksnom upravljačkom problemu nameće razvoj zasebnih modula upravljanja i sinkronizacija njihovog rada kroz hijerarhijsku koordinaciju između pojedinih podsustava [13, 38]. Uvođenjem hijerarhijske dekompozicije omogućeno je značajno smanjenje računalne kompleksnosti i povećanje učinkovitosti samog algoritma upravljanja. Razina upravljanja u zonama zgrade oblikuje toplinsku potrošnju u zonama te kao takva predstavlja najnižu razinu u identificiranoj hijerarhijskog strukturi. Razina zona pritom obuhvaća sve zone zgrade, elemente za grijanje i hlađenje te pripadne senzorske elemente i aktuatore.

Klasične metode upravljanja temperaturom u zonama zgrade koje se temelje na lokalnim upravljačkim petljama i koriste samo trenutna lokalna mjerenja iz razmatrane zone, značajno se razlikuju od MPCa koji kao izlaz daje profil optimalnih toplinskih energija po različitim zonama zgrade. U takvom pristupu ne postoji direktna kompenzacija utjecaja nemjerljivih poremećaja poput rasvjete, elektroničke opreme ili položaja sjenila. Kako bi se osiguralo regulacijsko odstupanje jednako nuli, u zatvorenu petlju upravljanja uvodi se estimator nemjerljivih poremećaja. Ostvarivanje zahtijevanog toplinskog ulaza u pojedinu prostoriju zgrade, proračunatog od strane centralnog MPCa, osigurava se pomoću sučelja prema elementima za grijanje/hlađenje (radijatori, ventilokonvektori, itd.) koje služi kao sprega između energetske zahtjeva i upravljačkih naredbi za aktuatore elemenata za grijanje/hlađenje potrebnih da bi se traženi zahtjevi ostvarili. Upravljanje energijom po zonama zgrade omogućuje koordinaciju te razine s ostalim podsustavima zgrade čime se ostvaruje sinkronizacija rada svih podsustava zgrade i postizanje učinkovitog rada zgrade kao cjeline. Prednosti direktnog upravljanja toplinskom energijom su: *i*) jednostavna interakcija s ostalim podsustavima u zgradi poput centralne pripreme medija za grijanje/hlađenje, mikromreže ili pametne mreže [13, 38], *ii*) minimizacija ukupnog troška energije uz poznatu cijenu energije, *iii*) mogućnost smanjenje varijance toplinske snage čime se značajno smanjuju troškovi održavanja centralnog sustava za pripremu medija kao i troškovi penalizacije vršne vrijednosti snage [39], *iv*) mogućnost povratnog djelovanja na temperaturu prostorije uz veoma striktna ograničenja komfora, te *v*) modularnost i fleksibilnost pristupa čime se osigurava jednostavna replikacija na različitim konfiguracijama zgrada.

Do danas, upravljanje komforom u zonama zgrade temeljeno na MPCu implementirano je na svega nekoliko zgrada [14, 15, 16, 17, 18, 19, 20]. U svim studijama implementacijom MPCa osigurano je poboljšanje energetske učinkovitosti u usporedbi sa standardnim algoritmima korištenim prije instalacije. Uštede energije značajno variraju, između 5%

i 63%, ovisno o sveobuhvatnosti instalacije, sustavima kojima se upravlja i stanju zgrade prije instalacije. U svim studijama MPC je implementiran kao dio više upravljačke razine koja služi za optimiranje trajektorije unutarnjih referentnih vrijednosti sustava pri čemu je slijeđenje tih vrijednosti zadaća upravljana na nižoj razini. Referentne vrijednosti se pritom optimiraju direktno [17, 15, 20, 19, 18] ili se proračunavaju na temelju optimiranih vrijednosti ostalih varijabli sustava [14]. Prednost pristupa upravljanju komforom u zonama zgrade koji je razvijen u sklopu disertacije je u direktnom optimiranju energijom po zonama zgrade umjesto opće prihvaćenog pristupa temeljenog na optimizaciji referentnih vrijednosti. Takav pristup omogućuje modularnost i fleksibilnost pristupa koji su temelj za replikaciju razvijenih algoritama na velikom broju različitih zgrada. Također, optimiranje referentnih vrijednosti temperature vrlo je upitno sa stajališta komfora krajnjih korisnika prostora zgrade.

Iako je upotreba MPCa za upravljanje komforom u zonama zgrade već uvriježeni pojam u istraživačkim krugovima, jedinstven, jasan i robustan pregled svih koraka potrebnih za njegovu implementaciju nije dostupan. U sklopu disertacije prezentirana je generalna metodologija za smanjenje potrošnje energije u zonama zgrade korištenjem naprednih upravljačkih algoritama uz minimalna ulaganja i korištenje trenutno dostupnih izvora energije. Razvijeni pristup temelji se na postojećem sustavu automatizacije (ukoliko takav postoji) te omogućuje jednostavno prebacivanje na standardno upravljanje u slučajevima prekida komunikacije. Upravljanje komforom u zonama zgrade, razvijeno u sklopu disertacije, predstavlja temelj za hijerarhijsko gospodarenje energijom u zgradi. Implementacija sustava opisana je do razine komunikacije sa sustavom automatizacije u zgradi i zatvorenih petlji upravljanja svih komponenata koje osiguravaju stabilan rad sustava. Veza između upravljačkih i estimacijskih algoritama na jednoj strani i stvarnih fizičkih komponenata u zgradi pritom je dvosmjerna baza podataka koju se koristi za spremanje svih relevantnih digitalnih podataka iz zgrade kao i unutarnjih varijabli programskih modula za upravljanje. Razvijeni algoritmi verificirani su na simulacijskim studijama i kroz on-line implementaciju na primjeru neboderske zgrade Sveučilišta u Zagrebu Fakulteta elektrotehnike i računarstva (FERa). Istaknuti su sljedeći znanstveni doprinosi predloženih algoritama:

- metoda za identifikaciju energetskog modela sustava ventilokonvektora koja daje direktnu vezu između toplinske energije prenesene u zone zgrade, upravljačkih akcija na aktuatorima ventilokonvektora, stanja medija za grijanje/hlađenje i temperature zraka u zonama zgrade,
- metoda za identifikaciju termodinamičkog modela zgrade pogodnog za upravljanje i estimaciju nemjerljivih toplinskih poremećaja po zonama zgrade,
- strategija modelskog prediktivnog upravljanja temperaturom u zonama zgrade s mogućnošću hijerarhijske koordinacije s centralnim sustavom pripreme medija

za grijanje/hlađenje, mikromrežom ili nekim drugim podsustavom zgrade koji je spregnut sa zonama preko energije,

- validacija razvijenog sustava za hijerarhijsko prediktivno upravljanje u smislu ostvarenog komfora i ušteda energije na primjeru neboderske zgrade Sveučilišta u Zagrebu Fakulteta elektrotehnike i računarstva,
- validacija razvijenih algoritama za upravljanje temperaturom u zonama zgrade implementacijom sustava za rad u stvarnom vremenu na cijeloj neboderskoj zgradi Sveučilišta u Zagrebu Fakulteta elektrotehnike i računarstva.

Doktorska disertacija podijeljena je u tri cjeline koje obuhvaćaju neophodne korake implementacije modelskog prediktivnog upravljanja temperaturom u zonama zgrade: identifikacija potrebnih matematičkih modela, sinteza upravljačkih algoritama te implementacija i obavljanje razvijenih algoritama u stvarnom vremenu u operativnom okruženju zgrade. U uvodnom *Poglavlju 1*, opisuje se motivacija za provedeno istraživanje, s pregledom trenutnog stanja područja i opisom problematike.

Cjelina I: Modeliranje i identifikacija termodinamičkih procesa u zgradama

Napredni algoritmi upravljanja, koji se temelje na matematičkom modelu procesa, poput MPCa, dokazano su primjenjivi za ostvarivanje značajnih ušteda u zgradama. Temelj za daljnji napredak i rasprostranjenu implementaciju takvih algoritama su jednostavni i pouzdani matematički modeli termodinamičkih procesa u zgradama. U *Cjelini I* opisuju se razvijene metodologije za identifikaciju takvih modela.

- Metodologija za identifikaciju energetskog modela sustava ventilokonvektora detaljno je opisana u *Poglavlju 2*. Tako identificirani model daje direktnu vezu između toplinske energije prenesene u zone zgrade, upravljačkih akcija na aktuatorima ventilokonvektora, stanja medija za grijanje/hlađenje i temperature zraka u zonama zgrade. Uvedena jednostavna i precizna dinamička karakterizacija energije prenesene s ventilokonvektora u zone zgrade omogućuje upravljanje po energiji u zonama zgrade čime se omogućuje implementacija prediktivnih algoritama za optimizaciju potrošnje toplinske energije u zonama zgrade.
- U *Poglavlju 3* opisana je metodologija za identifikaciju polu-fizikalnog modela zgrade pogodnog za upravljanje. Razvijena metodologija temelji se na modificiranom nederivacijskom Kalmanovu filtru s ograničenjima. Metodologija je validirana identifikacijom matematičkog modela neboderske zgrade FERa. Validacijom je potvrđeno da razvijena metodologija osigurava numeričku stabilnosti i poboljšanje konvergencije u odnosu na standardne varijante Kalmanova filtra. Primjenjivost razvijene metodologije potvrđena je korištenjem skupa podataka od samo tjedan dana za identifikaciju modela koji pouzdano predviđa ponašanje temperature u zonama zgrade na horizontu od 24 sata unaprijed.

Cjelina II: Modelsko prediktivno upravljanje u zonama zgrade

U drugoj cjelini opisan je razvoj modelskog prediktivnog upravljanja temperaturom u zonama zgrade koje osigurava osnovna svojstva upravljanja u zatvorenoj petlji i kompenzaciju poremećaja. Razvijeni algoritam predstavlja najnižu razinu u hijerarhijskoj dekompoziciji podsustava zgrade te je stoga poseban fokus stavljen na razvoj mogućnosti interakcije s ostalim podsustavima s ciljem osiguravanja sinkronizacije svih podsustava u zgradi i optimizacije ponašanja zgrade kao cjeline.

- U *Poglavljju 5* prikazan je razvoj modelskog prediktivnog upravljanja temperaturom u zonama zgrade. Kompenzacija nemjerljivih poremećaja osigurana je uvođenjem estimatora u strukturu zatvorenog kruga upravljanja. Ostvarivanje optimalnih toplinskih zahtjeva po zonama zgrade osigurano je korištenjem sučelja prema elementima za grijanje/hlađenje koji služe kao veza između energetske zahtjeva i stvarnih upravljačkih naredbi prema aktuatorima potrebnih da bi se ti zahtjevi ostvarili. Uštede energije ostvarive implementacijom takvog sustava potvrđene su simulacijom ponašanja zgrade FERa na intervalu od godinu dana uz pretpostavku različitih algoritama upravljanja temperaturom u zonama zgrade.
- Mehanizam modularne koordinacije razine zona s ostalim podsustavima u zgradi predstavljen je u *Poglavljju 6*. Modularnost pristupa ogleda se u jednostavnoj interakciji između razina koja se temelji na razmjeni profila predviđene potrošnje energije i profila cijene te energije generiranog od strane modula s više hijerarhijske razine. Pristup je verificiran optimizacijom ponašanja zgrade FERa na horizontu od 24 sata.

Cjelina III: Primjena na nebodersku zgradu

Treća cjelina prikazuje implementaciju razvijenog upravljanja temperaturom u zonama zgrade na primjeru neboderske zgrade FERa.

- Tehnički preduvjeti za implementaciju razvijenog sustava upravljanja detaljno su opisani u *Poglavljju 8*. Pregled osnovnih principa upravljanja temperaturom u zonama razmatrane zgrade i arhitekture razvijenog sustava popraćen je opisom i detaljnom analizom rada svih programskih modula potrebnih za rad razvijenog sustava u stvarnom vremenu.
- U *Poglavljju 9* prikazan je praktičan postupak detekcije začepljenja zrakom ventilokonvektora. Razvijeni postupak validiran je na neboderskoj zgradi FERa.

Zaključci te razrada daljnjih mogućnosti istraživanja i razvoja vezani za pojedine dijelove disertacije dani su u poglavljima na kraju svake cjeline (*Poglavlje 4*, *Poglavlje 7* i *Poglavlje 10*). Generalni zaključak i kratak osvrt na razvijenu metodologiju i dobivene rezultate dan je u *Poglavljju 11*.

Disertacija sadrži također i dva priloga. U *Prilogu A* dan je detaljan opis neboderske zgrade FERa. Zgrada je u potpunosti opremljena sklopovskom i informacijsko komunikacijskom tehnologijom potrebnom za testiranje i validaciju algoritama za upravljanje i estimaciju u zgradama. Svi eksperimenti i studije u sklopu disertacije provedeni su na razmatranoj zgradi. U *Prilogu B* dan je postupak izračuna sunčeve dozračenosti na nagnutu plohu, kao jedan od glavnih preduvjeta za proračun utjecaja sunčeve dozračenosti na temperature u prostorijama zgrade.

Ključne riječi: gospodarenje energijom u zgradama, upravljanje komforom u zonama zgrade, modelsko prediktivno upravljanje, matematičko modeliranje, identifikacija, energetska učinkovitost, termodinamički procesi u zgradama, nederivacijski Kalmanov filter s ograničenjima, polu-fizikalno modeliranje, model ventilokonvektora pogodan za upravljanje, hidrauličko i termodinamičko modeliranje, višeparametarsko modelsko prediktivno upravljanje, hijerarhijska koordinacija

CONTENTS

1	Introduction	1
1.1	Contributions	2
1.2	Thesis outline	5
I	Modelling and Identification of Thermodynamic Processes in Buildings	9
2	Mathematical modelling and identification of a system of fan coil units	11
2.1	Energy model of a system of fan coil units	13
2.1.1	Hydraulic model	14
2.1.2	Thermodynamic model	16
2.1.3	Electrical energy consumption model	18
2.2	The identification methodology	19
2.2.1	Sensor calibration	19
2.2.2	Identification of the hydraulic model of the system	21
2.2.3	Identification of the thermodynamic model of the system	22
2.3	Experimental validation	25
3	Mathematical modelling and identification of building temperature dynamics	37
3.1	Heat transfer processes in buildings	40
3.2	Thermal Resistance-Capacitance models	42
3.2.1	The Resistance-Capacitance model of a single zone	43
3.2.2	State-space model of a building	49
3.3	Building simulation software models	51
3.4	Low-order semi-physical building model	53
3.5	Identification framework for simplified low-order building models based on Unscented Kalman filter	54

3.5.1	Standard Unscented Kalman filter	55
3.5.2	Constrained Unscented Kalman filter with improved weight selection scheme	57
3.5.3	General UKF-based framework for identification of low-order semi-physical building models	61
3.6	Mathematical model of the case-study skyscraper building	64
3.6.1	IDA-ICE model of the case-study building	64
3.6.2	The Resistance-Capacitance model	65
3.6.3	Simplified low-order model	72
3.6.4	Suitability of the developed models for prediction of the heating/cooling loads	85
4	Part I conclusion and future research opportunities	89
II	Zone Model Predictive Control	91
5	Optimal zone temperature control - design	93
5.1	Introduction to model predictive control for zone temperature control . . .	96
5.2	Model predictive control for energy-savings and comfortable temperature control	98
5.3	Optimal zone temperature control in the presence of unmeasurable states and disturbances	103
5.4	Simulation case-study for assessment of a performance bound and possible energy savings	105
5.4.1	Simulation case-study results	109
5.5	Optimal control of heating/cooling elements in zones	118
5.5.1	Optimal control of fan coil units	119
5.5.2	Verification of optimal fan coil unit control	127
6	Modular hierarchical building energy management	131
6.1	Building zones optimal control for high comfort demands	134
6.2	Multi-parametric coordination of zone level with higher hierarchy levels . .	136
6.2.1	Multi-parametric model predictive control and single critical region calculation	137
6.2.2	Iterative revisiting between optimization levels	139
6.3	Simulation results and case-study analysis	142
6.3.1	Simulation scenario	142
6.3.2	Results	147
7	Part II conclusion and future research opportunities	159

III	Application to a full-scale skyscraper building	161
8	Zone model predictive control – real-time implementation	163
8.1	Basic principles of the case-study BEMS infrastructure	166
8.1.1	Temperature control system specifications	166
8.1.2	Information communication infrastructure architecture	167
8.2	Real-time operation of the model predictive control for zone temperature control	170
8.2.1	Prediction and estimation modules	172
8.2.2	Model predictive control module	183
8.2.3	Fan coil unit interface module	196
9	Fault detection in a system of fan coil units	205
10	Part III conclusion and future research opportunities	211
11	General conclusion	213
	Appendices	219
A	Case-study skyscraper building	219
A.1	Living-lab on predictive building zones control	222
A.2	Building construction and materials	226
A.3	List of controllable building zones	236
B	Solar irradiance incident on a tilted surface	241
	Bibliography	245
	Notation	259
	Curriculum Vitae	269
	Životopis	271
	List of publications	273

Introduction

The increasing global energy demand and noticeable effects of irrational energy consumption highlighted the reduction in energy consumption as a key element for ensuring long-term energy security. According to [1, 2], buildings account for 40% of worldwide primary energy consumption. As a result, there has been a considerable push towards designing policies and initiatives directed towards their energy efficiency increase. The EU2030 Energy Strategy, built on promising results and well-adopted research and implementation trends of the previous 20-20-20 strategy (CO₂ reduction - renewables share - energy savings), targets towards 40-27-27 by the end of year 2030 [40]. This economical motivation brought highly efficient building categories such as *Energy Star* (USA) or *Passivhaus Standard* (EU), with the final goal of reaching *Zero-energy buildings*. While new buildings can be constructed with high-performance levels, it is the older buildings, representing the vast majority of the building stock, which are predominantly of low energy performance and subsequently in need of refurbishment, which often demands significant investment [2, 3]. The systems with the largest potential for improvement of buildings sector energy efficiency, with estimated nearly 60% of overall energy consumption in buildings, are systems for maintaining the thermal comfort [2]. Therefore, a much more productive approach for achieving the strict energy cuts is to focus on the retrofitting of the existing buildings through the improvement of building automation systems and the underlying control algorithms. Motivated by this, energy management in buildings has become an increasing trend in their transformation to smart and efficient utilization of energy resources.

Over the past few years, many terms have been used in the building sector to describe the latest technological advances. Smart buildings, Big Data, Internet of Things are just a few of the most commonly used ones. The subject focus of all the terms is digital information from the building. The advances in information and communication technology (ICT) increased comfort, energy efficiency and the reliability of the automation systems in buildings. As a result, the majority of commercial buildings are equipped with Building Energy Management Systems (BEMSs) to monitor and control different

components of building automation. The data collected from the BEMS sensors and energy meters create a great value both for building owner and the energy grid operator. That data are crucial to construct better models, predict future building behaviour and optimize the overall building performance. The advances in the field of smart model-based control algorithms for buildings enabled the buildings to respond to the volatile pricing signals by shifting the loads either by preheating/precooling the buildings massive structure, by the use of an active energy storage system or through the combination of both approaches. Even though the consumption of the thermal energy on the zone level may increase, the overall building operational costs are significantly reduced. The more sophisticated building automation increases the achievable energy savings even further by enabling the use of the buildings as storage elements that could enhance the performance and the robustness of the power grid by becoming ancillary service providers [4]. The growing spread of renewable energy systems combined with the increasing importance of demand response and rising energy prices is evidently changing the paradigm of energy and the role of the buildings in the grid.

1.1 Contributions

The Model Predictive Control (MPC) approach applied in BEMSs has been recognized as one of the most promising solutions for improving comfort and achieve considerable energy savings. Its distinctive advantages over conventional control algorithms, make the MPC approach a promising solution for widespread problems of energy management within buildings. The estimated theoretical energy-saving potential is up to 70% in particular comprehensive applications [5, 6, 7, 8, 9, 10, 11, 12, 13]. Recently, MPC has found its place in practice, with experimentally-validated building energy efficiency increase by 15-63% [14, 15, 16, 17, 18, 19, 20, 21, 22, 23]. Although it is clear that MPC applied for building climate control offers many benefits, its practical implementation is still a major challenge due to the high computational demand followed by the required investment in sensing and ICT equipment required to collect, store, and analyse the building-related data. Additionally, the inherent complexity of building systems with uncertain and time-varying dynamics, as well as the presence of unmeasurable disturbances, present serious challenges for the development of corresponding efficient control, fault detection and diagnosis algorithms.

The practical experience has shown that acquiring the MPC essence – the model – is the most time-consuming and costly part of the corresponding design and on-site implementation process that generates around 70% of the engineering costs [21, 24]. Building models based on fundamental physical laws, usually used in building simulation tools [25, 26, 27], accurately describe the relevant building dynamics. However, they are hardly usable for real-time control implementation due to large state and parameters dimensions accompanied by nonlinearities or non-explicit model forms. The most usual

physically based approach in thermal modelling of buildings is based on a well established linear resistance-capacitance (RC) representation where each building element is represented with a finite number of states [28, 29, 30]. The model parameters are calculated analytically, based on the detailed physical properties of the building elements which are often unknown, especially for the older buildings. While nonlinear and higher-order models provide better accuracy, they tend to be computationally too intensive for the real-time implementation of MPC. Therefore, from the control viewpoint, the goal is to get a linear low-order model in a way that the model uncertainty is lowest possible. Thus, the main approaches categorized in the development of control-oriented models are data-driven approaches in which the model structure is assumed a priori while the constituting model parameters have to be identified [31, 32, 33, 34, 35, 36, 37].

Buildings are complex systems composed of many coupled subsystems responsible for maintaining safe and steady operation such as digital temperature control in building zones, central heating, ventilation and air conditioning (HVAC) system, microgrid with energy production units, storages and controllable or passive loads, etc. Typical applications of BEMS are oriented only locally to a specific subsystem while neglecting interconnections and cooperation among all constituent subsystems. As a result, building as a whole achieves uncoordinated and non-optimal behaviour. The key for ensuring the energy-efficient operation of the whole building is the ability for mutual coordination between different building subsystems: from those in charge of shaping energy consumption in building zones to those on the grid side that balance the energy market conditions. These subsystems are all very different in dynamics, priorities, means of operation but also implementation aspects such as energy levels, protocols, maintenance services, etc. Rather than having a large complex control structure to handle all the subsystems at once, it is more natural to separate it into BEMS submodules in a hierarchical way [13, 38]. Such hierarchical decomposition introduces significant computational relaxation and improvement of algorithm efficiency. The zone level, as the level in charge of shaping the thermal energy consumption in zones, represents the lowest hierarchical level in the identified hierarchical structure. On the physical level, the zone level MPC encompasses all building zones, heating/cooling elements (HCEs) inside zones and accompanying sensing and actuation equipment.

The MPC approach that uses thermal model of the building and computes optimal thermal energy inputs in different building zones substantially differs from generally accepted temperature control via local reactive control loops where only local measurements are used when deciding on the control actions for HCEs in zones (fan coils, radiators, floor heating, etc.). In such a set-up, the unmodelled disturbances, such as occupancy, lighting or electronic equipment, are no longer implicitly compensated. To ensure offset-free control and to be able to compensate such disturbances, an estimator is introduced in the control loop. The realization of the optimal thermal energy inputs is then enforced by HCE interfaces acting as a link between the optimal thermal inputs and real actuation

commands required for those inputs to be realized. Direct optimization of thermal energy consumption enables coordination with the higher-levels in building hierarchy with the aim to achieve the synchronization of all building subsystems and near-optimal behaviour of the whole building. Up to date, the practical implementation of MPC for building climate control has been reported on several buildings [14, 15, 16, 17, 18, 19, 20]. All addressed studies report a successful operation of MPC and efficiency improvement when compared with a baseline control. The experimentally confirmed energy savings vary significantly from 5% up to 63%, depending on the comprehensiveness of the study, controlled system and baseline used for the comparison. In all presented studies, the MPC control is implemented as a part of supervisory (management) level used to optimize the trajectory of internal setpoints whereas the tracking of those setpoints is a task of low-level control. The internal building setpoints are either optimized directly [17, 15, 20, 19, 18] or obtained by post-processing the optimal MPC variables [14]. The distinct advantage of the approach developed within the thesis is in direct optimization of energy inputs per zone rather than generally accepted temperature setpoints. The advantages of the direct control of thermal energy inputs are: *i*) simple interaction with other building subsystems [13, 38], *ii*) possibility of direct economic cost minimization by using the known price of the energy, *iii*) possibility of thermal power variance minimization lowering thus the maintenance cost for central HVAC system and reducing the peak operation costs [39], *iv*) possibility to act in tight comfort requirements where the required reference temperature following is not possible with conventional controllers, and *v*) high level of modularity and flexibility for different HCEs in zones and buildings configurations, enabling thus the fast replication of the method.

Although the MPC for building temperature control has been broadly discussed in many studies found in the literature, a unique, clear and robust framework summarizing the necessary steps for its deployment does not exist. In the thesis, a general methodology of minimizing energy consumption using current energy sources and minimal retrofitting through the use of advanced control techniques is presented. The developed approach relies on the existing building automation system (if such exists), enabling an easy switch to standard building operation in case of communication errors or some other system malfunction. The thesis describes the on-line implementation of the zone MPC as a basis for hierarchical energy management, including communication of the optimal control scheme with the building automation system and the component-level feedback loops, as well as the measured energy and indoor comfort performance benefits from the demonstration. The interface between control and estimation applications developed as software modules, and the physical world is a two-way real-time database including relevant building data, exterior variables and internal variables for mutual software modules synchronization. The developed algorithms have been verified through the extensive simulation case-studies and via on-line implementation on the University of Zagreb Faculty of Electrical Engineering and Computing (UNIZGFER) skyscraper

building which is a living-lab on MPC algorithms. The following contributions of the developed approach are highlighted:

- a method for identification of an energy model of a system of fan coil units, which gives a direct relation between the thermal energy provided to a zone, actuation commands, heating/cooling medium conditions and the zone temperature,
- a method for identification of a thermodynamic building model suitable for predictive control design and disturbance estimation,
- predictive control strategy for zone temperature control and hierarchical coordination with the central heating/cooling medium conditioning system, building microgrid, smart grid or some other building subsystem sharing a common energy link with zones,
- validation of the developed hierarchical predictive control system within a living-lab environment in terms of achieved thermal comfort and energy cost reduction,
- validation of the developed zone temperature control via on-line implementation on a full-scale skyscraper building.

1.2 Thesis outline

The thesis is organized into three parts that encompass needed steps for model predictive control of temperature in building zones: identification of needed mathematical models, synthesis of control algorithms as well as implementation and running of the developed algorithms in real-time in operative environment of the building. After the introductory words presented before, the remainder of the thesis is outlined as follows.

- **Part I: Modelling and identification of thermodynamic processes in buildings**

Model-based energy management of buildings, through MPC framework, proved to be the promising solution for improving the energy efficiency of the buildings sector. The keystone for further improvements and real implementation are reliable and accurate mathematical models simple enough to be used in real-time control. In *Part I* the developed modelling methodologies, necessary for a fast deployment of the model-based energy management strategies in buildings are presented.

- In *Chapter 2* a methodology for identification of a control-oriented energy model for a system of fan coil units (FCUs) is presented. The model gives a direct relation between the thermal energy provided by the FCU to a zone, actuation commands, heating/cooling medium conditions and the zone temperature. The introduced simple and accurate dynamic characterization of energy transmitted

from a FCU to zone air fills the gap between thermal and energy management for buildings. This enables implementation of predictive building controls and unleashes significant energy and cost-saving potentials in building equipped with FCUs.

- In *Chapter 3*, a general identification framework for acquiring control-oriented semi-physical thermal model of a building based on modified constrained unscented Kalman filter algorithm is presented and validated. The experimental validation results obtained by applying the framework to case-study building show that the developed algorithm applied to short-term operation data outperforms the standard Kalman filter forms, both in convergence rate and numerical stability. The true utility of the developed algorithm is demonstrated by showing that the simplified building models able to make reliable 24 hours ahead predictions are identified by using less than one week of normal operation building data.

- **Part II: Zone Model Predictive Control**

The focus of *Part II* of the thesis is the development of real-time MPC method for zone temperature control which guarantees the essential properties of closed-loop feasibility as well as offset-free control. The developed zone temperature control is envisioned as the lowest level in the hierarchical decomposition of building subsystems, thus a special focus is put on developing the possibility for interaction and coordination with the higher-level modules in order to achieve the near-optimal behaviour of the building as a whole.

- In *Chapter 5* an MPC based control scheme for energy-saving and comfortable temperature control in buildings is presented. The offset-free control and disturbance compensation is ensured through introduction of an estimator in the control loop. The realization of the optimal thermal energy inputs is then enforced by HCE interfaces acting as a link between the optimal thermal inputs and real actuation commands required for those inputs to be realized. The performance bound and possible energy savings are calculated via simulation case-study based on one year simulation of temperature control in the case-study building with the different control approaches applied for zone temperature control.
- *Chapter 6* proposes a modular coordination mechanism between building zones comfort control and higher-levels in building hierarchy such as central HVAC system, building microgrid or smart grid. The imposed modularity is based on a simple interface for exchanging thermal energy consumption and thermal energy price profiles shaped by higher hierarchical levels. The approach is verified by optimizing the one-day ahead operation of the case-study building

consisting of three hierarchical levels: building zones, central heating/cooling medium conditioning system and microgrid.

- **Part III: Application to a full-scale skyscraper building**

The developed zone temperature approach is validated in *Part III* by deploying it on a full-scale skyscraper building described in details in *Appendix A*.

- *Chapter 8* focuses on technological prerequisites for implementation of zone temperature control via MPC as a lowest level among identified hierarchical building subsystems. The basic principles of the case-study BEMS infrastructure related to zone temperature control are given, followed by the architecture of the developed zone temperature control system with detailed description of all software modules required for its deployment and results of their on-line operation.
 - In *Chapter 9* a practical procedure for detection of an airlock in a system of FCUs is presented and verified in on-line operation with a detailed elaboration of the obtained results.
- Concluding remarks with elaboration of the main results and further research and development possibilities related to certain thesis parts are provided at the end of each Part (*Chapter 4*, *Chapter 7* and *Chapter 10*). In *Chapter 11* a brief summary of the results presented in this thesis and an outlook to possible directions for future research on these topics is given.
 - The thesis contains two appendices. In *Appendix A* a detailed description of UNIZGFER skyscraper building is given. The building is fully equipped with required hardware and ICT infrastructure for testing and validating a wide range of control and estimation algorithms in buildings. The building itself is a living-lab on MPC algorithms. Within the thesis, all experiments and case studies are performed on the UNIZGFER building. In *Appendix B* the procedure for calculation of solar irradiance incident on a tilted surface, which is the main prerequisite for calculation of solar impact on zone temperature, is presented.

Part I

Modelling and Identification of Thermodynamic Processes in Buildings

Mathematical modelling and identification of a system of fan coil units

Fan Coil Units (FCUs) are one of the most common heating/cooling elements found in office buildings today. A FCU consists of a fan and one or more air-water heat exchangers. Multiple FCUs connected in parallel to a common supply line form a system of FCUs (Fig. 2.1).

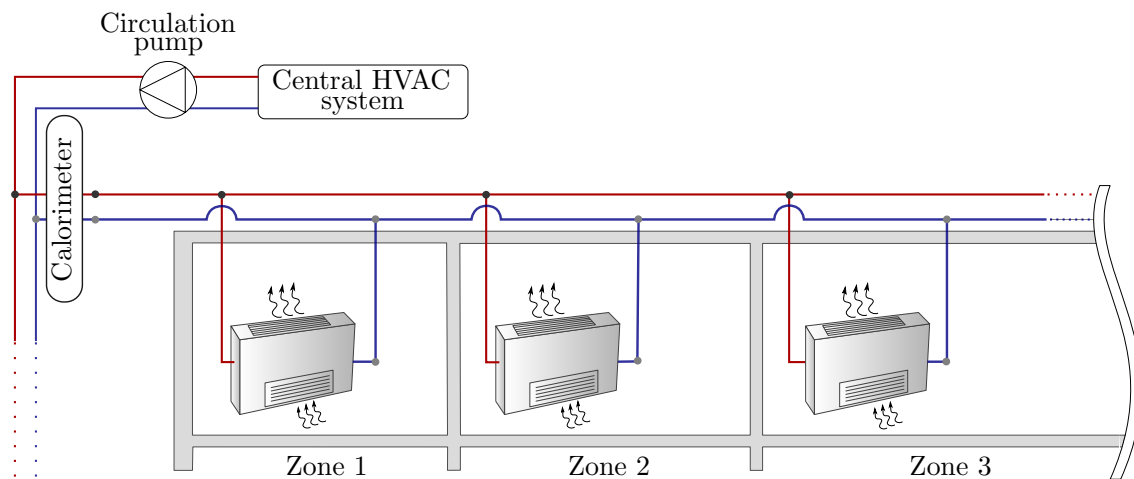


Figure 2.1. *Illustration of a system of FCUs.*

Overall performance of a FCU as a part of the system is described with a *i*) hydraulic model characterizing the distribution of the heating/cooling medium through the system and *ii*) a thermodynamic model for assessment of thermal energy provided by each FCU.

In general, thermodynamic heat exchanger models in literature are divided into three groups: *i*) physical models relied on fundamental physical laws or based on well known heat exchanger analysis methods such as logarithmic mean temperature difference or number of transfer units relations [41, 42, 43, 44, 45], *ii*) non-physical models completely relied

on the experimental data and *iii*) semi-physical models as a compromise between the first two groups. Physical models require detailed physical properties of a FCU, such as fin thickness or tube dimensions, which are often omitted from manufacturer's catalogue and are hardly measurable on the final on-site product [46, 47, 48, 49, 50, 51]. Non-physical models, usually put in a form of simple linear approximations around an operating point [17] or neural networks [52, 53, 54, 55], decrease in accuracy when operating outside the training range. Semi-physical models exploit physical knowledge or some other a priori information to specify the model structure while the unknown parameters are identified based on the experimental [56, 57, 58] or manufacturer's catalogue data [56]. Whilst the experimental analysis of heat exchangers in general is widely elaborated, experimental analysis of a FCU is scarcely considered in only few papers that concern with mainly a single FCU [59, 17].

While thermodynamic model of a single FCU can be easily assessed if measurements of the medium flow through the unit as well as measurements of supply and return medium and air temperatures are available, such information is often unavailable for a system of FCUs. A hydraulic performance of a FCU and sensors-free solution for determining the medium flow through the individual unit is rarely discussed. The use of pressure drop sensors [60] tends to be cost-intensive when applied to individual FCUs due to a large number of expensive sensors required and corresponding installation costs. By developing the hydraulic model of the system, the individual flows are easily assessed based on a single central measurement of the flow through the entire system (typically measured with calorimeters installed on major supply ducts). Use of the hydraulic model for the system design and subsequently its management significantly reduces operating costs [61, 62]. Inclusion of both, hydraulic and thermodynamic model into the building management system offers further savings by enabling dynamic flow control with respect to the thermal demands per zones [63].

2.1 Energy model of a system of fan coil units

Control-oriented energy model for a system of FCUs consists of a hydraulic model of the system and thermodynamic and electrical energy consumption models of all FCUs equal for the same FCU types. The overall scheme of the model is given in Fig. 2.2. The model inputs are: *i*) central measurement of medium mass flow through the entire

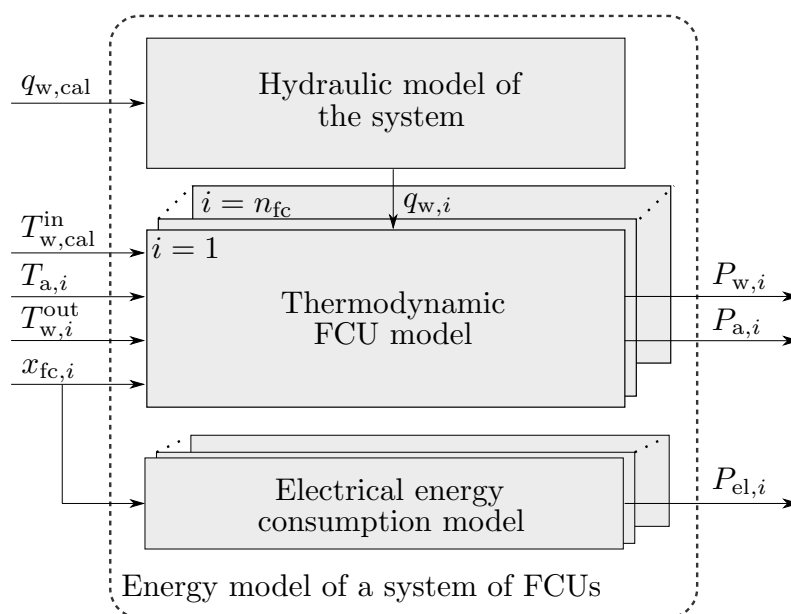


Figure 2.2. Scheme of the control-oriented energy model of a system of FCUs.

system $q_{w,o}^m$, *ii*) individual measurements of fan speeds $x_{fc,i}^m$, *iii*) zone air temperatures in every considered zone $T_{a,i}^{in,m}$ and *iv*) central or individual measurements of supply medium temperature $T_{w,i}^{in,m}$. Index i in subscripts denotes measurements related to the i^{th} FCU and n_{fc} is the overall number of FCUs in the system. Outputs of the hydraulic system model are individual medium mass flows through every FCU in the system $q_{w,i}$. Individual medium mass flows are subsequently used in the thermodynamic models to calculate the thermal powers provided to the zones $P_{a,i}$ and return medium temperatures $T_{w,i}^{out}$ for every considered FCU.

The developed energy model gives a direct relation between the thermal energy provided by the FCU to a zone, actuation commands, heating/cooling medium conditions and the zone temperature. As such, the model is suitable for: *i*) acquiring thermal powers per zone required for identification of building thermodynamic model, *ii*) estimation of unmeasured thermal loads affecting the zone for a very broad use in building monitoring and control, *iii*) usage of an advanced FCU control algorithm for direct control of thermal energy inputs per zone via fan speeds, which makes it possible to realize optimized thermal energy inputs computed via predictive energy management schemes for maintaining zones thermal comfort [64, 13] and *iv*) development of fault detection and diagnosis algorithms for FCUs [65, 66, 67].

2.1.1 Hydraulic model

The medium flow through a FCU depends on the pressure drop across the various elements that form up the entire system. A practical way of modelling complex hydraulic systems is the transition to an analogous electrical model where medium mass flow q_w , pressure drop Δp and hydraulic resistance R_h behave equivalently to electrical current, voltage and electrical resistance, respectively. The equation relating pressure drop and mass flow through a hydraulic network element is equal to:

$$\Delta p = R_h \cdot q_w^{\alpha_h}, \quad (2.1)$$

where R_h is a constant hydraulic resistance. The values of α_h depend on the methodology used for calculation of R_h and the element type.

Pressure loss in pipes consists of three components: *i*) hydrostatic pressure loss Δp_h , *ii*) frictional pressure loss Δp_f and *iii*) kinetic pressure loss. For most applications in heating/cooling system, kinetic losses are minimal. Thus, the equation that describes the overall pressure loss in pipes is expressed as a sum of two major terms:

$$\Delta p_p = \Delta p_f + \Delta p_h. \quad (2.2)$$

The hydrostatic pressure drop occurs only when there are differences in elevation from the inlet to the outlet of a pipe segment:

$$\Delta p_h = \rho \cdot g \cdot \Delta h, \quad (2.3)$$

where g is acceleration of gravity and Δh is change in pipe elevation. The frictional pressure drop in a circular pipe with constant inner diameter d and length l is defined by Darcy-Weisbach equation:

$$\Delta p_f = f_D \frac{8 \cdot l}{\rho \cdot \pi^2 \cdot d^5} \cdot q_w^2, \quad (2.4)$$

where ρ is the density of heating/cooling medium and f_D is the friction factor. For hydraulically smooth pipes, f_D is defined by Blasius equation:

$$f_D = 0.3164 \cdot \text{Re}^{-0.25}, \quad (2.5)$$

where Re is Reynolds number defined as:

$$\text{Re} = \frac{4}{\mu \cdot d \cdot \pi} \cdot q_w, \quad (2.6)$$

with μ as dynamic viscosity of the medium. In addition to the losses due to the friction or elevation difference, there are also losses associated with flow through valves and fittings. These, so called minor pressure losses, are accounted by using the equivalent

length method [68]. The method uses empirical tables to convert each fitting into an equivalent length of the straight pipe l_{eq} which is then added to the pipe length l . The l_{eq}/d ratio for most common types of fittings can be found in Tab. 2.1.

Table 2.1. Equivalent length of fittings [68], [69].

Type of fitting	l_{eq}/d
Tee - along the straight	20
Tee - to the branch	60
Elbow 90 (smooth radius)	30
Three way valve (fully opened - through flow)	30
Sudden pipe diameter expansion	4*
Sudden pipe diameter contraction	20*

* used with inlet velocity.

By inserting (2.6) and (2.5) into (2.4) and including the minor losses, the final form of frictional pressure drop across the circular pipe section is defined as:

$$\Delta p_f = 0.241 \cdot \frac{\mu^{0.25} \cdot (l + \sum l_{eq})}{d^{4.75} \cdot \rho} \cdot q_w^{1.75}. \quad (2.7)$$

Hydraulic resistance of the FCU and medium mass flow through the unit are fully determined with the pressure drop within it:

$$\Delta p = R_{h,fc} \cdot q_w^{\alpha_{h,fc}}, \quad (2.8)$$

where $R_{h,fc}$ and $\alpha_{h,fc}$ are parameters to be found based on the experiments or pressure drop data from the manufacturer's catalogue.

Based on the electric-hydraulic analogy an equivalent electrical model of the system is derived for a most common heating/cooling network topology (Fig. 2.3).

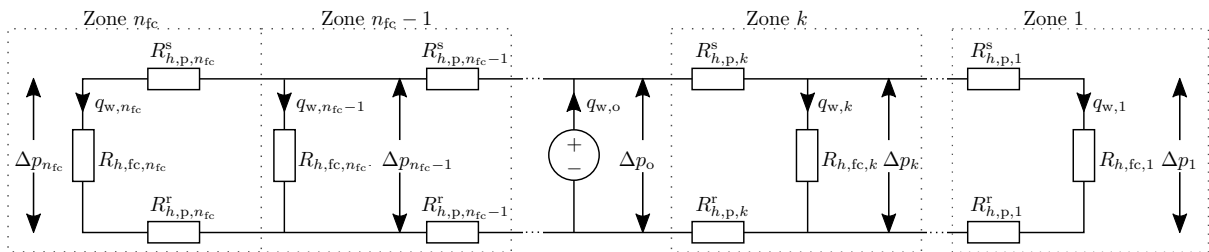


Figure 2.3. The analogous electrical model of standard heating/cooling installations.

Supply pipe, return pipe and FCU hydraulic resistances are denoted as $R_{h,p}^s$, $R_{h,p}^r$ and $R_{h,fc}$, respectively. For clarity, hydraulic resistances of pipes in parallel branches are omitted. For every closed loop of the circuit, once the hydraulic resistances and mass flows are

known, the pressure drop is defined with Kirchhoff's circuit laws $\forall j = 1, \dots, n_{fc} - 1$:

$$\Delta p_j = \begin{cases} \Delta p_{j+1} - \sum_{i=1}^j q_{w,i}^{1.75} (R_{h,p,j}^s + R_{h,p,j}^r) & \text{for } j \leq k, \\ \Delta p_{j+1} + \sum_{i=j}^{n_{fc}} q_{w,i}^{1.75} (R_{h,p,j}^s + R_{h,p,j}^r) & \text{for } j > k, \end{cases} \quad (2.9)$$

where Δp_j is the overall pressure drop in a parallel branch including pressure drop through FCU and pressure drop in associated vertical supply and return pipes, $\Delta p_{k+1} = \Delta p_o$ is the overall pressure drop in the entire system, n_{fc} is the total number of FCUs in the system and $q_{w,i}$ is the medium mass flow through the i^{th} FCU. For known overall medium mass flow denoted with $q_{w,o}^m$, the individual FCU mass flows $q_{w,i}$ are found by solving the following optimization problem:

$$\begin{aligned} \min_{\Delta p_o} \quad & |q_{w,o}^m - q_{w,o}| \\ \text{s.t.} \quad & q_{w,o} = \sum_{i=1}^{n_{fc}} q_{w,i}, \end{aligned} \quad (2.10)$$

(2.2), (2.3), (2.7), (2.8), (2.9).

The optimization problem (2.10) belongs to a class of nonlinear programs which can be efficiently solved with e.g. genetic algorithms [70]. Flow share through the i^{th} FCU is defined as $\eta_{fc,i} = q_{w,i}/q_{w,o}$ where $q_{w,i}$ is recalculated based on (2.9) and the optimal Δp_o obtained as solution of the optimization problem (2.10). For installations with operable valves, where flow distribution is time-varying and based on the valve positions, the procedure is extended by introducing variable valves hydraulic resistances in the network.

2.1.2 Thermodynamic model

Heat transfer within a FCU consists of three parts: convection of the heating/cooling medium (e.g. water), heat conduction through the heat exchanger and convection of air to be heated or cooled. For modelling, the following assumptions are made:

- FCU fan has four possible fan speeds: off, Low, Medium and High, denoted respectively as off, L, M, H,
- air mass flow q_a inside the FCU varies with the fan speed and is assumed to be constant for each speed,
- mean water temperature inside the FCU, $\overline{T_w}$, is approximately the average of water inlet temperature T_w^{in} and water outlet temperature T_w^{out} , i.e. $\overline{T_w} = 0.5(T_w^{\text{in}} + T_w^{\text{out}})$,
- air intake temperature T_a^{in} is assumed to be equal to zone air temperature,
- heat transfer from water to air is driven by the temperature difference $(\overline{T_w} - T_a^{\text{in}})$,

- properties of air and water are assumed to be constant.

With set assumptions, the following dynamics equations are derived for each FCU:

$$m_w c_w \dot{T}_w^{\text{out}} = q_w c_w (T_w^{\text{in}} - T_w^{\text{out}}) - U_o (\bar{T}_w - T_a^{\text{in}}), \quad (2.11)$$

$$m_a c_a \dot{T}_a^{\text{out}} = q_a c_a (T_a^{\text{in}} - T_a^{\text{out}}) + U_o (\bar{T}_w - T_a^{\text{in}}), \quad (2.12)$$

where T_a^{out} is the outgoing air temperature, q_w is medium mass flow through the FCU, c_a and c_w are the specific heat capacity of dry air and specific heat capacity of water, respectively. Parameter m_a is the mass of air and m_w is the mass of water inside the FCU, available from manufacturer's catalogue. Heat transfer coefficient $U_o = f(q_a, q_w)$ is a nonlinear function of medium mass flow q_w and air flow q_a defined as [71, 60, 66]:

$$U_o(q_a, q_w) = \frac{a_{fc} \cdot q_a^{c_{fc}}}{1 + b_{fc} \cdot \left(\frac{q_a}{q_w}\right)^{c_{fc}}}, \quad (2.13)$$

where a_{fc} , b_{fc} and c_{fc} are parameters determined based on physical system properties or through identification. For FCUs with fixed set of fan speeds, the air mass flow q_a for a certain fan speed x_{fc} does not deviate over time significantly (if there are no external impacts blocking the air path). Thus, it is reasonable to estimate separate functional dependencies for all available fan speeds avoiding thus the need for knowing the exact, hardly measurable, information on the air flow. By linking the air flow information to a fan speed, (2.13) obtains the form:

$$U_o(x_{fc}, q_w) = \begin{cases} \frac{a_{fc}^{\text{off}}}{1 + b_{fc}^{\text{off}} \cdot q_w^{-c_{fc}}}, & \text{for } x_{fc} = \text{off}, \\ \frac{a_{fc}^{\text{L}}}{1 + b_{fc}^{\text{L}} \cdot q_w^{-c_{fc}}}, & \text{for } x_{fc} = \text{L}, \\ \frac{a_{fc}^{\text{M}}}{1 + b_{fc}^{\text{M}} \cdot q_w^{-c_{fc}}}, & \text{for } x_{fc} = \text{M}, \\ \frac{a_{fc}^{\text{H}}}{1 + b_{fc}^{\text{H}} \cdot q_w^{-c_{fc}}}, & \text{for } x_{fc} = \text{H}, \end{cases} \quad (2.14)$$

with individual parameters $\mathbf{a}_{fc} := \{a_{fc}^{\text{off}}, a_{fc}^{\text{L}}, a_{fc}^{\text{M}}, a_{fc}^{\text{H}}\}$ and $\mathbf{b}_{fc} := \{b_{fc}^{\text{off}}, b_{fc}^{\text{L}}, b_{fc}^{\text{M}}, b_{fc}^{\text{H}}\}$ defined for every fan speed. Parameter c_{fc} does not depend on the air flow so one common parameter for all fan states is defined. For switched-off fan a FCU behaves as a normal radiator unit with a constant heat transfer coefficient, thus for fan switched off $b_{fc}^{\text{off}} = 0$.

The thermodynamic performance of the floor mounted units is downgraded during the cooling season. While during the heating season, incoming air temperature is considered equal to the zone temperature, during the cooling season cooled outgoing air tends to settle at the floor without mixing with the zone air. As a result, incoming air temperatures are lower than the zone temperature. The described seasonal effect is anticipated through

introduction of correction coefficients ε_{fc}^x for every fan speed:

$$U_o(x_{fc}, q_w) = \varepsilon_{fc}^x \cdot \frac{a_{fc}^x}{1 + a_{fc}^x \cdot q_w^{-c_{fc}}}, \quad x_{fc} \in \{\text{off}, \text{L}, \text{M}, \text{H}\}. \quad (2.15)$$

The water side thermal power P_w is defined as:

$$P_w = q_w c_w (T_w^{\text{in}} - T_w^{\text{out}}). \quad (2.16)$$

The m_a/q_a ratio is typically less than 1 s and therefore negligible compared to water time constant. The air side thermal process of a FCU is therefore observed as a stationary process ($\dot{T}_a^{\text{out}} = 0$):

$$\underbrace{q_a c_a (T_a^{\text{out}} - T_a^{\text{in}})}_{P_a} = \underbrace{U_o (\overline{T}_w - T_a^{\text{in}})}_{P_t}. \quad (2.17)$$

This further means that the thermal power affecting the zone, P_a , is equal to the overall transmitted thermal power P_t . The important feature of this approach is that the hardly measurable and unreliable T_a^{out} measurement is omitted. For a fixed medium mass flow q_w , the final thermodynamic model of a FCU is in a form of a switched-linear model:

$$\begin{aligned} \dot{T}_w^{\text{out}} = & \left[-\frac{q_w}{m_w} - \frac{U_o(x_{fc}, q_w)}{2m_w c_w} \right] T_w^{\text{out}} \\ & + \left[\frac{q_w}{m_w} - \frac{U_o(x_{fc}, q_w)}{2m_w c_w} \quad \frac{U_o(x_{fc}, q_w)}{2m_w c_w} \right] \begin{bmatrix} T_w^{\text{in}} \\ T_a^{\text{in}} \end{bmatrix}, \end{aligned} \quad (2.18)$$

$$P_a = \left[\frac{U_o(x_{fc}, q_w)}{2} \right] T_w^{\text{out}} + \left[\frac{U_o(x_{fc}, q_w)}{2} \quad -U_o(x_{fc}, q_w) \right] \begin{bmatrix} T_w^{\text{in}} \\ T_a^{\text{in}} \end{bmatrix}, \quad (2.19)$$

where $U_o(x_{fc}, q_w)$ is defined in (2.14) and the fan speed x_{fc} is used for switching.

2.1.3 Electrical energy consumption model

Electrical power of FCU's fan P_{el} is assumed constant for every fan speed:

$$P_{el} = \begin{cases} 0, & \text{for } x_{fc} = \text{off}, \\ P_{el}^L, & \text{for } x_{fc} = \text{L}, \\ P_{el}^M, & \text{for } x_{fc} = \text{M}, \\ P_{el}^H, & \text{for } x_{fc} = \text{H}. \end{cases} \quad (2.20)$$

The FCU's fan powers in certain fan speed P_{el}^L , P_{el}^M and P_{el}^H are defined based on fan motor technical data from the manufacturer's catalogue.

2.2 The identification methodology

The methodology for identification of an energy-model of a system of FCUs consists of three major parts: *i*) sensors calibration, *ii*) identification of a hydraulic system model and *iii*) identification of thermodynamic FCUs models. The considered system configuration (Fig. 2.4) consists of: *i*) multiple FCUs connected in parallel, *ii*) temperature sensors installed on the FCU return pipes measuring the return medium temperature $T_{w,i}^{\text{out,m}}$, *iii*) zone units for measuring the zone air temperature $T_{a,i}^{\text{in,m}}$ and fan speed $x_{f,c,i}^{\text{m}}$, and *iv*) central calorimeter for measuring the overall medium mass flow through the system $q_{w,o}^{\text{m}}$, supply medium temperature $T_{w,\text{cal}}^{\text{in,m}}$, return medium temperature $T_{w,\text{cal}}^{\text{out,m}}$ and thermal consumption of the entire system $P_{\text{cal}}^{\text{m}}$.

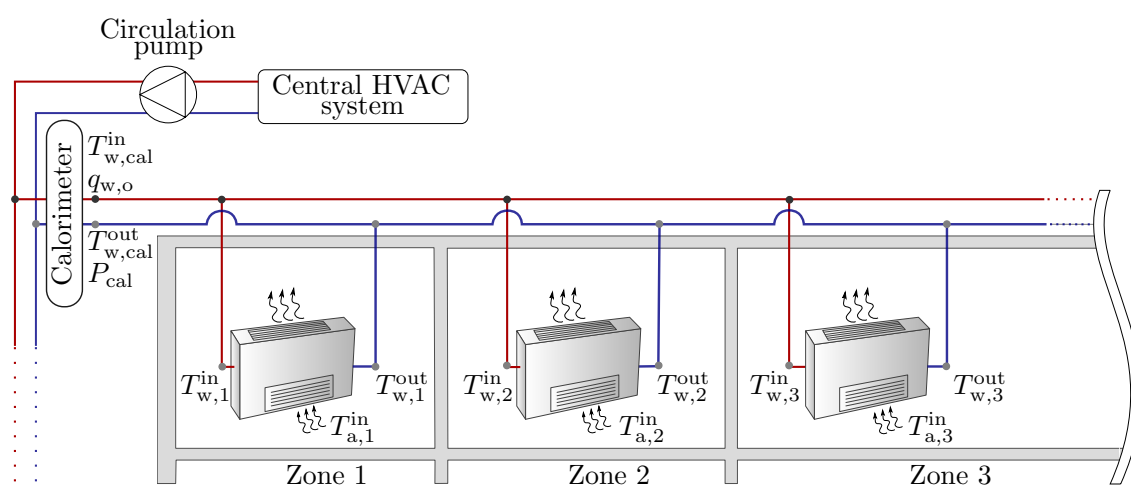


Figure 2.4. Considered configuration of a system of FCUs.

For negligible transmission heat losses FCU inlet water temperature $T_{w,i}^{\text{in}}$ is considered to be equal to the supply temperature measured by the calorimeter $T_{w,\text{cal}}^{\text{in,m}}$, i.e. $T_{w,i}^{\text{in}} = T_{w,\text{cal}}^{\text{in,m}}$. If the temperature drop along the network is significant, it should be modelled or additional temperature sensors have to be mounted at the FCU water inlet. Supply and return pipes are assumed to be isolated. All measurements are collected with a time resolution of T_s . Superscript 'm' denotes measured variable.

2.2.1 Sensor calibration

Indirect measurement of the return medium temperature, typically performed with temperature sensor mounted on the FCU return pipe is subject to various effects (e.g. lead wires acting as a thermal sink, sensor insulation, effects of ambient temperature, etc.) that cause its deviation from the real temperature. The so-called two-point calibration method, comparison with trusted sensor at lower and upper bound of the operating range, essentially re-scales the output and is capable of correcting both slope and offset errors. For systems with three-way valves (see Fig. A.4(a) in Appendix A.2) and well-insulated supply pipelines, the sensor characteristics can be determined by using historical measurements.

In intervals with switched-off fan and closed FCU valve (total flow goes through the bypass branch), calibrated sensor measurements should be equal to calorimeter measurement of supply temperature $T_{w,\text{cal}}^{\text{in,m}}$. The sensor calibration curve, defined with slope $p_{1,i}$ and offset $p_{2,i}$, is then found by solving the following optimization problem for every FCU return medium temperature sensor:

$$\begin{aligned} \min_{p_{1,i}, p_{2,i}} \quad & \sum_{k=1}^{M_i} \left(T_{w,i}^{\text{out,c}}(k) - T_{w,\text{cal}}^{\text{in,m}}(k) \right)^2, \\ \text{s.t.} \quad & T_{w,i}^{\text{out,c}} = p_{1,i} T_{w,i}^{\text{out,raw}} + p_{2,i}, \end{aligned} \quad (2.21)$$

where k denotes measurement samples, M_i is overall number of samples used for calibration of the i^{th} FCU temperature sensor, $T_{w,i}^{\text{out,c}}$ is the calibrated sensor measurement and $T_{w,i}^{\text{out,raw}}$ is a raw sensor measurement of the i^{th} FCU. If temperature sensor is mounted close to the bypass branch, measurements may be additionally distorted due to the high thermal conductivity of the pipes. Since supply and return pipes are thermally coupled through the bypass, large thermal gradient between them influences the sensor measurements proportionally to temperature difference between the pipes. True temperature measurement $T_{w,i}^{\text{out,m}}$ is thus defined as:

$$T_{w,i}^{\text{out,m}} = T_{w,i}^{\text{out,c}} - \psi_{\text{fc}} (T_{w,i}^{\text{in,m}} - T_{w,i}^{\text{out,m}}), \quad (2.22)$$

where ψ_{fc} is the unknown heat transfer coefficient equal for all FCUs in the system with the same bypass pipe configuration and $T_{w,i}^{\text{in,m}}$ is the i^{th} FCU supply temperature considered equal to $T_{w,\text{cal}}^{\text{in,m}}$. For ideal mixing of the return medium from different FCUs and only the i^{th} FCU operating at the time (valves on all other FCUs closed) once stationary state is reached, the following holds:

$$q_{w,i} (T_{w,i}^{\text{in}} - T_{w,i}^{\text{out}}) = q_{w,o} (\Delta T_{\text{cal},i} - \Delta T_{\text{cal},0}). \quad (2.23)$$

where $\Delta T_{\text{cal},i}$ is temperature difference between the system supply and return measured on the central calorimeter,

$$\Delta T_{\text{cal},i} = T_{w,\text{cal}}^{\text{in,m}} - T_{w,\text{cal}}^{\text{out,m}}, \quad (2.24)$$

and $\Delta T_{\text{cal},0}$ is the temperature difference in the system with valves of all FCUs closed. Since $\sum_{i=1}^{n_{\text{fc}}} q_{w,i} = q_{w,o}$, by combining (2.22) and (2.23) heat transfer coefficient ψ_{fc} is defined as:

$$\psi_{\text{fc}} = 1 - 1 / \sum_{i=1}^{n_{\text{fc}}} \left(\frac{\Delta T_{\text{cal},i} - \Delta T_{\text{cal},0}}{T_{w,i}^{\text{in}} - T_{w,i}^{\text{out,c}}} \right), \quad (2.25)$$

where n_{fc} is the total number of FCUs in the system.

2.2.2 Identification of the hydraulic model of the system

The prerequisites for development of an analogous electrical model of the heating/cooling system are *i*) the availability of system documentation with known diameters and lengths of individual pipe segments and *ii*) FCUs manufacturers' catalogues with specified pressure drop characteristics. Based on the developed analogous electrical model, the flow shares through different FCUs are defined by the solution of optimization problem (2.10). If the pressure drop at the system entrance is changed, new flow distribution is found by re-solving (2.10) based on new measurement of overall flow through the system $q_{w,o}^m$.

If the piping data or FCUs pressure drop characteristics are not available, the approach based on running an individual experiment on every FCU is proposed. It is important to note that so obtained flow distribution is valid only for operating points for which the experiments are performed. If the overall pressure drop of the system is changed, experiments have to be performed again under new conditions. Thus, the approach is not advisable for systems with variable flow. Since such approach is time-consuming for large systems, herein it is used for validation of the approach based on electric-hydraulic analogy. The individual experiments are performed by switching off all the units in the system (or assuring their constant operation) and running a test sequence on one particular unit. Valves remained fully opened for all units. In such a set-up, the central calorimeter measures the heat consumption of the particular unit with a constant offset equal to the thermal power of the remaining part of the system. To assure constant losses, supply medium mass flow and temperature are required to be constant during the test. The test sequence consists of switching on the highest fan speed on the i^{th} unit and keeping it on until the stationary state is reached. The water-based heating and cooling systems are inevitably subject to transport delays. To account for the effect, calorimeter and return medium temperature measurements are considered as ideal with variable transport delay τ estimated based on the known pipe length and diameter as well as the medium mass flow. After performing experiments on every FCU, flow share through the i^{th} unit $\eta_{fc,i}$ is found by solving the following optimization problem:

$$\begin{aligned} \min_{\eta_{fc,i}, P_d} \quad & \sum_{k=1}^{M_i} \left(\eta_{fc,i} \cdot P_{w,i}^a(k) - (P_{cal}^m(k + \tau_{cal}) - P_d) \right)^2 \\ \text{s.t.} \quad & P_{w,i}^a(k) = q_{w,o}^m(k) c_{w,cal} \left(T_{w,i}^{\text{in},m}(k) - T_{w,i}^{\text{out},m}(k + \tau_{fc}) \right), \\ & 0 \leq \eta_{fc,i} \leq 1, \end{aligned} \quad (2.26)$$

where k denotes measurement samples, M_i is overall number of the samples in the experiment with the i^{th} FCU, $c_{w,cal}$ is a nominal water heat capacity used by the calorimeter (usually set to heat capacity of distilled water 4180 J/(kg·K)), P_{cal}^m is thermal power measurement from the calorimeter, $P_{w,i}^a$ is a priori calculated water side thermal power of the i^{th} FCU and P_d is constant thermal power of the rest of the system. For clarity, the transport delay τ_{fc} is assumed to be already accounted when using the return

medium temperature measurements in the rest of the thesis.

For available measurement of the system return medium temperature $T_{w,\text{cal}}^{\text{out,m}}$ and medium mass flow and supply temperature constant during the experiment, simple algebraic equations for calculation of flow share through the i^{th} FCU are derived. Flow share of the i^{th} FCU is defined as the ratio of temperature differences of the system and FCU return temperature with all FCUs' fans switched off (denoted with superscript 'off') and measured once stationary state of return medium temperature of the excited unit is reached (denoted with superscript 'on'):

$$\eta_{\text{fc},i} = \left| \frac{(T_{w,\text{cal}}^{\text{out,m,off}} - T_{w,\text{cal}}^{\text{out,m,on}})}{(T_{w,i}^{\text{out,m,off}} - T_{w,i}^{\text{out,m,on}})} \right|. \quad (2.27)$$

2.2.3 Identification of the thermodynamic model of the system

In a majority of water-based heating and cooling systems, medium mass flow is controlled to a constant value while supply temperature is altered to meet the building thermal demand. Thus, from the operation data of one FCU only the number of points on the $U_o = f(x_{\text{fc}}, q_w)$ characteristics equal to the number of available distinct fan speeds can be obtained. To obtain multiple points for different medium mass flows the non-uniform distribution of the flow through the system is exploited, i.e. several FCUs of the same type with different estimated flow shares are examined. For a fixed medium mass flow and fan speed, overall heat transfer coefficient is a scalar value (2.14). The identification of the U_o characteristic is thus divided into two parts. First, a set of scalars $\mathbf{U}_o = \{U_o^{\text{off}}, U_o^{\text{L}}, U_o^{\text{M}}, U_o^{\text{H}}\}$ is found by solving the following optimization problem for every dataset related to the considered FCUs of the same type:

$$\begin{aligned} \min_{\mathbf{U}_o, c_w} \quad & \sum_{k=1}^{M_i} |T_{w,i}^{\text{out,m}}(k) - T_{w,i}^{\text{out}}(k)| \\ \text{s.t.} \quad & q_{w,i}(k) = \eta_{\text{fc},i} \cdot q_{w,o}^{\text{m}}(k), \end{aligned} \quad (2.28)$$

(2.15).

Index k denotes measurement samples, c_w is unknown water heat capacity, $T_{w,i}^{\text{out,m}}$ is measured return medium temperature of the i^{th} FCU and M_i is the length of the considered data set. The output of the thermodynamic FCU model $T_{w,i}^{\text{out}}(k)$ is defined as:

$$T_{w,i}^{\text{out}}(k+1) = h \left(x_{\text{fc},i}^{\text{m}}(k), q_{w,i}(k), T_{w,i}^{\text{in,m}}(k), T_{a,i}^{\text{in,m}}(k), T_{w,i}^{\text{out}}(k) \right), \quad (2.29)$$

with function $h(\cdot)$ representing numerical integration of (2.18) over the interval $[k, k+1]T_s$ and model inputs assumed to be constant within that interval. For systems with known heat capacity of the medium c_w operating in a stationary state, values of the \mathbf{U}_o set for

a fixed medium mass flow $q_{w,i}$ and fan speed x_{fc} are defined as:

$$U_o^x = \frac{q_{w,i} c_w (T_{w,i}^{\text{in,m}} - T_{w,i}^{\text{out,m,x}})}{(0.5 \cdot (T_{w,i}^{\text{in,m}} + T_{w,i}^{\text{out,m,x}}) - T_{a,i}^{\text{in,m}})}. \quad (2.30)$$

The result of the first part of the thermodynamic model identification is a set of value triplets $\{(q_{w,i}^*, x_{fc,i}^*, U_o^{x*})_j : j = 1, \dots, K\}$, where K is their overall number and $q_{w,i}^*$ is mean value of the medium mass flow of the considered data set if the triplets are obtained by solving (2.28) or it is equal to medium mass flow used in (2.30).

The second part of the identification is related to finding the unknown coefficients of the U_o characteristics (2.15). The unknown coefficients are found by minimizing the squared error between the model (2.15) and value triplets obtained experimentally:

$$\min_{\mathbf{a}_{fc}, \mathbf{b}_{fc}, \boldsymbol{\varepsilon}_{fc}, c_{fc}} \sum_{j=1}^K (U_o(x_{fc,i}^*, q_{w,i}^*) - U_o^{x*})^2, \quad (2.31)$$

where $\boldsymbol{\varepsilon}_{fc}$ is a set of FCU efficiencies in every fan speed $\boldsymbol{\varepsilon}_{fc} := \{\varepsilon_{fc}^{\text{off}}, \varepsilon_{fc}^{\text{L}}, \varepsilon_{fc}^{\text{M}}, \varepsilon_{fc}^{\text{H}}\}$. To improve the performance of the model outside the current operating range of the system additional value pairs are calculated from the catalogue data based on the stationary equation (2.17).

Following from (2.14), it is evident that heat transfer coefficient U_o increases with the medium mass flow q_w . However, due to distinctively higher heat capacity of the medium compared to air, for fixed fan speed the U_o value starts to stagnate after some amount of medium mass flow:

$$\lim_{q_w \rightarrow \infty} U_o(x_{fc}, q_w) = a_{fc}^x, \quad x_{fc} \in \{\text{off}, \text{L}, \text{M}, \text{H}\}. \quad (2.32)$$

This part of the U_o characteristics is typically covered in manufacturer's catalogue. The heat capacity tables from the catalogue consist of stationary values of the sensible thermal power data P_a^{cd} , supply $T_w^{\text{in,cd}}$ and return $T_w^{\text{out,cd}}$ temperature of the heating/cooling medium and entering air temperature data $T_a^{\text{in,cd}}$ for different fan speeds. Thus, if such data are available it is possible to calculate values in the \mathbf{a}_{fc} coefficient set from the stationary condition (2.17) as:

$$a_{fc}^x = \left| \frac{P_a^{\text{cd,x}}}{\left(T_a^{\text{in,cd,x}} - 0.5 \left(T_w^{\text{in,cd,x}} + T_w^{\text{out,cd,x}} \right) \right)} \right|. \quad (2.33)$$

It is important to note that, even without the use of the manufacturer's catalogue data, it is possible to estimate the model covering the operating range of the system. Since the catalogue data cover the constant part of the U_o characteristics, it represents a sort of performance bound for the considered FCUs.

The workflow of the overall identification methodology is given in Fig. 2.5.

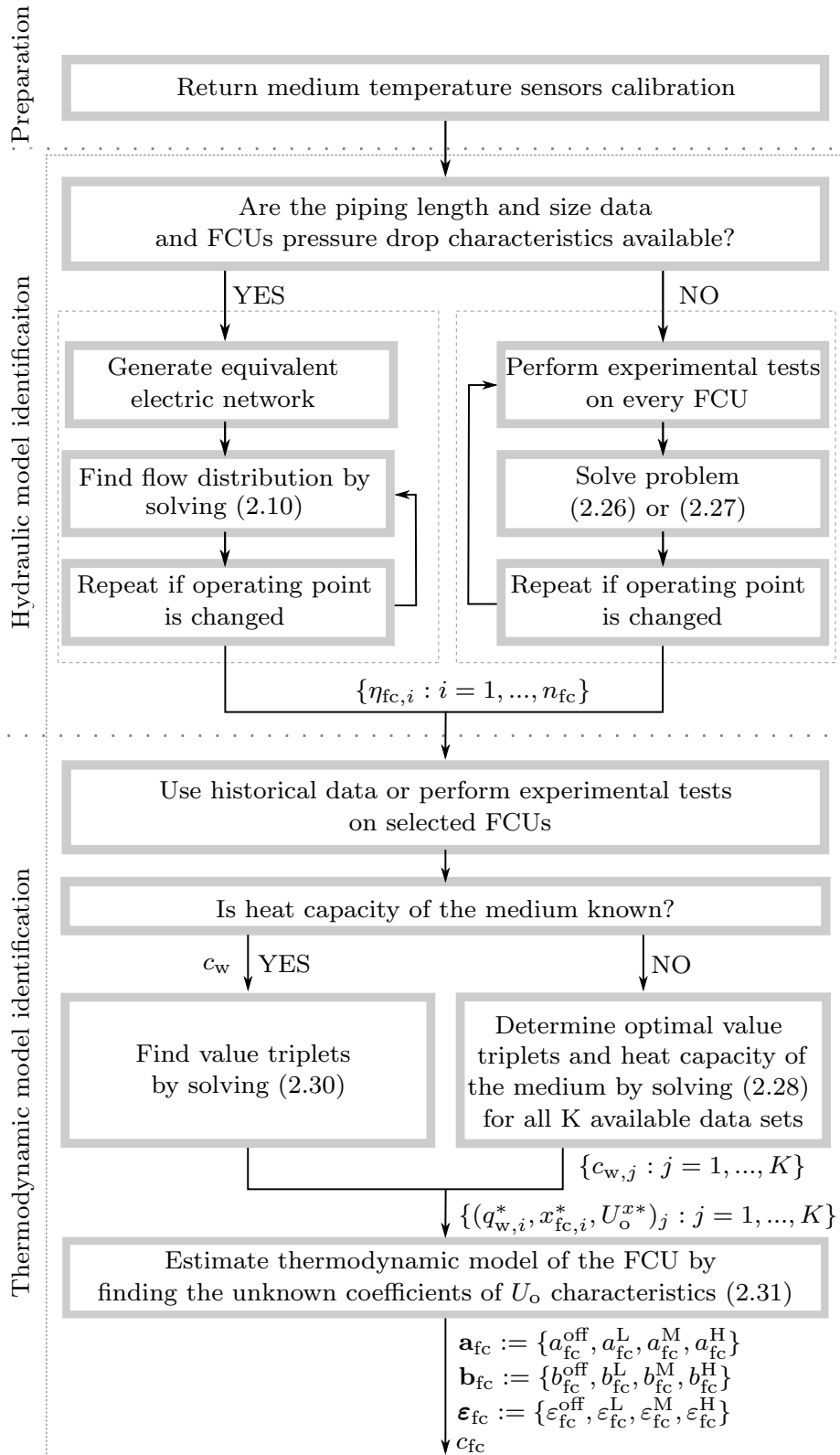


Figure 2.5. The workflow of the methodology for identification of an energy model for a system of FCUs.

2.3 Experimental validation

Experimental validation of the methodology is performed on the south-side piping on the 9th floor of the case-study building. The experimental setup consists of 13 zones with 17 vertical FCUs mounted on the floor, 12 units of type FCC06 and 5 units of type FCC04 (Fig. 2.6).

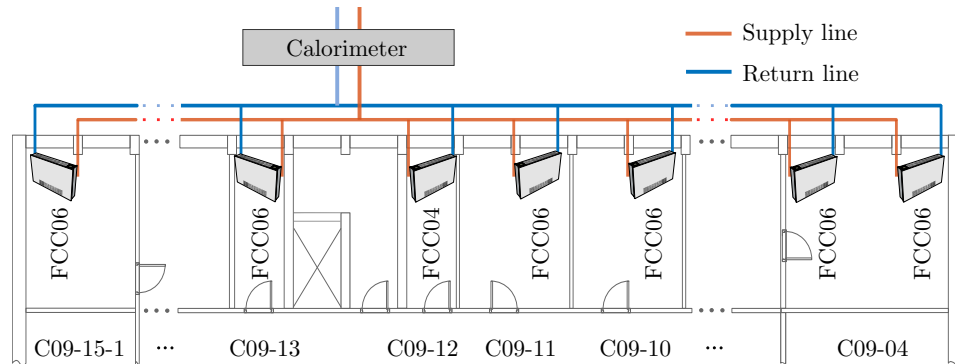


Figure 2.6. Layout of the southern supply duct on the 9th floor of the case-study building.

The arrangement of units with included geometry of horizontal supply pipes (length and diameter) is given in Tab. 2.2.

Table 2.2. Configuration of a system of FCUs on the 9th floor of the case-study building.

Zone	FCU No. i	d [mm]	l [m]	Unit type
C09-04	1	18	1.7	FCC06
	2	22	3.5	FCC06
C09-05	3	28	1.7	FCC06
	4	35	3.5	FCC06
C09-06	5	35	3.5	FCC06
C09-07	6	35	3.5	FCC06
C09-08	7	42	3.5	FCC06
C09-09	8	42	1.7	FCC04
	9	42	3.5	FCC04
C09-10	10	42	3.5	FCC06
C09-11	11	42	1.7	FCC06
C09-12	12	42	2.1	FCC04
C09-13	13	28	5	FCC06
C09-14	14	28	1.7	FCC06
C09-15	15	28	3.5	FCC04
	16	22	1.7	FCC04
C09-15-1	17	18	3.5	FCC06

The length of the pipe is defined as the length of the horizontal segment between two consecutive FCUs or the length between the FCU and the calorimeter (see Fig. 2.6).

The equivalent length of vertical supply and return pipes (including fittings) is identical for all units and amounts 6.26 m. In the following subsections, transmission heat losses are neglected due to the good thermal insulation of the pipeline. This means that the FCU water inlet temperature is considered to be equal to the supply temperature measured by the calorimeter $T_{w,cal}^{in,m}$, i.e. $T_{w,i}^{in} = T_{w,cal}^{in,m}$. The FCUs, produced by manufacturer Trane (models FCC06 and FCC04) [72], are equipped with a centrifugal fan with four different fan speeds (off, Low, Medium and High) and a three-way valve (on-off type). The performance of the FCUs is monitored by measuring the return medium temperature with temperature sensors installed on the FCUs return pipes. On two selected FCUs, additional temperature sensors are mounted on air exhaust and intake to monitor incoming and outgoing air temperatures. Zone air temperatures are measured within the local digital temperature controllers placed in every controllable zone. Every floor supply duct is equipped with calorimeter used for measurement of supply and return medium temperature, temperature difference, medium flow, thermal power and consumed thermal energy. All measurements are collected with sampling time of one minute ($T_s = 1$ min). The list of all relevant measurements is given in Tab. 2.3.

Table 2.3. Available measurements used for identification of energy model of the considered system of FCUs.

DATA SOURCE		SAMPLING TIME
FCUs ($i = 1, \dots, n_{fc}$)		
Fan speed	$x_{fc,i}$ (off, L, M, H)	1 min
Return medium temperature	$T_{w,i}^{out}$ [$^{\circ}$ C]	1 min
ZONES		
Zone temperature	$T_{a,i}$ [$^{\circ}$ C]	1 min
CALORIMETER		
Supply medium temperature	$T_{w,cal}^{in}$ [$^{\circ}$ C]	1 min
Return medium temperature	$T_{w,cal}^{out}$ [$^{\circ}$ C]	1 min
Mass flow	$q_{w,o}$ [kg/s]	1 min
Thermal power	P_{cal} [kW]	1 min
Thermal energy	E_{cal} [kWh]	1 min

To confirm the air mass flow q_a can be considered constant for a certain fan speed the airflow through one exemplary FCU is determined by using an electrical energy meter and fan performance data from the manufacturer's catalogue. The air flow through the FCU is defined as:

$$q_a = f_{el}^x(P_{el}), \quad x_{fc} \in \{L, M, H\}, \quad (2.34)$$

where P_{el} is electric FCU fan power and $f_{el}^x(\cdot)$ is nonlinear function identified based on the manufacturer's catalogue data (see e.g. Fig. 2.7 for identified functional dependence between the electrical power of FCU fan and airflow for Trane FCC06). Since FCUs' air intake filters performances vary slowly over time, one electrical energy meter is used to monitor electrical power of all FCUs placed on the 9th floor and connected to the same supply lines.

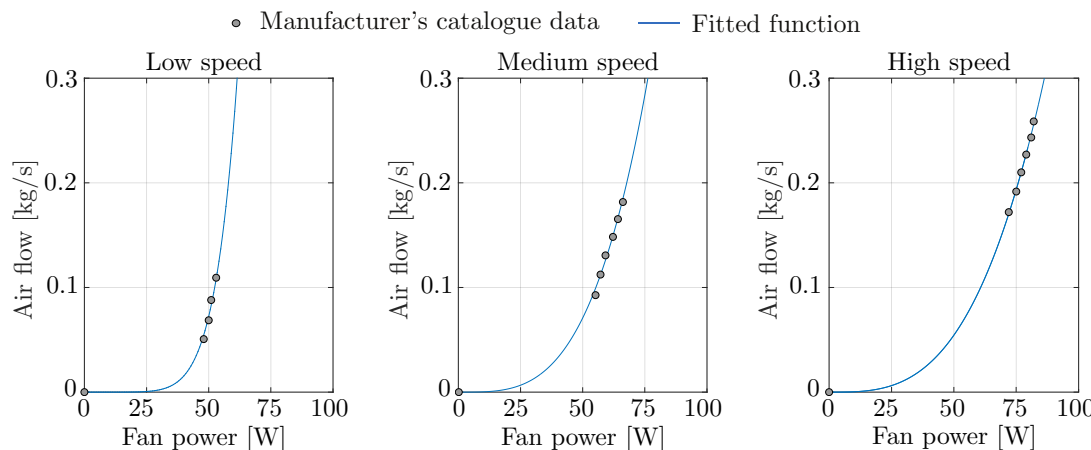


Figure 2.7. Identified FCU fan power model for Trane FCC06.

In Fig. 2.8 the results of on-line monitoring of the exemplary FCU performance are shown. Tests are performed by turning the highest fan speed for two minutes during unoccupied hours. All other FCUs' fans were switched off. To see the impact of the air path blockage, the FCU air exhaust was blocked by placing the obstacle on roughly 70% of the air exhaust. The result is degradation of the airflow by approximately 11%. By performing the experiment it is proved that the air flow does not deviate significantly from the nominal air floor rate listed in manufacturer's catalogue at pressure difference 0 Pa if there is no external impact blocking the air path. Thus, in the thesis air flow and electrical FCU power are assumed to be constant and equal to the nominal values at 0 Pa for each fan speed.

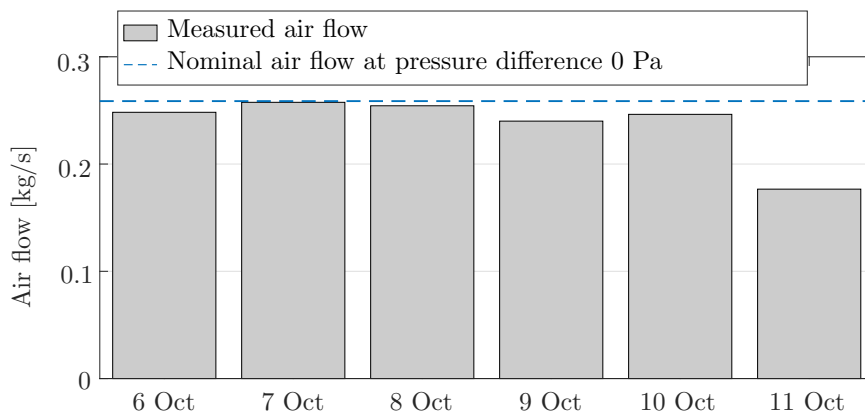


Figure 2.8. Air mass flow variation for 6 days period in 2017.

1-wire return medium temperature sensors calibration

Due to the well-insulated supply pipelines, large thermal conductivity of the copper pipes and 1-wire sensor mounted near to the bypass branch, offset characteristics is determined using historical measurements of supply medium temperature. To avoid the transient impact of the medium stalled inside the heat exchanger, only stationary values are used. Figure 2.9 shows the calibration curve obtained by calibrating the 1-wire sensor mounted on the FCU return pipe in zone C09-10.

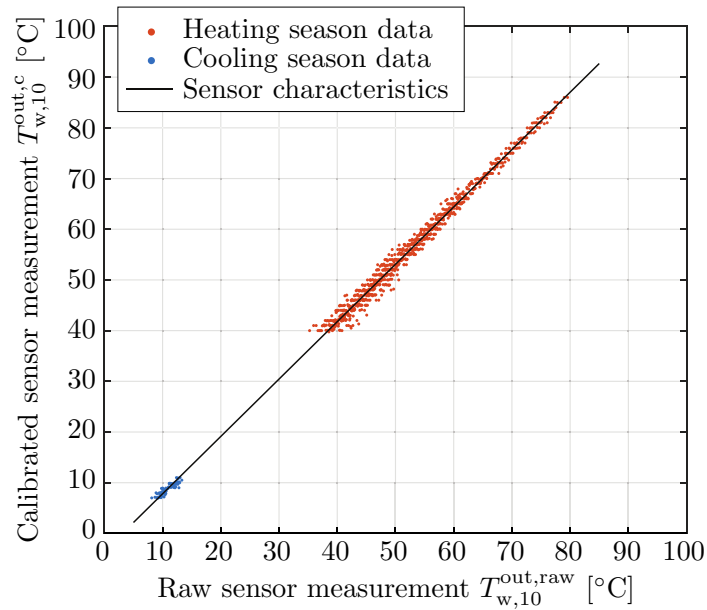


Figure 2.9. 1-wire return medium temperature sensor characteristics (FCU $i = 10$).

To determine the coefficient ψ_{fc} , the identification procedure according to (2.25) was performed. The resulting ψ_{fc} value for the considered system of FCUs and described scenario amounts $\psi_{fc} = 0.1534$.

Identification experiments

Since validation of both thermodynamic and hydraulic model requires experiments, one common set of experiments per FCU is used. The experiments are performed by shutting down all the units and running a test sequence on one particular unit. Valves remained fully opened for all units. The test sequence consists of sequential fan speed changes from off to other possible fan speeds. The duration of every fan speed engagement is chosen to be 8 min, which proved to be enough to cover both the transient and steady-state behaviour. Alternatively, the identification of the thermodynamic model is also applicable on FCU historical data with the requirement of recorded stationary operation for each fan speed. Measurements obtained after running the experiment test on the selected zone C09-10 during the heating season 2016/17 are shown in Fig. 2.10.

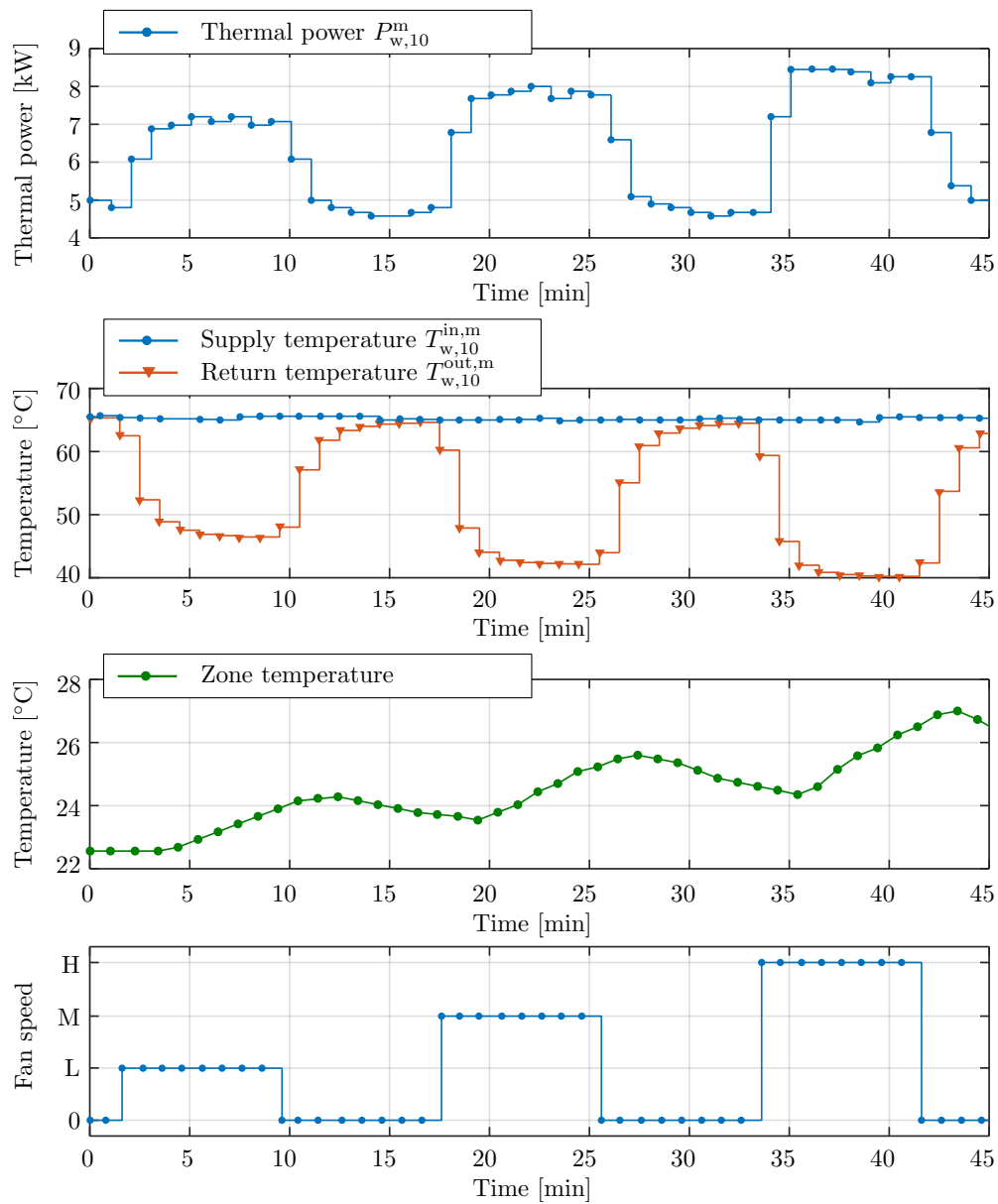


Figure 2.10. Measurements obtained after running the experiment test in zone C09-10 (FCU $i=10$).

Identification of hydraulic model of the considered system of FCUs

With known topology and geometry of the pipes (see Table 2.2), an analogous electrical model of the hydraulic installations is developed. The correlation between pressure drop and mass flow for both FCU types is found by identifying the unknown coefficients $R_{h,fc}$ and $\alpha_{h,fc}$ based on the data from the manufacturer's catalogue (see e.g. Fig. 2.11 for FCC06 FCU type).

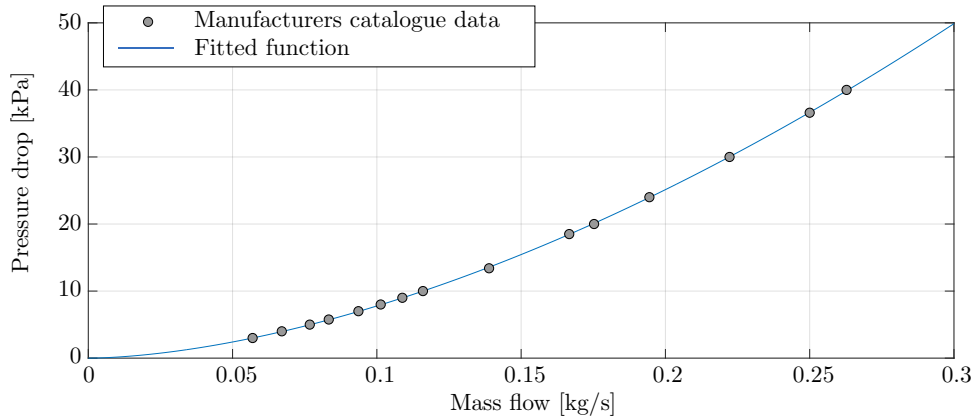


Figure 2.11. Identified pressure drop function for Trane model FCC06.

To set up the optimization problem (2.10), a single measurement of the overall medium mass flow $q_{w,o}^m$ from the calorimeter is used. The flow distribution through the entire network is found by solving the optimization problem (2.10) in MATLAB with the genetic algorithm from [70]. The resulting flow distribution, defined as $\eta_{fc,i} = q_{w,i}/q_{w,o}$ and expressed as percentage, is listed in column 4 in Tab. 2.4 and graphically illustrated in Fig. 2.12.

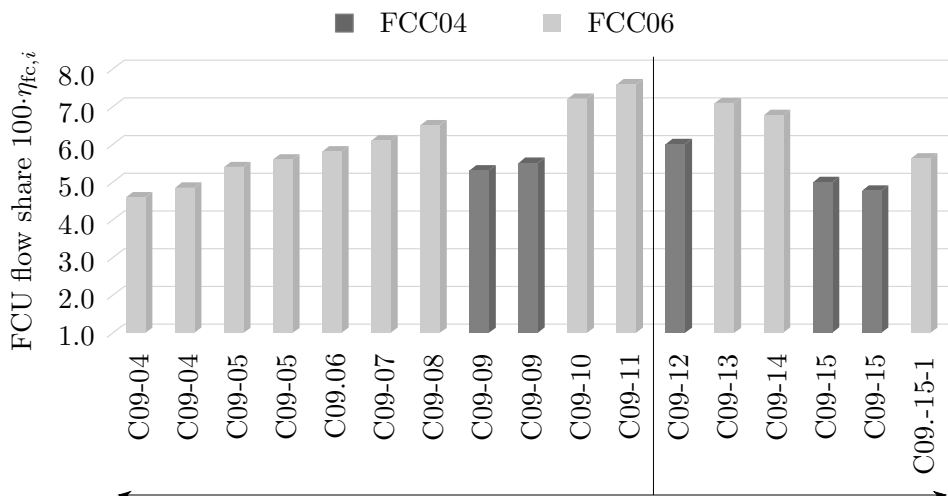


Figure 2.12. Flow distribution of the medium mass flow among FCUs connected to south supply line on the 9th floor.

Table 2.4. Estimated flow share for the south supply line on the 9th floor for $q_{w,o}^m \approx 0.36$ kg/s.

Zone	FCU No. i	Unit type	$100 \cdot \eta_{fc,i}$ [%]	$100 \cdot \bar{\eta}_{fc,i}$ [%]	Error $100 \cdot \frac{ \eta_{fc,i} - \bar{\eta}_{fc,i} }{\eta_{fc,i}}$ [%]
C09-04	1	FCC06	4.62	4.73	0.04
	2	FCC06	4.85		
C09-05	3	FCC06	5.40	5.49	0.13
	4	FCC06	5.60		
C09-06	5	FCC06	5.81	5.88	1.22
C09-07	6	FCC06	6.09	5.97	1.87
C09-08	7	FCC06	6.49	6.50	0.24
C09-09	8	FCC04	5.31	x	x
	9	FCC04	5.51		
C09-10	10	FCC06	7.20	7.40	2.84
C09-11	11	FCC06	7.58	7.66	1.06
C09-12	12	FCC04	6.01	6.15	2.27
C09-13	13	FCC06	7.08	x	x
C09-14	14	FCC06	6.77	6.71	0.79
C09-15	3.5	FCC04	5.00	4.94	1.13
	16	FCC04	4.77		
C09-15-1	17	FCC06	5.62	x	x

Flow shares, identified based on individual experiments for 8 tests performed in the exemplary zone C09-10 during winter 2015 and 2016, are shown in Tab. 2.5. The mean flow share is $\bar{\eta}_{fc,10} = 7.40\%$, which deviates from the calculated value based on the electric-hydraulic analogy by only 2.84% (see Tab. 2.4). The identified flow distribution through

Table 2.5. Estimated flow share for Trane FCC06 in zone C09-10 (FCU $i = 10$).

Test No.	1	2	3	4	5	6	7	8
$q_{w,10}$ [kg/s]	0.027	0.028	0.027	0.028	0.029	0.023	0.022	0.030
$100 \cdot \eta_{fc,10}$ [%]	7.26	7.35	7.35	7.57	7.34	7.26	7.78	7.31

the considered system of FCUs is listed in column 5 in Tab. 2.4. Since all FCUs in a single zone are actuated simultaneously, for zones with more than one FCU, the mean flow share of all units is calculated instead of individual shares. Average relative error, mainly due to sensor accuracy, is 1.16%, which proves the adequate accuracy of electric-hydraulic analogy based calculation of flow distribution through the system. In zones marked with 'x', measurements were unavailable.

Identification of thermodynamic FCU model

Value triplets for identification of the thermodynamic model of the selected FCU type (FCC06) are identified by solving the optimization problem (2.28) for the data collected during 32 test sequence runs on the units of type FCC06 in different zones during heating season 2015/2016, 2016/2017 and cooling season 2017. The heat capacity of water c_w identified according to (2.28) for all the experiments is shown in Fig. 2.13. The model (2.29) is initialized by using known measurements of the return medium temperature at the beginning of the experiment.

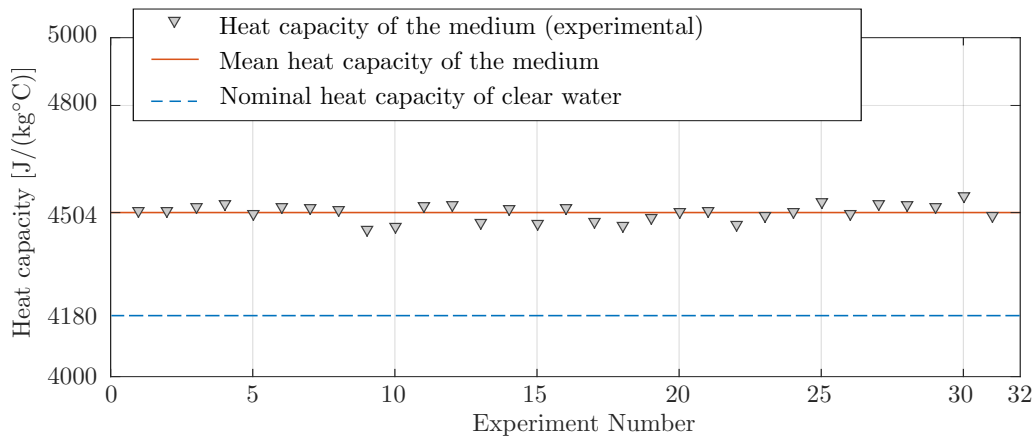


Figure 2.13. Identified heat capacity of the heating/cooling medium.

During the heating season incoming air temperature can be considered equal to the zone temperature, thus ε_{fc}^x coefficients are set to one for all speeds. During the cooling season cooled outgoing air tends to settle at the floor without mixing with the zone air (Fig. 2.14). To anticipate the effect, separate efficiency coefficients ε_{fc}^x are identified for every fan speed (2.15). The identified parameter sets \mathbf{a}_{fc} , \mathbf{b}_{fc} and ε_{fc} and parameter c_{fc} for Trane FCC06 thermodynamic model obtained through (2.31), based on the above obtained value triplets, are shown in Tab. 2.6.

Table 2.6. Estimated $U_o(x, q_w)$ function parameters for Trane FCC06.

Fan speed $x_{fc}/$ Model parameters	off	L	M	H
a_{fc}^x	5.30	96.45	152.90	201.80
b_{fc}^x	0	$1.73 \cdot 10^{-3}$	$3.58 \cdot 10^{-3}$	$5.40 \cdot 10^{-3}$
ε_{fc}^x (cooling)	0	0.35	0.47	0.52
ε_{fc}^x (heating)			1	
c_{fc}			1.86	

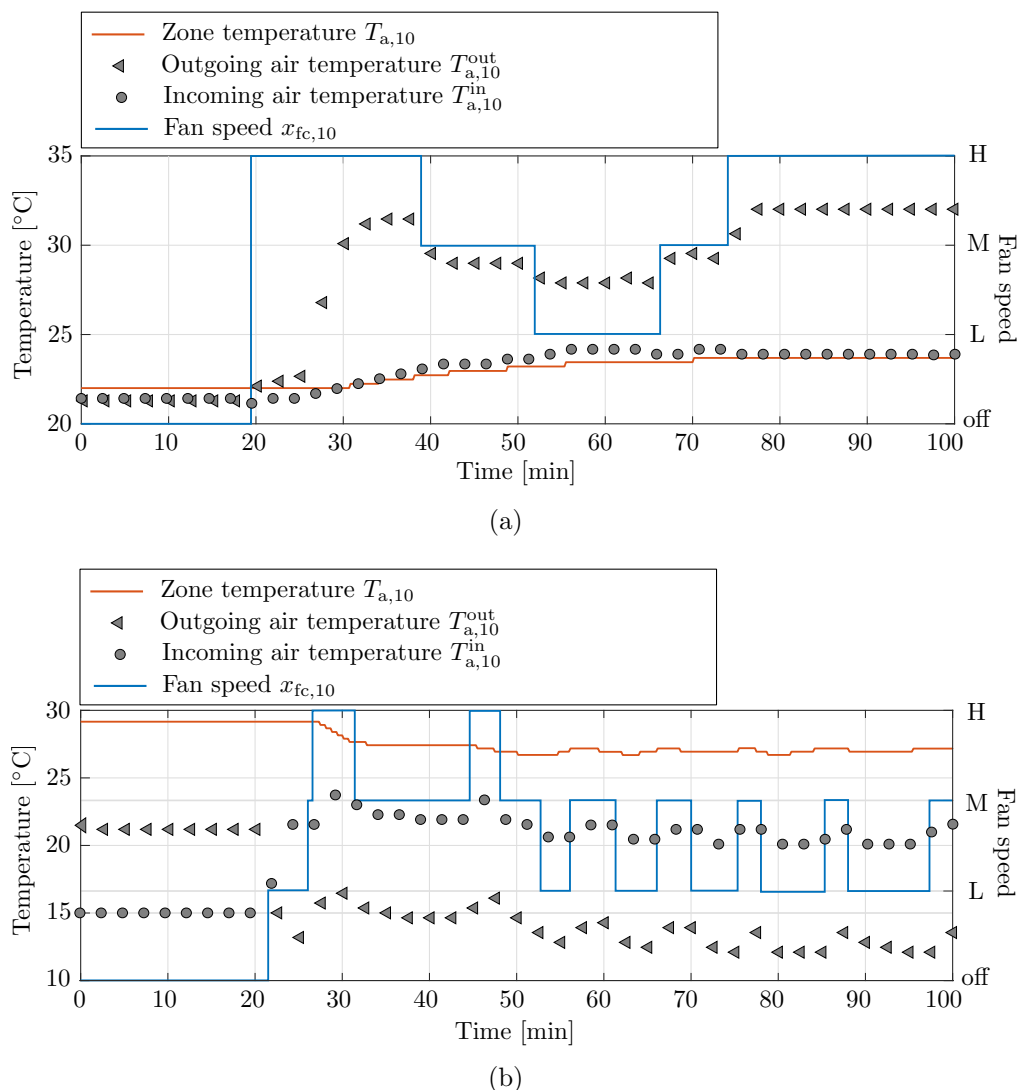


Figure 2.14. Measurements of incoming and outgoing air temperature in zone C09-10 (FCU $i = 10$) collected during the a) heating season, b) cooling season.

Time responses of the identified FCU thermodynamic model in the exemplary zone C09-10, tested on the verification data set, are shown in Fig. 2.15. The model is simulated by using known model input data to calculate the prediction of the return medium temperature without considering available measurements during that period (so-called open-loop prediction). Estimated heat capacity of the medium is considered (see Fig. 2.13) such that calorimeter power measurements are scaled and de-offsetted for the remaining piping consumption $P_{\text{cal}}^* = P_{\text{cal}}^{\text{m}} \cdot c_{\text{w}} / c_{\text{w,cal}} - P_{\text{d}}$. As it can be seen from the figure, the model successfully captures the FCU dynamics.

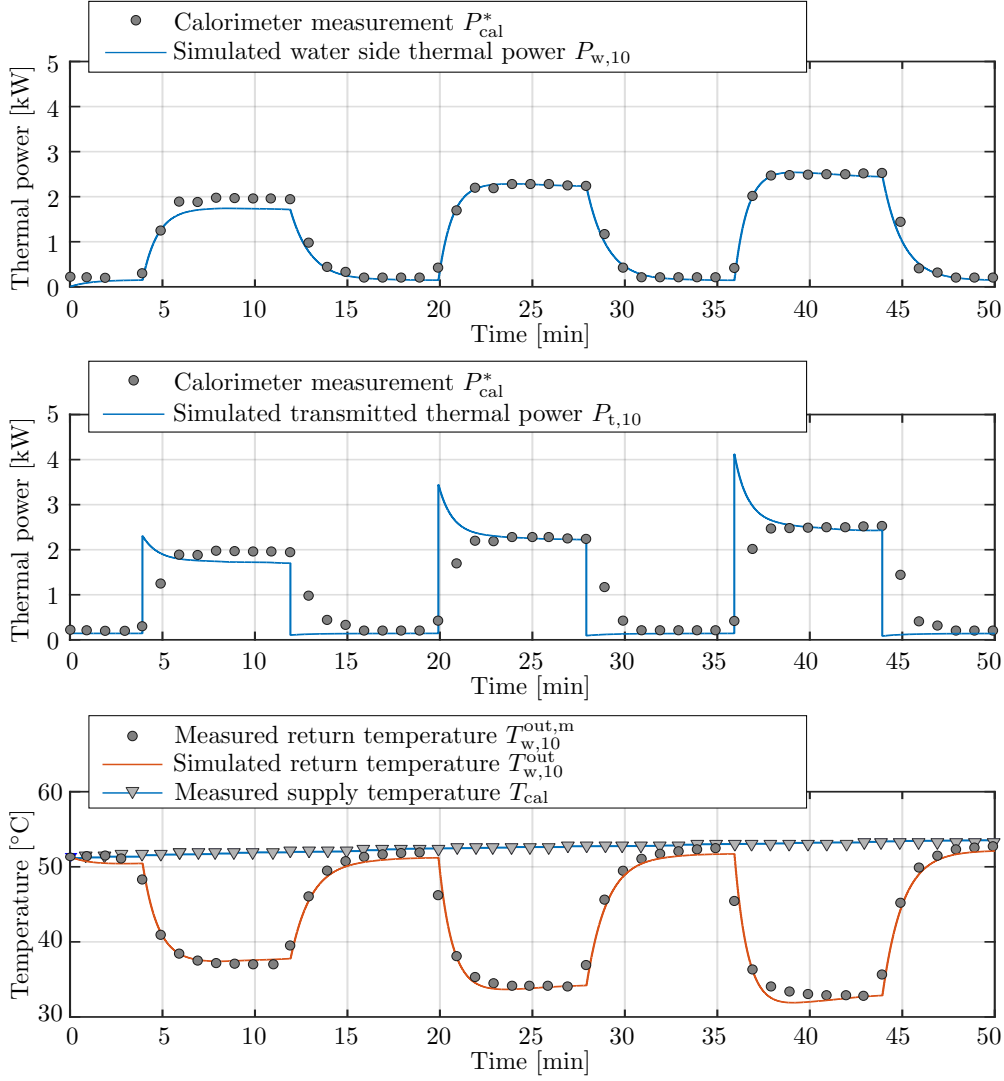


Figure 2.15. Identified FCU model (FCU $i=10$) response over the verification data set.

The estimated functional dependence $U_o(x_{fc}, q_w)$ for three non-zero fan speeds of Trane FCC06 is shown in Fig. 2.16. In Fig. 2.17, normalized root mean squared error (NRMSE) of model return temperature response compared with minutely sampled measurements is given. The NRMSE is calculated as:

$$\text{NRMSE} = \frac{1}{\bar{T}_{w,i}^{out,m}} \sqrt{\frac{\sum_{k=1}^{M_i} (T_{w,i}^{out,m}(k) - T_{w,i}^{out}(k))^2}{M_i}}, \quad (2.35)$$

where $\bar{T}_{w,i}^{out,m} = \sum_{k=1}^{M_i} T_{w,i}^{out,m}(k) / M_i$ is the mean value of return medium temperature taken over considered data samples for a particular i^{th} FCU, M_i is overall number of samples collected during the experiment on the particular FCU and k denotes the measurement sample.

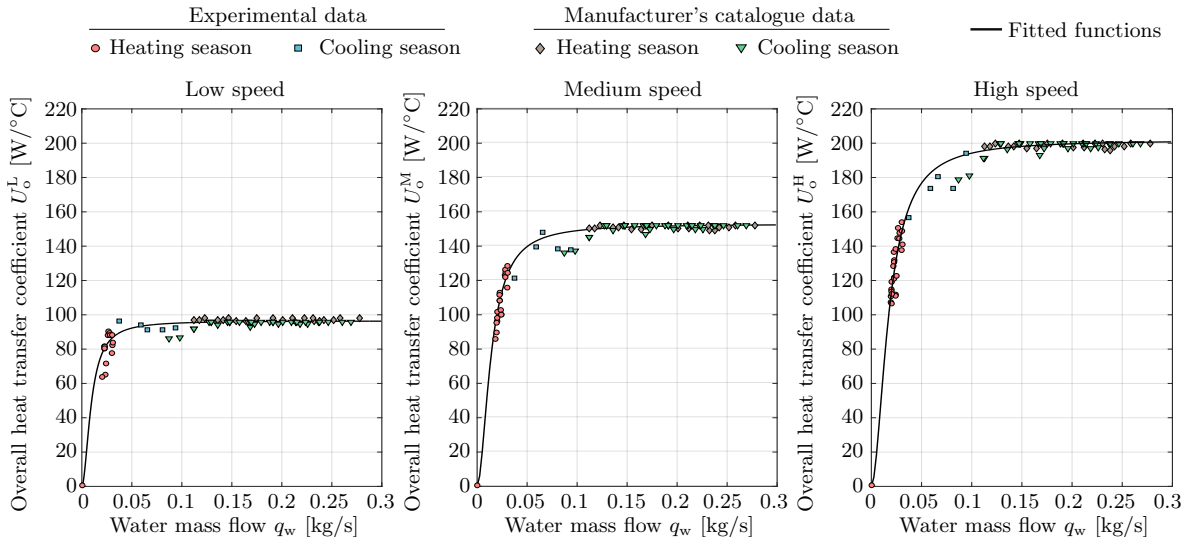


Figure 2.16. Identified heat transfer coefficient function for low, medium and high fan speed of Trane FCC06.

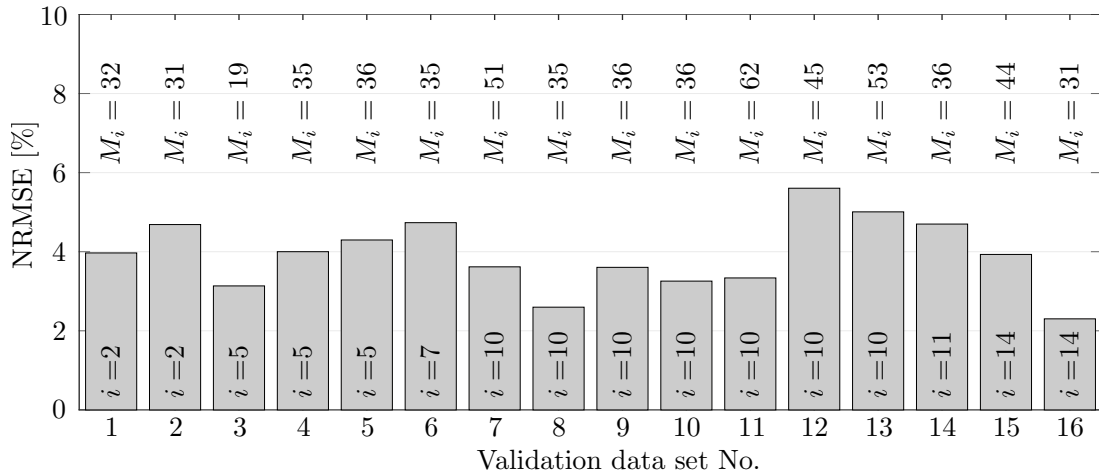


Figure 2.17. NRMSE of the identified model return medium temperature response compared to the measurements for FCU $i = \{2, 5, 7, 10, 11, 14\}$.

Electrical energy consumption model

The FCU's fan powers in certain fan speed P_{el}^L , P_{el}^M and P_{el}^H are defined based on the manufacturer's catalogue data (Tab. 2.7).

Table 2.7. FCU's fan power for different fan speeds at pressure difference 0 Pa.

FCU type	Fan power [W]		
	P_{el}^L	P_{el}^M	P_{el}^H
FCC04	54	56	66
FCC06	53	66	82

Mathematical modelling and identification of building temperature dynamics

Buildings are complex nonlinear dynamic systems with uncertain and time-varying dynamics. The practical experience has shown that acquiring the Model Predictive Control (MPC) essence – the model – is the most time-consuming and costly part of the corresponding design and on-site implementation process that generates around 70% of the engineering costs [21, 73]. Despite clear benefits of MPC, its wide-scale deployment is still hindered due to the lack of replicable, low-cost procedures for obtaining suitable mathematical models able to predict the building behaviour sufficiently accurate for several hours ahead.

Building models based on fundamental physical laws, usually used in building simulation tools such as IDA - Indoor Climate and Energy (IDA-ICE) [25], EnergyPlus [26] and Transient System Simulation Program (TRNSYS) [27], accurately describe the relevant building dynamics. Those tools use detailed descriptions of thermal properties and dimensions of building elements such as walls, floors, ceilings and windows, to generate the dynamic simulation models. With available weather data for the building location, the models accurately calculate heating and cooling loads of the building useful for optimizing the building design, sizing the HVAC equipment or planning the energy efficiency retrofit [74, 75, 76]. However, they are hardly usable for real-time control implementation due to large state and parameters dimensions accompanied by nonlinearities or non-explicit model form. To be applicable for the control system design generally, the model of the process should be simple and yet accurate enough. While nonlinear and higher order models provide better accuracy, they tend to be computationally too intensive for the real-time implementation of the MPC. Therefore, from the control viewpoint, the goal is to get a linear low-order model in a way that the model uncertainty is lowest possible.

Several approaches exist to develop a control-oriented model, including *i*) non-physical data-driven methods such as subspace state-space system identification (4SID) algorithm [31], linear parametric models (e.g. autoregressive moving average with external inputs (ARMAX)) [32, 33, 77] or neural networks, *ii*) physical lumped-parameters methods based on the analogy between thermodynamic processes in buildings and electrical networks, and *iii*) semi-physical methods, where model structure is assumed to be known based on the building physics or some other a priori information while the constituting model parameters with physical meaning have to be estimated.

Non-physical methods do not require any specific knowledge about the system structure but to identify the model a long period of a widely varying operational data for parameters tuning is required. The most usual physically based approach in thermal modelling of buildings is based on a well established linear resistance-capacitance (RC) representation where heat storage is represented by capacitors and heat transmission by resistors. The methodology is based on lumped-parameters approach where each building element (outside wall, window, inside wall, floor, roof, etc.) is represented with a finite number of states [28, 29, 30]. The model parameters are calculated analytically, based on the detailed physical properties of the building elements, such as wall layers, layer's thickness and materials, materials properties, etc., which are often unknown, specially for the older buildings. Since every building element is represented with its analogous RC model, as the number of building elements increases, complexity of the model increases as well. For large buildings, the number of the system states can be over a couple of thousands with many of these states being unmeasurable (e.g. wall temperatures, ceiling temperatures, etc.). To determine those states the online estimation is required. Although the resulting estimation problem is linear, the estimation of a large number of unmeasurable states based on a limited set of measurable variables tends to be unreliable. To cope with the problem in [78, 79, 80] methods for reducing the order of the full-scale RC model are proposed. Authors of [81] proposed simplified model structure where zones are represented with only two states and the parameters are calculated analytically based on the known thermal properties of the building elements. The mismatch between the documented and real thermal properties of the building elements as well as the availability of those data motivated several authors to tune the parameters of the simplified model structures, developed based on the RC analogy, to the available data sets of temperature and energy consumption [21, 82, 37, 31, 73, 83, 84, 85, 86]. These models, combining the benefits of physical modelling and identification methods, are often referred to as grey-box or semi-physical models.

Semi-physical methods incorporate a priori information and physical knowledge directly into the system model, resulting thus with more reproducible results and less bias [34]. The particular benefits of the semi-physical building models are demonstrated in several studies by comparing their performance with the specialised building simulation software [21, 82, 37, 31] or measurements collected in real buildings [73, 83, 84, 85].

Although simulation studies provide a good alternative for identification when the real measurements are not available, such an approach necessitates additional engineering hours for deployment of the simulation models while the developed estimation procedure may not be replicable on the real building due to the mismatch between the documented and realized building construction, limited number of measured variables, noisy sensor observations, unknown heating/cooling elements dynamics and poorly excited building operation data. The algorithms mostly used for identification are Nonlinear Problem (NLP) solving algorithms (e.g. genetic algorithms, gradient methods, etc.) employed to minimize one-step-ahead [33, 87, 88] or multi-steps-ahead predictions [84], maximum likelihood methods [73, 89] and filtering approaches like Extended Kalman Filter (EKF) and Unscented Kalman Filter (UKF). To solve the problem of possibly non-physical behaviour of the identified model, e.g. negative thermal resistances, the developed models are subsequently tested for the oscillatory behaviour or unstable modes [84] or a set of supervisory rules is employed to detect and discard physically meaningless estimates [90].

The rest of the Chapter is organized as follows. First, a short overview of heat transfer processes in buildings is given in Section 3.1 followed by detailed description of thermal RC models and accompanying modelling methodology in Section 3.2. Section 3.3 gives a brief description of building simulation software and models developed within it. The structure of the considered low-order semi-physical zone temperature model is given in Section 3.4. In Section 3.5 an identification framework for simplified low-order building models based on Unscented Kalman filter is developed. Finally, in Section 3.6 the presented methodologies are applied on the case-study building followed with the thorough performance analysis of the developed building simulation models.

3.1 Heat transfer processes in buildings

The heat is transferred from one place to another by three methods:

- conduction in solids, with heat being transferred between substances which are in direct contact with each other,
- convection in fluids or between a fluid and a solid body due to the fluid motion, and
- radiation, where energy is transferred by electromagnetic waves.

Illustration of the heat flows between two adjacent zones separated by a solid wall is shown in Fig. 3.1.

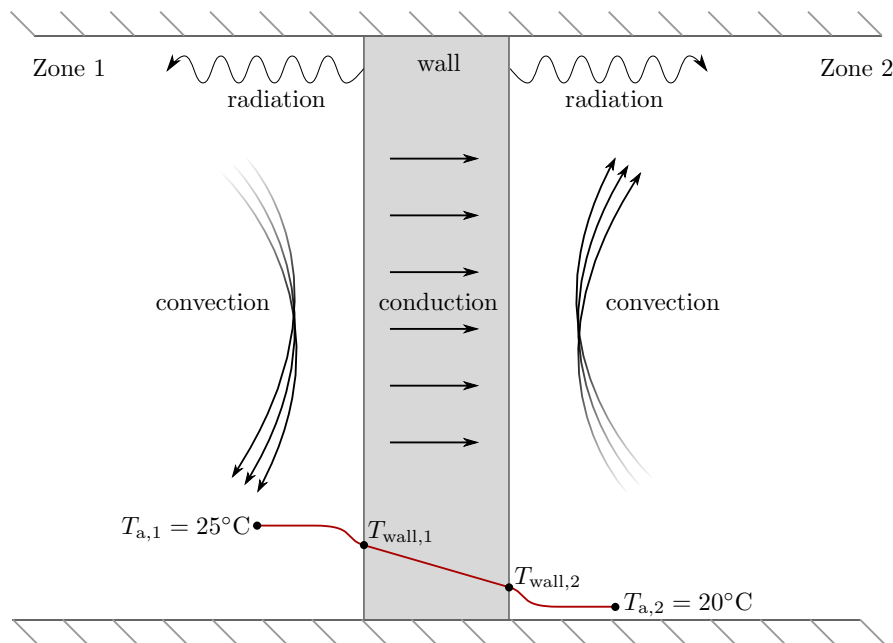


Figure 3.1. An illustration of different modes of heat transfer in a thermal zone.

Heat transfer occurs by: *i*) convection from the warmer air in zone 1 at temperature $T_{a,1}$ to one surface of the wall at temperature $T_{wall,1}$, *ii*) conduction through the wall, *iii*) convection from the other surface of the wall at temperature $T_{wall,2}$ to the colder zone air at temperature $T_{a,2}$ and *iv*) radiation. For any building element (wall, window, door, etc.), a rate of temperature change dT/dt corresponds to the sum of all heat transfer rates affecting the object:

$$C \cdot \frac{dT}{dt} = Q_{\text{cond}} + Q_{\text{conv}} + Q_{\text{rad}}, \quad (3.1)$$

where T is the temperature, t denotes time, $d/(dT)$ denotes a first time derivative, Q_{cond} , Q_{conv} and Q_{rad} are conductive, convective and radiant heat transfer rates, respectively,

and C is thermal capacity of the building element defined as:

$$C = m \cdot c, \quad (3.2)$$

where m is the building element mass and c is its specific heat capacity. The conductive heat transfer rate Q_{cond} through a homogeneous building element is described by one-dimensional form of Fourier's law:

$$Q_{\text{cond}} = -k \cdot A \cdot \frac{dT}{dx}, \quad (3.3)$$

where dT/dx is the temperature gradient in the direction x normal to the area of the building element A and k is thermal conductivity of the element. Under the steady state condition ($dT/dt = 0$) the temperature distribution in wall is linear, and the temperature gradient can be considered as:

$$\frac{dT}{dx} = \frac{(T_2 - T_1)}{L}, \quad (3.4)$$

where T_1 and T_2 are temperatures of element surfaces and L is the thickness of the element. From (3.3) and (3.4) it follows:

$$Q_{\text{cond}} = \frac{(T_1 - T_2)}{R_{\text{cond}}}, \quad (3.5)$$

where R_{cond} is conductive thermal resistance defined as:

$$R_{\text{cond}} = \frac{L}{k \cdot A}. \quad (3.6)$$

For a convective heat transfer process the rate of heat being transferred Q_{conv} is defined as:

$$Q_{\text{conv}} = \frac{(T_{\text{sur}} - T_{\text{a}})}{R_{\text{conv}}}, \quad (3.7)$$

where T_{sur} is the temperature of the considered solid body surface, T_{a} is the temperature of the surrounding air and R_{conv} is the convective thermal resistance defined as:

$$R_{\text{conv}} = \frac{1}{h \cdot A}, \quad (3.8)$$

with h being convective heat transfer coefficient. Any body at any temperature above absolute zero will radiate to some extent, the intensity and frequency distribution of the radiation depend on the detailed structure of the body. The radiant heat transfer rate Q_{rad} is defined as:

$$Q_{\text{rad}} = \sigma \cdot \varepsilon \cdot A \left((T_{\text{sur}} + 273.15)^4 - (T_{\text{a}} + 273.15)^4 \right), \quad (3.9)$$

where σ is the Stefan-Boltzmann constant and ε is the emissivity of the surface. Similarly

to conductive and convective heat transfers, radiant heat transfer rate is described as:

$$Q_{\text{rad}} = \frac{(T_{\text{sur}} - T_{\text{a}})}{R_{\text{rad}}}, \quad (3.10)$$

where R_{rad} is thermal resistance to radiant heat transfer defined as:

$$R_{\text{rad}} = \frac{(T_{\text{sur}} - T_{\text{a}})}{\sigma \cdot \varepsilon \cdot A ((T_{\text{sur}} + 273.15)^4 - (T_{\text{a}} + 273.15)^4)}. \quad (3.11)$$

3.2 Thermal Resistance-Capacitance models

Thermal RC models are established as simple, computationally efficient and accurate enough models. The methodology, based on the analogy between the thermodynamic processes and electrical networks, uses the resistance and capacitance elements to model thermodynamic processes in buildings. To represent a thermal circuit using an equivalent RC network the temperature of an element is viewed as the electrical voltage, heat flow is analogous to the electrical current, the thermal resistance of a building element is represented by an electrical resistance and the heat capacitance, i.e. the thermal mass of the building element, is represented by a capacitance (Tab. 3.1).

Table 3.1. *The analogy between thermodynamics processes in buildings and electrical networks.*

Electrical circuit	Thermal process
Voltage	Temperature
Current	Heat flow
Electrical resistance	Heat resistance
Electrical capacity	Heat capacity

The basic strategy of this methodology is to represent building elements (or complete zones) with a finite number of electrical network elements. This way, building elements are treated as if they were concentrated (lumped) into nodes (points) with uniform temperature. By doing so, instead of using partial differential equations, heat conduction is described by using ordinary differential equations the order of which is equal to the number of dynamic electrical network elements (capacitances) used to describe the building elements [91, 28, 79, 92, 93]. To derive differential equations from the electrical circuit diagram, electrical circuit analysis techniques, such as Kirchhoff's current and voltage laws, are applied. The resulting model is linear and time-invariant, with nodes temperatures as system states. Due to a very low range of building operation temperatures, radiant heat transfer between the building elements is not considered [94].

3.2.1 The Resistance-Capacitance model of a single zone

For a multilayer building element, with n_l overall material layers, heat capacity C is defined as:

$$C = A \sum_{i=1}^{n_l} L_i \cdot \rho_i \cdot c_{l,i}, \quad (3.12)$$

where L_i is thickness, ρ_i is the density and $c_{l,i}$ is the specific heat capacity of i^{th} layer material. Thermal resistance for conduction in a multilayer building element is

$$R_{\text{cond}} = \sum_{i=1}^{n_l} \frac{L_i}{k_i \cdot A}, \quad (3.13)$$

where k_i is thermal conductivity of the i^{th} layer material.

Zone air

Zone, i.e. air inside a zone is represented with a single capacitance defined as:

$$C_a = \rho_a \cdot V \cdot c_a = m_a \cdot c_a, \quad (3.14)$$

where ρ_a is the air density, V is the volume of the air in the zone, c_a is specific heat capacity of the air and m_a is mass of the air inside the zone.

Solar irradiance

Solar irradiance is absorbed by solid external surfaces or absorbed and transmitted into the zone through external windows. The rate of absorbed solar irradiance depends on the absorptivity a of the wall. Overall radiation absorbed by the external wall $Q_{s,a}$ is defined as:

$$Q_{s,a} = a \cdot A_{\text{wall}} \cdot (I_{\theta}^{\text{dir}} + I_{\theta}^{\text{diff}}), \quad (3.15)$$

where I_{θ}^{diff} and I_{θ}^{dir} are diffuse and direct solar irradiances per unit area incident on the exterior surface of area A_{wall} . The solar incidence angle θ is the angle between direct solar ray and a line normal to the irradiated surface. Typically, only measurements of direct normal I_n^{dir} and diffuse horizontal I_h^{diff} solar irradiance are available. The direct solar irradiance incident on a tilted surface I_{θ}^{dir} , e.g. wall or window, is easily calculated with the known surface azimuth angle, tilt angle, and solar zenith and azimuth angle (see Appendix B).

The main uncertainty in modelling the solar irradiance impact on zone temperature lies in modelling the overall solar heat gain transmitted into the zone and calculation of the areas influenced by this gain. Part of the overall transmitted irradiance is absorbed by the air inside a zone and part by internal zone surfaces (e.g. walls or furniture). A thorough calculation of this effect would determine the position of the Sun at each moment, and,

based on the position of the windows, the fraction of the transmitted solar irradiance that is incident on each surface in the zone. This calculation is not only time-consuming, but also needs a follow-up in which the multiple reflections between the different surfaces are determined. The most common approach for modelling the transmitted solar irradiance uses constant Solar Heat Gain Coefficient (SHGC) and assumes that the entire transmitted irradiance is absorbed by the zone air [94] or the floor surface [79].

Direct solar irradiance comes straight from the Sun and falls on the window surface under specified angle - angle of incidence θ . Therefore it is possible to determine the area that is affected. Herein, it is assumed that part of the transmitted direct solar irradiance, which is not absorbed by the zone air, affects the zone floor. Overall direct solar irradiance transmitted into the zone $Q_{s,t}^{\text{dir}}$ is defined as [95, 96]:

$$Q_{s,t}^{\text{dir}} = \text{SHGC}(\theta) \cdot A_{\text{window}} \cdot I_{\theta}^{\text{dir}}, \quad (3.16)$$

where A_{window} is the area of the window and SHGC is function of a solar incidence angle θ (see. e.g. Fig. 3.2 for $\text{SHGC}(\theta)$ function of the glazing installed on the case-study building described in Appendix A and calculated with Window software [96])

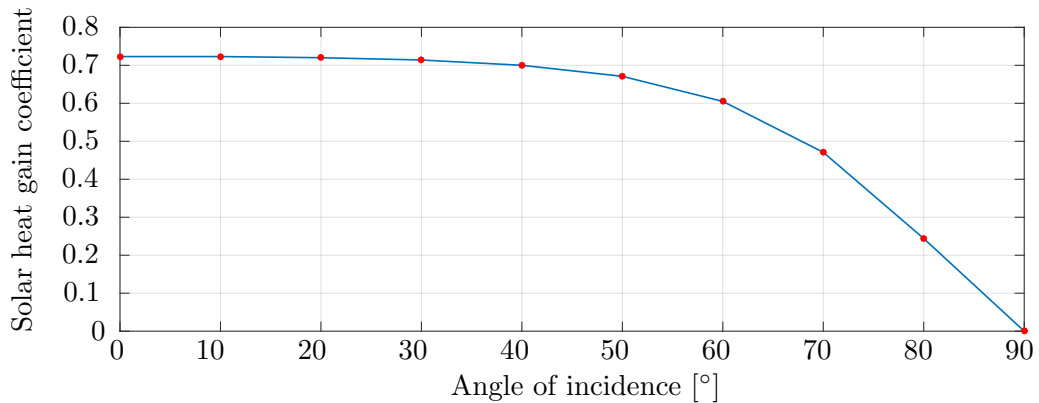


Figure 3.2. The SHGC value as a function of angle of incidence θ .

Diffuse solar irradiance falls on the windows surface under dispersed arrival angles, so it is very difficult to determine the areas which are affected and the amount of irradiance that affects a particular area. Under the assumption of uniformly distributed arrival angles, it can be concluded that the part of the transmitted diffuse irradiance which is not absorbed by the zone air affects all zone surfaces except the surface containing the window [97]. Amount of the irradiance that affects a particular area is a function of the surface area and overall area of the affected surfaces, i.e. transmitted diffuse solar irradiance which is not absorbed by the zone air is uniformly distributed to all affected surfaces. Since the diffuse solar irradiance falls on the window surface at different angles, for calculation of the transmitted diffuse irradiance, the hemispherically averaged solar heat gain coefficient $\overline{\text{SHGC}}$ is used:

$$\overline{\text{SHGC}} = \int_0^{\pi/2} \text{SHGC}(\theta) \cos(\theta) d\theta. \quad (3.17)$$

The transmitted diffuse solar irradiance $Q_{s,t}^{\text{diff}}$ is then defined as:

$$Q_{s,t}^{\text{diff}} = \overline{\text{SHGC}} \cdot A_{\text{window}} \cdot I_{\theta}^{\text{dir}}. \quad (3.18)$$

Overall solar irradiance transmitted into the zone $Q_{s,t}$ through windows is defined as:

$$Q_{s,t} = Q_{s,t}^{\text{diff}} + Q_{s,t}^{\text{dir}}. \quad (3.19)$$

To avoid lengthy calculations and complicated distribution functions it is assumed that there are no reflections between surfaces inside the zone. The final solar irradiance model is nonlinear but significantly improves the accuracy of the model.

Walls and windows

While temperature of the air in the zone is typically represented with a single state (3.14), the number of the states used to describe a wall typically differs from number of states equal to number of different material layers inside the wall to a single state. Intuitively, for modelling the external walls at least two capacitances are necessary - one representing temperature of the outer surface of the wall and one representing temperature of the inner surface of the wall. Representing the external walls with a single capacitance was subject of many studies. The studies showed significant deviations from real measurements, especially in the case of high thermal capacity buildings [97]. An analogous RC network model of an external wall, represented with two capacitances, is given in Fig. 3.3. The model has four nodes with potentials T_{out} , $T_{\text{wall}}^{\text{out}}$, $T_{\text{wall}}^{\text{in}}$ and T_{a} corresponding to outside air, the external surface of the wall, internal surface of the wall and air in the zone, respectively. The capacities representing temperature of external and internal wall surface are defined as:

$$C_{\text{wall}}^{\text{out}} = C_{\text{wall}}^{\text{in}} = 0.5 \cdot C, \quad (3.20)$$

where C is defined as in (3.12). The conductive heat resistances R_{wall} and R_{window} are defined as in (3.13). The thermal resistance for convection on the internal and external surfaces of the wall (3.8) are denoted as,

$$R_{\text{wall}}^{\text{in}} = \frac{1}{h^{\text{in}} \cdot A}, \quad R_{\text{wall}}^{\text{out}} = \frac{1}{h^{\text{out}} \cdot A}, \quad (3.21)$$

where h^{in} and h^{out} are internal and external convective heat transfer coefficients, respectively. Typical values of the convective heat transfer coefficients are $h^{\text{in}} = 3 \text{ W}/(\text{m}^2\text{K})$ for the internal and $h^{\text{out}} = 18 \text{ W}/(\text{m}^2\text{K})$ for the external coefficient. Due to the significantly lower heat capacity than the wall, windows are represented with resistors only.

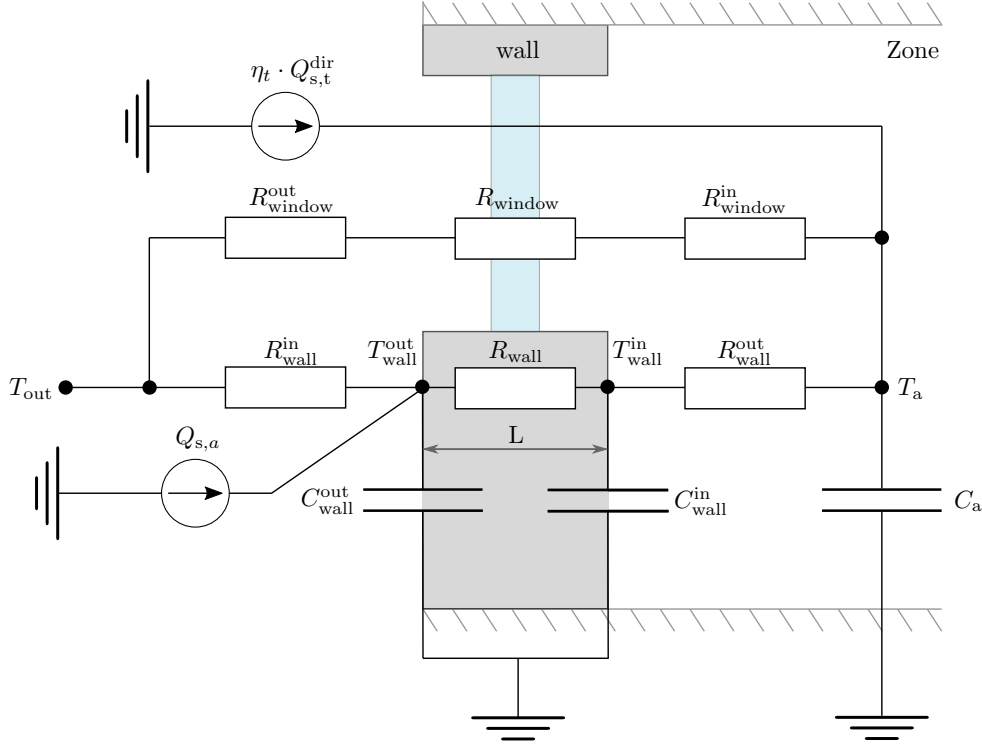


Figure 3.3. An analogous RC network model of an external wall with a window.

Energy balance for two wall nodes results in a set of first order differential equations

$$C_{\text{wall}}^{\text{out}} \frac{dT_{\text{wall}}^{\text{out}}}{dt} = \frac{(T_{\text{out}} - T_{\text{wall}}^{\text{out}})}{R_{\text{wall}}^{\text{out}}} + \frac{(T_{\text{wall}}^{\text{in}} - T_{\text{wall}}^{\text{out}})}{R_{\text{wall}}} + Q_{s,a}, \quad (3.22)$$

$$C_{\text{wall}}^{\text{in}} \frac{dT_{\text{wall}}^{\text{in}}}{dt} = \frac{(T_{\text{wall}}^{\text{out}} - T_{\text{wall}}^{\text{in}})}{R_{\text{wall}}} + \frac{(T_{\text{zone}} - T_{\text{wall}}^{\text{in}})}{R_{\text{wall}}^{\text{in}}}, \quad (3.23)$$

with energy balance of the zone air node defined as:

$$C_{\text{zone}} \frac{dT_{\text{zone}}}{dt} = \frac{(T_{\text{wall}}^{\text{in}} - T_{\text{zone}})}{R_{\text{wall}}^{\text{in}}} + \frac{(T_{\text{out}} - T_{\text{zone}})}{R_{\text{window}}^{\text{out}} + R_{\text{window}} + R_{\text{window}}^{\text{in}}} + \eta_t \cdot Q_{s,t}, \quad (3.24)$$

where η_t is the share of the transmitted solar irradiance absorbed by the zone air.

Due to the smaller temperature difference between the wall surfaces and lower thermal capacity than external walls, internal walls are typically represented with a single state such that the temperature of a wall across its volume is assumed to be equal to its centerline temperature. An analogous RC model of an internal wall is shown in Fig. 3.4. It is assumed only Zone 1 has external windows and the share of the transmitted diffuse solar irradiance absorbed by the internal wall is denoted with η_d . Energy balance for the node representing the internal wall results in the following first order differential equation:

$$C_{\text{wall}} \frac{dT_{\text{wall}}}{dt} = \frac{(T_{\text{zone1}} - T_{\text{wall}})}{0.5 \cdot R_{\text{wall}}} + \frac{(T_{\text{zone2}} - T_{\text{wall}})}{0.5 \cdot R_{\text{wall}}} + \eta_d \cdot Q_{s,t}^{\text{diff}}, \quad (3.25)$$

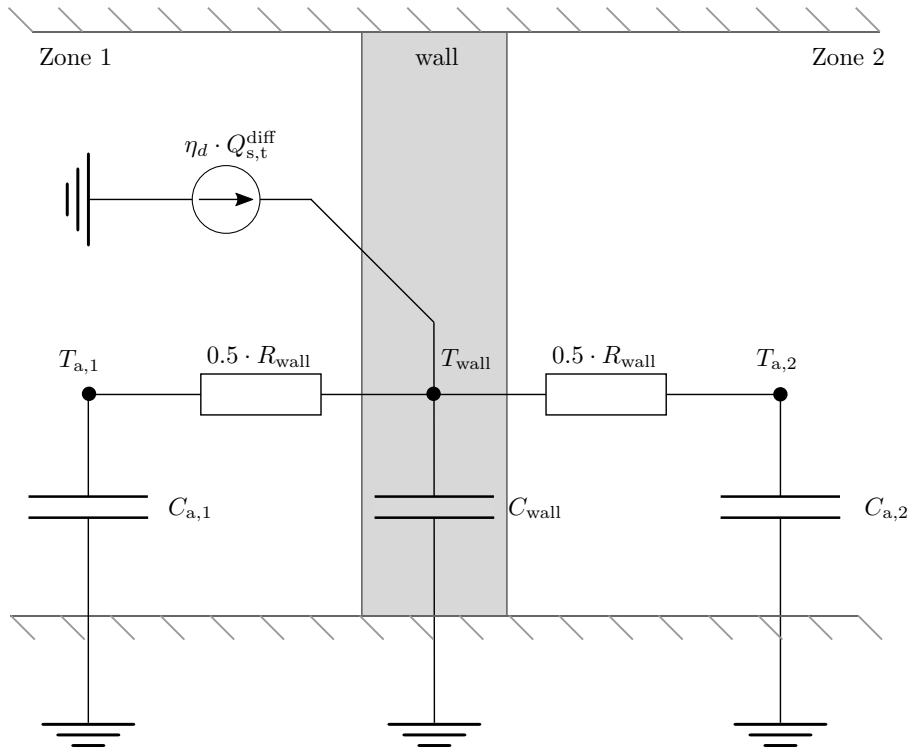


Figure 3.4. An analogous RC network model of an internal wall.

where R_{wall} is defined as a sum of conductive thermal resistance (3.13) and convective thermal resistances (3.8) for both surfaces of the wall

$$R_{\text{wall}} = \frac{1}{h^{\text{in}} \cdot A_{\text{wall}}} + R_{\text{cond}} + \frac{1}{h^{\text{in}} \cdot A_{\text{wall}}}, \quad (3.26)$$

A_{wall} is the area of the wall surfaces and C_{wall} is calculated according to (3.12).

Building zones

Figure 3.5 shows an analogous RC network model for the typical building zone with two external and two internal walls, one window and heating/cooling element heat transfer rate denoted with $P_{a,1}$ (e.g. heat transfer rate from fan coil unit, radiator, etc.). The temperature in the zone above of the exemplary Zone 1 is denoted as $T_{a,5}$ and temperature in the zone below as $T_{a,4}$. Solar irradiance affecting the external wall facing north is denoted with superscript 'N' while the one affecting the external wall oriented towards west is denoted with superscript 'W'. For simplicity, transmitted diffuse solar irradiance is omitted.

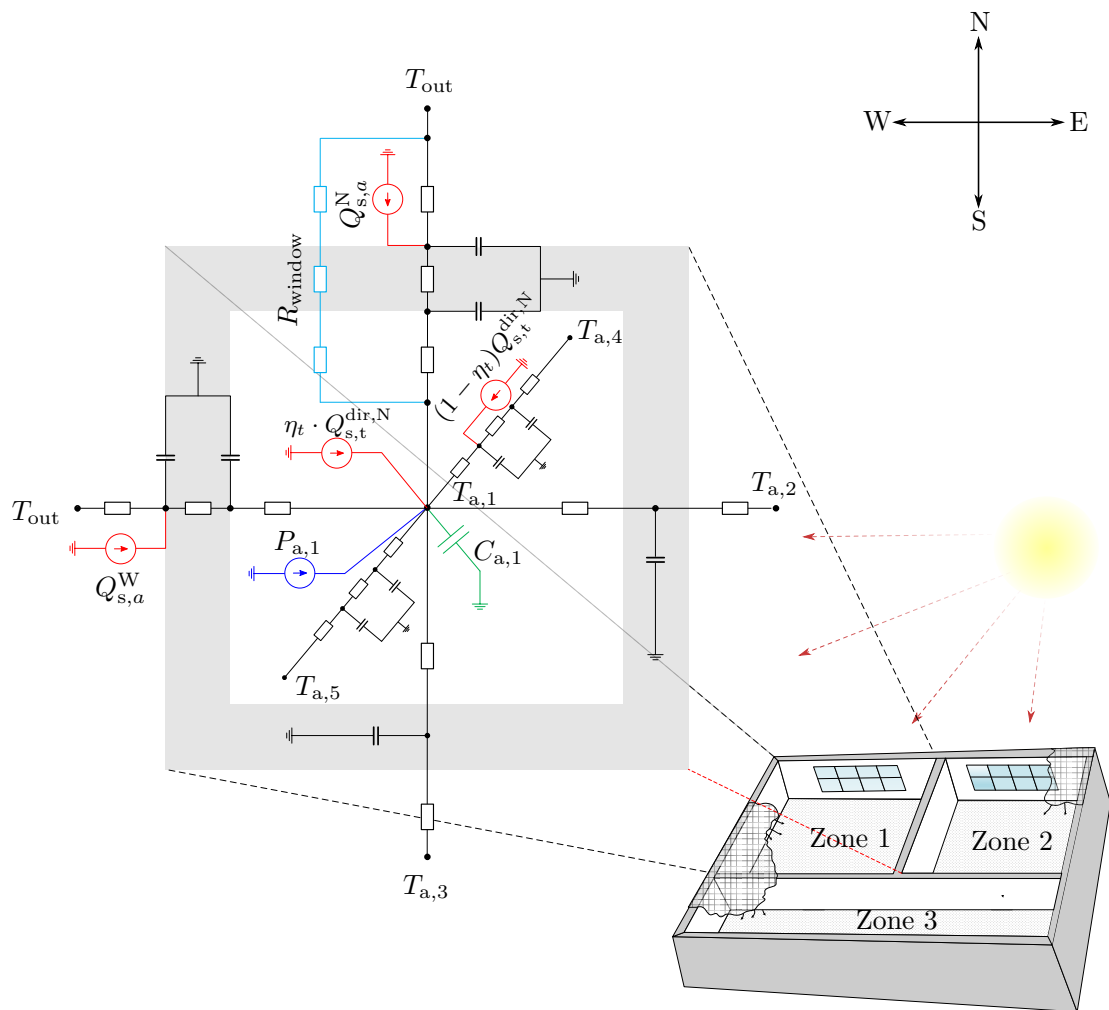


Figure 3.5. An analogous RC network model for the typical zone with two external and two internal walls and one window.

3.2.2 State-space model of a building

For a multi-zone building, the network consist of three types of nodes: wall nodes, zone air nodes and external conditions nodes. There are total m nodes, n_x of which represent zones and wall temperatures and the rest of them representing external and boundary conditions. To keep the building model linear, nonlinear calculations of solar irradiation effects are separated from the model into two types of preprocessing procedures (Fig. 3.6). The first procedure calculates solar incidence angle θ and direct and diffuse solar irradiances incident on the external building surface, I_{θ}^{dir} and I_{θ}^{diff} , respectively, based on the known solar zenith angle θ_z , solar azimuth angle ϕ_s , surface azimuth angles ϕ , direct normal I_n^{dir} and diffuse horizontal solar irradiance I_h^{diff} . Outputs of the first procedure are used to calculate the overall radiation absorbed by the external wall $Q_{s,a}$ (3.15) and as inputs to the second procedure in which the SHGC of window surfaces is determined and based on it solar irradiances transmitted through the windows into the zones are calculated. The number of required preprocessing procedures calls can be significantly reduced by grouping the external walls and windows by surface azimuth angles and window types.

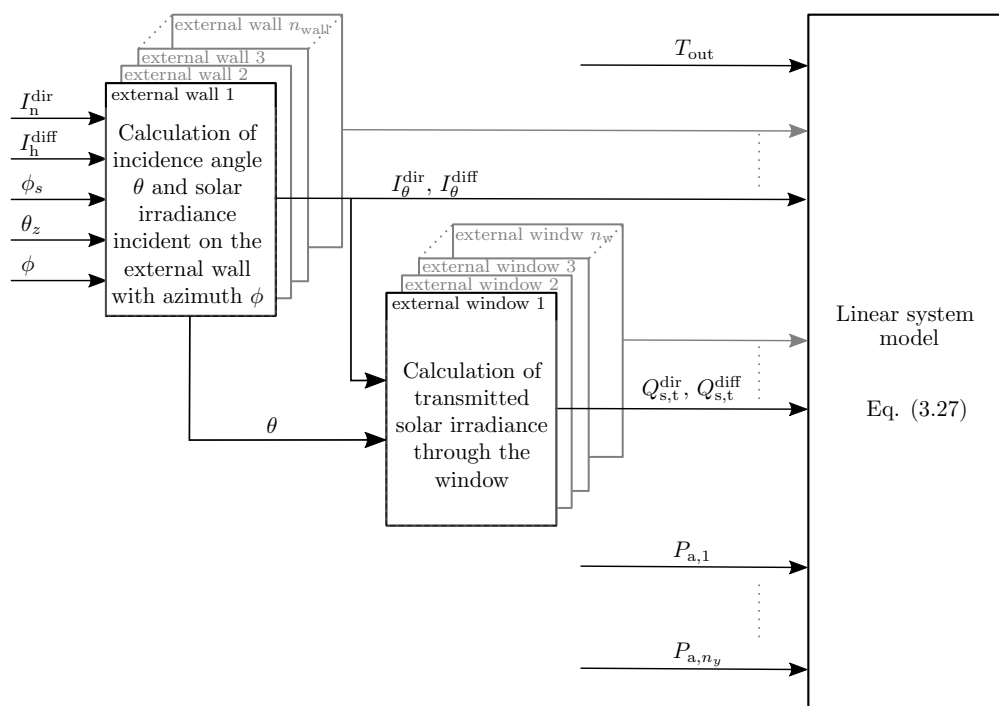


Figure 3.6. Preprocessing of nonlinear solar irradiance effects.

Since the calculation of the absorbed radiation is linear function of the solar irradiances incident on the external building surface, instead of having additional procedure for its calculation (3.15) it is integrated into the linear system model such that solar irradiances incident on the external building surfaces are treated as inputs into the linear system model. If the energy balance equations (3.22)-(3.25) are written for every building element,

the obtained first order differential equations can be put in the following state-space form:

$$\dot{x}(t) = A \cdot x(t) + B \cdot u(t), \quad (3.27)$$

where $x(t) \in \mathbb{R}^{n_x}$ is the state vector containing the temperatures of all wall and zone air nodes in the building, the dot denotes time derivation ($\dot{x} = dx/dt$), and $u(t) \in \mathbb{R}^{n_u}$ is the input vector consisting of external weather conditions, pre-calculated solar irradiances and heating/cooling elements thermal powers P_a . Matrix $A \in \mathbb{R}^{n_x \times n_x}$ is the system matrix and $B \in \mathbb{R}^{n_x \times n_u}$ is the accompanying system input matrix. System output $y(t) \in \mathbb{R}^{n_y}$ comprises available temperature measurements, typically only the zone air temperatures:

$$y(t) = C \cdot x(t). \quad (3.28)$$

3.3 Building simulation software models

Building simulation software has been recognized as an important decision support tool in many sectors, most notably the architecture, engineering and construction. Major use of the building simulation software includes:

- architectural design: comparing different designs quantitatively in order to assure optimal energy-efficient design,
- HVAC equipment sizing: avoiding oversizing by sizing the HVAC equipment with respect to the simulated building thermal loads,
- building performance rating: demonstrating the compliance of the building with energy certificates,
- building retrofitting: assessing the possible energy savings by testing the building performance under different building operation conditions.

With the use of the advanced model-based algorithm in buildings that is recognized as a promising solution for achieving significant energy savings, building simulation software is intensively used *i*) for verification of advanced control algorithms and *ii*) as a source of data for identification of simplified building simulation models [21, 82, 37, 31]. The accuracy of the building simulation software is highly determined by the input data. The data necessary for development of building simulation model within specialised building simulation software are:

- geometry of the building: typically, in form of AutoCAD building drawings,
- location information: location and orientation of the building, shading by the surrounding buildings,
- building physics: materials and construction, windows and shading, thermal bridges, infiltration, etc.
- climate data: ambient air temperature, relative humidity, direct and diffuse solar irradiance, wind speed and direction,
- interior building loads: occupancy, lighting, electric equipment,
- operation strategies and schedules.

Among the most commonly used simulation software tools are Energy Plus [26], IDA-Indoor Climate and Energy (IDA-ICE) [25] and Transient System Simulation Program (Trnsys) [27]. Depending on the primary use of the software different tools have unique benefits and drawbacks for different conditions. Within the thesis, two simulation tools are tested, Trnsys and IDA-ICE. IDA-ICE is a whole-year detailed and dynamic multi-zone simulation software developed by EQUA Simulation AB [25]. The program is validated with ASHRAE 140-2004 [98] and EN 15255-2007, 15265-2007 [99], showing

that IDA-ICE can give accurate calculations of buildings' energy and indoor climate performances in comparison to measured data or other state-of-the art simulation programs. Trnsys is a transient system simulation software tool with a modular structure that is designed to develop an energy system with a wide range from simple to complex systems [27].

3.4 Low-order semi-physical building model

The building zone temperature behaviour is well captured with two thermal masses: one with smaller thermal capacity related to the air temperature inside a zone referred to as temperature fast dynamics and one with larger thermal capacity related to the solid zone parts like walls and furniture referred to as temperature slow dynamics [83]:

$$\begin{aligned} C_1 \dot{T}_a &= \sum_{j \in \mathcal{V}} \frac{(T_a^j - T_a)}{R_j} + \frac{(T_{\text{out}} - T_a)}{R_{\text{out}}} + \frac{(T_z - T_a)}{R} + p_t^{\text{dir}} I_\theta^{\text{dir}} + p_t^{\text{diff}} I_\theta^{\text{diff}} + P_a, \\ C_2 \dot{T}_z &= \frac{(T_a - T_z)}{R}, \end{aligned} \quad (3.29)$$

where T_a and T_z are the temperatures of lumped smaller and larger thermal masses capacities C_1 and C_2 , respectively. The dot denotes time derivation ($\dot{T} = dT/dt$). Outside air temperature and corresponding thermal resistance between outside and the zone are denoted with T_{out} and R_{out} , respectively. Resistance R_j models the thermal resistances between the adjacent zones where \mathcal{V} is a set of all zones adjacent to the considered zone and j^{th} adjacent zone temperature is denoted as T_a^j . The parameter P_a is a thermal load affecting the zone, I_θ^{diff} and I_θ^{dir} are diffuse and direct solar irradiances per unit area incident on the exterior zone surface, affecting the zone through the corresponding solar transmittance parameters p_t^{diff} and p_t^{dir} . In order to avoid multiplication of the unknown system capacities and thermal resistances, model (3.29) is reformulated to

$$\begin{bmatrix} \dot{T}_a \\ \dot{T}_z \end{bmatrix} = \begin{bmatrix} -(p_1 + p_3 + p_7) & p_1 \\ p_2 & -p_2 \end{bmatrix} \begin{bmatrix} T_a \\ T_z \end{bmatrix} + \begin{bmatrix} p_3 & p_4 & p_5 & p_6 & p_7 \\ 0 & 0 & 0 & 0 & 0 \end{bmatrix} u. \quad (3.30)$$

The unknown system parameters form the parameter vector

$$\Theta = \begin{bmatrix} p_1 & \cdots & p_7 \end{bmatrix}^\top, \quad (3.31)$$

while input vector is defined as

$$u = \begin{bmatrix} T_{\text{out}} & I_\theta^{\text{diff}} & I_\theta^{\text{dir}} & P_a & T_a^{\text{adj}} \end{bmatrix}^\top. \quad (3.32)$$

System capacities and thermal resistances can easily be recalculated through algebraic relations from Θ . For simplicity of notation it is assumed that the zone has just one adjacent zone denoted with T_a^{adj} . The unknown parameters vector Θ is to be determined analytically based on the available data on building physics [81] or through identification [21, 82, 37, 31, 73, 83, 84, 85, 86].

3.5 Identification framework for simplified low-order building models based on Unscented Kalman filter

Unscented Kalman Filter (UKF) is a well-known technique for estimation of states and parameters of a dynamic system mathematical model [100]. Many different variations of the original UKF were derived in order to improve its numerical stability or to adjust the filter to special model forms [101, 102, 103]. The fundamental part of UKF is Unscented Transformation (UT) which uses a minimal set of appropriately chosen weighted points (so-called sigma points) to capture the mean and covariance of a random vector that undergoes a nonlinear mapping. It is shown that UT can capture this posterior mean and covariance correctly up to the fourth term in the corresponding Taylor series [100]. In practice, almost all physical parameters and states are limited in some sense. One of the first nonlinear estimation algorithms developed to efficiently handle constraints is Moving Horizon Estimator (MHE) [104]. MHE formulates the estimation problem as a nonrecursive constrained Quadratic Program (QP). Solving the constrained QP at each step makes this algorithm computationally expensive and difficult to use in different real-time applications. For time-critical applications a special form of MHE with unitary moving horizon is derived, which resulted in constrained Extended Kalman Filter (EKF) [105] as a less computationally demanding derivative of the general MHE.

General idea on how to modify the original UKF to account for constraints on states and parameters subject to estimation was first presented by authors of the original UKF in [106] through introduction of the scaled UT. First intuitive attempts to incorporate inequality constraints into the UKF approach were based on a simple clipping approach, i.e setting all sigma points outside the allowed set to the boundaries [37, 107, 108]. The constrained sigma points are not necessary symmetric, therefore in [109, 110, 111] the weights associated with them are modified. Alternative approach, presented in [107], handles the constraints by solving a Nonlinear Problem (NLP) in the correction step. An overview of the possible ways to handle the constraints within filtering estimation algorithms is given in [112, 113, 110]. The UKF has been largely adopted in specific fields complementary to energy-efficient buildings [114, 42, 115]. However, the research related to application of UKF for estimation of control-oriented building models is mostly limited to the application on simulation data [82, 37] as there are only few studies with the experimental results [85, 116]. In [85], an UKF approach is validated by using short-term (10 h) measurement data from a real building affected by the outside temperature and adjacent zones temperatures. A 13-days sequence of minute-sampled data is validated in [116]. While UKF has shown good tracking properties, some parameters of the assumed semi-physical model structure adopted negative values whilst this is not physically possible and may result in unwanted behaviour when the model is utilized for prediction.

The reasons for UKF being rarely used for identification of thermal building models lie in practical issues of *i*) dealing with non-physical model parameters, *ii*) handling the problem of non-informative system excitation (e.g. solar irradiance at night) *iii*) limited number of installed sensors (available measurements), *iv*) filter sampling time selection issues and *v*) accounting for dynamics of the heating/cooling elements installed in the building.

3.5.1 Standard Unscented Kalman filter

Consider the nonlinear system represented with the following standard discrete-time equations:

$$\begin{aligned}x_k &= f(x_{k-1}, u_{k-1}) + w_{k-1}, \\y_k &= h(x_k) + v_k,\end{aligned}\tag{3.33}$$

where $x_k \in \mathbb{R}^{n_x}$ is the system state, $w_k = \mathcal{N}(0, Q_k) \in \mathbb{R}^{n_w}$ the process noise, $v_k = \mathcal{N}(0, R_k) \in \mathbb{R}^{n_v}$ observation noise, u_k the system input vector and y_k the noisy observation of the system. Gaussian random variable distribution with the corresponding mean and variance (square of standard deviation) is denoted with $\mathcal{N}(\cdot, \cdot)$. The nonlinear functions $f(\cdot)$ and $h(\cdot)$ are not necessarily differentiable. For the identification of a continuous-time system $f(\cdot)$ results from integration of the continuous-time model function over the interval of one filter sampling time. For system and measurement noises considered as additive, the original UKF algorithm is described in Algorithm 1 [106]. Parameter γ is a scaling parameter defined as:

$$\gamma = \sqrt{n_x + \lambda}, \quad \lambda = \alpha^2(n_x + \kappa) - n_x,\tag{3.34}$$

where n_x is the number of system states while α , κ and β are tuning parameters. To guarantee the semi-definiteness of the covariance matrix it must be $\kappa + n_x \neq 0$ [102]. A good default choice is $\kappa = 0$, $\beta = 2$ [106]. The parameter α defines the spread of the sigma points around the current estimate and is usually set to a small positive value $10^{-4} \leq \alpha \leq 1$. Parameter β is a parameter used to incorporate the prior knowledge of the distribution of x_k . For a Gaussian prior the optimal choice is $\beta = 2$ [106].

Algorithm 1 Standard UKF algorithm**Initialization** at $k = 0$:

$$\hat{x}_0 = E[x_0], \quad (3.35)$$

$$P_{x_0} = E[(x_0 - \hat{x}_0)(x_0 - \hat{x}_0)^\top]. \quad (3.36)$$

For $k = 1, 2, 3, \dots$ **Time update**Calculate sigma points $\chi_{k-1,i}$:

$$\chi_{k-1,i} \triangleq \begin{cases} \hat{x}_{k-1} & i = 0, \\ \hat{x}_{k-1} + \gamma \sqrt{P_{x_{k-1}}} & i = 1, \dots, n_x, \\ \hat{x}_{k-1} - \gamma \sqrt{P_{x_{k-1}}} & i = n_x + 1, \dots, 2n_x. \end{cases} \quad (3.37)$$

Transform the sigma points through the state-update nonlinear function:

$$\chi_{k|k-1,i}^x = f(\chi_{k-1,i}, u_{k-1}), \quad i = 0, 1, \dots, 2n_x. \quad (3.38)$$

Calculate the a priori state estimate \hat{x}_k^- and a priori covariance $P_{x_k}^-$:

$$\hat{x}_k^- = \sum_{i=0}^{2n_x} W_i^{(m)} \chi_{k|k-1,i}^x, \quad (3.39)$$

$$P_{x_k}^- = \sum_{i=0}^{2n_x} W_i^{(c)} (\chi_{k-1,i}^x - \hat{x}_k^-)(\chi_{k-1,i}^x - \hat{x}_k^-)^\top + Q_k. \quad (3.40)$$

The weights $W_i^{(m)}$ and $W_i^{(c)}$ are defined as:

$$W_i^{(m)} \triangleq \begin{cases} \frac{\lambda}{(n_x + \lambda)} & i = 0, \\ \frac{1}{2(n_x + \lambda)} & i = 1, \dots, 2n_x, \end{cases} \quad (3.41)$$

$$W_i^{(c)} \triangleq \begin{cases} \frac{\lambda}{(n_x + \lambda)} + (1 - \alpha^2 + \beta) & i = 0, \\ \frac{1}{2(n_x + \lambda)} & i = 1, \dots, 2n_x. \end{cases} \quad (3.42)$$

Transform the sigma points through the measurement update function $h(\cdot)$:

$$Y_{k|k-1,i} = h(\chi_{k|k-1,i}^x), \quad i = 0, 1, \dots, 2n_x, \quad (3.43)$$

and calculate the mean \hat{y}_k^- and covariance of the measurement $P_{\hat{y}_k}$:

$$\hat{y}_k^- = \sum_{i=0}^{2n_x} W_i^{(m)} Y_{k|k-1,i}, \quad (3.44)$$

$$P_{\hat{y}_k} = \sum_{i=0}^{2n_x} W_i^{(c)} (Y_{k|k-1,i} - \hat{y}_k^-)(Y_{k|k-1,i} - \hat{y}_k^-)^\top + R_k, \quad (3.45)$$

where R_k is the measurement noise covariance matrix.

The cross covariance $P_{x_k y_k}$ is defined as:

$$P_{x_k y_k} = \sum_{i=0}^{2n_x} W_i^{(c)} (\chi_{k-1,i}^x - \hat{x}_k^-) (Y_{k|k-1,i} - \hat{y}_k^-)^\top. \quad (3.46)$$

Kalman gain K_k is computed as:

$$K_k = P_{x_k y_k} P_{\hat{y}_k}^{-1}. \quad (3.47)$$

Finally, UKF estimate \hat{x}_k and its covariance P_{x_k} are computed from the standard Kalman update equations:

$$P_{x_k} = P_{x_k}^- - K_k P_{\hat{y}_k} K_k^\top. \quad (3.48)$$

Measurement update

$$\hat{x}_k = \hat{x}_k^- + K_k (y_k - \hat{y}_k^-). \quad (3.49)$$

3.5.2 Constrained Unscented Kalman filter with improved weight selection scheme

The weighted sigma point set (3.37) has the same sample mean, covariance and all higher odd-ordered central moments as original distribution $\mathcal{N}(\hat{x}_{k-1}, P_{x_{k-1}})$:

$$\hat{x}_{k-1} = \sum_{i=0}^{2n_x} W_i^{(m)} \chi_{k-1,i}, \quad (3.50)$$

$$P_{x_{k-1}} = \sum_{i=0}^{2n_x} W_i^{(c)} [\chi_{k-1,i} - \hat{x}_{k-1}] [\chi_{k-1,i} - \hat{x}_{k-1}]^\top, \quad (3.51)$$

where $W_i^{(m)} \in \mathbb{R}^1$ and $W_i^{(c)} \in \mathbb{R}^1$ are the weights associated with the i^{th} sigma point. To account for interval constraints, in Interval-Constrained Unscented Transformation (ICUT) [110] original sigma point set (3.37) is modified such that in each filtering step k the original sigma point spread defined by scaling parameter γ is reduced for every sigma-point violating the constraints:

$$\chi'_{k,i} \triangleq \begin{cases} \hat{x}_k & i = 0, \\ \hat{x}_k + \Delta_{k,i} \text{col}_i(S_{x_k}) & i = 1, \dots, 2n_x, \end{cases} \quad (3.52)$$

$$S_{x_k} = \begin{bmatrix} \sqrt{P_{x_k}} & -\sqrt{P_{x_k}} \end{bmatrix}, \quad (3.53)$$

where $\chi'_{k-1,i}$ is constrained sigma point set, $\text{col}_i(\cdot)$ represents the i^{th} column of matrix and modified scaling parameter $\Delta_{k,i}$ is defined as:

$$\Delta_{k,i} \triangleq \min(\text{col}_i(\Upsilon)), \quad (3.54)$$

$$\Upsilon(j, i) \triangleq \begin{cases} \gamma & \text{if } S_{x_k}(j, i) = 0, \\ \min\left(\gamma, \frac{U_k(j) - \hat{x}_k(j)}{S_{x_k}(j, i)}\right) & \text{if } S_{x_k}(j, i) > 0, \\ \min\left(\gamma, \frac{L_k(j) - \hat{x}_k(j)}{S_{x_k}(j, i)}\right) & \text{if } S_{x_k}(j, i) < 0, \end{cases} \quad (3.55)$$

where $i = 1, \dots, 2n_x$, $j = 1, \dots, n_x$, $L_k \in \mathbb{R}^{n_x}$ and $U_k \in \mathbb{R}^{n_x}$ are vectors of lower and upper bounds of system state variable, respectively. If all unconstrained sigma points are within the boundaries, or in absence of bounds, the ICUT (3.52) results in sigma points identical to those in UT (3.37), keeping thus the same order of accuracy as original UT. If unconstrained sigma points violate the constraints, the constrained sigma point set is in general not symmetric, i.e. its weighted mean and covariance may not be in accordance with (3.50) and (3.51). As a results, the properties related to the UT may not be preserved. In spite of this, the ICUT approach has shown to outperform UT in several case studies [110, 111].

To counter-act the asymmetry the corresponding sigma point weights are also modified. The sigma points weights can be positive or negative but, to provide an unbiased estimate, they must obey¹ [100]:

$$\sum_{i=0}^{2n_x} W_i = 1. \quad (3.56)$$

In [109, 110, 111] affine reformulation of original weighting scheme which allows weights to be both positive and negative is proposed (denoted here as ICUT[±]). From (3.51) it is evident that positive semi-definiteness of the covariance matrix can be guaranteed only for strictly positive weights since the quadratic summands are always positive semi-definite [106]. In accordance with that, weighting reformulation in a form of a linear function is proposed:

$$W_i = a_k \cdot \Delta_{k,i}, \quad \forall i = 1, \dots, 2n_x, \quad (3.57)$$

where $a_k > 0$ is a parameter to be determined while $\Delta_{k,i}$ is equal to the original UKF step γ for sigma points within constraints and equal to the linearly reduced original step, in the amount required to keep the constrained sigma points within the limits, for sigma points violating the constraints.

To keep the mean within the limits, at the end of measurement update stage all state components violating the constraints are projected back onto the constraint boundary

¹The parameter $(1 - \alpha^2 + \beta)$ which makes the difference between the $W^{(m)}$ and $W^{(c)}$ is additionally added to the $W_0^{(c)}$ to include the effect of the sigma-points scaling into the weights.

before the start of the next iteration. The mean is thus always within the limits, so the weight W_0 is chosen to be equal as in the original algorithm. From (3.56) and (3.57) it follows:

$$\sum_{i=0}^{2n_x} W_i = W_0 + \sum_{i=1}^{2n_x} W_i = \frac{\lambda}{(n_x + \lambda)} + \sum_{i=1}^{2n_x} a_k \cdot \Delta_{k,i} = 1. \quad (3.58)$$

Therefore:

$$a_k = \frac{n_x}{(n_x + \lambda) \sum_{i=1}^{2n_x} \Delta_{k,i}}. \quad (3.59)$$

So defined weighting scheme guarantees positive weights W_i for $i = 1, \dots, 2n_x$. Just like in the original UKF algorithm, only W_0 may be negative for a specific combination of tuning parameters ($\alpha \neq 1$, $\beta = 2$, $\kappa = 0$). For that case positive definiteness cannot be strictly guaranteed. Due to the strictly positive non-zero weights, the presented algorithm enables easier integration in efficient Square Root implementation of the UKF algorithm [117] (no need of additional modifications as required for ICUT $^\pm$). The detailed modified ICUT algorithm is given in Algorithm 2.

Algorithm 2 Modified ICUT algorithm.

Calculate constrained sigma points set $\chi'_{k,i}$:

$$\chi'_{k,i} \triangleq \begin{cases} \hat{x}_k & i = 0, \\ \hat{x}_k + \Delta_{k,i} \text{col}_i(S_{x_k}) & i = 1, \dots, 2n_x, \end{cases} \quad (3.60)$$

$$S_{x_k} = \begin{bmatrix} \sqrt{P_{x_k}} & -\sqrt{P_{x_k}} \end{bmatrix},$$

where $\text{col}_i(\cdot)$ represents the i^{th} column of matrix and step $\Delta_{k,i}$ is defined as:

$$\Delta_{k,i} \triangleq \min(\text{col}_i(\Upsilon)), \quad (3.61)$$

$$\Upsilon(j, i) \triangleq \begin{cases} \gamma & \text{if } S_{x_k}(j, i) = 0, \\ \min\left(\gamma, \frac{U_k(j) - \hat{x}_k(j)}{S_{x_k}(j, i)}\right) & \text{if } S_{x_k}(j, i) > 0, \\ \min\left(\gamma, \frac{L_k(j) - \hat{x}_k(j)}{S_{x_k}(j, i)}\right) & \text{if } S_{x_k}(j, i) < 0, \end{cases}$$

$$i = 1, \dots, 2n_x, \quad j = 1, \dots, n_x.$$

Adjust weights:

$$W_i^{(c)} = W_i^{(m)} \triangleq \begin{cases} \frac{\lambda}{(n_x + \lambda)} & i = 0, \\ a_k \cdot \Delta_{k,i} & i = 1, \dots, 2n_x, \end{cases} \quad (3.62)$$

$$W_0^{(c)} = W_0^{(c)} + (1 - \alpha^2 + \beta). \quad (3.63)$$

Figure 3.7 illustrates the ICUT on a two-dimensional state variable with

$$L_k = \begin{bmatrix} 0 & -1 \end{bmatrix}^\top, \quad U_k = \begin{bmatrix} 3 & 2 \end{bmatrix}^\top, \quad \hat{x}_k = \begin{bmatrix} 1 & 1 \end{bmatrix}^\top, \quad (3.64)$$

$\alpha = 0.7$, $\beta = 2$, $\kappa = 0$ and $P_{x_k} = 2 \cdot \mathbf{I}_2$ where \mathbf{I}_2 is the second order identity matrix, $\mathbf{I}_2 \in \mathbb{R}^{2 \times 2}$. Unlike in UT, sigma points are not necessarily symmetric. However, the constrained sigma points mean and covariance include information on the constraints.

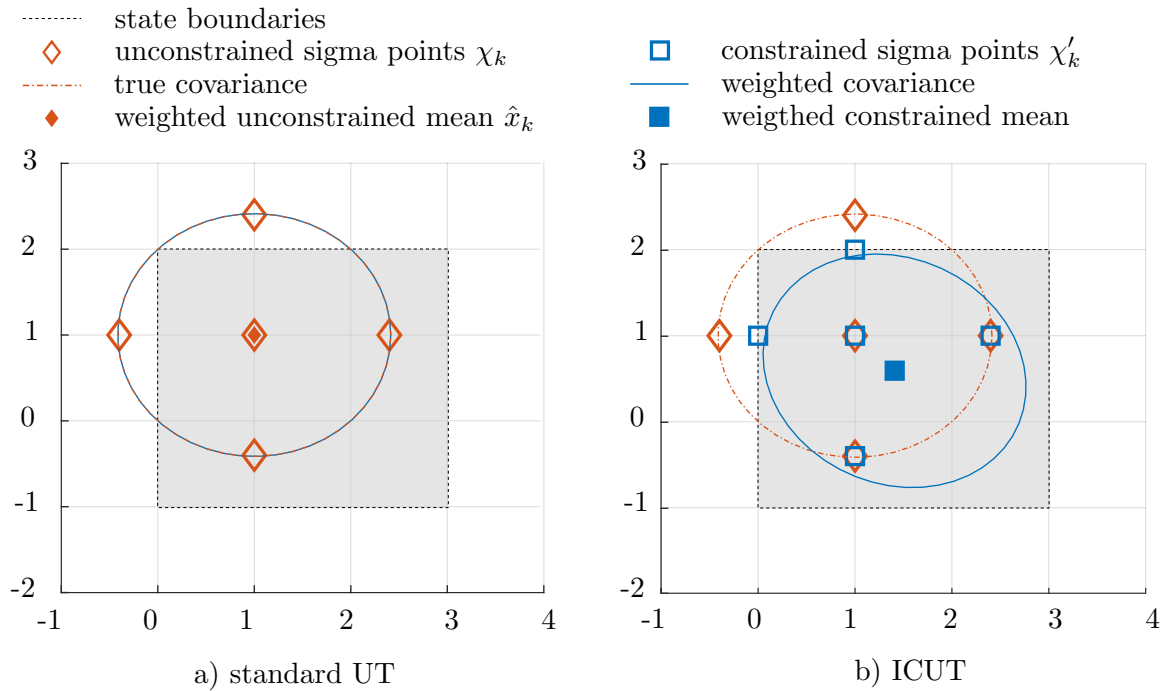


Figure 3.7. Geometrical interpretation of the proposed modified ICUT.

3.5.3 General UKF-based framework for identification of low-order semi-physical building models

To address the problem of simultaneous states and parameters identification, the parameter vector Θ is also treated as a dynamical variable with $\dot{\Theta} = 0$ [101]:

$$x_k = \begin{bmatrix} f(x_{k-1}, u_{k-1:k}) \\ \Theta_{k-1} \end{bmatrix} + w_{k-1}, \quad (3.65)$$

where $x_k = \begin{bmatrix} T_{a,k} & T_{z,k} & \Theta_k^\top \end{bmatrix}^\top \in \mathbb{R}^{n_x}$ is the augmented state vector while $f(\cdot)$ denotes the integration of the continuous-time model function (3.29) over the interval of one sampling time T_s using input vector measurements $u_{k-1:k}$ available over interval $[k-1, k]T_s$. The particular benefit of continuous-time identification, rather than direct identification of the discrete-time model, is the generality of the approach since the model is valid for an arbitrary sampling time.

Normalization

The augmented state vector x_k typically contains multiple physical variables and parameters of distinctively different orders of magnitude. Thus, the state vector limits are utilized to normalize the vector x_k to interval $[0, 1]$ such that:

$$x_k^n = \frac{x_k - L_k}{U_k - L_k}, \quad (3.66)$$

where $x_k^n \in \mathbb{R}^{n_x}$ is the normalized augmented state vector. Due to the simplicity of notation in the upcoming part of the thesis it is assumed that $x_k = x_k^n$. In accordance with (3.66) measurement update is performed on normalized measurement.

Non-informative system excitation

Inputs which do not excite the building in an informative way cause degradation of the filter behaviour and in the worst case even its divergence. Typical examples of non-informative excitation are solar irradiance and heating/cooling elements thermal loads. In intervals when solar irradiance is equal to zero (e.g. during night) the related estimated parameters gradually deviate from their true values since they can be put into any value (parameter is constantly multiplied with zero). To overcome this issue original algorithm is further modified in a way that the filtering in the k^{th} step is performed only on parameters related to informative input data while the other parameters are treated as constants. To check the informativeness, the integrals of possibly non-informative inputs between previous and current filtering step are calculated and compared with threshold value. If the integrals are below the threshold the parameters related to those inputs are treated

as unexcited. To incorporate the methodology within UKF algorithm at the beginning of every filtering step k , state estimates and their corresponding covariance matrices are modified and filtering is performed using x_{k-1}^* and $P_{x_{k-1}}^*$:

$$x_{k-1}^* = x_{k-1}(e_k), \quad P_{x_{k-1}}^* = P_{x_{k-1}}(E_k), \quad (3.67)$$

where $e_k = \{\}$ is a set of indices of excited states, $E_k = \{e_k \times e_k\}$ while operator \times denotes Cartesian product, i.e. set of all ordered pairs. In the end of current filtering step updated covariance matrix and states are reassembled such that:

$$\begin{aligned} P_{x_k}(E_k) &= P_{x_k}^*, & P_{x_k}(N_k) &= P_{x_{k-1}}(N_k), \\ x_k(e_k) &= x_k^*, & x_k(n_k) &= x_{k-1}(n_k), \end{aligned} \quad (3.68)$$

where $n_k = \{\}$ is a set of indices of all unexcited states and $N_k = \{n_k \times n_k\} \cup \{e_k \times n_k\}$. The approach is graphically illustrated in Fig. 3.8.

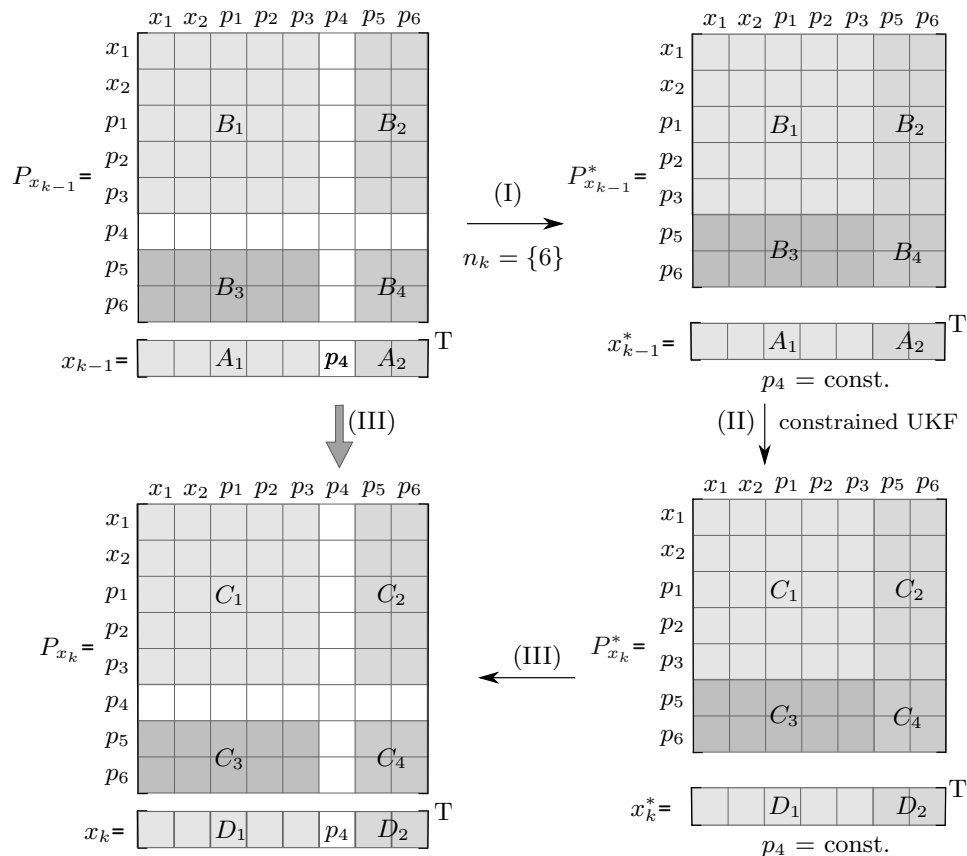


Figure 3.8. Graphical illustration of handling the unexcited parameters within the UKF.

Sampling time selection

The filter sampling time selection, although often completely neglected part of the estimation process, significantly influences the estimation results, especially if it is not selected properly. This is particularly noticeable in systems of second or higher order with two or more distinctly different time constants. The sampling time should be large enough to capture the slow system dynamics characterised by larger time constants and small enough to capture the transient behaviour of the fast dynamics. Buildings are typical examples of systems with largely different time constants. Although selection of the sampling time is mostly based on heuristics, in [118, 119] a general framework for selection of a convenient sampling time is given:

$$\frac{\tau_y}{20} \leq T_s \leq \frac{\tau_y}{10}, \quad (3.69)$$

where τ_y is the time of the first minimum of the correlation function Φ_{yy} :

$$\Phi_{yy}(\tau_c) = E[(y(k) - \overline{y(k)})(y(k - \tau_c) - \overline{y(k)})], \quad (3.70)$$

$E[\cdot]$ is the mathematical expectation, $y(k)$ is the measured system state and $\overline{\cdot}$ represents time-averaging.

3.6 Mathematical model of the case-study skyscraper building

A reliable thermodynamic model of a building is a key for the exploitation of significant energy savings potential of model-based control algorithms in buildings. In the following subsection detailed IDA-ICE model of the case-study building is presented. Based on the RC analogy between thermodynamic processes in buildings and electrical network described in Section 3.2, an analogous RC model of two selected floors of the case-study building is developed. The model is validated by comparing its temperature response with the response obtained in specialised building simulation software IDA-ICE [25] and Trnsys [27]. The identification framework developed within Section 3.5 is utilized to identify simplified low-order models of the building zones. Numerical stability of the approach and applicability of the identified models to be used within the MPC framework are verified using real measurements from the building. The suitability of all developed models for prediction of heating/cooling building loads is then tested through comparison with the measured thermal energy consumption data from the building.

3.6.1 IDA-ICE model of the case-study building

The distinct advantages of IDA-ICE are:

- equation based modelling, using the Modelica-like Neutral Model Format (NMF), enabling quick expansion of the software with new modelling capabilities,
- model transparency, i.e. every underlying equation can be browsed and every variable can be logged,
- user-friendly interface,
- the software is certified based on measured data,
- customer support available on demand.

The case-study building has in total 248 controllable zones, mainly offices (Fig. 3.9) and classrooms (Fig. 3.10). The 13 building floors span over the total area of 10690 m², including non-controllable zones like hallways and restrooms. The material properties, window properties, thermal bridges, infiltration and wall types are aligned with the specifications of the building physics described in Appendix A.2. Based on the available specifications a detailed building simulation model is developed. Figure 3.11 shows a 3D view of the 6th floor, while a 3D view of the whole building is given in Fig. 3.12.

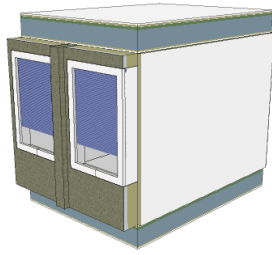


Figure 3.9. Typical zone used as an office.

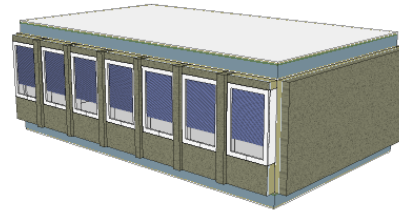


Figure 3.10. Typical zone used as a laboratory or classroom.

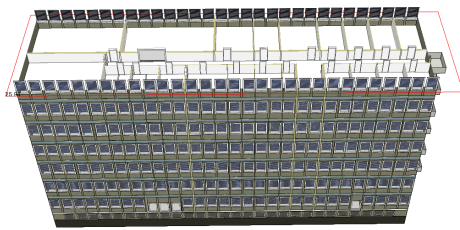


Figure 3.11. IDA-ICE 3D view of the 6th floor layout.

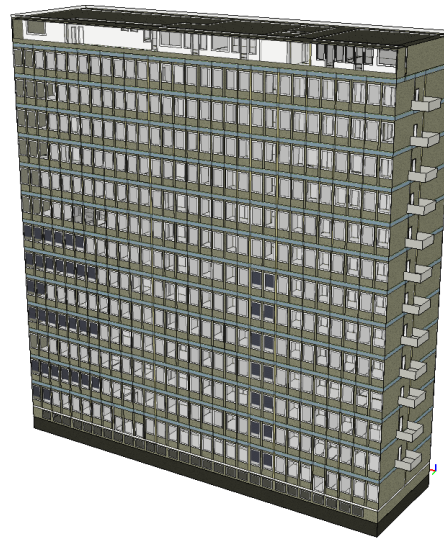


Figure 3.12. IDA-ICE 3D view of the case-study building.

3.6.2 The Resistance-Capacitance model

Based on the lumped-parameters method and RC analogy between thermodynamic processes in buildings and electrical network, an analogous RC model of two selected floors of the skyscraper building (9th and 10th floor) is developed. The selected two floors have 50 zones, both controllable and non-controllable, spanning over the area of 1510 m². Low thermal capacity elements, such as doors and internal glass or polycarbonate windows, are just as external windows modelled with resistors only. Detailed specifications of the building construction elements required for calculation of the capacitances and resistances are given in Appendix A.2.

To validate the developed RC model, the selected two floors are also modelled in specialised building simulation software IDA-ICE [25] and Trnsys [27]. The zones on the 8th and 11th floor as well as zones marked with an arrow in Fig. 3.13 are not modelled, instead the temperature in these zones is used as a boundary condition for the considered RC model.

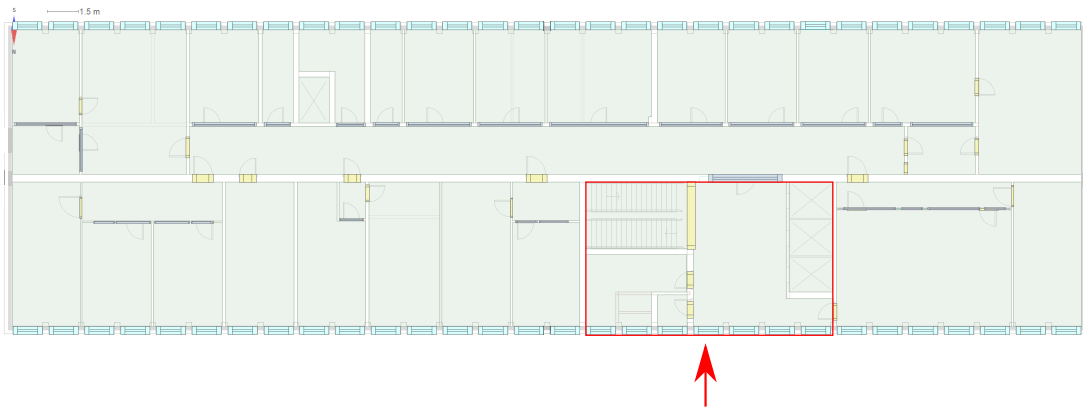


Figure 3.13. IDA-ICE layout of the 9th floor with marked spaces which are not included into RC model.

Final model in a state-space form has 516 model states representing wall and zone temperatures and 19 inputs. Inputs consist from:

- outside temperature,
- direct and diffuse solar irradiances per unit area incident on external wall surfaces recalculated for all external wall orientations (4 different orientations),
- direct and diffuse solar irradiance transmitted into zones recalculated for all different window types and orientations (one window type and 2 different window orientations),
- boundary air temperatures on the 8th and 11th floor and other zones which are not considered in the RC model.

Within the developed RC model typical values of the convective heat transfer coefficient of $h^{\text{in}} = 3 \text{ W}/(\text{m}^2\text{K})$ for the internal and $h^{\text{out}} = 18 \text{ W}/(\text{m}^2\text{K})$ for the external coefficient are used. The share of the transmitted solar irradiance absorbed by the zone air is set to $\eta_t = 0.6$

Model validation

The developed RC model is validated through comparison of the model performance with the performance of the models developed within IDA-ICE and Trnsys. All models are simulated by using Typical Meteorological Year (TMY) data for the building location [27], consisted of hourly sampled values of:

- outside temperature T_{out} (Fig. 3.14(a)),
- direct normal solar irradiance I_n^{dir} (Fig. 3.14(b)),
- diffuse horizontal solar irradiance I_h^{dif} (Fig. 3.14(c)),
- humidity, wind speed and direction.

The TMY data are selected from historical hourly data recorded over a longer time period (normally 10 years or more). For each month in the year the data have been selected from the year that was considered most 'typical' for that month. It is specially selected so that it presents the range of weather phenomena, while still giving annual averages that are consistent with the long-term averages for the building location.

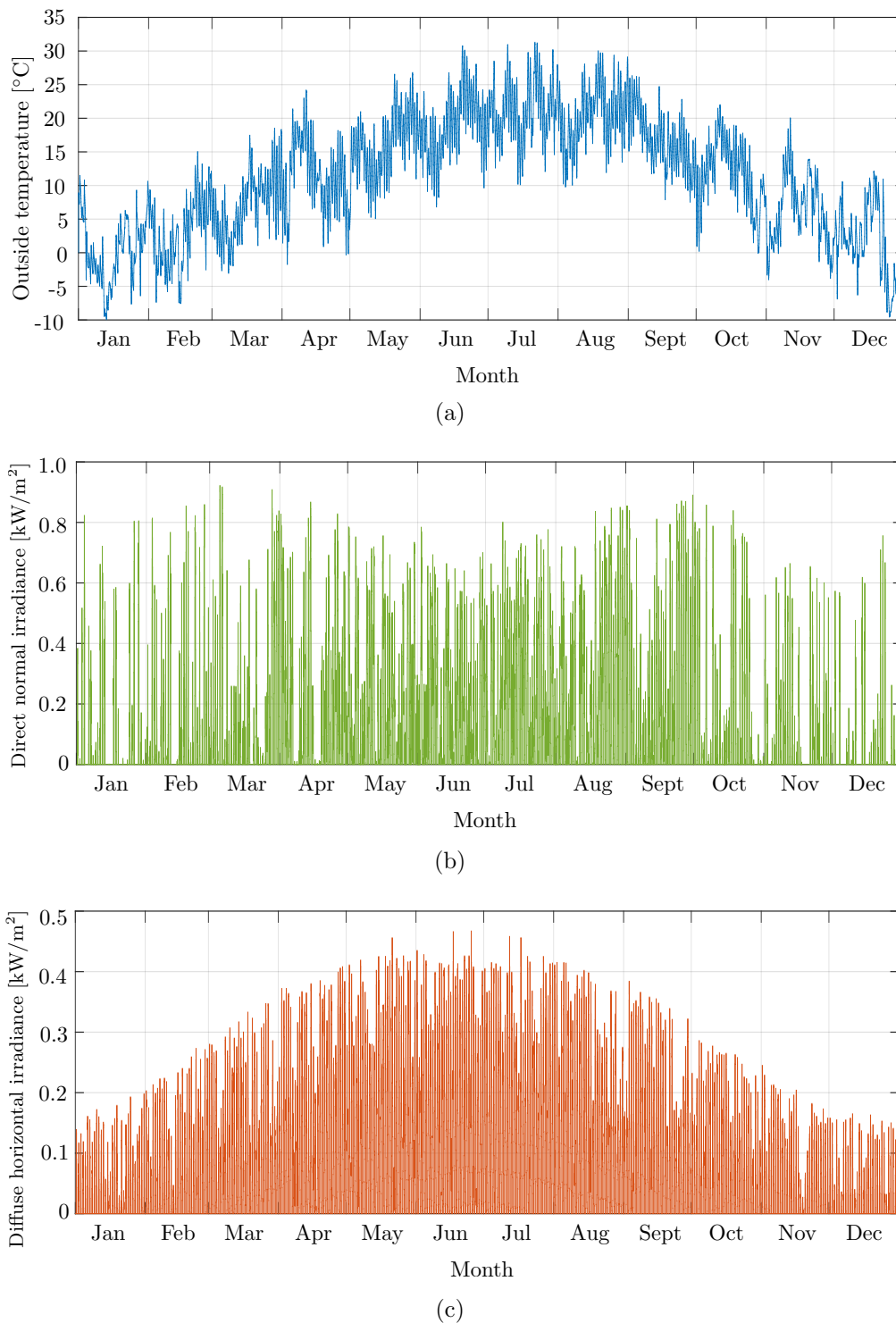


Figure 3.14. TMY data for location Zagreb: a) outside temperature, b) direct normal solar irradiance and c) diffuse horizontal solar irradiance.

The RC model uses only outside temperature and solar irradiance as inputs, model in Trnsys additionally uses humidity data while model in IDA-ICE uses all available information. It is assumed the temperature in the building is influenced only by the external weather conditions. All auxiliary heat sources, such as fan coil units or radiators, are omitted. The RC model of the considered two floors is developed and simulated within MATLAB/Simulink environment [70]. All models are simulated through two year period, while only second year of data is used for comparison to annul the impact of different model initial conditions. For a fair comparison, when comparing the RC model with other models, boundary conditions are imported from the simulation programs and used as inputs into the RC model. Outputs of all models are sampled with a sampling time of one hour. The comparison of the simulated RC model temperature in one exemplary south-oriented zone with the IDA-ICE and Trnsys simulation results is shown in Fig. 3.15. The selected zone has two external walls, concrete west-oriented external wall and south-oriented external wall made of brick. South-oriented wall has large external window. Model mismatch is quantified in terms of temperature difference between the models:

$$\text{Error} = T_a^{\text{RC}} - T_a^{\text{SS}}, \quad (3.71)$$

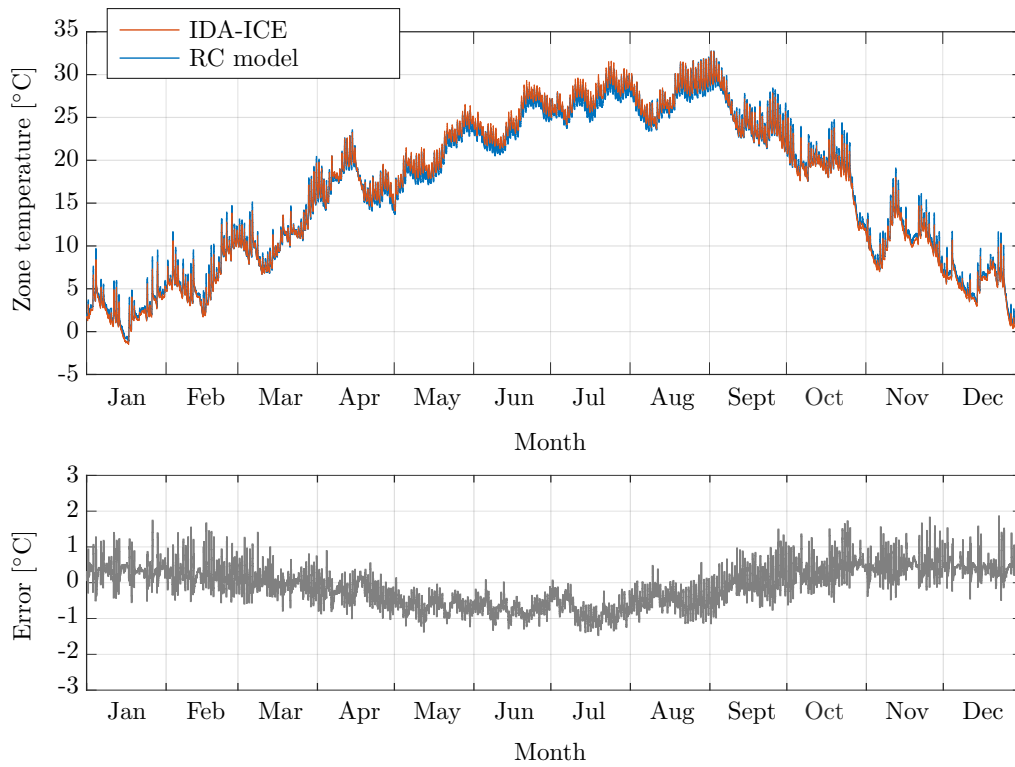
where T_a denotes the zone temperature, superscript RC denotes temperature simulated by RC model while SS in superscript denotes temperature simulated by using building simulation software (IDA-ICE or Trnsys). The comparison of the simulated RC model temperature in one exemplary north-oriented zone with the IDA-ICE and Trnsys simulation results is shown in Fig. 3.16. The selected zone has only one external wall, made from brick, oriented towards north and containing a large external window. The calculated Mean Absolute Error (MAE) and Normalized Root Mean Squared Error (NRMSE) between the RC model and simulation software is given in Fig. 3.17. MAE is calculated as:

$$\text{MAE} = \frac{1}{n_y \cdot 8760} \sum_{i=1}^{n_y} \sum_{j=1}^{8760} |T_{a,i}^{\text{RC}}(j) - T_{a,i}^{\text{SS}}(j)| \quad (3.72)$$

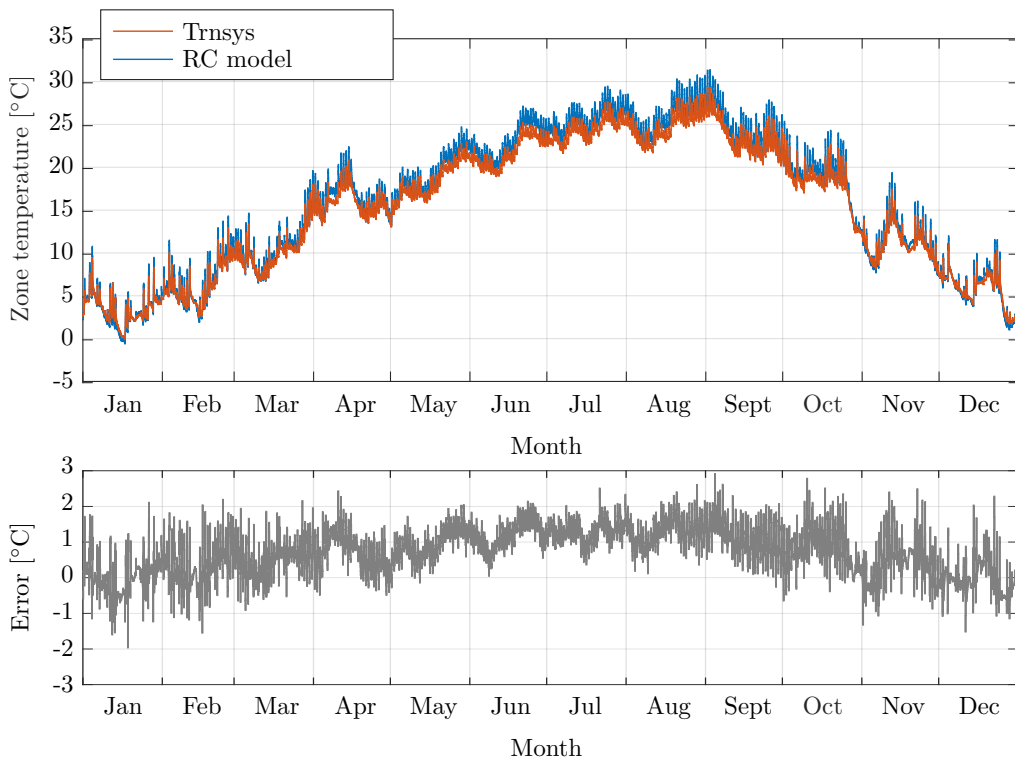
where $n_y = 50$ is the overall number of zones on the considered two floors, 8760 is the overall number of hourly temperature samples per zone, $T_{a,i}(j)$ is the temperature in the i^{th} zone simulated at the j^{th} hour in the year. NRMSE is calculated as:

$$\text{NRMSE} = \frac{1}{\max(T_a^{\text{RC}}) - \min(T_a^{\text{RC}})} \sqrt{\frac{1}{8760 \cdot n_z} \sum_{i=1}^{n_z} \sum_{j=1}^{8760} (T_{a,i}^{\text{RC}}(j) - T_{a,i}^{\text{SS}}(j))^2} \quad (3.73)$$

where $\max(T_a^{\text{RC}})$ and $\min(T_a^{\text{RC}})$ denote maximum and minimum building temperature simulated by using the developed RC model on a time span of one year.

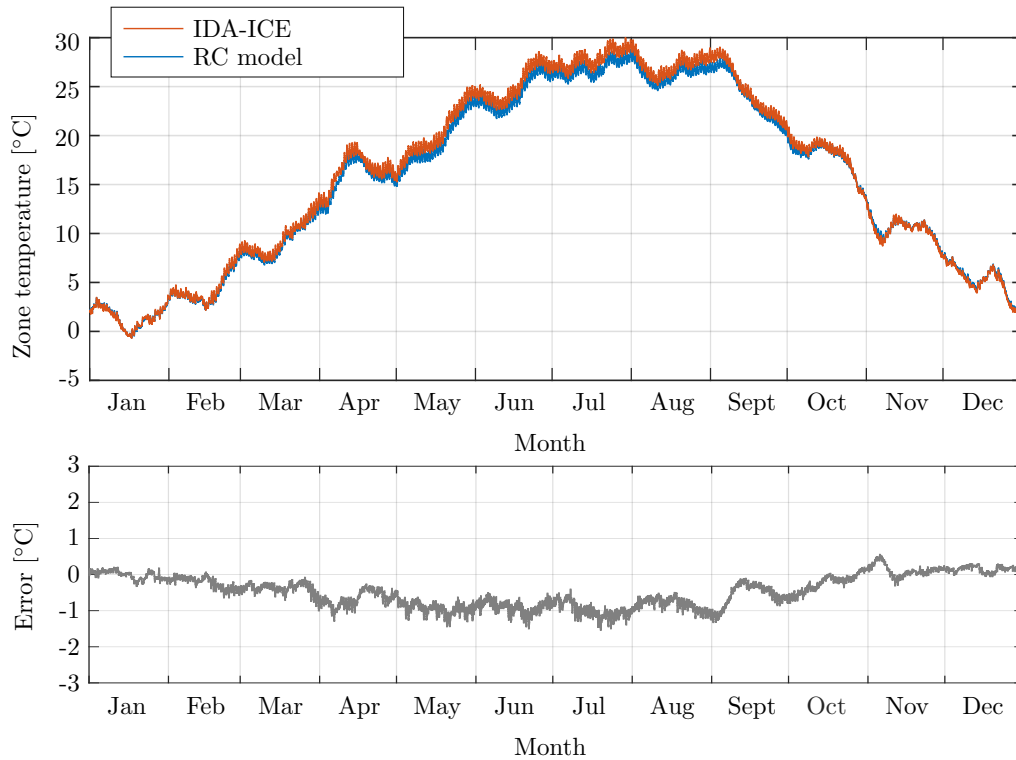


(a)

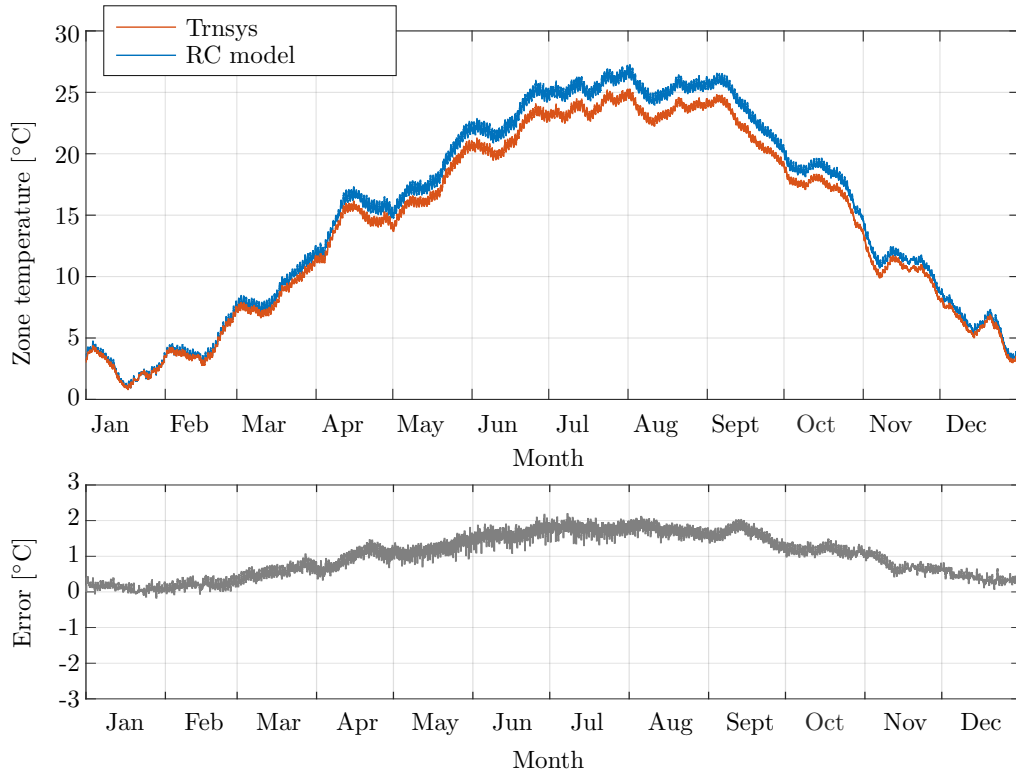


(b)

Figure 3.15. Simulated temperature response of exemplary south-oriented zone (C09-04) during period of one year in Matlab (RC model) and in a) IDA-ICE, b) Trnsys.

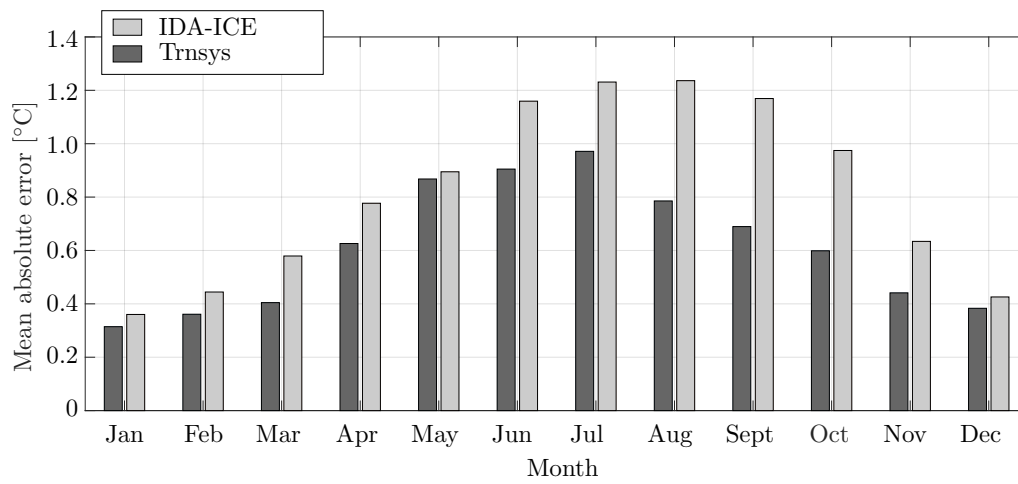


(a)

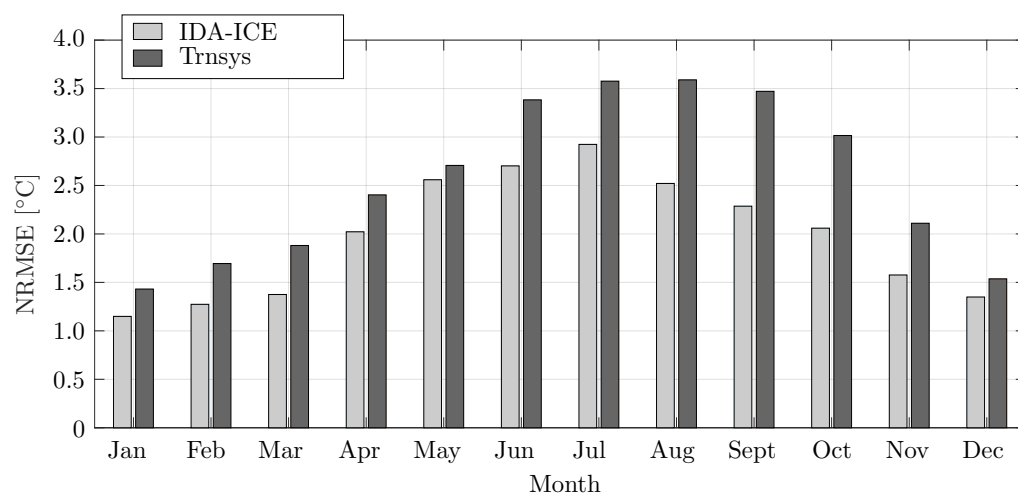


(b)

Figure 3.16. Simulated temperature response of exemplary north-oriented zone (C09-17) during period of one year in Matlab (RC model) and in a) IDA-ICE, b) Trnsys.



(a)



(b)

Figure 3.17. Validation of the developed RC model in terms of a) MAE and b) NRMSE of the model response compared to the model temperature response in IDA-ICE and Trnsys

Despite the simplicity, the developed RC model performance does not deviate significantly from the performance of the specialised building simulation software which accurately models all relevant thermodynamic processes.

3.6.3 Simplified low-order model

Since heat transfer between the zones is driven by the temperature difference, due to the similar temperature in zones and well-insulated internal walls, heat flow between the zones is assumed to be zero. Table 3.2 contains a detailed list of measurements used for identification of the building thermodynamic model. Due to the well-insulated piping the transmission heat losses are neglected which means that the fan coil unit (FCU) water inlet temperature is considered to be equal to the supply temperature measured by the calorimeter.

Table 3.2. Measurements used for the identification of the simplified building model.

DATA SOURCE		SAMPLING TIME
ZONES		
Zone temperature	T_a [°C]	1 min
FCUs		
Fan speed	x_{fs} (off, L, M, H)	1 min
Return medium temperature	T_w^{out} [°C]	1 min
CALORIMETER		
Supply medium temperature	$T_{w,cal}^{in}$ [°C]	1 min
Mass flow	$q_{w,cal}$ [kg/s]	1 min
WEATHER STATION		
Outside temperature	T_{out} [°C]	1 min
Global solar irradiance	I_n^{dir} [W/m ²]	1 min
Diffuse solar irradiance	I_h^{diff} [W/m ²]	1 min

Measurements of solar irradiance components are available for the direct normal I_n^{dir} and diffuse horizontal I_h^{diff} solar irradiance per unit area. The direct and diffuse solar irradiance incident on a tilted surface I_θ^{dir} and I_θ^{diff} are easily calculated with the known direct normal and diffuse horizontal irradiance, surface azimuth angle, tilt angle, and solar zenith and azimuth angle (see Appendix B).

The suitability of the developed approach for identification of semi-physical building models is tested by applying it on the measurements collected during winter holidays 2018/2019 (21 December 2018 - 2 January 2019) when the building was unoccupied. The data set for identification of simplified zone model contains: *i*) outside air temperature (Fig. 3.18), *ii*) diffuse and *iii*) direct solar irradiance incident on the exterior surfaces of the zone (Fig. 3.19) *iv*) fan coil unit thermal power and *v*) zone temperature (Fig. 3.20).

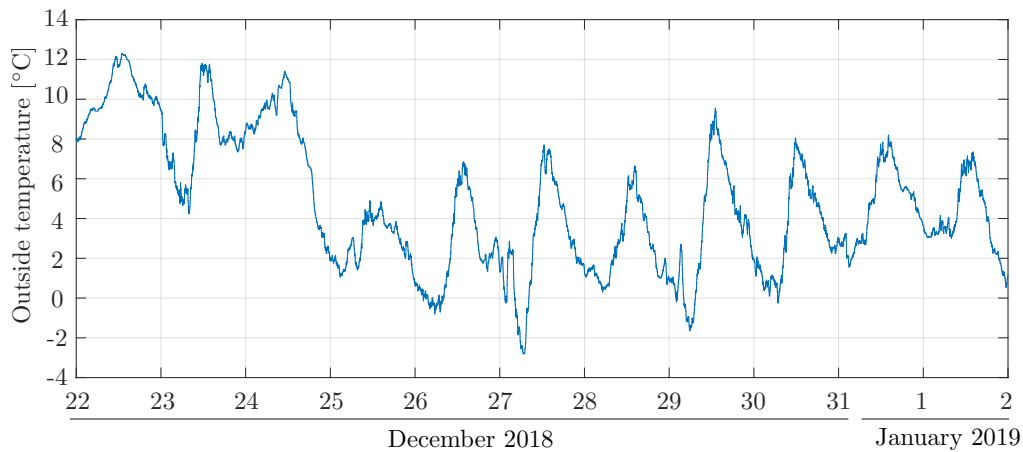


Figure 3.18. Measurements of outside temperature used for identification.

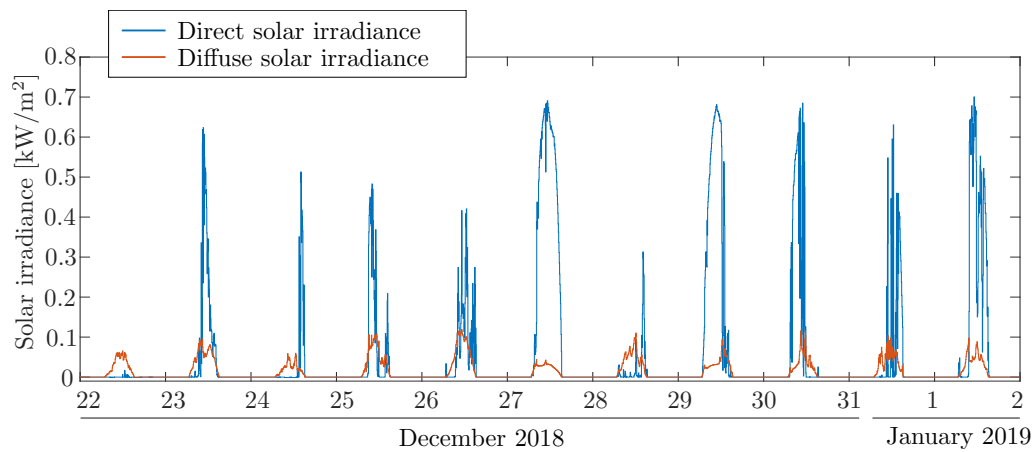


Figure 3.19. Direct and diffuse solar irradiance incident on south-oriented external walls.

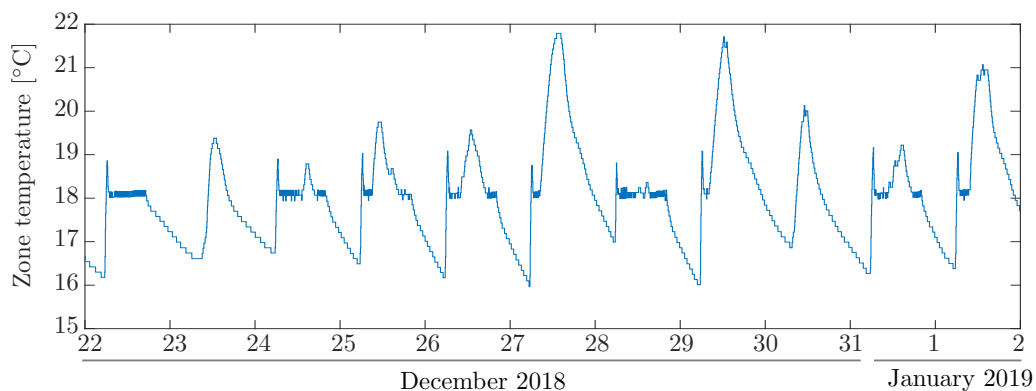


Figure 3.20. Measured zone air temperature in one exemplary south-oriented zone (C09-10).

Acquiring of accurate thermal energy load from the heating/cooling elements in building zones is the main prerequisite for identification of accurate building thermal models that transform zone energy input into temperature output. The detailed procedure for identification of the thermal and hydraulic model of a FCU is in detail described in

Chapter 2. The thermal power transferred from the FCU to the zone air, P_a , is defined as (2.19):

$$P_a = U_o (\bar{T}_w - T_a^{\text{in}}), \quad (3.74)$$

where \bar{T}_w is the mean water temperature inside the FCU, approximately equal to the average of water inlet temperature T_w^{in} and water outlet temperature T_w^{out} , i.e. $\bar{T}_w = 0.5(T_w^{\text{in}} + T_w^{\text{out}})$, T_a^{in} is the air intake temperature equal to the zone temperature T_a and $U_o = f(x_{\text{fc}}, q_w)$ is the heat transfer coefficient, dependent on the medium mass flow q_w and current fan speed x_{fc} defined as in (2.14). For installations with static hydraulic situation (FCUs without valves), medium mass flow through a certain unit is defined as $q_w = \eta_{\text{fc}} \cdot q_{w,o}$, where $q_{w,o}$ is the overall mass flow measured by the floor calorimeter and η_{fc} is the identified fixed share of the flow which goes through the considered FCU. More details on identification of the hydraulic model of the FCU can be found in Chapter 2. Calculated FCU thermal power inserted into one exemplary zone is shown in Fig. 3.21.

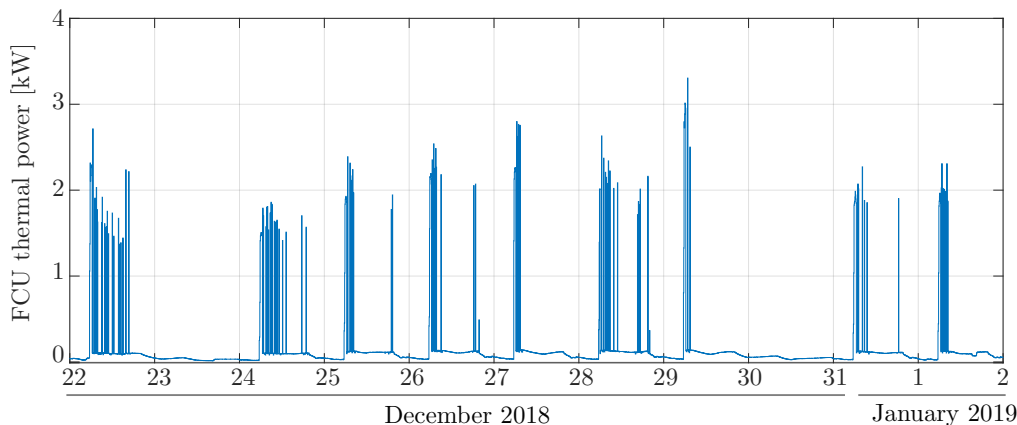


Figure 3.21. Calculated FCU thermal power inserted into one exemplary zone (C09-10).

Sampling time is selected as described in Subsection 3.5.3. The times of the first minimum τ_y of one exemplary zone temperature autocorrelation functions for 24th and 30th December are 371 min and 627 min, respectively (Fig. 3.22). The selected days are characterised by two distinctively different temperature responses: external conditions driven response and response driven by internal factors such as FCU operation. The filter sampling time is thus selected to cover both intervals, i.e. $T_s = 30$ min.

Parameter limits are calculated by performing non-recursive batch parameter identification on the historical data, limits are then determined to be one order of magnitude higher/lower than the batch identified parameters. Limits on zone state variables are selected to be slightly higher/lower than maximum/minimum zone temperature in used data set. The initial state value is set to be in the middle of the scaled interval, i.e. starting from value $x_0 = 0.5 \cdot \mathbf{1}_n^T$ ($n = 8$), where $\mathbf{1}_n$ is the n -dimensional row-vector of ones. Both initial parameters and limits can also be easily assessed based on the well adopted formulas for calculating thermal resistances and capacitances of building elements (see Section 3.2). The filter parameters are set to be $\alpha = 0.5$, $\kappa = 0$ and

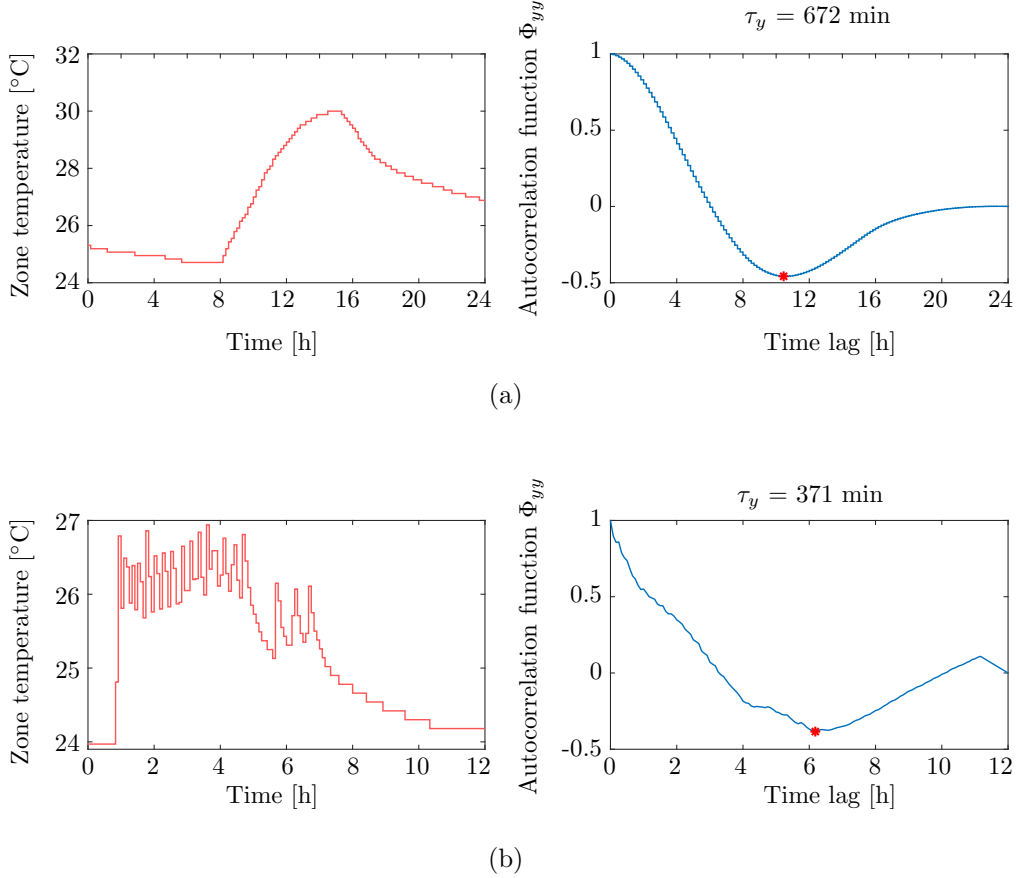


Figure 3.22. Normalized autocorrelation function of the exemplary zone temperature a) excited only by external conditions (24 December 2018), b) excited by the external conditions and FCU (30 December 2018).

$\beta = 2$ with the initial augmented state covariance matrix $P_{x_0} = 0.50^2 \cdot \mathbf{I}_{n_x}$, where \mathbf{I}_{n_x} is the n_x^{th} order identity matrix, $\mathbf{I}_{n_x} \in \mathbb{R}^{n_x \times n_x}$. State and measurement noise matrices are set to be $Q = \text{blkdiag}(0.04^2, 0.01^2, 10^{-10} \cdot \mathbf{I}_{n_x-2})$ and $R = 0.08^2$, respectively. The $\text{blkdiag}(\cdot)$ denotes a block-diagonal matrix form consisted of the matrices listed as arguments. Convergence of the estimated parameters for two exemplary zones is shown in Fig. 3.23 and Fig. 3.24. For both selected zones, limit parameters are set to be $L_k = \begin{bmatrix} 20 & 20 & 10^{-5} & 10^{-6} \mathbf{1}_2 & 10^{-7} \mathbf{1}_3 \end{bmatrix}^\top$, $U_k = \begin{bmatrix} 35 & 35 & 10^{-3} & 10^{-4} \mathbf{1}_2 & 10^{-5} \mathbf{1}_3 \end{bmatrix}^\top$. It can be noted that for both zones the unknown system parameters p_1, p_2, p_3, p_4, p_5 and p_6 defined as in (3.30) managed to converge within one week.

To test the suitability of the model to be used within the predictive control strategies, the identified models are discretised with the sampling time of one minute. Since only one model state is measurable, linear Kalman filter [120] is used to estimate the slow-dynamic temperature states of all identified models every one minute (see e.g. Fig. 3.25 for estimated states in zone C09-10).

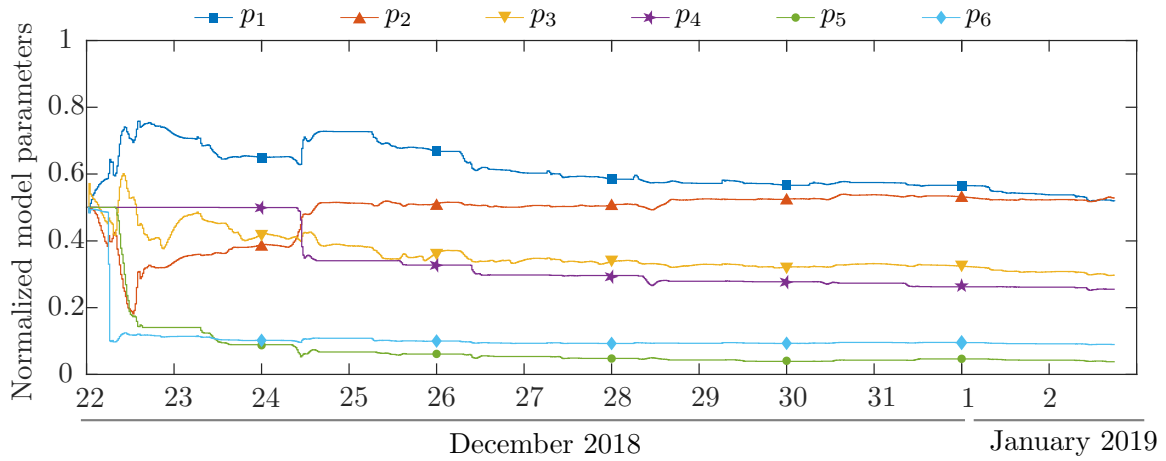


Figure 3.23. Estimated model parameters of south-oriented exemplary zone (C09-08).

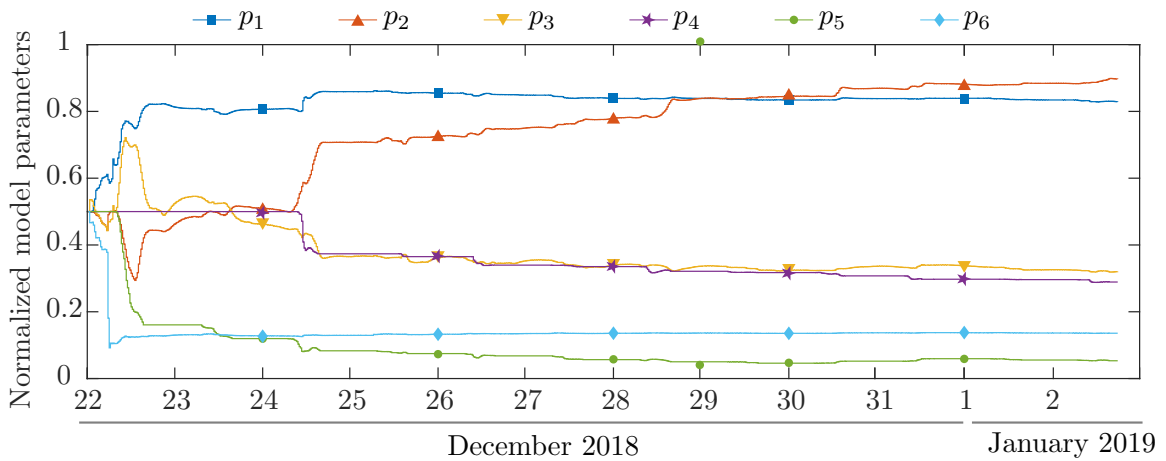


Figure 3.24. Estimated model parameters of south-oriented exemplary zone (C09-10).

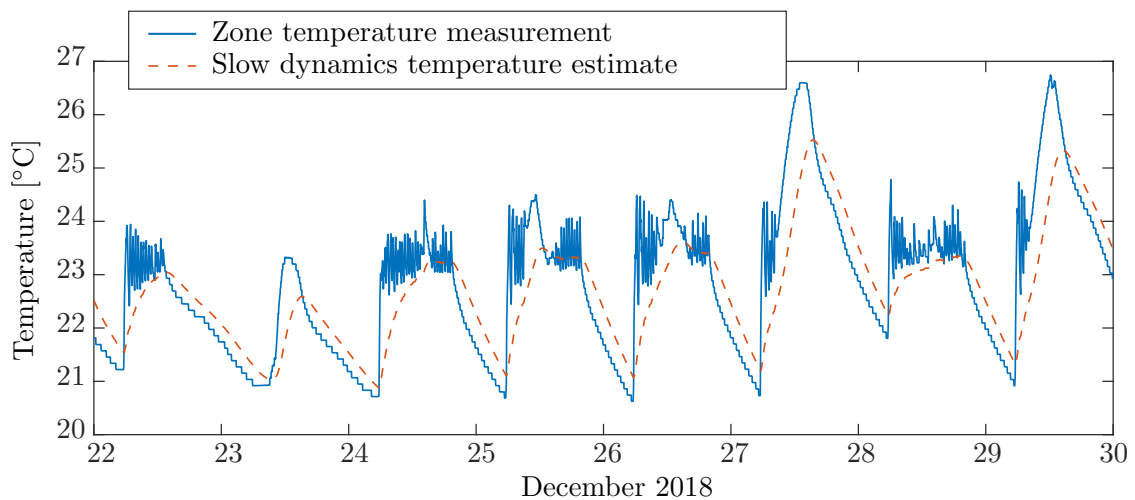


Figure 3.25. Estimated slow dynamics state for zone C09-10.

After both model states are acquired through the entire 12-days time sequence, every one minute ($T'_s = 1$ min) known input data are used to calculate the prediction of the zone temperature along the prediction horizon. Prediction is started from the current states estimates without considering any available zone temperature measurements along the prediction horizon (so-called open-loop prediction). The Mean Absolute Error (MAE) of the prediction along the prediction horizon of length H at step k is calculated as:

$$\text{MAE}(k) = \frac{1}{H} \sum_{i=k}^{k+H} |T_{a,i} - T_{a,i}^m|, \quad (3.75)$$

where H is prediction horizon expressed in minutes, $T_{a,k}$ is the zone temperature at time $k \cdot T'_s$ predicted by using the identified system model with fixed parameters and $T_{a,k}^m$ is the measured zone temperature at that time. The Normalized Mean Squared Error (NRMSE) is calculated as:

$$\text{NRMSE}(k) = \frac{1}{\max(T_a) - \min(T_a)} \sqrt{\frac{1}{H} \sum_{i=k}^{k+H} (T_{a,i}(j) - T_{a,i}^m(j))^2} \quad (3.76)$$

with $\max(T_a)$ and $\min(T_a)$ as maximum and minimum predicted temperature on the considered prediction horizon H . The comparison of the MAE and NRMSE calculated by testing the prediction of the identified models of several building zones for different prediction horizon lengths H and averaged over the time interval between 22 December 2018 and 2 January 2019 are given in Fig. 3.26 and Fig. 3.27. The comparison of real and predicted building air temperature for selected zones is given in Fig. 3.28 and Fig. 3.29. The detailed list of physical properties of the selected building zones, placed on different building floors, can be found in Appendix A.3.

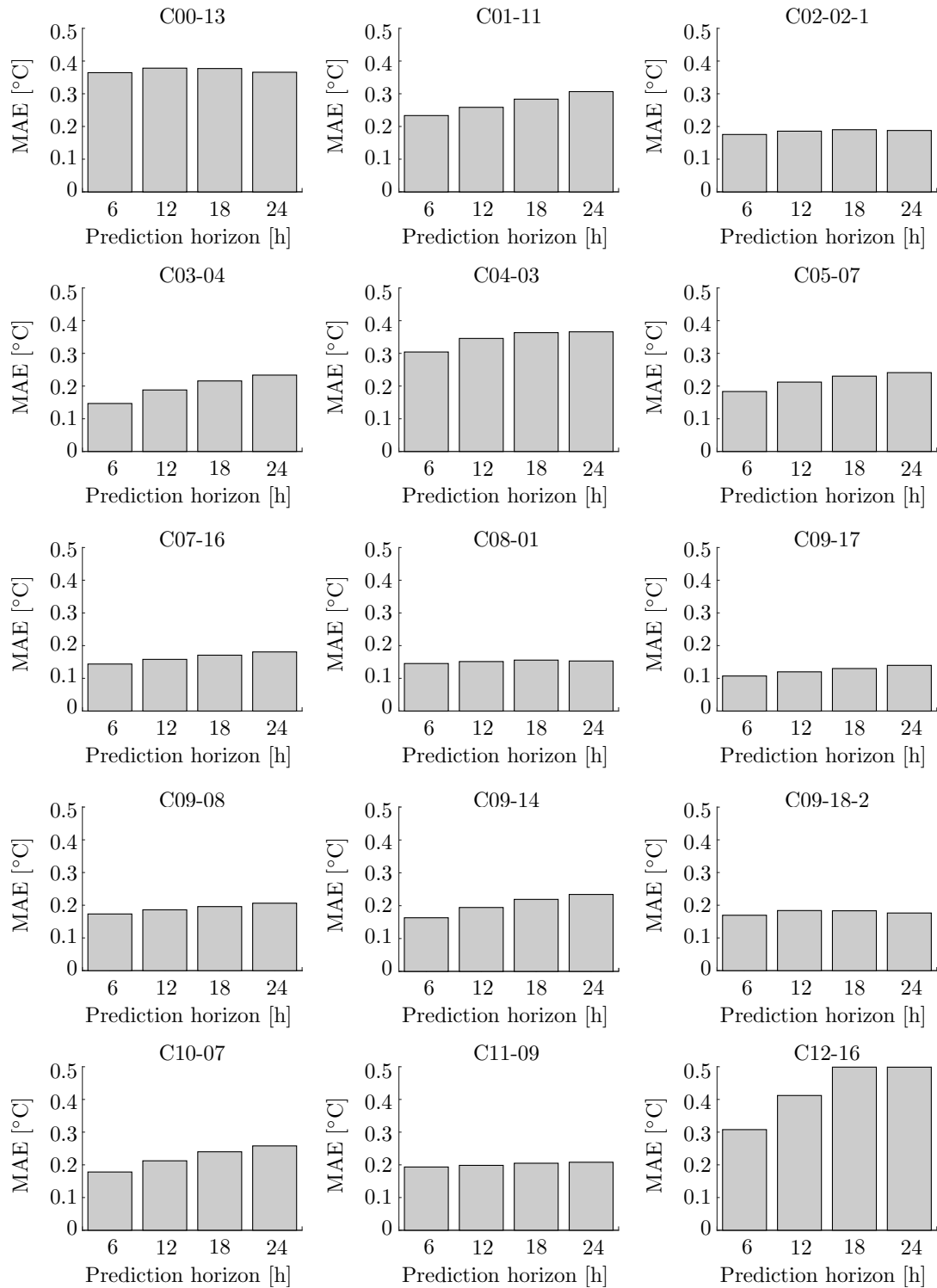


Figure 3.26. Mean absolute error of the identified zone air temperature models simulated over different prediction horizon lengths and averaged on the time frame between 22 December 2018 and 2 January 2019.

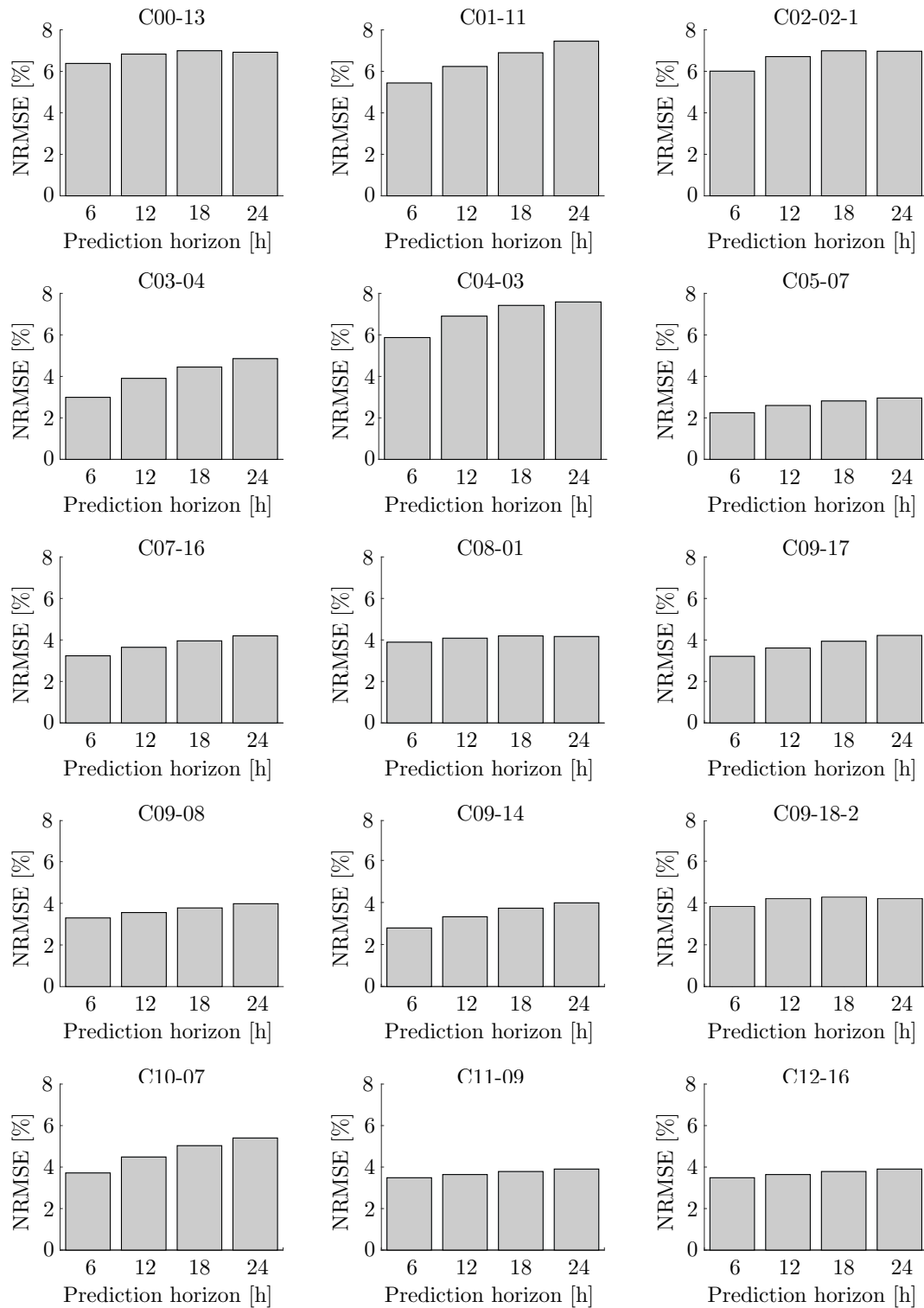


Figure 3.27. Normalized mean squared error of the identified zone air temperature models simulated over different prediction horizon lengths and averaged on the time frame between 22 December 2018 and 2 January 2019.

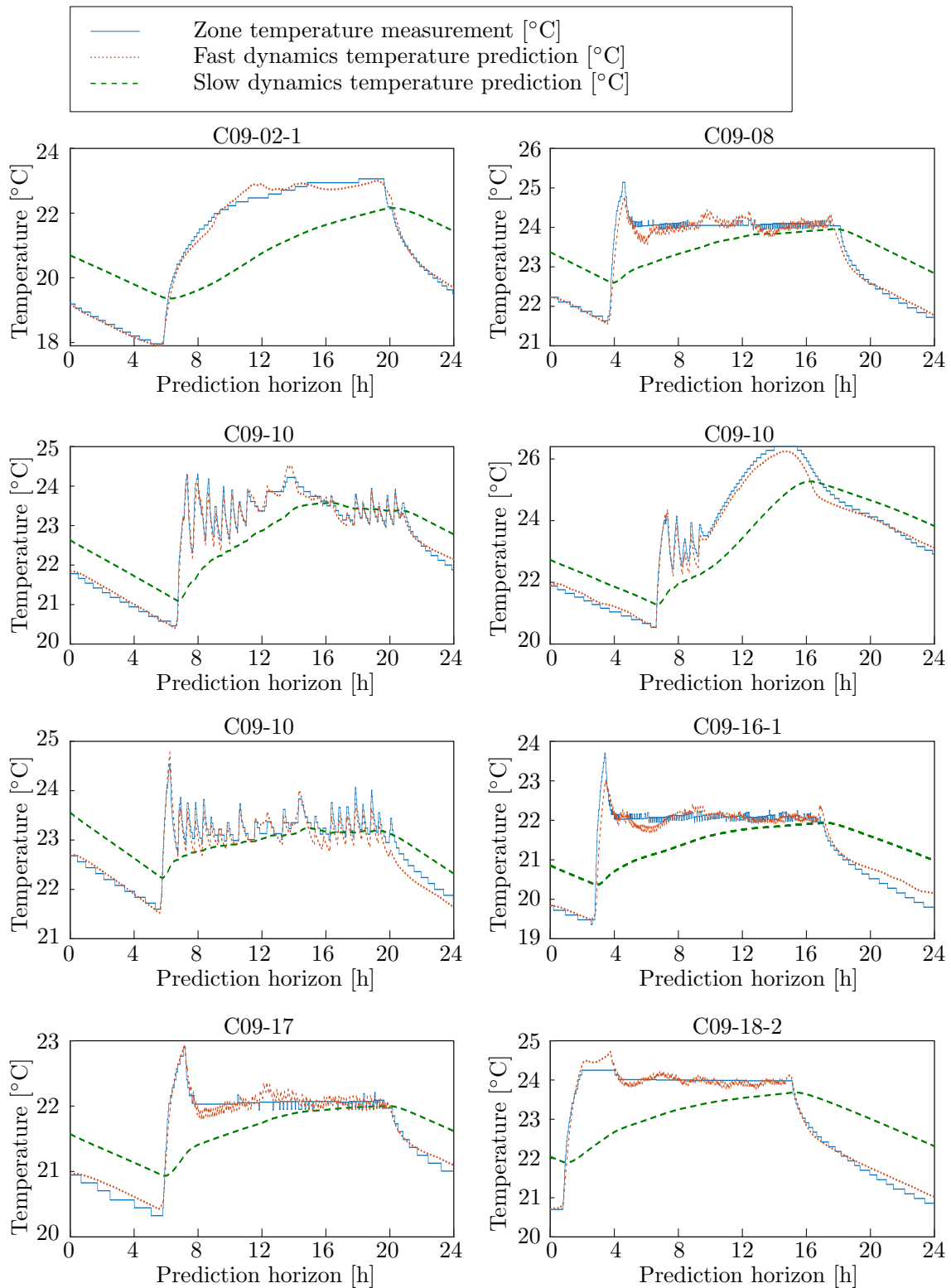


Figure 3.28. Comparison of the measurements and the predicted states of the estimated model for a 24-h-ahead prediction.

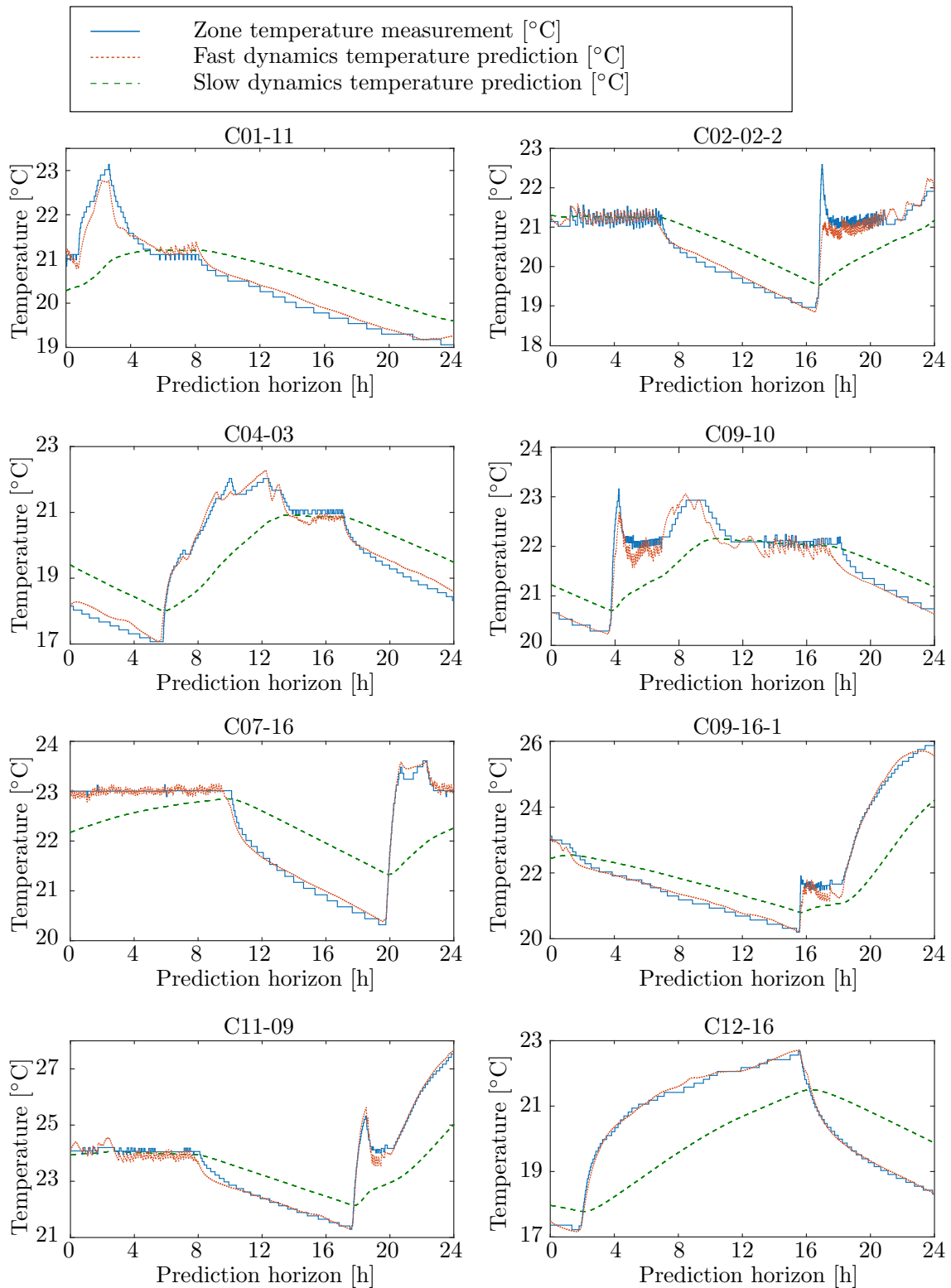


Figure 3.29. Comparison of the measurements and the predicted states of the estimated model for a 24-h-ahead prediction.

Numerical stability of the proposed UKF-framework

The numerical stability and convergence speed of the improved constrained UKF (CUKF) algorithm is verified by comparing it with the well established Kalman filters, i.e. EKF, standard UKF and CUKF based on ICUT[±]. All filters are implemented with the same augmented state vector, process and measurement noise values and the same initial augmented state estimates and covariance matrix. To make a fair comparison, normalization and treatment of non-excited building parameters are implemented in all algorithms. In the EKF algorithm, scaling and un-scaling procedure is integrated into the system dynamics equation. The filters performances with different initial covariance matrices are given in Fig. 3.30 and Fig. 3.31.

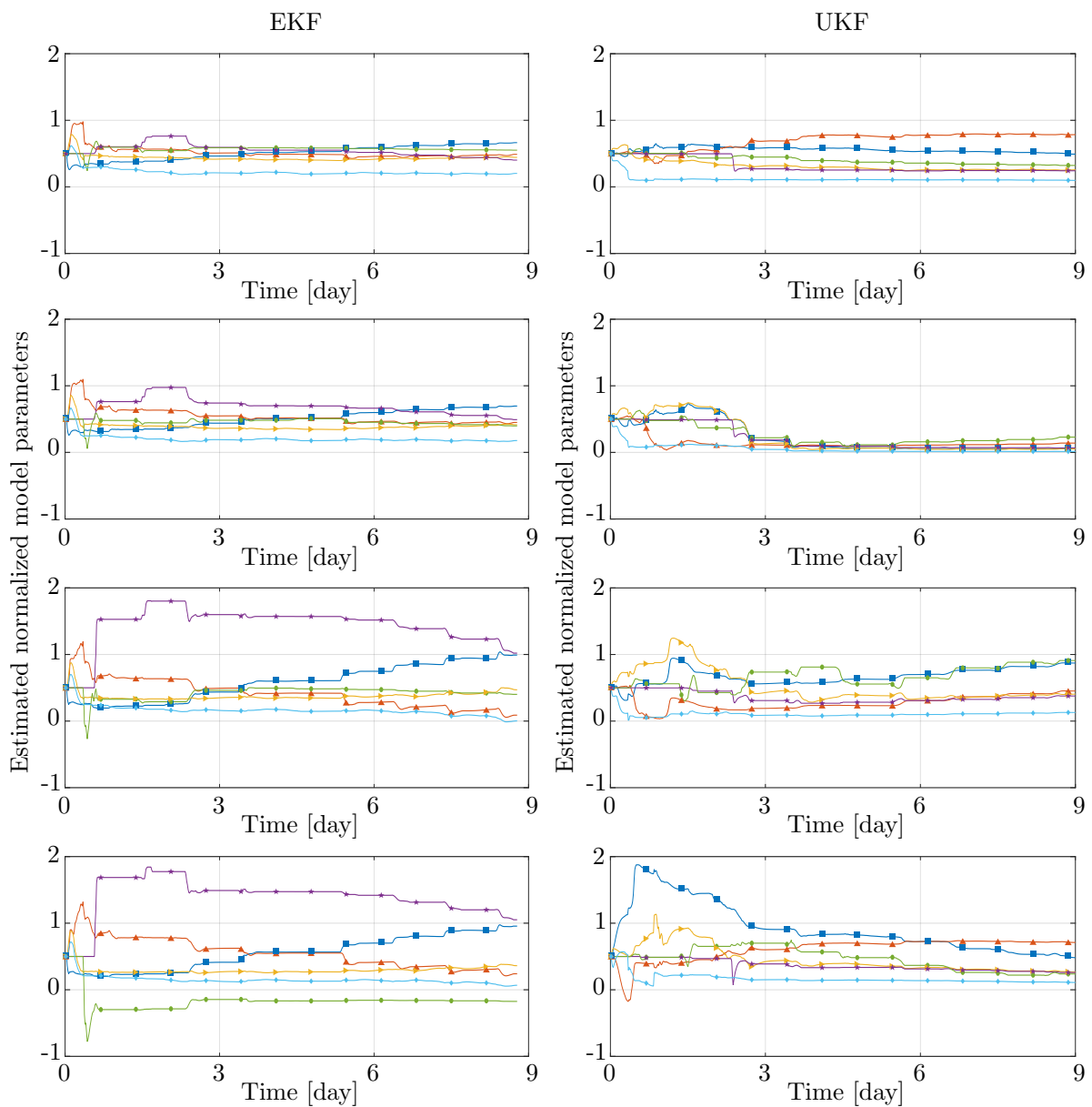


Figure 3.30. Estimated parameters of the exemplary zone using EKF and UKF with $P_{x_0} = 0.25 \cdot \mathbf{I}_{n_x}$ (first row), $P_{x_0} = 0.5 \cdot \mathbf{I}_{n_x}$ (second row), $P_{x_0} = \mathbf{I}_{n_x}$ (third row), $P_{x_0} = 2 \cdot \mathbf{I}_{n_x}$ (last row). Different parameters are marked in the same way as in Fig. 3.23.

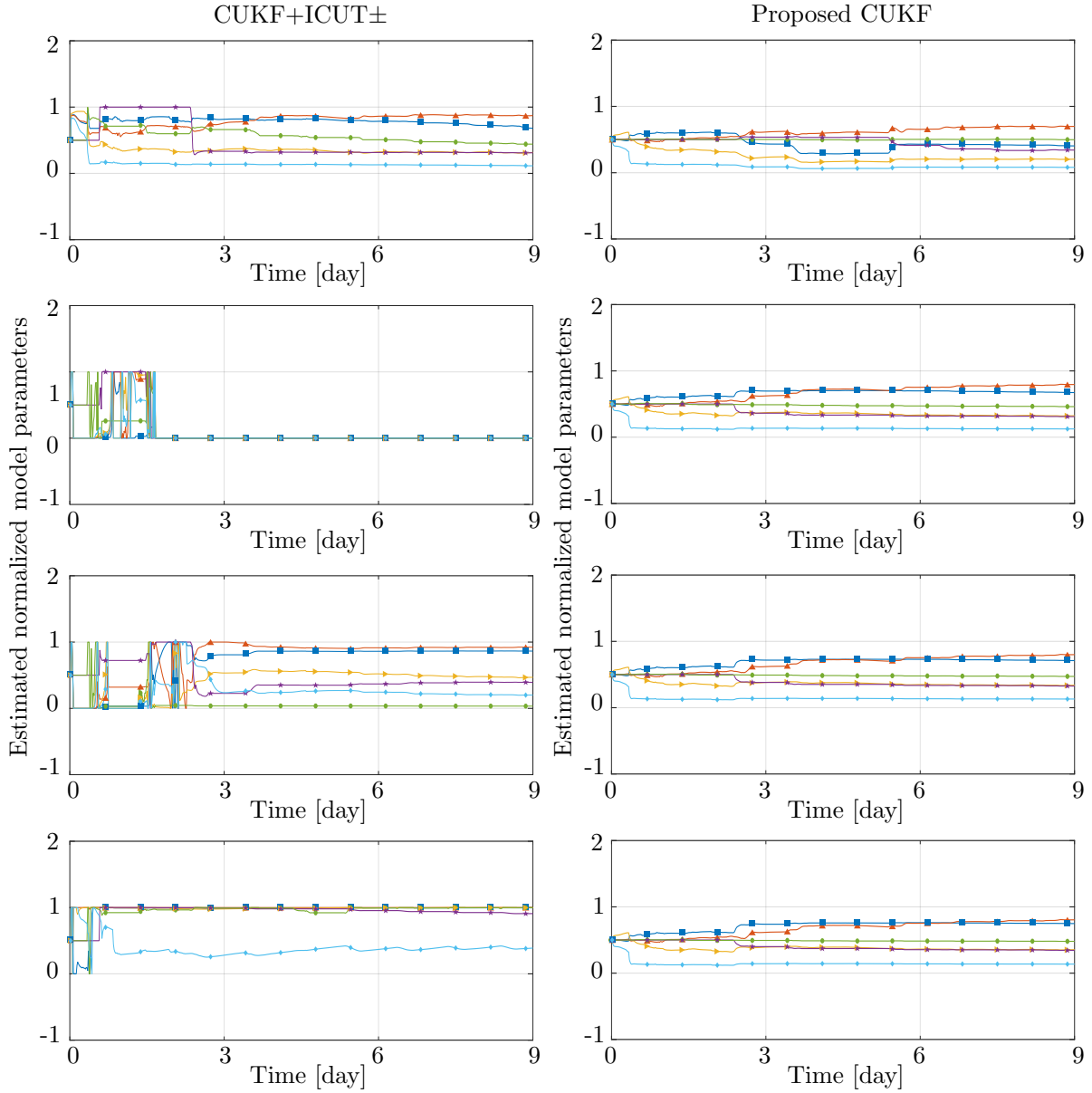


Figure 3.31. Estimated parameters of the exemplary zone using CUKF based on ICUT $^{\pm}$ and the proposed CUKF algorithm with $P_{x_0} = 0.25 \cdot \mathbf{I}_{n_x}$ (first row), $P_{x_0} = 0.5 \cdot \mathbf{I}_{n_x}$ (second row), $P_{x_0} = \mathbf{I}_{n_x}$ (third row), $P_{x_0} = 2 \cdot \mathbf{I}_{n_x}$ (last row). Different parameters are marked in the same way as in Fig. 3.23.

Small process noise in parameter estimation problems can lead to the negative definiteness of the covariance matrix and thus to numerical instability of the algorithm. To treat the ill-conditioning of the covariance matrix P_{x_k} its definiteness is checked before the calculation of the square root in (3.37). If the matrix is not positive definite, its closest symmetric positive definite matrix is found by minimizing the Frobenius norm of the difference [121]. In Tab. 3.3 number of steps with ill-conditioned covariance matrix, evaluated on the test-set data, is given. Results of the performance comparison demonstrate that the improved constrained UKF outperforms other algorithms, both in the convergence speed and numerical stability. Additionally, it is noted that both standard UKF and CUKF based

Table 3.3. Numerical instability count for different algorithms. Within the test each filtering algorithm is invoked overall 648 times.

Algorithm	Proposed CUKF	CUKF +ICUT [±]	UKF
$P_{x_0} = 0.25 \cdot \mathbf{I}_{n_x}$	0	9	8
$P_{x_0} = 0.50 \cdot \mathbf{I}_{n_x}$	0	26	12
$P_{x_0} = 1.00 \cdot \mathbf{I}_{n_x}$	0	30	7
$P_{x_0} = 2.00 \cdot \mathbf{I}_{n_x}$	0	21	6

on ICUT[±] suffer from bad initialization issues, i.e. choosing the wrong initial covariance matrix of the system causes large estimation errors and, in some cases, divergence of the estimation procedures. Both filters converge only when the initial uncertainty was low ($P_{x_0} = 0.25 \cdot \mathbf{I}_{n_x}$). The convergence of the EKF algorithm has been rather slow, i.e. parameters did not converge within 9 days. Both constrained approaches managed to keep the estimates within the limits while the estimates of EKF and UKF adopted negative values in certain filter steps whilst this is not physically possible. The robustness and numerical stability of the improved algorithm are clearly evident due to the demonstrated insensitivity to the bad initialization issues and zero number of the numerical instability occurrences.

3.6.4 Suitability of the developed models for prediction of the heating/cooling loads

Suitability of the developed models for prediction of building heating/cooling loads is tested by comparing the heating/cooling load estimated using the models with real measurements of heating and cooling energy on the considered two floors from January 2015 until June 2019. The building consumption data is determined by averaging the thermal consumption of the considered two floors on monthly scale. The validated models are: *i*) Trnsys model, *ii*) IDA-ICE model, *iii*) RC model and *iv*) identified semi-physical model of the considered two floors. The identified semi-physical model consists of individual zone models (see Chapter 3 Section 3.4) of all controllable zones on the 9th and 10th floor stacked into a compact model form. Heating/cooling loads of all models are estimated by simulating the thermal power required to keep the temperatures in all controllable zones on 22°C during the heating season and on 24°C during the cooling season. The cooling season starts on 1st June and ends on 30th of September. The rest of the year only heating is available. The temperature in zones is required to be equal to the selected reference temperatures only during the occupancy periods defined as stated in Tab. 3.4.

Table 3.4. Weekly occupancy schedule for simulation scenario.

	workday	Saturday	Sunday
occupancy schedule	06:00 - 18:00	06:00-15:00	-

Comparison of the simulated heating/cooling loads with real measured loads is given in Fig. 3.32. The detailed overview of the thermal energy consumption per month is given in Tab. 3.5. Since the beginning and end of the cooling season highly depend on external weather conditions all thermal energies are considered as positive to enable comparison with the simulation data.

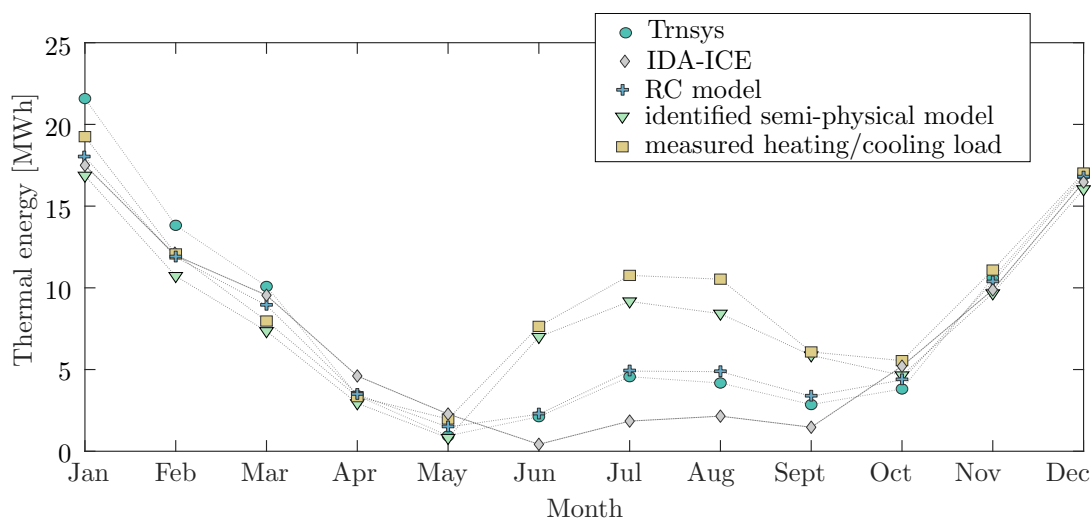
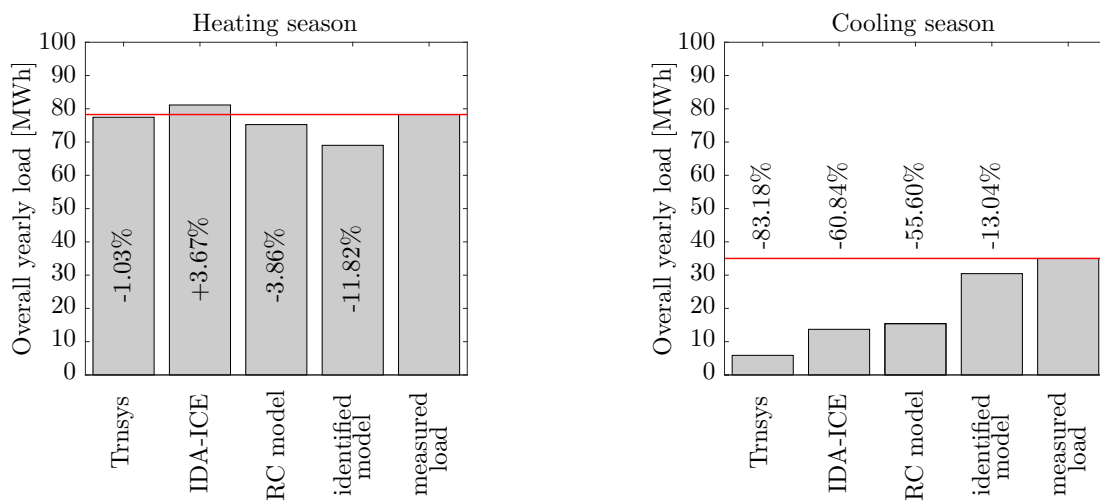


Figure 3.32. Monthly heating/cooling load of the considered two floors.

Table 3.5. Overall heating/cooling load of the considered two floors.

Month	Thermal energy consumption [MWh]				
	Trnsys model	IDA-ICE model	RC model	Identified model	Measured load
January	17.50	21.58	18.00	16.86	19.25
February	11.98	13.83	11.88	10.72	12.08
March	9.55	10.09	8.92	7.35	7.97
April	4.61	3.41	3.47	2.94	3.34
May	2.28	0.94	1.48	0.82	1.98
June	0.42	2.12	2.27	6.99	7.64
July	1.85	4.56	4.90	9.17	10.76
August	2.15	4.18	4.87	8.42	10.53
September	1.47	2.86	3.36	5.87	6.08
October	5.20	3.81	4.36	4.64	5.54
November	9.88	10.60	10.36	9.66	11.09
December	16.47	16.89	16.77	16.03	17.02
Overall:	83.35	94.86	90.65	99.47	113.28

The comparison of overall yearly heating and cooling thermal load of the building, under the assumption that the heating and cooling season in measured data starts and ends as it is considered in the simulation scenario is given in Fig. 3.33.

**Figure 3.33.** Overall heating/cooling load of the considered two floors.

Although heating load of the building is calculated within $\pm 11\%$ of deviation from the real heating load, the simulated cooling load deviates from true measurements for up to 84%. The main reasons for so large deviation are in *i*) using the TMY data rather than real measurements from the location, *ii*) omission of additional disturbance heat fluxes such as lighting, occupancy and electronic equipment which highly influence the building consumption, *iii*) using the constant occupancy schedule and setpoint temperature. Expectedly, the model identified by using the building measurements shows the best performance when utilized to predict the required heating and cooling building loads. Since the model is identified by using the real data, permanent thermal loads (e.g. computers which are constantly turned on) and additional thermal masses, like e.g. furniture, are inherently included into the model which is not the case with the other models. Consequently, when using the identified model for simulating the air temperature in the building excited only by the weather conditions over the period of one year (by using TMY data and without heating/cooling elements) the temperature span in the building is much broader than the one obtained with other models (see e.g. Fig. 3.34 for comparison of the obtained temperature span with IDA-ICE simulation).

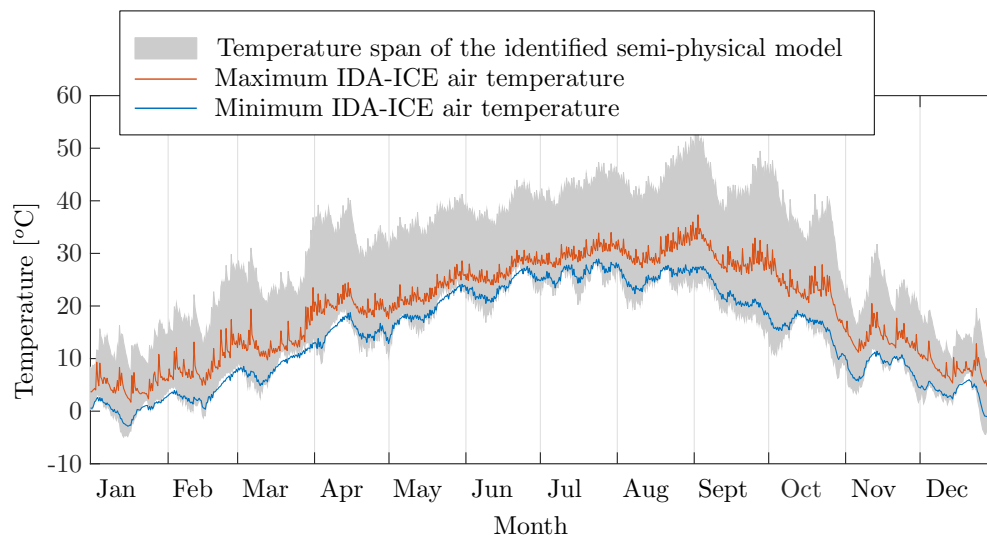


Figure 3.34. Obtained envelope of possible zone temperatures over one year.

When used for estimation of overall yearly thermal load (heating load + cooling load) the identified semi-physical model has the best performance with the real load underestimated for only 12.19%. Trnsys, IDA-ICE and RC model underestimate the overall yearly thermal load for 26.42%, 16.26% and 19.97%, respectively.

Part I conclusion and future research opportunities

The majority of modern commercial buildings are equipped with Building Energy Management Systems (BEMSs) to monitor and control different components of heating, ventilation, and air conditioning systems. Part I of the thesis encloses a methodology for the development of a control-oriented energy model for a system of fan coil units (FCUs) and mathematical model of the building, suitable for advanced model-based control algorithms. The developed models are validated on the experimental data collected from a 248-office living-lab. The proposed methodologies stand out in their simplicity, cost-effectiveness, non-invasiveness and amount of time required for model identification. The incorporation of the developed energy model for a system of FCUs into the BEMS offers several advantages such as: *i*) acquiring thermal powers per zone, *ii*) estimation of unmeasured thermal loads affecting the zone for a very broad use in building monitoring and control, *iii*) usage of an advanced control algorithm for direct control of thermal energy inputs per zone via fan speeds which makes it possible to realize optimized thermal energy inputs computed via predictive energy management schemes for maintaining zones thermal comfort and *iv*) development of fault detection and diagnosis algorithms. A reliable thermodynamic model of a building is a key for the exploitation of significant energy savings potential of model-based control algorithms in buildings. The true utility of the developed algorithm for identification of simplified building model is demonstrated by showing that the simplified building models able to make reliable 24 hours ahead predictions can be identified by using less than one week of normal operation building data. Despite the uncertainty of the input data arising as a consequence of solar irradiance and heating/cooling elements modelling errors, mean squared error for minutely sampled 24-hour long prediction was on the level of 0.3°C which proves the suitability of the identified model for control and fault detection purposes. The developed methodologies aim to fill the gap between the research and implementation by facilitating the deployment of the advanced BEMSs based on a model-based control algorithms.

Part II

Zone Model Predictive Control

Optimal zone temperature control - design

The challenging task of sustainable management of building heating and cooling systems is to assure comfort with high energy efficiency. Poor design and inefficient operation of these systems result with a significant amount of energy wastage [1, 2]. The key for rationalization of energy consumption and thus reduced energy wastage is the development of control algorithms that can effectively capture the trade-off between the user comfort and energy consumption. A Model Predictive Control (MPC) approach applied in Building Energy Management Systems (BEMSs) has been recognized as one of the most promising solutions for improving the user comfort and to achieve considerable energy savings. The estimated theoretical energy saving potential is up to 70% in particular comprehensive applications [9, 122, 123]. Recently, MPC has found its place in practice, with experimentally-validated building energy efficiency increase by 15-63% [14, 15, 16, 17, 18, 19, 20, 21, 22, 23].

The MPC is an advanced control strategy that relies on a dynamic model of the process. This way the control algorithm is designed for a particular building. The distinct advantages of the MPC compared to the conventional control algorithms are in: *i*) using the relevant future information in making control decisions; *ii*) routine handling of the multi-input multi-output (MIMO) systems; *iii*) routine respecting of system constraints (e.g. finite amount of heating/cooling power or comfort intervals) and *iv*) explicit orientation of the control actions towards the goals which can, for example, be economic, environmental or their combination. All the mentioned advantages make the MPC a favorable choice for the BEMS design. Conventional control algorithms mostly rely on a calibration of the algorithms designed for a typical building according to approximate rules of thumb or trial and error methods. The operation is commonly based on predefined constant schedules and operation modes. This often means that the controller constantly maintains certain zone temperature in order to avoid long transient periods between occupied and unoccupied zone operation, which is not optimal from the

energy viewpoint. The optimal set-back time depends on many factors such as outdoor and indoor temperatures, thermal inertia of the building, thermal power limitations, weather conditions, etc. The wastage of the energy during unoccupied period can be significantly reduced by incorporating the occupancy schedules directly into the MPC optimization problem, where based on the mathematical model of the system it is decided how early before the occupants arrival it is necessary to start heating or cooling in the zone in order to assure the requested thermal comfort during occupied hours [124].

The MPC approach that uses thermal model of the building and computes optimal thermal energy inputs in different building zones substantially differs from generally accepted temperature control via local reactive control loops where only local measurements are used when deciding on the control actions for heating/cooling elements (HCEs) in zones (fan coils, radiators, floor heating, etc.). In such a set-up, the unmodelled disturbances, such as occupancy, lighting or electronic equipment, are no longer implicitly compensated. To ensure offset-free control and to be able to compensate such disturbances, an estimator is introduced in the control loop. The realization of the optimal thermal energy inputs is then enforced by HCE interfaces acting as a link between the optimal thermal inputs and real actuation commands required for those inputs to be realized. The offset-free control is ensured through compensation of the estimated zone disturbances which are not accounted by the MPC. The advantages of the direct control of thermal energy inputs are: *i*) simple interaction with other building subsystems (e.g. smart grid or central heating, ventilation and air conditioning (HVAC) system) [13], *ii*) possibility of direct economic cost minimization by using the known price of the energy, *iii*) possibility of thermal power variance minimization lowering thus the maintenance cost for central HVAC system and reducing the peak operation costs [39], *iv*) possibility to act in tight comfort requirements where the required reference temperature following is not possible with conventional controllers, and *v*) high level of modularity and flexibility for different HCEs in zones and buildings configurations, enabling thus the fast replication of the method.

The focus of this Chapter is to demonstrate (via simulation) the improved efficiency of zone comfort control via MPC. The Chapter introduces a novel formulation of the MPC optimization criteria for optimal temperature control in buildings with high comfort demands and gives a fair comparison of the resulting MPC controller with conventional controllers with the same level of flexibility. Since the case-study building does not have the possibility for controlling the humidity or CO₂ level, within the thesis thermal comfort is managed with respect to the zone temperature only. All controllers are tested for a system with seasonal heating and cooling, which is the most common case in real applications. It is shown that the introduced optimization problem formulation leads to the MPC controller that outperforms conventional controllers both in energy consumption and users comfort even when applied to basic zone temperature control with flat energy prices and constant occupancy schedule.

The remainder of this chapter is organized as follows. In Section 5.1 short introduction to MPC applied for zone temperature control is presented. Section 5.2 gives the MPC formulation and detailed description of the optimization criterion for energy-saving and comfortable temperature control in buildings followed by an assessment of a performance bound and possible energy savings of the developed approach. Section 5.3 deals with the necessary upgrade of the developed MPC formulation required to assure offset-free control in the presence of disturbances affecting the system. In Section 5.5 an interface between the MPC for determining the optimal energy inputs into the zones and building automation system, consisted from HCEs and accompanying actuators, is presented. The development within the Section is oriented towards optimal operation of fan coil units (FCU) with adherence to the required optimal thermal energy input in zones.

5.1 Introduction to model predictive control for zone temperature control

Model predictive control is an advanced control strategy that optimizes future system behaviour by using an explicit mathematical model of the system in time domain. At each time step, optimal control problem is formulated and solved, and only the control action of the current time step is implemented on the system. In terms of building climate control this means that at the current point in time the optimal profile of the thermal energy consumption over the prediction horizon is calculated based on predictions of upcoming weather conditions and other available predictions which influence the building behaviour. Schedules (e.g. building occupancy schedules), time-dependencies of the control cost (e.g. volatile energy prices), or the constraints (e.g. physical system limitations) can be readily included into the optimization. Only the first step of the optimal energy profile is implemented and the optimization problem is re-solved at the next time step, using the new measured values of the system variables. By this receding horizon feedback is introduced into the system (Fig. 5.1).

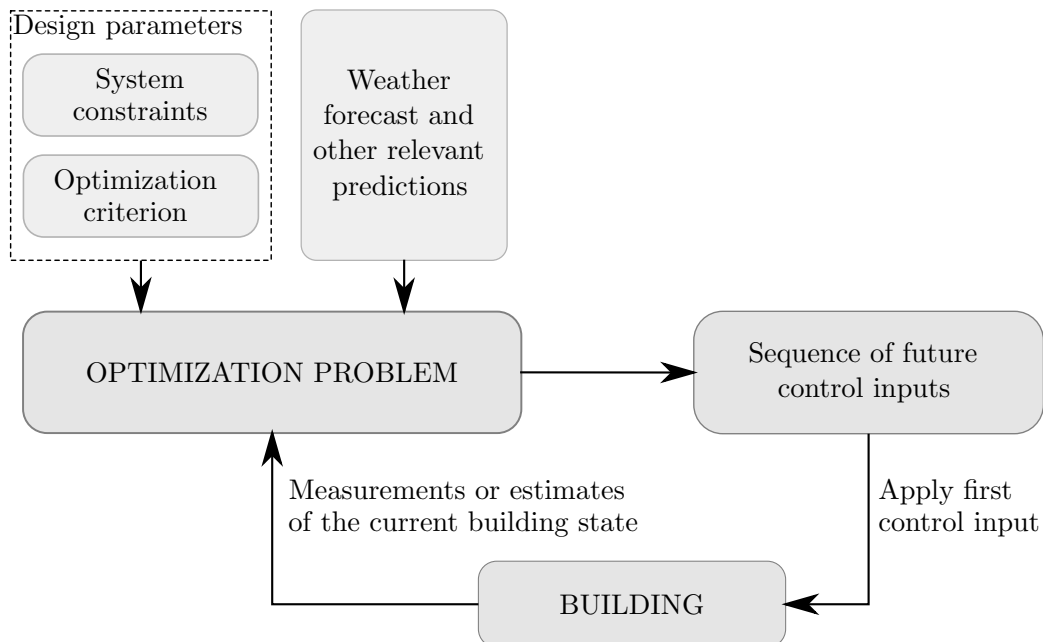


Figure 5.1. MPC scheme for building comfort control.

The MPC optimization problem can be formulated in the following way:

$$\begin{aligned} \min_{u_0, \dots, u_{H-1}} \quad & \sum_{k=0}^{H-1} l(x_k, u_k) \\ \text{s.t.} \quad & x_{k+1} = f(x_k, u_k, d_k), \\ & g(x_k, u_k, d_k) \leq 0, \\ & h(x_H) \leq 0, \end{aligned} \tag{5.1}$$

where x_k , u_k and d_k denote, respectively, values of system states, inputs and disturbances predicted at step k of the prediction horizon H . The prediction of the system behaviour is obtained from the prediction model $f(x_k, u_k, d_k)$. The term $l(x_k, u_k)$ is called a stage cost and its purpose is to assign a cost to a particular choice of x_k and u_k . For a specific disturbance profile and initial system state x_0 , the optimization (5.1) yields the sequence of control inputs that are optimal with respect to the defined cost,

$$\mathbf{u}^* = [(u_0^*)^\top \quad (u_1^*)^\top \quad \dots \quad (u_{H-1}^*)^\top]^\top. \tag{5.2}$$

Only the first element of that sequence, i.e. u_0^* , is applied to the plant and the procedure is repeated at the next sampling time interval. In the sequel, bold notation is used to denote variables stacked over the prediction horizon and '*' in the superscript denotes optimal values obtained by optimization.

Computational complexity of obtaining the optimal sequence depends on the type of the prediction model employed in (5.1) and on the type of the cost function and the constraints. Over the years different variations of the nominal MPC such as distributed [125], decentralized [126], nonlinear [124], robust [127] and stochastic [29, 128] are developed in order to achieve the maximal efficiency and/or robustness of the control algorithm. The recent studies on MPC applied for zone temperature control are divided into two categories. The optimization criteria used in a first category of studies is mainly focused on minimizing the use and cost of energy, while the zone temperature is constrained to be within a permissible comfort interval [129]. Productivity of occupants in commercial buildings depends largely on comfort levels, but also on lots of the subjective factors [95, 130], so a second category of studies focuses not only on controlling the energy consumption for reducing cost but also on user comfort. The comfort is typically included directly into the optimization criteria through penalization of temperature deviation from user defined temperature reference [131] or more complex metric for defining the user comfort is used (e.g. Predicted Mean Vote index (PMV)) [130, 3]. The MPC temperature control approach developed within the thesis allows the individual setting of comfort level with the aim of user satisfaction and increased productivity rather than achieving additional energy savings.

5.2 Model predictive control for energy-savings and comfortable temperature control

Mathematical model of a building is a basis for MPC implementation. The benefits and drawbacks of different building modelling approaches are analysed within Chapter 3. Zone temperature dynamics is described with linear state-space model of the following form:

$$\begin{aligned} x_{k+1} &= A^d x_k + B_d^d d_k + B_u^d u_k, \\ y_k &= C^d x_k, \end{aligned} \quad (5.3)$$

where $x_k \in \mathbb{R}^{n_x}$ denotes system state vector, $y_k \in \mathbb{R}^{n_y}$ is an output vector consisted of zone temperatures, $u_k \in \mathbb{R}^{n_u}$ is a vector of thermal energy inputs from controllable heating/cooling elements into each of n_y controllable zones and $d_k \in \mathbb{R}^{n_d}$ is the disturbance input (outside temperature, solar irradiance, internal gains, temperatures of adjacent rooms, etc.). Matrices A^d , B_d^d , B_u^d and C^d are of appropriate dimensions and are obtained either based on first principles modelling or by use of identification methods (see Chapter 3, Section 3.4).

The MPC uses the dynamic model of the building and information on the future disturbance profiles to predict future building behaviour and, based on these predictions, computes the optimal control input trajectory. Predicted states and outputs along the prediction horizon $H \in \mathbb{N}$ are conveniently written as:

$$\mathbf{y} = \boldsymbol{\alpha} x_{k|k} + \boldsymbol{\beta} \mathbf{u} + \boldsymbol{\gamma} \mathbf{d}, \quad (5.4)$$

where \mathbf{y} is a stack of future outputs:

$$\mathbf{y} = [y_{k+1|k}^\top \quad y_{k+2|k}^\top \quad \cdots \quad y_{k+H|k}^\top]^\top, \quad (5.5)$$

\mathbf{u} is a stack of future inputs:

$$\mathbf{u} = [u_{k|k}^\top \quad u_{k+1|k}^\top \quad \cdots \quad u_{k+H-1|k}^\top]^\top, \quad (5.6)$$

vector \mathbf{d} is a stacks of future disturbances:

$$\mathbf{d} = [d_{k|k}^\top \quad d_{k+1|k}^\top \quad \cdots \quad d_{k+H-1|k}^\top]^\top, \quad (5.7)$$

$x_{k|k} \in \mathbb{R}^{n_x}$ is current system state and $\boldsymbol{\alpha}$, $\boldsymbol{\beta}$ and $\boldsymbol{\gamma}$ are matrices based on the discrete-time building model matrices (5.3). Subscript $k+j|k$ denotes prediction at time k for a time step $k+j$, $j \in \mathbb{N}$, e.g. $y_{k+j|k}$ denotes predicted zones temperature at time $k+j$, obtained by applying the input sequence \mathbf{u} to the system starting from current system state $x_{k|k}$ up to the moment $k+j$.

The most frequent MPC problem formulation for temperature control in buildings consists of a simplistic minimization of energy consumption with respect to the temperature constraints set by the end-users and physical limitations of heating/cooling elements [129]:

$$\begin{aligned}
\min_{\mathbf{u}} \quad & \|\mathbf{u}\|_1 \\
\text{s.t.} \quad & \mathbf{y} = \boldsymbol{\alpha}x_{k|k} + \boldsymbol{\beta}\mathbf{u} + \boldsymbol{\gamma}\mathbf{d}, \\
& \mathbf{y}_{\min} \leq \mathbf{y} \leq \mathbf{y}_{\max}, \\
& \mathbf{u}_{\min} \leq \mathbf{u} \leq \mathbf{u}_{\max},
\end{aligned} \tag{5.8}$$

where operator $\|\cdot\|_1$ denotes L_1 norm, \mathbf{y}_{\min} and \mathbf{y}_{\max} are lower and upper bounds of zone temperature, while \mathbf{u}_{\min} and \mathbf{u}_{\max} are minimum and maximum attainable thermal powers \mathbf{u} . Although in general, the sensitivity is higher for L_1 norm optimization cost (leading to Linear Program (LP)) than for problems with a quadratic L_2 norm (leading to Quadratic Program (QP)), the LP is preferred since the energy bill is directly proportional to the optimization cost. Initial system state $x_{k|k}$ is measured or provided by means of Kalman filter if all system states are not measurable. The MPC formulation (5.8) handles users temperature constraints as hard constraints, which often results in infeasibility, especially when sign change of \mathbf{u} is not possible (only heating or only cooling available at certain time step). To solve the problem, temperature constraints are "softened" by introducing them into the cost function through slack variables $\sigma_k \in \mathbb{R}^{n_y}$. Slack variables are additional decision variables that are heavily penalized through non-negative weight g in situations when zone temperature reaches upper or lower temperature bounds (e.g. $g = 10^6$). The resulting optimization problem is as follows:

$$\begin{aligned}
\min_{\mathbf{u}, \boldsymbol{\sigma}} \quad & \|\mathbf{u}\|_1 + g\mathbf{1}^\top \boldsymbol{\sigma}, \\
\text{s.t.} \quad & \mathbf{y} = \boldsymbol{\alpha}x_{k|k} + \boldsymbol{\beta}\mathbf{u} + \boldsymbol{\gamma}\mathbf{d}, \\
& \mathbf{y}_{\min} - \boldsymbol{\sigma} \leq \mathbf{y} \leq \mathbf{y}_{\max} + \boldsymbol{\sigma}, \\
& \mathbf{u}_{\min} \leq \mathbf{u} \leq \mathbf{u}_{\max}, \\
& \boldsymbol{\sigma} \geq 0,
\end{aligned} \tag{5.9}$$

where $\mathbf{1}^\top$ is appropriately sized row vector of ones. Bold notation for optimizer $\boldsymbol{\sigma}$ stands for vectors stacked over the prediction horizon H .

In most situations, occupants want the exact temperature to the one they have chosen on the zone thermostat. This is ensured by defining the MPC problem as a classic reference tracking problem:

$$\begin{aligned}
\min_{\mathbf{u}, \sigma} \quad & \mathbf{r}^\top |\mathbf{u}| + \mathbf{q}^\top |\mathbf{y}^{\text{ref}} - \mathbf{y}| + g \mathbf{1}^\top \sigma, \\
\text{s.t.} \quad & \mathbf{y} = \boldsymbol{\alpha} x_{k|k} + \boldsymbol{\beta} \mathbf{u} + \boldsymbol{\gamma} \mathbf{d}, \\
& \mathbf{y}_{\min} - \sigma \leq \mathbf{y} \leq \mathbf{y}_{\max} + \sigma, \\
& \mathbf{u}_{\min} \leq \mathbf{u} \leq \mathbf{u}_{\max}, \\
& \sigma \geq 0.
\end{aligned} \tag{5.10}$$

where operator $|\cdot|$ denotes absolute value which is applied element-wise on the vector, weights $\mathbf{r} \in \mathbb{R}^{H \cdot n_u}$ and $\mathbf{q} \in \mathbb{R}^{H \cdot n_y}$ penalize the energy consumption and deviation from the temperature reference, respectively. The temperature reference between step k and $k + 1$, $\mathbf{y}_k^{\text{ref}} \in \mathbb{R}^{n_y}$, is defined as:

$$\mathbf{y}_k^{\text{ref}} = [T_{a,1,k}^{\text{ref}} \quad T_{a,2,k}^{\text{ref}} \quad \dots \quad T_{a,n_y,k}^{\text{ref}}]^\top, \tag{5.11}$$

where $T_{a,i,k}^{\text{ref}}$ is temperature reference in the i^{th} zone. The MPC formulation (5.10), combined with a receding horizon strategy, often results in either minimum energy performance at the cost of completely disregarded temperature comfort or in permanent reference following with disregarded energy consumption. A compromise between the two options is made through the mentioned weights, \mathbf{r} and \mathbf{q} .

To tackle the opposing criteria of energy savings and reference following, weights \mathbf{r} and \mathbf{q} have to be chosen in a way which enables smart switching between these two requirements based on predicted disturbance profiles. To be comparable, both parts of optimization cost have to be expressed in the same or similar units. Since the first part of the optimization criterion (5.10) is related to thermal power and it is thus defined in watts, weight of the temperature related part of the optimization criterion (5.10) is selected such that it makes deviation from the reference expressed in degrees Celsius comparable to the first part of the criterion. The amount of energy which can be saved by allowing the zone temperature to slide below the temperature reference during the heating season or above the reference during the cooling season, under the same weather conditions, is linear function of system dynamics. Sensitivity of the energy consumption to the zone temperature is defined as:

$$\frac{\partial \mathbf{u}}{\partial \mathbf{y}} = \frac{\partial (\boldsymbol{\beta}^{-1} (\mathbf{y} - \boldsymbol{\alpha} x_{k|k} - \boldsymbol{\gamma} \mathbf{d}))}{\partial \mathbf{y}} = \boldsymbol{\beta}^{-1}. \tag{5.12}$$

Matrix $\boldsymbol{\beta}^{-1}$ is lower bidiagonal matrix with all elements on the main diagonal equal to $(C^d \cdot B_u^d)^{-1}$ and to the $-((B_u^d)^{-1} \cdot A^d \cdot (C^d)^{-1})$ on the secondary diagonal.

Optimization cost which considers both energy and comfort and enables easy switching between these two requirements is as follows:

$$\begin{aligned}
& \min_{\mathbf{u}, \boldsymbol{\sigma}_1, \boldsymbol{\sigma}_2} \quad |\mathbf{u}|_1 + \gamma_e \cdot \boldsymbol{\delta}^\top \cdot |\mathbf{Q}(\mathbf{y}^{\text{ref}} - \mathbf{y})| + g_1 \mathbf{1}^\top \boldsymbol{\sigma}_1 + g_2 \mathbf{1}^\top \boldsymbol{\sigma}_2, \\
& \text{s.t.} \quad \mathbf{y} = \boldsymbol{\alpha} x_{k|k} + \boldsymbol{\beta} \mathbf{u} + \boldsymbol{\gamma} \mathbf{d}, \\
& \quad \mathbf{y}^{\text{ref}} - \boldsymbol{\Delta}^{\text{ref}} - \boldsymbol{\sigma}_1 \leq \mathbf{y} \leq \mathbf{y}^{\text{ref}} + \boldsymbol{\Delta}^{\text{ref}} + \boldsymbol{\sigma}_2 \\
& \quad \mathbf{u}_{\min} \leq \mathbf{u} \leq \mathbf{u}_{\max}, \\
& \quad \boldsymbol{\sigma}_1 \geq \mathbf{0}, \quad \boldsymbol{\sigma}_2 \geq \mathbf{0},
\end{aligned} \tag{5.13}$$

where weighting matrix $\mathbf{Q} \in \mathbb{R}^{(H \cdot n_u) \times (H \cdot n_u)}$ is selected to be equal to sensitivity of energy consumption to the zone temperature (5.12), i.e. $\mathbf{Q} = \boldsymbol{\beta}^{-1}$. The non-negative parameter γ_e is introduced for easy trade-off possibility between the comfort and energy savings parts. The comfort is defined with temperature reference \mathbf{y}^{ref} and acceptable temperature deviation from the temperature reference $\boldsymbol{\Delta}_k^{\text{ref}} \in \mathbb{R}^{n_y}$ where $\boldsymbol{\Delta}^{\text{ref}}$ is stack of the acceptable deviations along the prediction horizon. Slack variables $\boldsymbol{\sigma}_1$ and $\boldsymbol{\sigma}_2$ guarantee temperature within the permissible interval. Different weights $g_1 \neq g_2$ enable asymmetric penalization of upper and lower temperature limit violations (e.g. penalization of lower temperature bound violation is higher during the heating season). The vector $\boldsymbol{\delta}_k \in \mathbb{R}^{n_y}$ is zone occupancy vector, where i^{th} element presents occupancy profile for the i^{th} zone, $\delta_{k,i} \in \{0, 1\}$ defined as:

$$\delta_{k,i} = \begin{cases} 1, & \text{if } i^{\text{th}} \text{ zone is occupied at time step } k + j, \\ 0, & \text{if } i^{\text{th}} \text{ zone is unoccupied at time step } k + j. \end{cases} \tag{5.14}$$

During occupancy periods the deviation $\boldsymbol{\Delta}^{\text{ref}}$ can be set individually or one common value can be set for all zones in the building. Typical values are in interval $[0, 1.5]^\circ\text{C}$. During unoccupied periods, there are no strict requirements on users comfort ($\delta_{k,i} = 0$) so the focus is put solely on energy consumption part of the criterion (5.13) and keeping the minimal temperature requirements, assured by matching building protect temperature limits with the allowed temperature span. The temperature related part of the optimization criterion (5.13), for prediction horizon $H = 1$, can be interpreted as four-segmented convex PieceWise Affine (PWA) penalty function (Fig. 5.2).

Weighting factor γ_e determines the importance of reference tracking with respect to the minimization of energy consumption (Fig. 5.3). For $\gamma_e = 1$ both energy consumption and reference tracking have the same weights so the controller will decide what is best from the energy viewpoint. Energy savings are therefore solely the result of the predictive control property and ahead knowledge of weather and possibly other available forecasts (e.g. occupancy or reference changes). With $\gamma_e < 1$, the controller maintains the temperature at the temperature boundary most of the time and large energy savings are directly a result of the deviation from the reference. For $\gamma_e > 1$ the control focus is

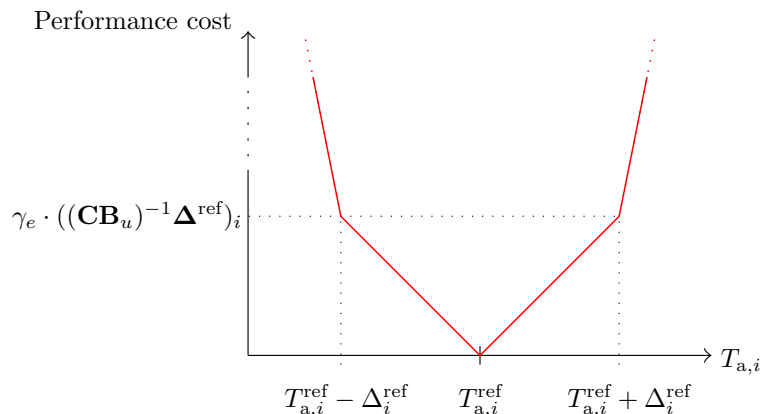


Figure 5.2. Convex PWA penalty function for the i^{th} zone, $H = 1$ and $\delta = 1$.

put on following the reference even if such behaviour will lead to the increased energy consumption.

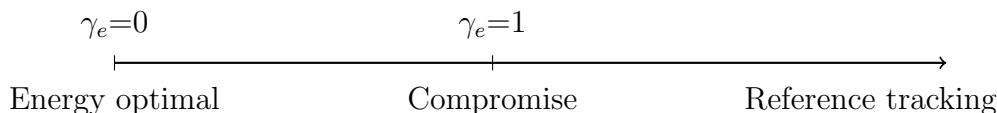


Figure 5.3. Dependence between weighting factor γ_e and system performance.

The performance of the MPC using optimization criterion (5.13) in the heating season highly penalizes solar irradiance influence that can result in overheating, which adversely forces the system to minimize overheating, i.e. to use the free energy from outdoors starting from the lower edge of the allowed range. Effectively, the heating/cooling elements are controlled such that the lower bound of the temperature range is reached prior to the stream of free energy from outdoors. In the cooling season system is forced to quit cooling the zone when free cooling can be utilized.

The optimization problem (5.13) is easily transformed from energy-optimal to price-optimal by introducing the energy price $c_{t,k} \in \mathbb{R}^{n_y}$ into the optimization problem such that:

$$\begin{aligned}
 \min_{\mathbf{u}, \boldsymbol{\sigma}_1, \boldsymbol{\sigma}_2} \quad & \mathbf{c}_t^\top |\mathbf{u}| + \gamma_e \cdot c_c \cdot \boldsymbol{\delta}^\top |\mathbf{Q}(\mathbf{y}^{\text{ref}} - \mathbf{y})| + g_1 \mathbf{1}^\top \boldsymbol{\sigma}_1 + g_2 \mathbf{1}^\top \boldsymbol{\sigma}_2, \\
 \text{s.t.} \quad & \mathbf{y} = \boldsymbol{\alpha} x_{k|k} + \boldsymbol{\beta} \mathbf{u} + \boldsymbol{\gamma} \mathbf{d}, \\
 & \mathbf{y}^{\text{ref}} - \boldsymbol{\Delta}^{\text{ref}} - \boldsymbol{\sigma}_1 \leq \mathbf{y} \leq \mathbf{y}^{\text{ref}} + \boldsymbol{\Delta}^{\text{ref}} + \boldsymbol{\sigma}_2 \\
 & \mathbf{u}_{\min} \leq \mathbf{u} \leq \mathbf{u}_{\max}, \\
 & \boldsymbol{\sigma}_1 \geq 0, \quad \boldsymbol{\sigma}_2 \geq 0,
 \end{aligned} \tag{5.15}$$

where $\mathbf{c}_t \in \mathbb{R}^{H \cdot n_u}$ is the thermal energy cost important for enabling coordination of zone level with higher-level building modules, such as central HVAC system or microgrid [38, 13] and $c_c \in \mathbb{R}^1$ is the cost associated to thermal comfort.

5.3 Optimal zone temperature control in the presence of unmeasurable states and disturbances

Closed-loop performance of MPC algorithm is directly related to the model accuracy. In practice, modelling errors and unmeasured disturbances can lead to steady-state offset unless precautions are taken in the control system design [132, 133]. A general approach to eliminate steady-state offset involves augmenting the process model to include constant step disturbance. The heat disturbances affecting the zone temperature indicate any additional heat input or sink compared to the current building model used for control (occupants, equipment, window blinds, etc.). To account the impact of the disturbance to the zone temperature along the prediction horizon, zone model developed in Chapter 3 Section 3.4 is augmented with an additive disturbance input P_d such that

$$\begin{bmatrix} \dot{T}_a \\ \dot{T}_z \end{bmatrix} = A^c \begin{bmatrix} T_a \\ T_z \end{bmatrix} + \begin{bmatrix} B^c & \begin{bmatrix} p_6 \\ 0 \end{bmatrix} \end{bmatrix} \begin{bmatrix} T_{\text{out}} \\ I_{\theta}^{\text{diff}} \\ I_{\theta}^{\text{dir}} \\ P_a \\ P_d \end{bmatrix}, \quad (5.16)$$

where T_a is the temperature of air inside the zone, T_z is the slow dynamics temperature, matrices $A^c \in \mathbb{R}^{n_x \times n_x}$ and $B^c \in \mathbb{R}^{n_x \times (n_u + n_d)}$ are continuous-time system matrices of the identified simplified zone model (3.30), and $p_6 \in \mathbb{R}^1$ is the parameter of system input matrix B^c related to the impact of the thermal load of the HCEs to the zone, e.g. radiator or FCU thermal load, noted as P_a . Due to the similar nature of thermal inputs P_a and P_d , their impact on the zone temperature is modelled with the same parameter. Outside air temperature is denoted as T_{out} while I_{θ}^{diff} and I_{θ}^{dir} are diffuse and direct solar irradiances incident on the exterior zone surface. The anticipation of the unmeasured heat load affecting the zone temperature is performed in three stages: *i*) online estimation of disturbance heat input, *ii*) prediction of the disturbance heat inputs along the prediction horizon, *iii*) optimization of the building performance regarding the predicted disturbance heat inputs.

Slow dynamics temperature T_z represents a substitute variable for all higher thermal capacity element temperatures (e.g. walls and furniture). As such, it is hardly measurable and has to be estimated online. In order to estimate the slow dynamic state T_z and disturbance input P_d , building model is augmented with a disturbance heat influence and disturbance propagation model:

$$\begin{bmatrix} \dot{T}_a \\ \dot{T}_z \\ \dot{P}_d \end{bmatrix} = \begin{bmatrix} A^c & \begin{bmatrix} p_6 \\ 0 \\ 0 \end{bmatrix} \\ \begin{bmatrix} 0 & 0 \end{bmatrix} & 0 \end{bmatrix} \begin{bmatrix} T_a \\ T_z \\ P_d \end{bmatrix} + \begin{bmatrix} B^c \\ \mathbf{0} \end{bmatrix} \begin{bmatrix} T_{\text{out}} \\ I_\theta^{\text{diff}} \\ I_\theta^{\text{dir}} \\ P_a \end{bmatrix}. \quad (5.17)$$

The estimation of unmeasurable system states and disturbance heat inputs is in a form of a linear estimation problem, so a classical linear Kalman filter is applied on the discretised augmented model. Separate estimation of the heat disturbance enables a possibility to tune models for heat disturbance predictions and exploit them for efficiency gains in predictive zone control (Fig. 5.4).

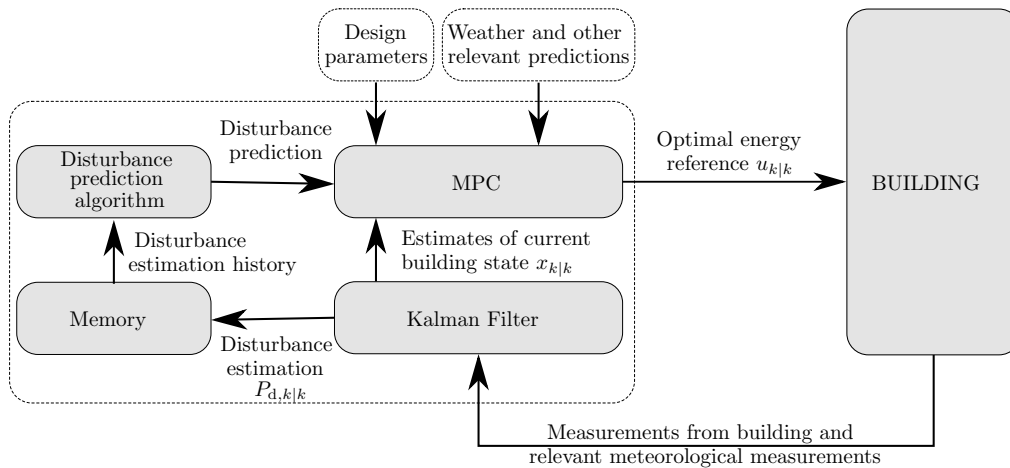


Figure 5.4. MPC control scheme for offset-free zone temperature control.

5.4 Simulation case-study for assessment of a performance bound and possible energy savings

The case-study building is described in detail in Appendix A. All controllers are employed to control directly the thermal powers required to achieve the desired temperature behaviour. Lower-level controllers required to calculate direct control actions on HCEs installed in zones, necessary for implementation of the developed MPC approach are not considered, instead it is assumed that power references can be tracked perfectly. The identified semi-physical model of the case-study building consists of identified second-order models (see Chapter 3 Section 3.4) of all 248 controllable zones ($n_y = 248$) stacked into compact model form:

$$\begin{aligned} \dot{x} &= A^c x + B_d^c d + B_u^c u, \\ y &= Cx \end{aligned} \quad (5.18)$$

where $x \in \mathbb{R}^{n_x}$ ($n_x=496$) is a stacked vector of zone fast- and slow-dynamics states $T_{a,i}$ and $T_{z,i}$, respectively, with $i = 1, 2, \dots, n_y$:

$$x = \begin{bmatrix} T_{a,1} & T_{a,2} & \cdots & T_{a,n_y} & T_{z,1} & T_{z,2} & \cdots & T_{z,n_y} \end{bmatrix}^\top, \quad (5.19)$$

$y \in \mathbb{R}^{n_y}$ is output vector consisted from zone fast-dynamics states which correspond to zone temperatures, $u \in \mathbb{R}^{n_u}$ ($n_u = 248$) is a vector of thermal energy inputs $P_{a,i}$ into each of n_y controllable zones

$$u = \begin{bmatrix} P_{a,1} & P_{a,2} & \cdots & P_{a,n_y} \end{bmatrix}^\top, \quad (5.20)$$

and $d \in \mathbb{R}^{n_d}$ ($n_d = 9$) is a vector of disturbances affecting the building temperature behaviour:

$$d = \begin{bmatrix} T_{\text{out}} & I_N^{\text{diff}} & I_E^{\text{diff}} & I_S^{\text{diff}} & I_W^{\text{diff}} & I_N^{\text{dir}} & I_E^{\text{dir}} & I_S^{\text{dir}} & I_W^{\text{dir}} & P_{d,1} & P_{d,2} & \cdots & P_{d,n_y} \end{bmatrix}, \quad (5.21)$$

where T_{out} is outside air temperature, I^{diff} and I^{dir} are diffuse and direct solar irradiances incident on the exterior zone surface and $P_{d,i} \in \mathbb{R}^1$ is heat disturbance input affecting i^{th} controllable zone. The irradiances on the surfaces oriented towards north, east, south and west are denoted with letters N, E, S, W in subscript, respectively. Positive values of u represent heating, while negative u stands for cooling. Continuous-time system matrix $A^c \in \mathbb{R}^{n_x \times n_x}$ and input matrices, $B_u^c \in \mathbb{R}^{n_x \times n_u}$ and $B_d^c \in \mathbb{R}^{n_x \times n_d}$, are constructed from continuous-time matrices of augmented identified simplified models of individual zones (5.16). To utilize known prediction of the external weather temperature T_{out} , influence of outside air temperature is discretised by employing first-order hold while the rest of the system is discretised by zero-order hold.

The resulting discrete-time system is as follows:

$$x_{k+1} = A^d x_k + B_d^d d_k + B_d^{d*} T_{\text{out},k+1} + B_u^d u_k, \quad (5.22)$$

$$y_k = C^d x_k,$$

where A^d , B_u^d , B_d^{d*} and B_d^d are appropriately sized matrices.

Data used for external conditions (outside air temperature and solar irradiances) are typical meteorological year (TMY) data for the building location (see Chapter 3, Fig. 3.14). The focus here is put on deterministic MPC with perfect knowledge of building thermal dynamics and future weather conditions while all other disturbances, including heat disturbance inputs $P_{d,i}$, are neglected. For real building implementations, with a lot of uncertain and unpredictable disturbances, their compensation is performed by introducing an estimator into the control loop (see Section 5.3). To assess energy and cost saving possibilities of different controllers, mutual ground has to be established for a fair comparison. Two main identifiers are usually observed: energy spent and comfort indicators. For the comparison, the following zone temperature controllers are considered:

1. *Proportional-integral (PI) controller.* Conventional PI controller represents a typical decentralized control approach which can be found in many building applications [134]. Building components using PI control are thermostats and thermostatic valves. Comparison with PI controller will give the baseline for energy consumption since PI controller ensures tracking of user temperature reference all the time when it is possible. The PI controller is implemented in standard closed-loop fashion as discrete-time controller with sampling time 30 s. The synthesis of PI controller is performed automatically within the MATLAB environment to ensure the best performance regarding reference tracking [70].
2. *Hysteresis controller (HYSC).* The HYSC is the most typical controller found in buildings with FCUs. The HYSC controller switches between available power outputs based on the temperature difference between current zone temperature T_a and temperature reference T_a^{ref} (Fig. 5.5). Hysteresis width $2\Delta^{\text{ref}}$ is predefined and equal for all zones. The amount of power in certain fan speed depends on the temperature and mass flow of the heating/cooling medium and is considered as constant for all zones. The HYSC controller is implemented in standard closed-loop fashion as discrete-time controller with sampling time 30 s.
3. *MPC controller for high comfort demands (cMPC).* The considered cMPC controller is based on the presented mathematical model of the building and optimization problem formulation (5.13) with $\gamma_e = 1$. Possible energy savings arise from the predictive knowledge of heat distribution thorough the building, occupancy information (working hours) and weather forecast such that unnecessary energy consumption is avoided.

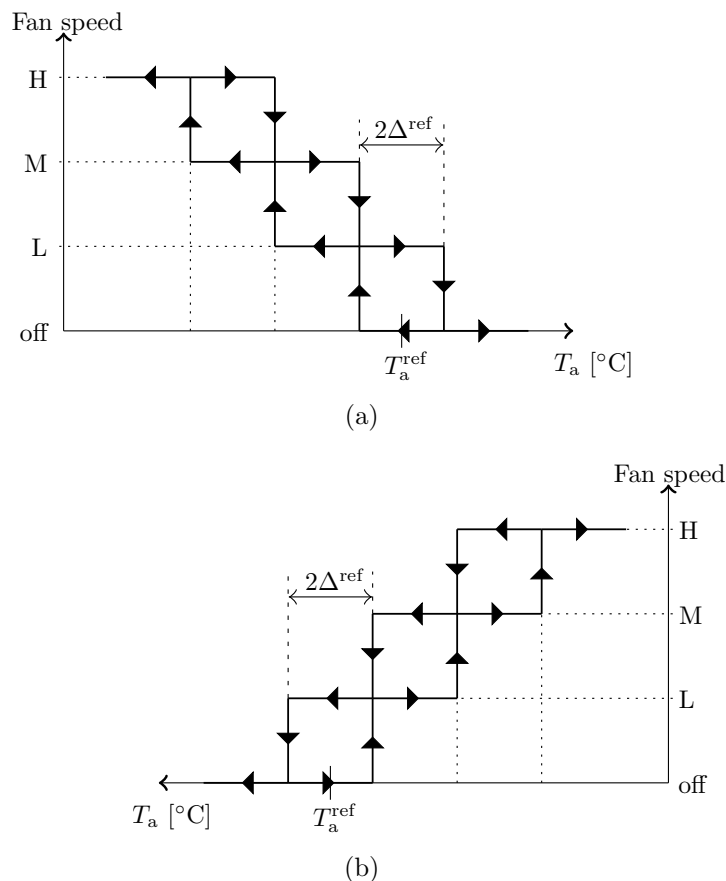


Figure 5.5. Hysteresis control law for the FCU fan speed control during a) heating season, b) cooling season.

4. *MPC controller with focus put on energy consumption (eMPC).* The considered eMPC controller is, just as cMPC controller, based on the presented mathematical model of the building and optimization problem formulation (5.13). The focus is put only on energy consumption by setting the energy-comfort parameter to $\gamma_e = 0$.

The temperature reference is followed only during periods when building is occupied. For a fair comfort level comparison, the PI controller and HYSC are switched 1 hour before the start of the occupancy period to meet the comfort requirements in occupancy periods in time. The optimization horizon of all MPC controllers is 24 h long with 15-min sampling time. Temperature references are set according to comfort guidelines from [135] to 22°C in the heating season and to 24°C in the cooling season. The allowed temperature deviation from the reference Δ^{ref} is set to 0.5°C, 1.0°C and 1.5°C, which is within the limits of cyclic temperature variations of A and B class of the thermal environment defined by ISO 7730 standard [136]. For a fair comparison, the allowed temperature deviation Δ^{ref} is matched with HYSC hysteresis width. For the considered scenario, only heating or only cooling is available at a certain moment. This corresponds to standard two pipe implementation of heating/cooling system present in many buildings. The cooling season starts on 1st June and lasts until 1st October. The zone occupancy schedule is equal for all zones and is

defined as:

$$\delta_{k+j|k,i} = \begin{cases} 1, & \text{if } k+j \text{ is within the interval } [7:00, 19:00] \text{ h,} \\ 0, & \text{if } k+j \text{ is outside of the interval } [7:00, 19:00] \text{ h.} \end{cases} \quad (5.23)$$

During unoccupied intervals the temperature is kept within the building protect limits defined as $22 \pm 6^\circ\text{C}$ in the heating season and $24 \pm 6^\circ\text{C}$ in the cooling season.

Physical limitations on maximum and minimum attainable thermal powers, put in the form of thermal energy constraints are obtained from the FCU models identified in Chapter 2. The highest attainable thermal power of the individual FCU is defined with the following algebraic equation:

$$u_H = \frac{2q_w c_w U_o^H}{2q_w c_w + U_o^H} (T_w^{\text{in}} - T_a) \quad (5.24)$$

where q_w is the medium mass flow through the unit, c_w is heat capacity of the heating/cooling medium, T_w^{in} is the FCU supply temperature, T_a is air temperature in the zone and U_o^H is overall heat transfer coefficient for highest FCU fan speed defined as:

$$U_o^H = \frac{a_{fc}^H}{1 + b_{fc}^H q_w^{-c_{fc}}}, \quad (5.25)$$

where a_{fc}^H , b_{fc}^H and c_{fc} are known parameters found through identification as described in Chapter 2. The FCU medium mass flow and supply temperature defined in Tab. 5.1 are assumed to be equal for all FCUs.

Table 5.1. Heating/cooling medium conditions for individual FCU.

	$\delta_{k+j k}$	$T_w^{\text{in}} [^\circ\text{C}]$	$q_w [\text{kg/s}]$
Heating season	1	60	0.032
	0	40	0.032
Cooling season	1	7	0.088
	0	-	0

Although the lowest thermal power of the individual FCU is defined by the natural convection of air around the unit with FCU's fan switched off, in the considered simulation case-study it is set to zero in order not to focus on thermal energy consumption which is unavoidable in standard operation of the case-study building. Thus, during the cooling season, the thermal power limits are set by replacing the minimum attainable thermal power u_{min} with u_H and setting u_{max} to zero vector of appropriate size. In the heating season, the thermal power limits are set by replacing the maximum attainable thermal power u_{max} with u_H and setting u_{min} to zero vector of appropriate size. In zones with multiple FCUs thermal power limits are calculated as superposition of individual FCU thermal power limitations.

5.4.1 Simulation case-study results

All simulations are performed within MATLAB environment [70, 137]. An overview of overall energy consumption during one year operation, for different types of control, different flexibilities Δ^{ref} and different weights γ_e is given in Tab. 5.2. Graphical illustration of results is given in Fig. 5.6. The results are given for $\gamma_e = 0$ and $\gamma_e = 1$ (cMPC and eMPC), but simulations with $\gamma_e \in \{0.5, 0.75, 1.1, 1.5\}$ yielded results with less than 1% difference.

Table 5.2. Overall energy consumption during the one year operation, for different types of control and different user flexibilities.

Controller	Season	Thermal energy [MWh]		
		$\Delta^{\text{ref}} = 0.5^\circ\text{C}$	$\Delta^{\text{ref}} = 1.0^\circ\text{C}$	$\Delta^{\text{ref}} = 1.5^\circ\text{C}$
PI	heating	454.78		
	cooling	177.08		
HYSC	heating	449.73	441.20	431.78
	cooling	173.72	168.06	168.06
cMPC	heating	446.10	443.46	162.38
	cooling	173.32	174.41	175.39
eMPC	heating	430.38	410.83	391.69
	cooling	166.82	157.00	147.52

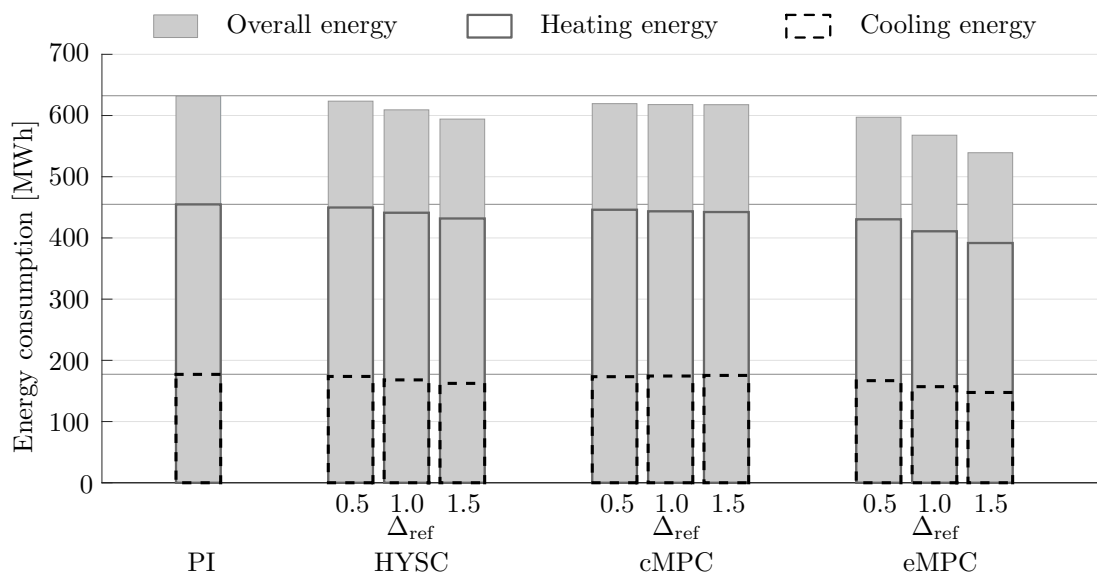


Figure 5.6. Overall energy consumption during one year operation, for different types of control, different flexibilities Δ^{ref} and different weights γ_e .

The overall energy consumption reflect the overall thermal energy needs for all 248 controllable zones. Within the simulation case-study only thermal energy that should be provided to zones is considered. Thermal energy demand of other zones which are considered as non-controllable, electrical energy consumption of the FCUs' fans and

thermal energy losses, which normally occur during transmission of the medium from the central system for its conditioning to the building zones, are not considered. The validity of the obtained results is confirmed through the comparison with the measured thermal energy consumption of the case-study building during 2014. For measuring the thermal energy consumption in 2014 one common heat meter was used for measuring both the heat consumption of radiators with 181 kW of installed power and FCUs with 573 kW of installed power. The estimated FCUs thermal energy consumption of 465 MWh is obtained by multiplying the overall measured thermal consumption with the ratio of the installed FCUs thermal power in overall installed thermal power (FCUs + radiators). The obtained simulation results are in close proximity to the measured thermal energy demand confirming the validity of the performed case-study. The obtained percentage savings of thermal energy demand in the heating and cooling season calculated relative to the PI configuration are given in Fig. 5.7.

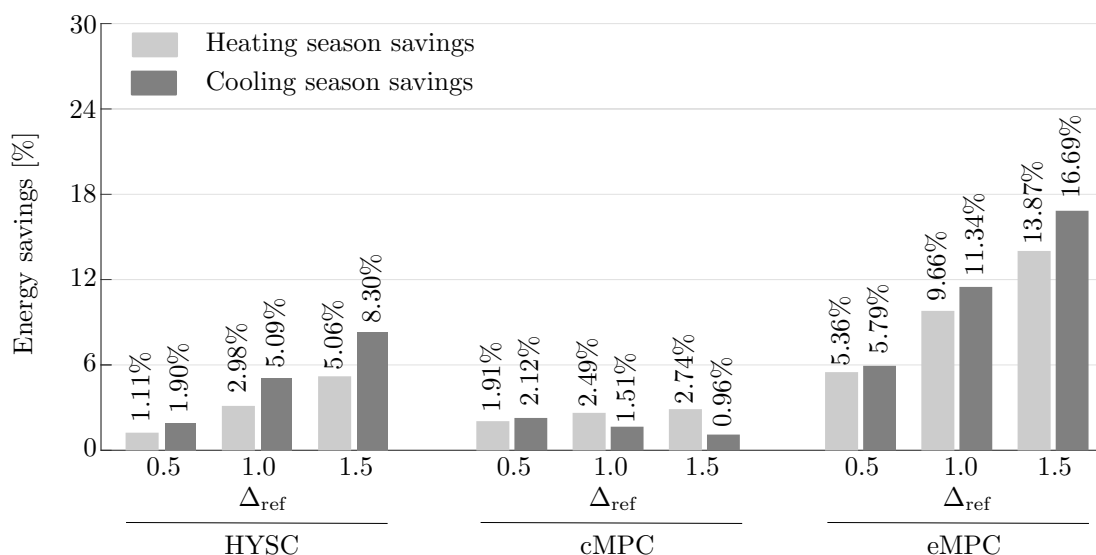


Figure 5.7. Energy savings for different types of control, different flexibilities Δ^{ref} and different weights γ_e .

Contrary to the conventional control algorithms, the MPC allows more advanced and specific system design, especially in terms of accounted hour-to-hour variable energy prices and coordination with central HVAC system. More comprehensive case-study, with accounted thermal energy losses, energy consumption of FCUs's fans, thermal energy demand of non-controllable zones and volatile energy prices is given in Chapter 6. The overall thermal energy consumption of controllable zones in the building for the considered control strategies and $\Delta^{ref} = 0.5^\circ\text{C}$ on one selected day during heating season is shown in Fig. 5.8. The figure shows the predictive feature of MPC algorithms where heating is initiated few sampling time instants in advance to satisfy comfort demands at the start of the occupancy period. The peak at the beginning of the operation is a result of the simultaneous thermal energy delivery to each of 248 zones. Typically, conventional zone level controllers, such as HYSC and PI, require the building climate system design to

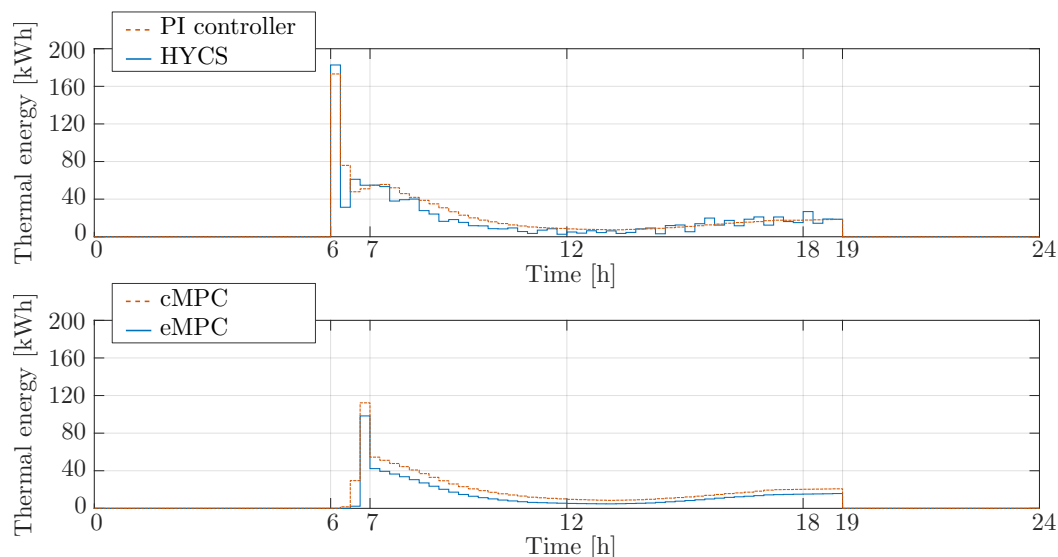


Figure 5.8. Overall thermal energy consumption of controllable zones in the building on one selected day in January for different control strategies.

withstand the worst case scenario of the simultaneous peak power operation in all zones. In most applications this results with largely oversized equipment. Further peak power reduction and its corresponding cost reduction by MPC employment is possible through coordination of zone level and superimposed central HVAC system or microgrid levels which is discussed in Chapter 6.

Comfort level indicators

In the considered case of seasonal heating and cooling, the comfort is significantly disrupted in cases when available thermal power is insufficient for covering the peak demand or inadequate for compensating the disturbance effect. This is highly expressed in cases when outside temperature and solar irradiance are too high in the heating season or too low in the cooling season. Comfort levels for different control strategies calculated during months when there is a clear need for only heating or cooling are shown in Fig. 5.9 and compared to the resulting energy consumption. Distinctive comfort levels for the same controllers and different user flexibilities of 0.5°C , 1.0°C and 1.5°C are denoted respectively with numbers 1, 2 and 3 next to the comfort level marker. The comfort level indicator is measured as average deviation (AD) from the temperature reference calculated as a ratio of the sum of all the deviation amounts during overall number of samples within the occupancy periods for all zones in the building and overall number of samples within the occupancy periods;

$$\text{AD} = \frac{1}{n_s n_y} \sum_{k \in \mathcal{O}} \|y_k^{\text{ref}} - y_k\|_1, \quad (5.26)$$

where \mathcal{O} is the set of all the time samples within the occupancy periods and n_s is its cardinal number. The comfort level indicator provides information on average expected

temperature in each time instant, e.g. for cMPC with $\Delta^{\text{ref}} = 1.5^\circ\text{C}$, the average expected temperature during summer time is within the $\pm 0.15^\circ\text{C}$ range around y^{ref} .

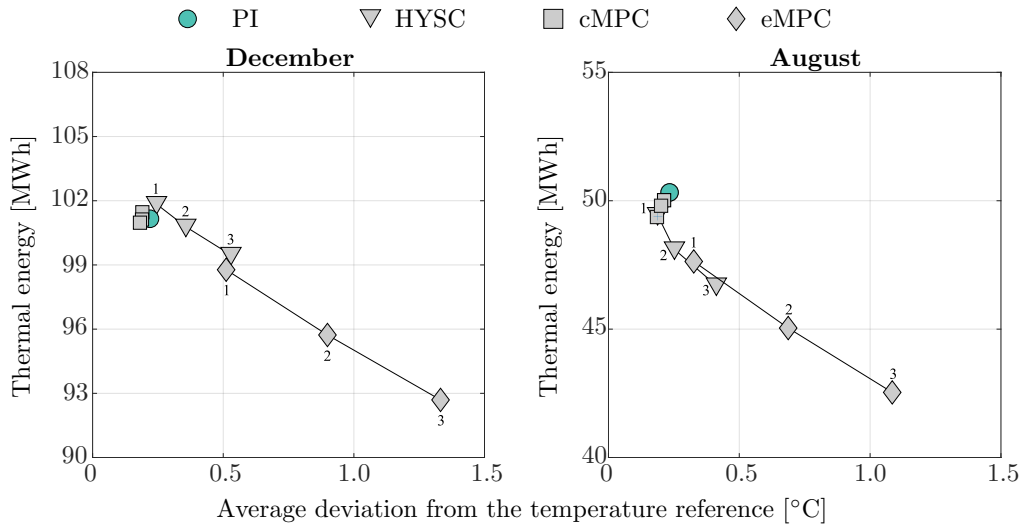


Figure 5.9. Comfort level indicators for different control strategies.

The considered cMPC approach shows better results than HYSC and PI due to the prediction of working hours requirements and timely applied preheating/precooling. The difference introduced with the γ_e parameter selection is evident. When compared with eMPC, the HYSC and PI perform better from the comfort quality aspect as eMPC is saturated at $y^{\text{ref}} \pm \Delta^{\text{ref}}$ temperatures for $\gamma_e < 1$. The measured comfort levels significantly differ for zones with different external windows orientation. Comfort levels, calculated for two exemplary zones, one oriented towards north and the other oriented towards south are shown in Fig. 5.10 and Fig. 5.11.

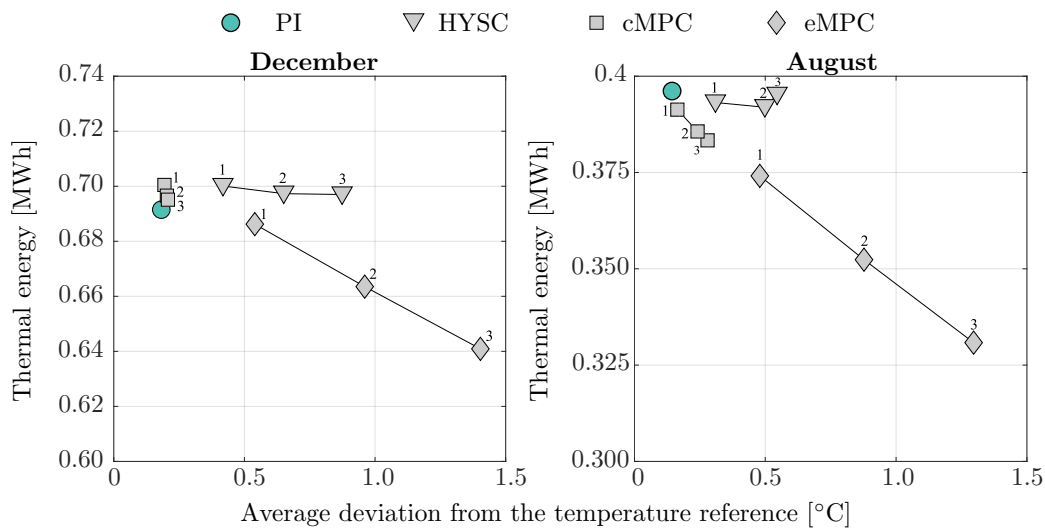


Figure 5.10. Comfort level indicators in one exemplary south-oriented zone for different control strategies.

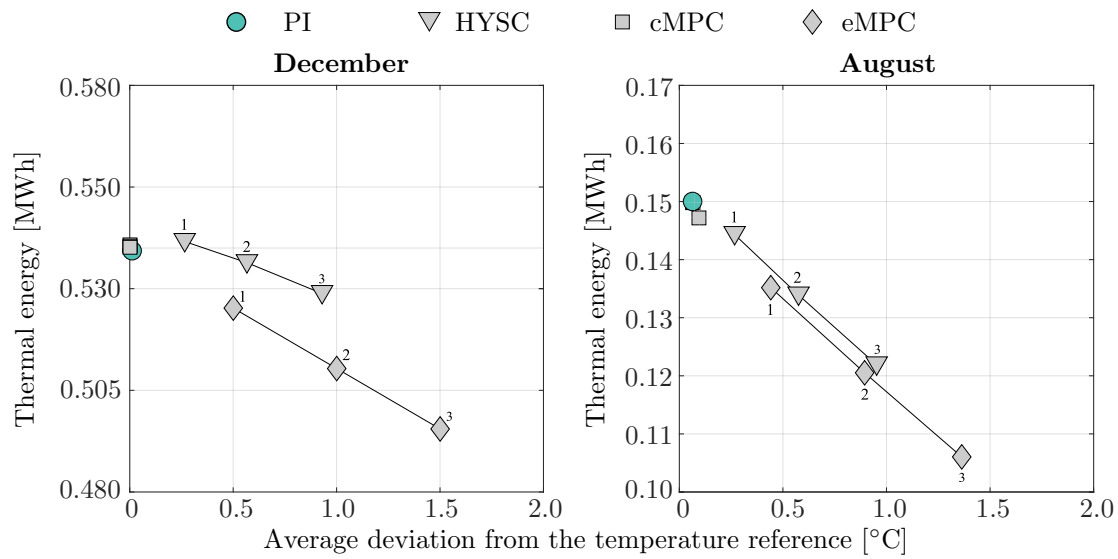


Figure 5.11. Comfort level indicators in one exemplary north-oriented zone for different control strategies.

Dynamic temperature response

Analysis of the considered controllers performances is further presented in terms of dynamic zone temperature response for different weather conditions. Figure 5.12 presents the weather conditions during the selected 7 semi-clouded days in December with significant temperature variation to illustrate the performance of various control strategies in the heating season. Depicted irradiances are the total incident irradiance on the south- and the north-facing building surface, where expressed peak at noon on 15 December is the result of a clear sunny day. The temperature responses of the exemplary north- and south-oriented zones for the PI, HYSC, cMPC and eMPC controller during the selected 7 days in the heating season are shown in Fig. 5.13 and Fig. 5.14.

To illustrate the performance of various control strategies in the cooling season 7 sunny days in August are selected (Fig. 5.15). The temperature responses of the exemplary north- and south-oriented zones for the P, HYSC, cMPC and eMPC controller during the cooling season are shown in Fig. 5.16 and Fig. 5.17. The results are shown for user flexibility of $\Delta^{\text{ref}} = 0.5^\circ\text{C}$.

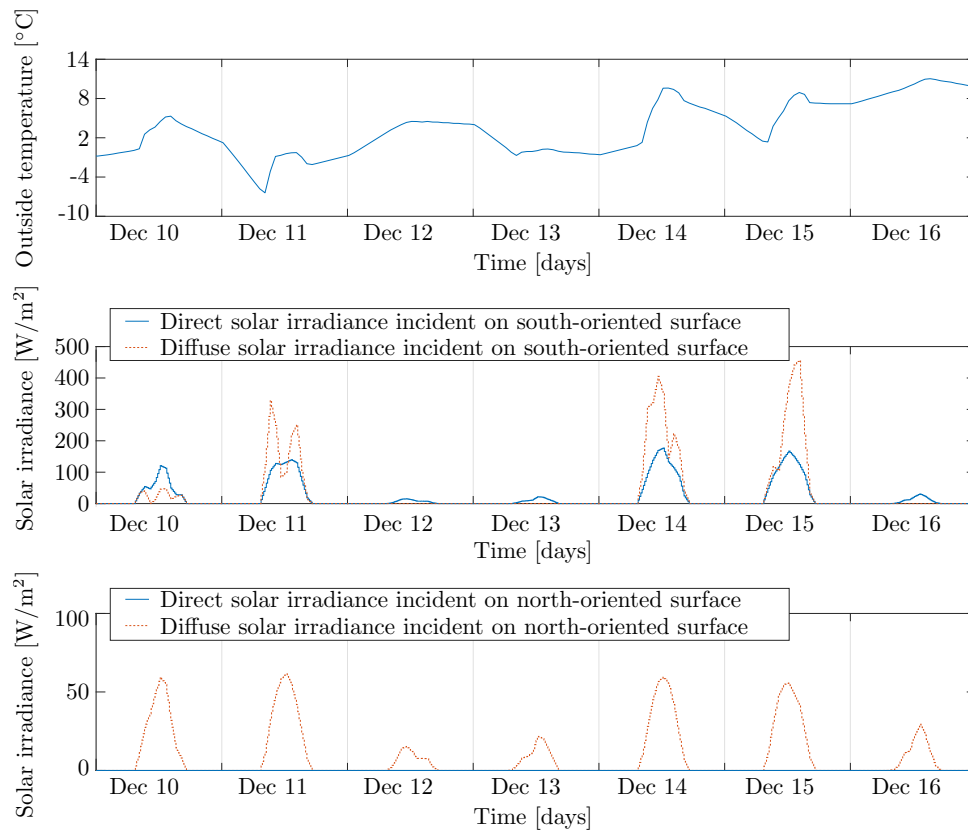


Figure 5.12. Weather conditions during the selected week in December.

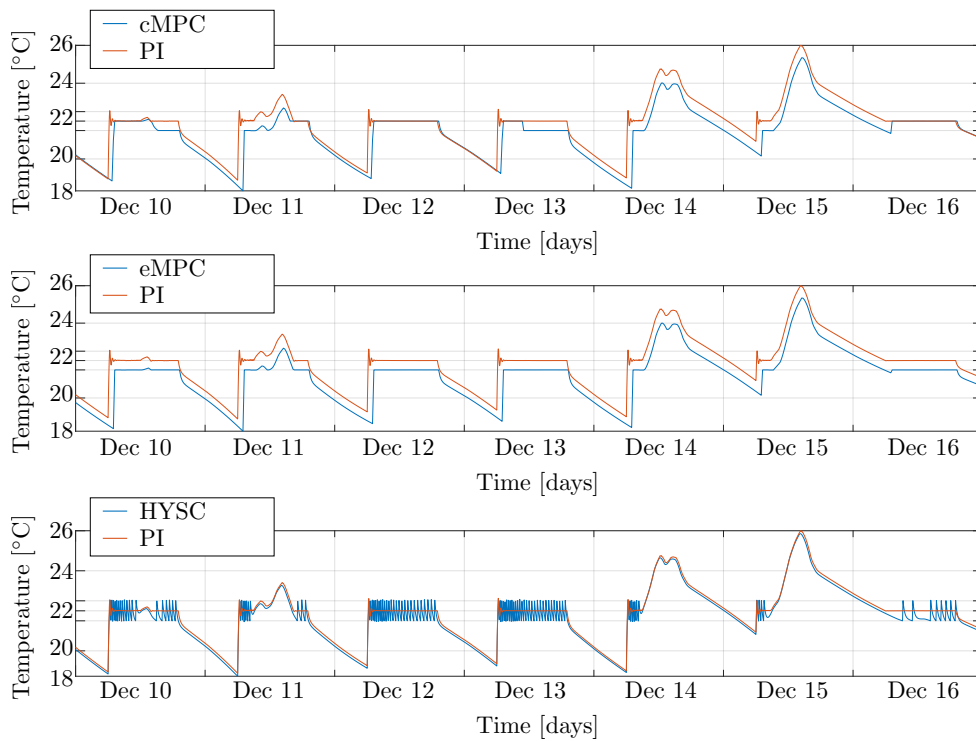


Figure 5.13. Temperature dynamics in one exemplary south-oriented zone for different control strategies in the heating season.

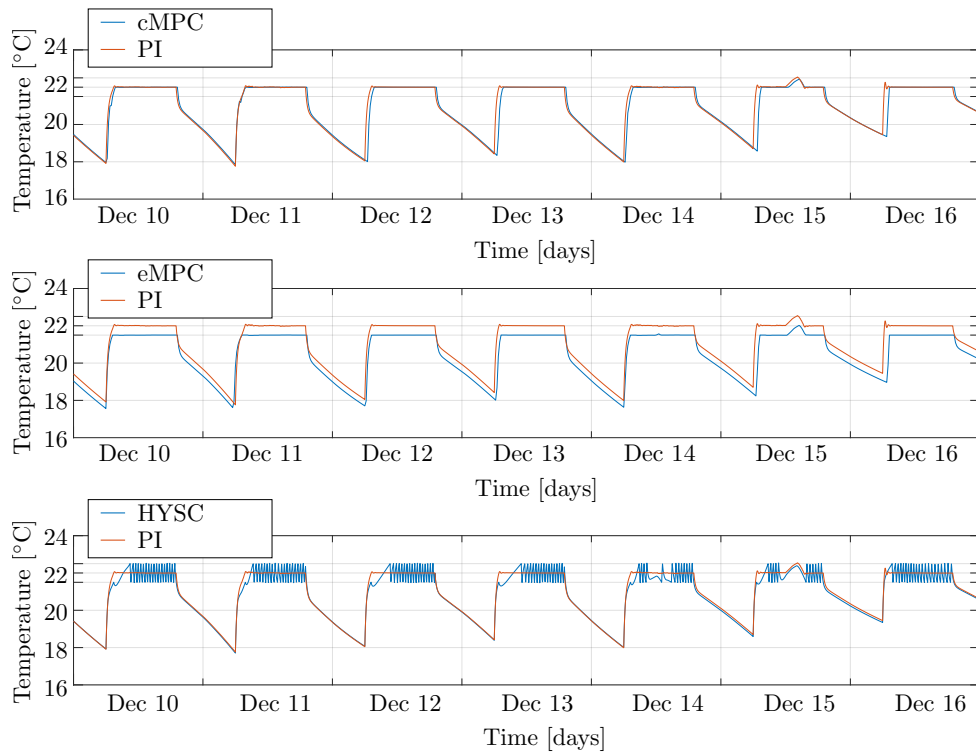


Figure 5.14. Temperature dynamics in one exemplary north-oriented zone for different control strategies in the heating season.

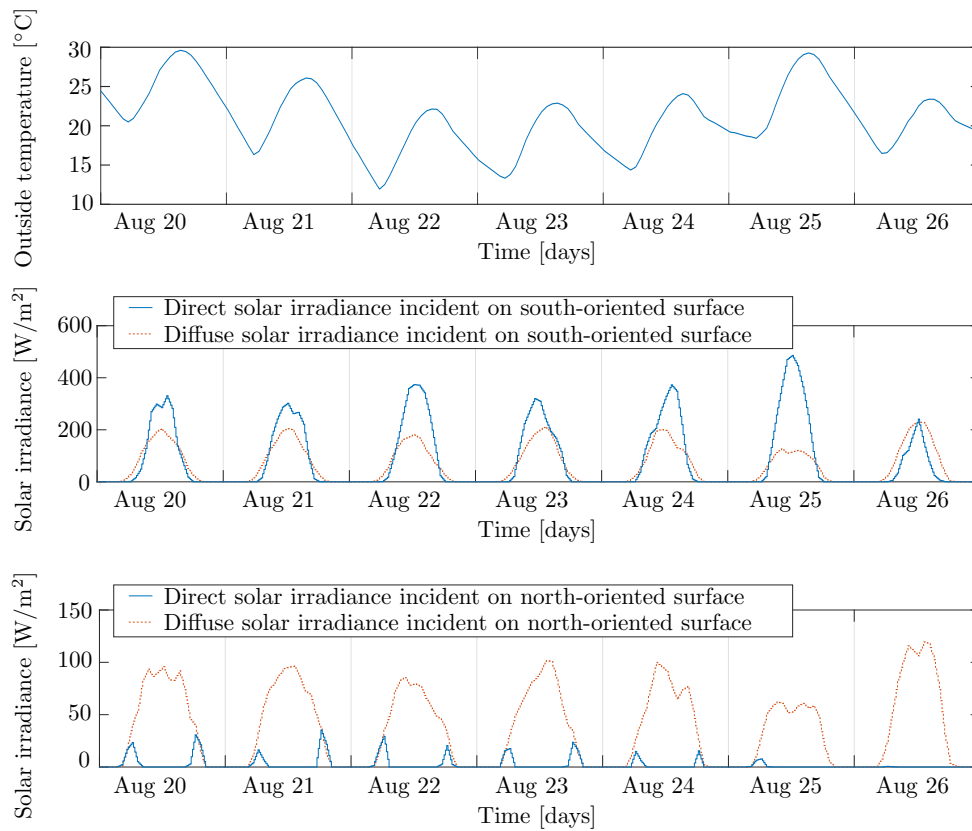


Figure 5.15. Weather conditions during the selected week in August.

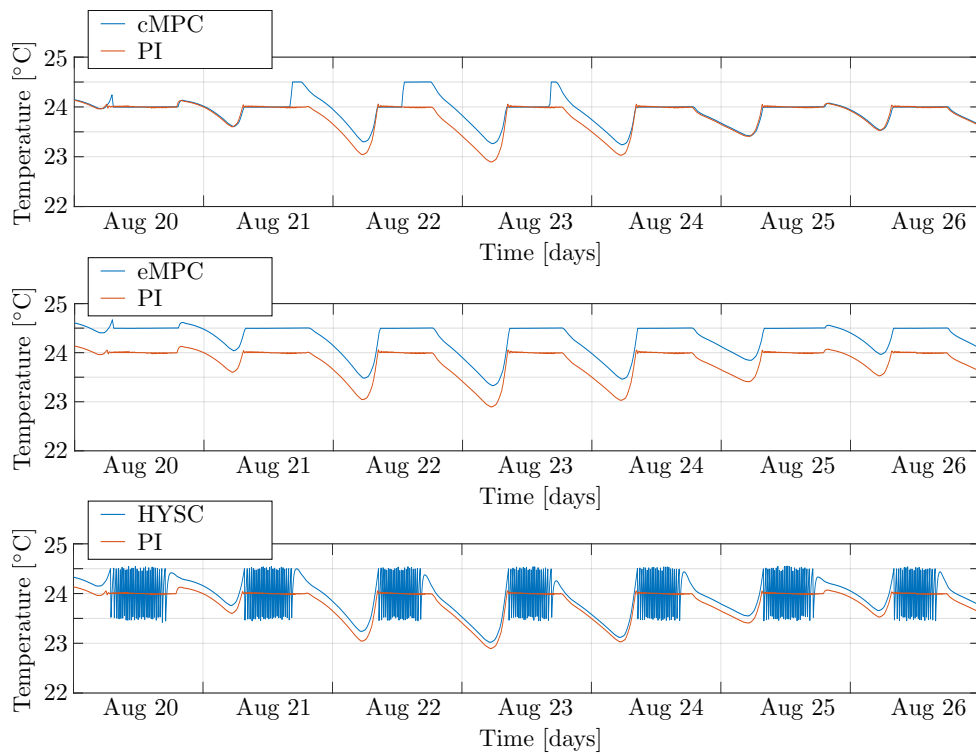


Figure 5.16. Temperature dynamics in one exemplary south-oriented zone for different control strategies in the cooling season.

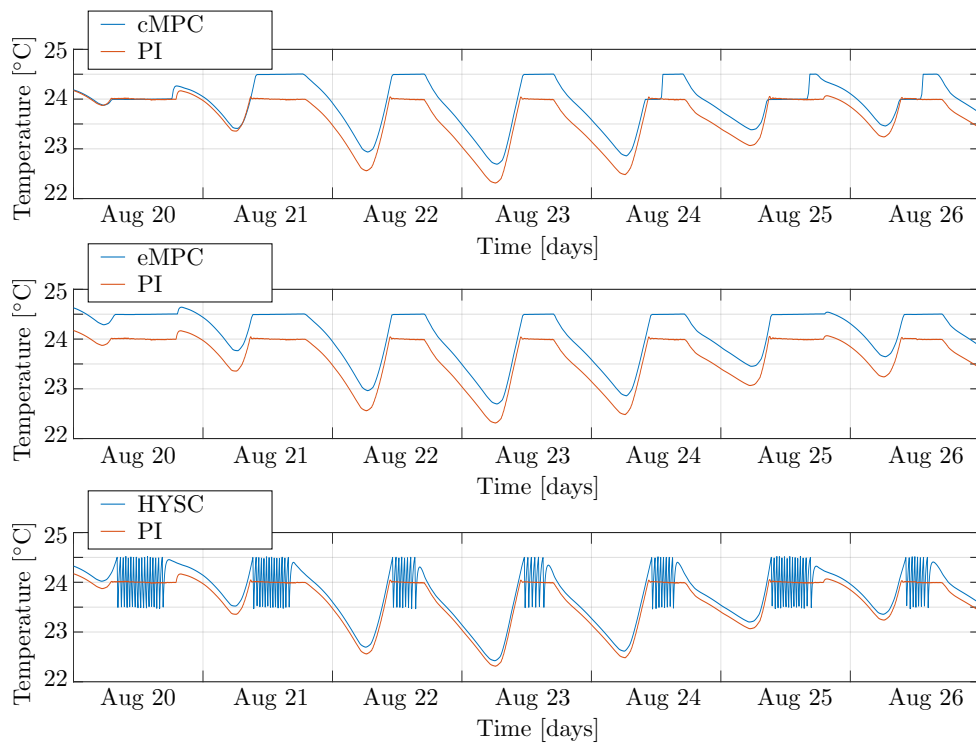


Figure 5.17. Temperature dynamics in one exemplary north-oriented zone for different control strategies in the cooling season.

From the results it is evident that cMPC forces the system to minimize overheating, i.e. to use the free energy from outdoors starting from the lower edge of the allowed range. The commanded thermal energy is selected such that the lower bound of the temperature range is reached prior to the stream of free energy from outdoors. In the cooling season system is forced to quit cooling the zone when free cooling can be utilized. It is also worth to note that TMY outside temperature data for the summer are relatively low, due to the averaging over the characteristic year, so the expected saving are even higher when applied to the real climate data. For the HYSC case intensive on/off switching between the available power units is clearly visible in terms of constant temperature oscillations. The results clearly show large cost-optimization opportunities of manipulations in tight comfort conditions with up to 16% additional savings of presented MPC approaches when compared to conventional control strategies. The expected savings are even much higher with MPC's full potential exploited in zone control, especially in terms of coordination with central HVAC system, building microgrid or smart grid.

5.5 Optimal control of heating/cooling elements in zones

Optimal control of HCEs in zones necessitates interfaces to the real building automation system which operate in adherence to the required thermal energy inputs in zones. As such, they are an extension to the MPC algorithms that calculate optimal thermal energy profiles per zones based on a thermodynamic model of the building (Section 5.2). The proposed zone level optimal energy management consists of two hierarchical control levels. Higher optimization level consists of MPC for calculation of optimal thermal energy profiles per zones. Lower hierarchical level consists of locally-distributed controllers (so called HCE interfaces), one per each zone, employed to control thermal actuators in an optimal way by respecting the commands given by the higher control level. The HCE interface acts a link between the commanded thermal energy variables from the higher-level MPC and the actuation profile of HCE required for these commands to be realized. The higher-level MPC calculates the optimal plan of heating/cooling for all included zones based on weather prediction, disturbance prediction, energy price prediction (in cases with volatile prices) and constraints such as temperature constraints or physical limitations of HCEs. The first control action per zone $u_{k|k}^*$ and disturbance assumed to be realized alongside that control action $P_{d,k|k}$ are then forwarded to low-level controllers (HCE interfaces) and the procedure is repeated at the next higher-level MPC time step.

The HCE interface can be realized in both centralized and decentralized fashion. Centralization is performed by grouping HCEs based on the major supply duct they are connected to. The use of a centralized controller for all elements in the group additionally reduces the operational cost by enabling control of the heating power variance and peak loads. Depending on the complexity of the heating/cooling set-up, decentralized implementation can offer significant reduction in computational power required to calculate the actuator commands. The proposed hierarchical organization is highly modular and thus applicable to various types of HCEs. For the set-up in the case-study building, which comprises FCUs, commands are fan speeds x_{fc}^* . For other FCU set-ups the commands may optionally also include valve positions x_v^* . The scheme of the above explained hierarchical organization is shown in Fig. 5.18.

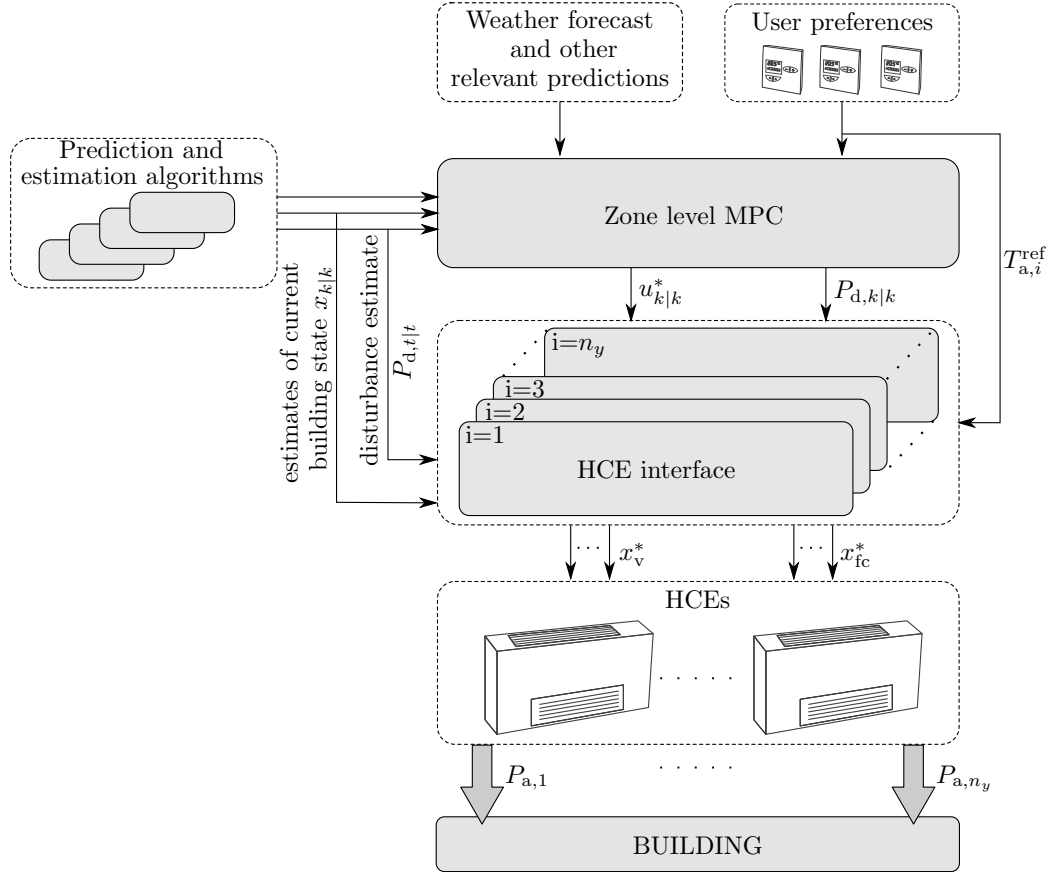


Figure 5.18. Hierarchical MPC for zones comfort control.

5.5.1 Optimal control of fan coil units

Due to their improved performance over classic radiators, FCUs are widely used for localized heating and cooling. However, MPC techniques, which are well-established in other industries, are still hardly used for FCUs due to the lack of appropriate mathematical models that are easy to parametrize. Traditional FCU control strategies include fuzzy, hysteresis and PID controllers [138], [139]. All the mentioned control approaches switch between fan speeds based on difference between temperature reference and current zone temperature. This mostly results with zone temperature oscillations of constant, predefined amplitude, leading to unnecessary energy consumption. The BEMSs that act by adjusting the optimal temperature reference usually neglect the performance of the local HCEs in the zone. Such systems are also practically inapplicable in tight comfort bounds with simple hysteresis controllers used locally for FCU control. Due to their inherent non-linearity, limited choice of fan speeds and inevitable unmeasurable heat disturbances affecting the zone temperature, FCUs represent a serious challenge for implementation of

real-time offset-free MPC that ensures adherence to the requested thermal energy inputs and comfort constraints.

Mathematical model of the FCU is derived in Chapter 2 in the following form:

$$\dot{T}_w^{\text{out}} = \underbrace{\left[\frac{q_w}{m_w} - \frac{U_o(x_{fc}, q_w)}{2m_w c_w} \right]}_{A_{fc}^c} T_w^{\text{out}} + \underbrace{\left[\frac{q_w}{m_w} - \frac{U_o(x_{fc}, q_w)}{2m_w c_w} \quad \frac{U_o(x_{fc}, q_w)}{2m_w c_w} \right]}_{B_{fc}^c} \begin{bmatrix} T_w^{\text{in}} \\ T_a^{\text{in}} \end{bmatrix}, \quad (5.27)$$

$$P_a = \underbrace{\left[\frac{U_o(x_{fc}, q_w)}{2} \right]}_{C_{fc}^c} T_w^{\text{out}} + \underbrace{\left[\frac{U_o(x_{fc}, q_w)}{2} \quad -U_o(x_{fc}, q_w) \right]}_{D_{fc}^c} \begin{bmatrix} T_w^{\text{in}} \\ T_a^{\text{in}} \end{bmatrix}, \quad (5.28)$$

where T_w^{in} is the water inlet temperature, T_w^{out} is the water outlet temperature, T_a is the zone air temperature, P_a is the thermal power provided by the FCU to the zone, q_w is the medium mass flow through the FCU, c_w is the specific heat capacity of the heating/cooling medium and m_w is the mass of water inside the FCU. It is assumed that there are four possible fan speeds x_{fc} : off, Low, Medium and High, denoted, respectively, as off, L, M and H. Heat transfer coefficient $U_o = f(x_{fc}, q_w)$ is a nonlinear function of the medium mass flow q_w and the fan speed x_{fc} , where fan speed is used for switching between different dynamics:

$$U_o(x_{fc}, q_w) = \begin{cases} \varepsilon_{fc}^{\text{off}} \cdot \frac{a_{fc}^{\text{off}}}{1 + b_{fc}^{\text{off}} \cdot q_w^{-c_{fc}}}, & \text{for } x_{fc} = \text{off}, \\ \varepsilon_{fc}^{\text{L}} \cdot \frac{a_{fc}^{\text{L}}}{1 + b_{fc}^{\text{L}} \cdot q_w^{-c_{fc}}}, & \text{for } x_{fc} = \text{L}, \\ \varepsilon_{fc}^{\text{M}} \cdot \frac{a_{fc}^{\text{M}}}{1 + b_{fc}^{\text{M}} \cdot q_w^{-c_{fc}}}, & \text{for } x_{fc} = \text{M}, \\ \varepsilon_{fc}^{\text{H}} \cdot \frac{a_{fc}^{\text{H}}}{1 + b_{fc}^{\text{H}} \cdot q_w^{-c_{fc}}}, & \text{for } x_{fc} = \text{H}. \end{cases} \quad (5.29)$$

The parameters $\{\varepsilon_{fc}^{\text{off}}, \varepsilon_{fc}^{\text{L}}, \varepsilon_{fc}^{\text{M}}, \varepsilon_{fc}^{\text{H}}\}$, $\{a_{fc}^{\text{off}}, a_{fc}^{\text{L}}, a_{fc}^{\text{M}}, a_{fc}^{\text{H}}\}$, $\{b_{fc}^{\text{off}}, b_{fc}^{\text{L}}, b_{fc}^{\text{M}}, b_{fc}^{\text{H}}\}$ and c_{fc} are known parameters found through identification as described in Chapter 2.

Attainable thermal powers along the prediction horizon depend on the HCE type, zone air temperature and heating/cooling medium temperature and mass flow. The information on future heating/cooling medium conditions is available either in a form of a scheduled central HVAC operation or it is considered as constant along the horizon by assuming persistence of currently measured system conditions. Since time constant of the FCU is relatively small compared to the time constants of the building, the maximum attainable thermal power from the FCU is defined with the following algebraic equation stemming from the (5.28) and (5.27):

$$u_{H,k} = \frac{2q_{w,k}c_w U_o^{\text{H}}}{2q_{w,k}c_w + U_o^{\text{H}}} (T_{w,k}^{\text{in}} - T_{a,k}^{\text{in}}), \quad (5.30)$$

where $U_o^H := U_o(H, q_w)$ is the overall heat transfer coefficient in the highest available fan speed (5.29) and $u_{H,k}$ is the maximum attainable thermal power averaged between time steps k and $k + 1$. Minimum attainable thermal power is either set to zero or it is calculated as the thermal power provided to the zone air with switched-off FCU fan. To assure thermal energy request from the higher-level MPC to be within the feasible FCU operation limits, minimum and maximum attainable thermal powers \mathbf{u}_{\min} and \mathbf{u}_{\max} on higher level should be matched with the FCUs' constraints. In zones with multiple FCUs thermal power limits are calculated as superposition of individual FCU thermal power limitations.

The goals of optimal energy management of FCUs are: *i*) to ensure that the zone temperature profile remains in the comfort limits, *ii*) to assure realization of energy input set by the higher-level MPC and *iii*) to guarantee the minimal disruption of the users and the minimum energy consumed by the fan by preferring lower fan speeds and minimizing the number of fan speed switching. To accomplish all the goals, FCU interface needs to operate on significantly lower time scales than higher-level MPC. It turns out that a time scale of $T_s = 60$ s is a good choice for reasonable data transfer and low enough for reducing the zone temperature oscillations, which are unavoidable in FCU operation, especially for FCUs without the possibility of the medium mass flow control. At the beginning of every T_s^c -long time-interval the interface receives an energy command E_a^{ref} defined as:

$$E_a^{\text{ref}} = u_{k|k}^* \cdot T_s^c, \quad (5.31)$$

from the higher-level MPC, where T_s^c is the sampling time of the higher-level MPC and $u_{k|k}^*$ is the optimal thermal power calculated by higher-level MPC. After receiving the energy command, the interface calculates the optimal fan speed trajectory $\mathbf{x}_{\text{fc},t}^*$ required to fulfil the energy request within the interval $[k, k + 1]T_s^c$:

$$\mathbf{x}_{\text{fc},t}^* = \left[x_{\text{fc},t|t}^* \quad x_{\text{fc},t+1|t}^* \quad \cdots \quad x_{\text{fc},t+((T_s^c/T_s)-1)|t}^* \right]^\top, \quad (5.32)$$

where $t \in \{0, 1, 2, \dots, (T_s^c/T_s) - 1\}$ is the current interface time step, H_{fc}^{\max} is the maximal time-offset from the higher-level MPC defined as $H_{\text{fc}}^{\max} \leq T_s^c/T_s$, and H_{fc} , defined as

$$H_{\text{fc}} = \min(H_{\text{fc}}^{\max}, (T_s^c/T_s) - t), \quad (5.33)$$

is the prediction horizon of the interface controller. The notation $x_{\text{fc},t+1|t}^*$ stands for predicted optimal fan speed at time step $t + 1$ calculated at time step t . In accordance with receding horizon principle, only the first control action $x_{\text{fc},t|t}^*$ is forwarded to the FCU and procedure is repeated at the next time interval. If the prediction horizon is outside the interval $[k, k + 1]T_s^c$, where k is the step of the higher-level MPC, the horizon is shortened so that $t + H_{\text{fc}} \leq H_{\text{fc}}^{\max}$ is satisfied.

To be able to predict future FCU behaviour, the FCU model (5.27) is discretised with

sampling time $T_d = 1$ s to preserve the model accuracy. With assumed constant system inputs within the interval $[t, t + 1]T_s$ the resulting discrete-time system equations are:

$$T_{w,t+1}^{\text{out}} = (A_{\text{fc}}^d)^M T_{w,t}^{\text{out}} + \sum_{j=0}^{M-1} (A_{\text{fc}}^d)^j B_{\text{fc}}^d \begin{bmatrix} T_{w,t}^{\text{in}} \\ T_{a,t}^{\text{in}} \end{bmatrix}, \quad (5.34)$$

where A_{fc}^d and B_{fc}^d are discrete-time counterparts of continuous-time system matrices A_{fc}^c and B_{fc}^c (5.27) while the parameter M is defined as $M = T_s/T_d$. Analogously, energy inserted into the zone within the time interval $[t, t + 1]T_s$ is defined as:

$$E_{a,t} = \sum_{i=0}^{M-1} C_{\text{fc}}^d (A_{\text{fc}}^d)^i T_{w,t}^{\text{out}} T_d + \left(D_{\text{fc}}^d T_s + C_{\text{fc}}^d \sum_{i=0}^{M-1} \sum_{j=0}^{i-1} (A_{\text{fc}}^d)^j B_{\text{fc}}^d T_d \right) \begin{bmatrix} T_{w,k}^{\text{in}} \\ T_{a,k}^{\text{in}} \end{bmatrix}, \quad (5.35)$$

where C_{fc}^d and D_{fc}^d are discrete-time counterparts of the continuous-time system matrices A_{fc}^c and D_{fc}^c from (5.28).

Goal i)

Temperature dynamics of single zone is described with a linear state-space model of the following form:

$$\begin{aligned} x_{t+1|t} &= A^d x_{t|t} + B_d^d d_t + B_u^d u_t, \\ y_{t|t} &= C^d x_{t|t}, \end{aligned} \quad (5.36)$$

where $x_t \in \mathbb{R}^{n_x}$ is the system state vector, $u_t \in \mathbb{R}^1$ is the thermal energy input and $d_t \in \mathbb{R}^{n_d}$ is the disturbance input (outside temperature, solar irradiance, internal gains, temperatures of adjacent rooms, etc.). Matrices A^d , B_d^d , B_u^d and C^d are of appropriate dimensions and are obtained either based on first principles modelling or by use of identification methods (see Chapter 3). To limit the zone temperature oscillations and to enforce the temperature trajectory to be within a defined comfort interval the following constraints need to be respected:

$$T_{a,i,t+j|t}^{\text{ref}} - \Delta_{i,t+j|t}^{\text{ref}} \leq T_{a,i,t+j|t} \leq T_{a,i,t+j|t}^{\text{ref}} + \Delta_{i,t+j|t}^{\text{ref}}, \quad \forall j = 1, \dots, H_{\text{fc}}, \quad (5.37)$$

where Δ_i^{ref} is the acceptable deviation from temperature reference $T_{a,i}^{\text{ref}}$ in the considered i^{th} zone, matched to the one used in higher-level MPC.

Goal ii)

At the beginning of $[k, k + 1]T_s^c$ interval, $t = 0$ for the prediction horizon equal T_s^c/T_s , the realization of the energy E_a^{ref} is enforced by minimizing the difference between the

requested and the energy planned to be realized with the FCU (5.35):

$$J_{\text{fc},1}(\mathbf{x}_{\text{fc},t}) = \left| E_{\text{a}}^{\text{ref}} - \sum_{j=0}^{(T_s^c/T_s)-1} E_{\text{a},t+j|t} \right|. \quad (5.38)$$

To assure offset-free control in presence of model-plant mismatch and for shorter prediction horizons than T_s^c/T_s the mismatch between the realized and requested energy up to the step t is introduced into the optimization criterion (5.38) such that:

$$J_{\text{fc},1}(\mathbf{x}_{\text{fc},t}) = \left| \frac{H_{\text{fc}}}{(T_s^c/T_s)} E_{\text{a}}^{\text{ref}} - \sum_{j=0}^{H_{\text{fc}}-1} E_{\text{a},t+j|t} + \Delta E_{\text{a},t} \right|, \quad (5.39)$$

where the energy backlogs $\Delta E_{\text{a},t}$ are defined as:

$$\Delta E_{\text{a},t} = \frac{t}{(T_s^c/T_s)} E_{\text{a}}^{\text{ref}} - \sum_{j=0}^{t-1} E_{\text{a},j}^{\text{m}}, \quad (5.40)$$

with $E_{\text{a},t}^{\text{m}}$ being the estimated energy provided by the FCU to the zone in the interval $[t, t+1]T_s$ recalculated based on measurements and known FCU thermal power model (5.28):

$$E_{\text{a},t}^{\text{m}} = \int_{k \cdot T_s^c + t \cdot T_s}^{k \cdot T_s^c + (t+1) \cdot T_s} P_{\text{a}} dt. \quad (5.41)$$

The integral action for disturbance compensation is introduced into the FCU interface algorithm by calculating the difference between the predicted and realized disturbance within the interval $[k \cdot T_s^c, k \cdot T_s^c + t \cdot T_s]$. The predicted heat disturbance energy within the interval $[k, k+1]T_s^c$ is defined as:

$$E_{\text{d}}^{\text{ref}} = P_{\text{d},k|k} T_s^c, \quad (5.42)$$

where $P_{\text{d},k|k}$ is the disturbance value predicted for the interval $[k, k+1]T_s^c$ used by the higher-level MPC. The difference between the predicted and the realized disturbance, $\Delta E_{\text{d},t}$ is then defined as:

$$\Delta E_{\text{d},t} = \frac{t}{(T_s^c/T_s)} E_{\text{d}}^{\text{ref}} - \sum_{j=0}^{t-1} P_{\text{d},j} T_s, \quad (5.43)$$

where $P_{\text{d},t}$ is the estimated disturbance affecting the zone temperature within the interval $[t, t+1]T_s$. Based on the known current realization of the disturbance $P_{\text{d},t}$ it is also possible to predict the mismatch along the rest of the horizon and correct the requested

thermal energy accordingly:

$$\Delta E_{d,H_{fc}} = \frac{E_d^{\text{ref}}}{H_{fc}} - P_{d,t} H_{fc} T_s. \quad (5.44)$$

For $t > 0$ the criterion J_1 is then defined as:

$$J_{fc,1}(\mathbf{x}_{fc,t}) = \left| \frac{H_{fc}}{(T_s^c/T_s)} E_a^{\text{ref}} - \sum_{j=0}^{H_{fc}-1} E_{a,t+j|t} + \Delta E_{a,t} + \Delta E_{d,t} + \Delta E_{d,H_{fc}} \right|. \quad (5.45)$$

Iterative update of ΔE_a and ΔE_d assures the offset-free input energy control as it emulates the integrator behaviour. The principle of integral behaviour is depicted in Fig. 5.19.

Goal *iii*)

Although one FCU consumes a small amount of electricity when its fan is on (~ 70 W), due to the large number of FCUs in the whole building and long working hours, the total electric energy consumption occupies a significant share of central heating and cooling system electricity consumption. Therefore, optimizing the FCU performance improves thermal comfort but also potentially contributes to the electrical energy savings:

$$J_{fc,2}(\mathbf{x}_{fc,t}) = \sum_{j=0}^{H_{fc}-1} E_{t+j|t}^{\text{el}}. \quad (5.46)$$

The electrical energy consumption model of FCU is defined in Chapter 2. By minimizing the electricity consumption, lower fan speeds are favoured thus minimizing also the noise. Since switching between fan speeds is the noisiest part of FCU operation, the following penalty function is introduced to reduce it:

$$J_{fc,3}(\mathbf{x}_{fc,t}) = \sum_{j=0}^{H_{fc}-1} \Delta x_{fc,t+j|t}, \quad (5.47)$$

$$\Delta x_{fc,t+j|t} = \begin{cases} 0, & \text{if } x_{fc,t+j|t} = x_{fc,t+j-1|t}, \\ 1, & \text{if } x_{fc,t+j|t} \neq x_{fc,t+j-1|t}, \end{cases} \quad (5.48)$$

$\forall j = 0, \dots, H_{fc} - 1$, with $x_{fc,t-1|t} = x_{fc,t-1|t-1}^*$, where $x_{fc,t-1|t-1}^*$ is the optimal fan speed calculated and applied to the FCU in the previous time step.

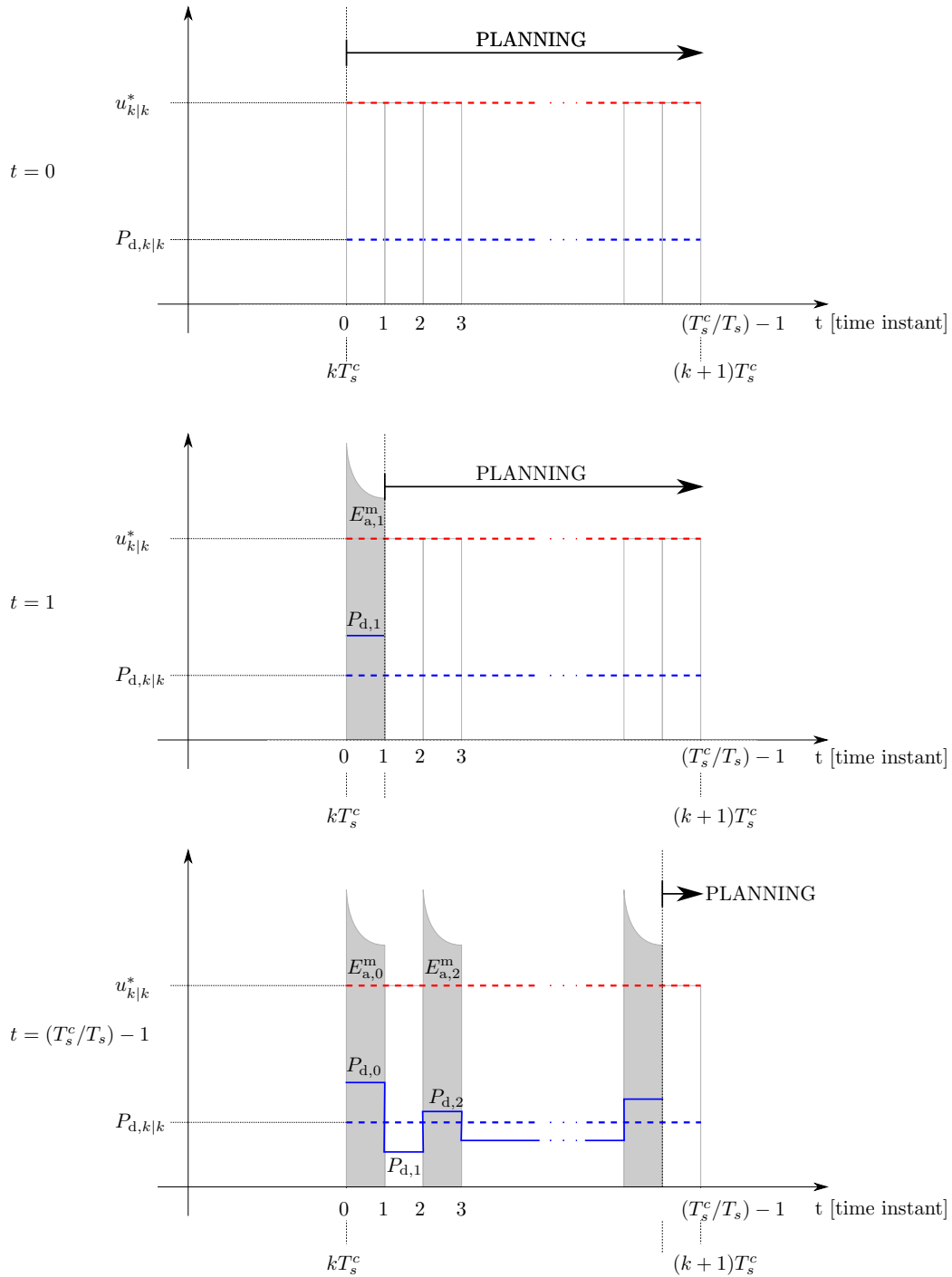


Figure 5.19. Principle of compensation of fast disturbances and mismatch between the realized and requested thermal energy, case when $H_{fc}^{\max} \leq T_s^c/T_s$.

The final consolidated interface optimization problem for FCU control, written in compact form, is as follows:

$$\begin{aligned}
\mathbf{x}_{\text{fc},t}^* &= \underset{\mathbf{x}_{\text{fc},t}}{\text{argmin}} && J_{\text{fc},1}(\mathbf{x}_{\text{fc},t}) + g_1 J_{\text{fc},2}(\mathbf{x}_{\text{fc},t}) + g_2 J_{\text{fc},3}(\mathbf{x}_{\text{fc},t}) \\
\text{s.t.} &&& (5.34), (5.35), (5.36), (5.37) \\
&&& x_{\text{fc},t+j|t} \in \{\text{off}, \text{L}, \text{M}, \text{H}\} \quad \forall j = 0, 1, \dots, H_{\text{fc}} - 1,
\end{aligned} \tag{5.49}$$

whereas, to enable implementation, constraints defined with (5.37) are included as soft constraints. The preferred behaviour is enforced by changing the non-negative weights g_1 and g_2 . The optimization problem (5.49) belongs to a class of Mixed Integer Linear Programs (MILPs) which can be efficiently solved with e.g. CPLEX [137]. The overall algorithm for the MPC energy management of FCUs is given in Algorithm 3.

Algorithm 3 Interface algorithm for optimal control of FCU.

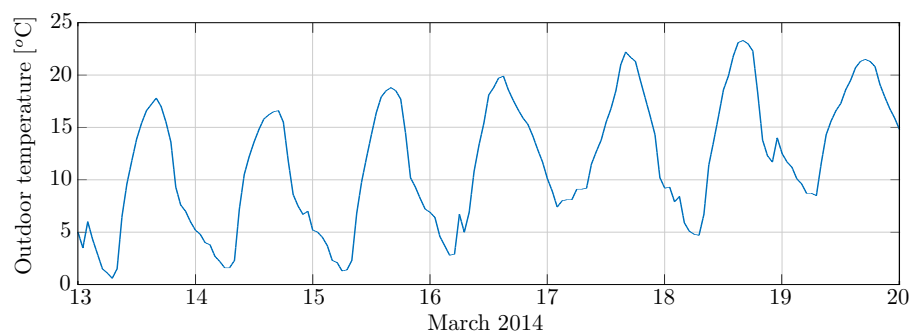
initialization: $t = 0$

repeat 1-8 every T_s :

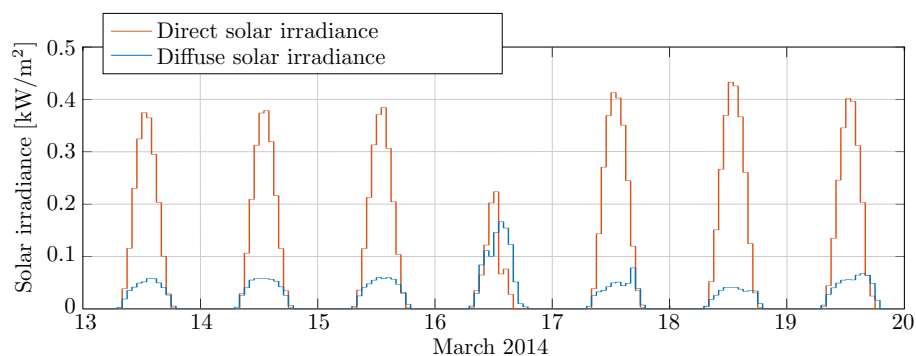
- 1: collect new building measurements: $q_w, T_a, T_w^{\text{in}}, T_w^{\text{out}}$;
 - 1: collect new meteorological measurements: $T_{\text{out}}, I_{\text{h}}^{\text{diff}}, I_{\text{n}}^{\text{dir}}$;
 - 2: collect estimates of current zone state $x_{t|t}$;
 - 3: check for SP and Δ^{ref} updates;
 - 4: **if** $t = T_s^c/T_s$ **or** $t = 0$:
 - 4.a: receive $u_{k|k}^*$ and $P_{d,k|k}$ from higher-level MPC;
 - 4.b: calculate energy reference E_a^{ref} (5.31);
 - 4.c: calculate predicted heat disturbance energy E_d^{ref} (5.42);
 - 4.d: initialize $t = 0, \Delta E_{a,t} = 0, \Delta E_{d,t} = 0, \Delta E_{d,H_{\text{fc}}} = 0, H_{\text{fc}} = H_{\text{fc}}^{\text{max}}$;
 - 5: **else:**
 - 5.a: $H_{\text{fc}} = \min(H_{\text{fc}}^{\text{max}}, (T_s^c/T_s) - t)$
 - 5.b: calculate realized thermal energy $E_{a,t}^{\text{m}}$ (5.41)
 - 5.c: calculate thermal energy mismatch $\Delta E_{a,t}$ (5.40)
 - 5.d: collect estimate of heat disturbance $E_{d,t}$
 - 5.e: calculate $\Delta E_{d,t}$ (5.43) and $\Delta E_{d,H_{\text{fc}}}$ (5.44)
 - 6: solve the FCU optimization problem (5.49);
 - 7: forward $x_{\text{fc},t|t}^*$ to the FCU;
 - 8: $t = t + 1$;
-

5.5.2 Verification of optimal fan coil unit control

The Algorithm 3 is realized and tested within MATLAB environment [70] for one selected zone from the case-study building described in detail in Appendix A. Data used as external conditions for dynamic building simulation are data from 13th to 20th March 2014 collected from the case-study building meteorological station. The weather conditions in the selected week (Fig. 5.20) are chosen as representative variable conditions.



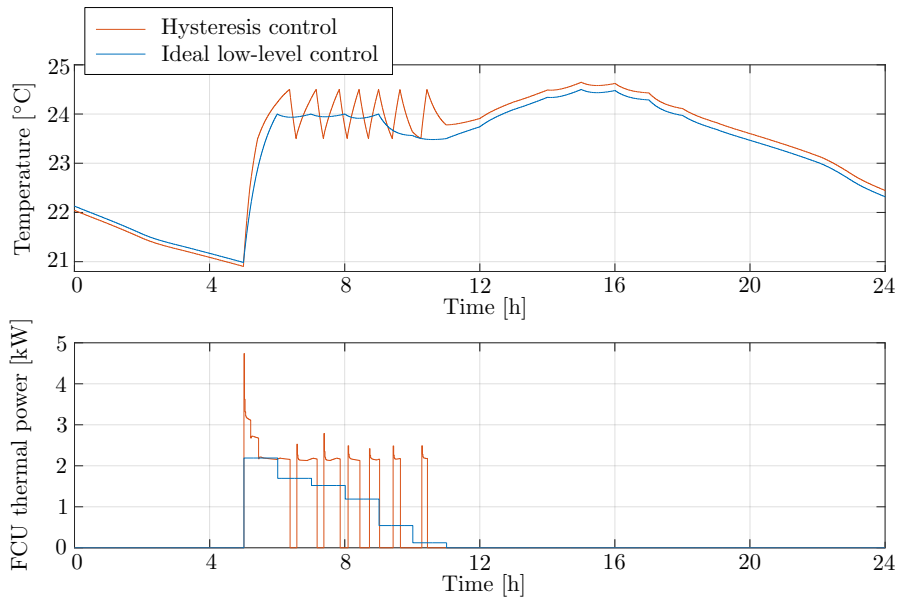
(a)



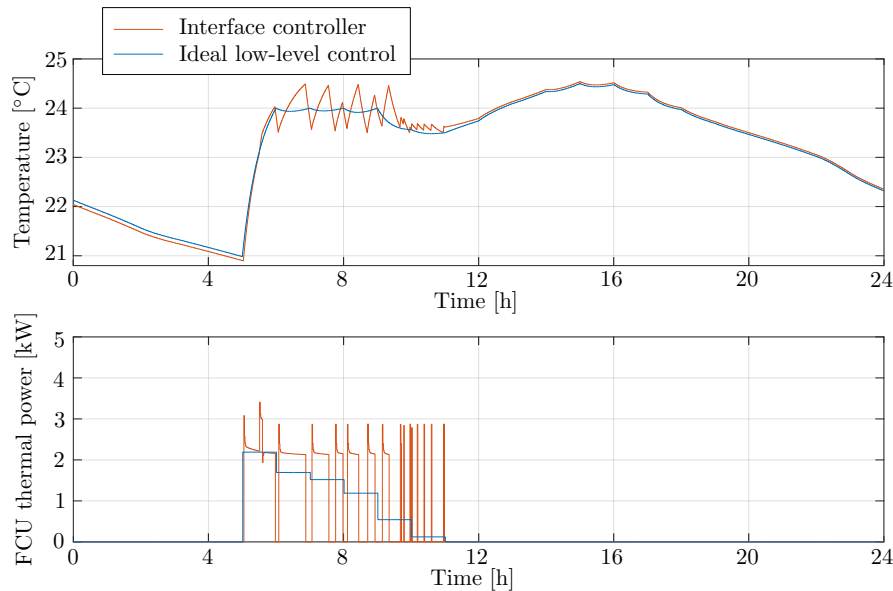
(b)

Figure 5.20. Weather conditions from 13th to 20th March 2014; a) outside temperature, b) solar irradiance.

All weather disturbances affecting the zone temperature are assumed to be perfectly known while unmeasured heat disturbance P_d is set to zero. Simulations are performed with the following parameters: $T_a^{\text{ref}} = 24^\circ\text{C}$, $\Delta^{\text{ref}} = 0.5^\circ\text{C}$, $H_{\text{fc}}^{\text{max}} = 10$, $T_s^c = 3600$ s and $T_s = 60$ s. The temperature is regulated only during occupancy period, from 6:00 to 18:00 h. Figure 5.21 shows a comparison of zone temperatures and the FCU thermal consumption for the three control approaches: continuous-time hysteresis control and two approaches based on thermal energy reference, the presented FCU interface and the idealized algorithm with uniform power tracking of thermal energy references. For a fair comparison, the hysteresis controller is switched on at 5:00 to meet the requirements of working hours in time. Preheating, as a well-known advantage of the MPC, suppresses the need for instant zone heating and thus flattens the energy consumption profile by reducing the peak power loads.



(a)



(b)

Figure 5.21. Zone temperature response and thermal FCU power with different types of control and $g_1 = g_2 = 100$ for 17 March 2014.

Figure 5.22 gives performance comparison of the developed control algorithm and the hysteresis one for the selected period in terms of the objective goals $J_{fc,2}$ and $J_{fc,3}$, overall thermal energy consumption, and average deviation from temperature reference for different weights g_1 and g_2 . For appropriately selected weights the developed algorithm outperforms the hysteresis one both in energy consumption and comfort with average number of switching per hour within the acceptable range.

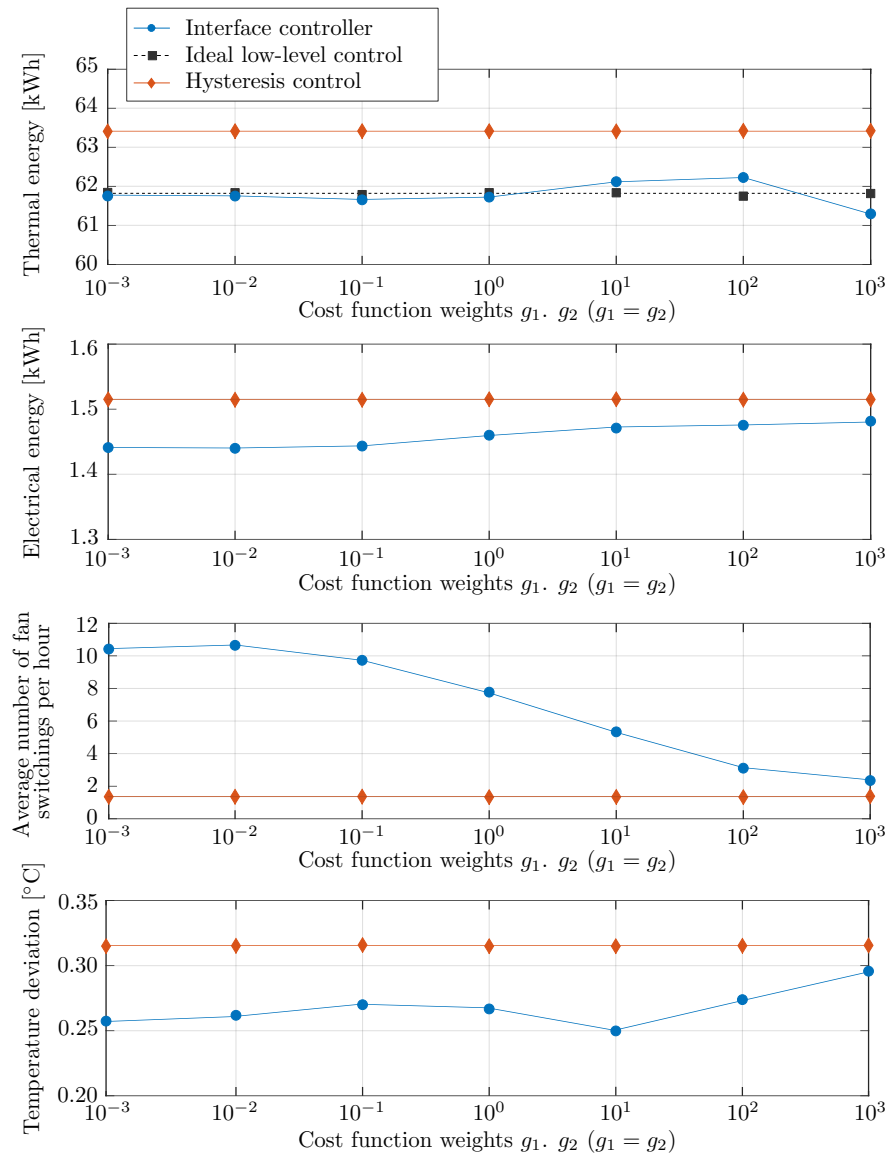


Figure 5.22. Performance comparison of the developed control algorithms for the period from 13th to 20th March 2014.

Use of the zone temperature model predictive control in modular hierarchical building energy management

Due to the proven flexibility, a model predictive control (MPC) approach emerged as a promising solution for wide spread problems of energy management within buildings. In addition to climate control, the MPC approach adds to increased savings of 13% when applied to heat pump [5], with load shifting by up to 61% [6, 7, 8] and to peak electricity power reduction by 35-72% [9]. Introduction of microgrid to buildings enables additional savings by providing ancillary services to the utility grid [10, 11] or through coordinated microgrid and building climate control [12]. In [13], the application of modular hierarchical coordination between predictive climate control and energy flows in the building microgrid ensured 23% revenue (123% savings) on a yearly scale. The advanced control methods are evidently transforming the buildings to active energy market participants.

Buildings are complex systems composed of many coupled subsystems responsible for maintaining safe and steady operation such as: building zones, central heating, ventilation and air conditioning (HVAC) system, microgrid with energy production units, storages and controllable or passive loads, etc. These subsystems are all very different in dynamics, priorities, means of operation but also implementation aspects such as energy levels, protocols, maintenance services, etc. Typical applications of building energy management system (BEMS) are oriented only locally to a specific subsystem, while neglecting interconnections and cooperation among all constituent subsystems. As a result, building as a whole achieves uncoordinated and non-optimal behaviour. The aim of the modular parametric hierarchical coordination is to separate building subsystems in a hierarchical fashion [13, 38] rather than having one large control structure to handle all the subsystems at once. Such hierarchical decomposition introduces significant computational relaxation

and improvement of algorithm efficiency [13].

The BEMS considered on the 3Smart project [140] consists of three levels following the building energy system vertical decomposition in its major parts: (A) building zones level, (B) central heating/cooling medium conditioning system level (referred to as central HVAC level), and (C) building microgrid level (Fig. 6.1).

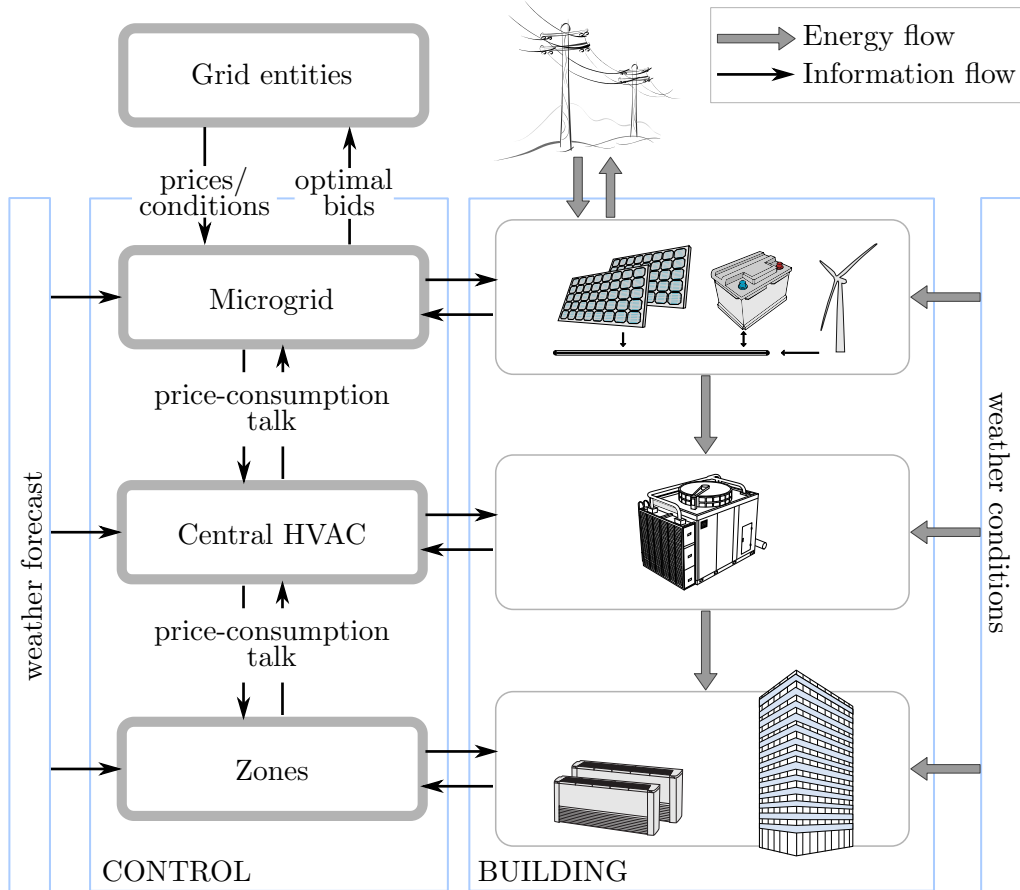


Figure 6.1. Modular control of main building subsystems.

Zone level comfort control, developed within the Chapter 5, is envisioned as the lowest-level in the proposed hierarchy. If other levels are missing, the improvement of energy-efficiency and comfort is achievable even through the application of only level (A) modules, if they take into account weather forecast and comfort requirements to decide on the optimal profile of energy consumption for maintaining comfort conditions in each zone. If no other building level is present, energy prices from the utility grids are directly transferred to level (A) which then induces energy-cost-optimal behaviour instead of the energy-optimal behaviour for maintaining comfort. By including also level (B) next to level (A) benefits can be multiplied since conventional solutions introduce only energy-connections with the central HVAC system, which consequently cannot take into account the current and near-future energy requirements in the zones, and thus operates with reduced efficiency. Especially important is the ability to intelligently shift the power demand based on the smart grid signals or predicted outside temperature that

shapes the efficiency of the central HVAC system. Finally, coming to the level (C), the BEMS introduces a possibility to manage energy storages, energy conversion systems and controllable loads on the building level. Hence, one can induce minimum energy costs with respect to the planned energy consumption and production profile while making the building an active entity on smart grids or of district-level smart energy distribution systems. Consequently, level (C) enables further modular build-up of the concept beyond the building area and towards smart districts, grids and cities.

The coordination in the imposed modular structure is based on the so-called "price-consumption" talk, where on each level the information about own optimal operation is communicated to the higher-level module and cost sensitivity with respect to the lower-level operation is communicated to the lower-level module. Cost sensitivity calculation resides on multi-parametric programming and critical regions (CRs). Segments of the algorithm introduced in [141] are utilized for that: only a single CR is determined at one iteration and no additional partitioning of the parameter space is performed. In such a set-up lower hierarchy level control variables are treated as a parametric disturbance on the higher-level and are further transformed towards global optimization criterion through a parametric value function. For convenience, the key elements of the original work [141] used here are concisely described in Section 6.2.

The development done within the thesis is focused on zone level only, thus within the Chapter the zone level, as the lowest level in the proposed hierarchy, is presented independently from the other parts of the system. In Section 6.1 the zone level MPC formulation developed within Chapter 5 is revisited and reformulated from energy-optimal to price-optimal form which can be easily included into hierarchical coordination with other building subsystems. In Section 6.2 the coordination mechanism between zone level and higher-levels is described. Section 6.3 gives description of the considered simulation scenario and elaborates the obtained results.

6.1 Building zones optimal control for high comfort demands

The zone level optimization problem used for modular hierarchical coordination of building subsystems is developed within the Chapter 5. For convenience, the main points of the developed MPC optimization criterion are in short described below.

Zone temperature dynamics is described with a linear discrete-time model of the following form (5.3):

$$x_{k+1} = A^d x_k + B_d^d d_k + B_d^{d*} T_{\text{out},k+1} + B_u^d u_k, \quad (6.1)$$

$$y_k = C^d x_k,$$

where $x_k \in \mathbb{R}^{n_x}$ denotes the zone level state vector, $y_k \in \mathbb{R}^{n_y}$ is an output vector consisted of zones temperatures, $u_k \in \mathbb{R}^{n_u}$ is a vector of thermal energy inputs into each of n_y controllable zones, $d_k \in \mathbb{R}^{n_d}$ is the disturbance input (outside temperature, solar irradiance, internal disturbance gains, etc.) and T_{out} is outside temperature. Matrices A^d , B_d^d , B_u^d , B_d^{d*} and C^d are of appropriate dimensions and are obtained either based on first principles modelling or by use of the identification methods (see Chapter 3, Section 3.4). In the sequel, bold notation is used to denote variables stacked over the prediction horizon of length H . To utilize known prediction of the outside weather temperature T_{out} , its influence is discretised by employing first-order hold while the rest of the system is discretised by zero-order hold.

A careful selection of weighting matrices for penalizing the energy consumption and deviation from the temperature reference enables easy switch between the two often opposing requirements based on the predicted disturbance and energy price profiles. Within such a set-up, comfort is defined through temperature reference $\mathbf{y}^{\text{ref}} \in \mathbb{R}^{H \cdot n_y}$ and permissible zone temperature interval:

$$\mathbf{y}^{\text{ref}} - \mathbf{\Delta}^{\text{ref}} - \boldsymbol{\sigma}_1 \leq \mathbf{y} \leq \mathbf{y}^{\text{ref}} + \mathbf{\Delta}^{\text{ref}} + \boldsymbol{\sigma}_2, \quad (6.2)$$

where $\mathbf{\Delta}^{\text{ref}} \in \mathbb{R}^{H \cdot n_y}$ is acceptable temperature deviation from the temperature reference stacked over the prediction horizon, and $\boldsymbol{\sigma}_1 \geq 0 \in \mathbb{R}^{H \cdot n_y}$ and $\boldsymbol{\sigma}_2 \geq 0 \in \mathbb{R}^{H \cdot n_y}$ are slack variables that allow highly penalized constraint violation and feasible implementation. The zone thermal heating/cooling element limitations are formulated as input constraints:

$$\mathbf{u}_{\text{min}} \leq \mathbf{u} \leq \mathbf{u}_{\text{max}}, \quad (6.3)$$

where \mathbf{u}_{min} and \mathbf{u}_{max} are minimum and maximum attainable thermal powers along the prediction horizon, dependant on the current and planned HVAC operation, heating/cooling elements properties and the zone temperatures. If no information on future HVAC operation is available, the current measured system state is presumed to be retained

along the prediction horizon. Maximum attainable fan coil unit thermal power is defined as in (5.30). The final optimization problem for energy-saving and comfortable zone temperature control, written in compact form, is as follows:

$$\begin{aligned}
J^1 = \min_{\mathbf{u}, \boldsymbol{\sigma}_1, \boldsymbol{\sigma}_2} \quad & \mathbf{c}_t^\top |\mathbf{u}| + \gamma_e \cdot c_c \cdot \boldsymbol{\delta}^\top |\mathbf{Q}(\mathbf{y}^{\text{ref}} - \mathbf{y})| + g_1 \mathbf{1}^\top \boldsymbol{\sigma}_1 + g_2 \mathbf{1}^\top \boldsymbol{\sigma}_2, \\
\text{s.t.} \quad & (6.1), (6.2), (6.3), \\
& \boldsymbol{\sigma}_1 \geq 0, \boldsymbol{\sigma}_2 \geq 0.
\end{aligned} \tag{6.4}$$

The operator $|\cdot|$ denotes absolute value which is applied element-wise on the vector, $\mathbf{c}_t \in \mathbb{R}^{H \cdot n_u}$ is the thermal energy cost, $c_c \in \mathbb{R}^1$ is the associated comfort cost expressed as mean value of the thermal energy cost \mathbf{c}_t , i.e. $c_c = \sum \mathbf{c}_t / (H \cdot n_u)$, $\mathbf{1}^\top$ is appropriately sized row vector of ones and g_1 and g_2 are non-negative weighting parameters for tuning the optimization criterion. The vector $\boldsymbol{\delta} \in \mathbb{R}^{H \cdot n_y}$ is the zone occupancy vector defined as in (5.14) consisted of zeros (indicating vacant zone) and ones (indicating occupied zone). Matrix $\mathbf{Q} \in \mathbb{R}^{H \cdot n_y \times H \cdot n_y}$ transforms temperature deviation from the reference to the corresponding thermal energy such that it is comparable to the energy consumption while the parameter $\gamma_e \in \mathbb{R}^1$ is introduced for trade-off possibility of comfort-savings criterion (for more details see Chapter 5 or [131]).

6.2 Multi-parametric coordination of zone level with higher hierarchy levels

In zone level optimization problem energy inputs per zone \mathbf{u} are control variables whereas they act as disturbance parameters for the higher-levels, e.g. microgrid or central HVAC level [38, 13].

- If there is no central HVAC level and the thermal energy is generated locally, the thermal energy demand per time step k and the corresponding electrical load are related through coefficient of performance (COP), a heating efficiency measure dependent on the outside conditions, targeted medium temperature and/or medium flow. A separate measure, energy efficiency ratio (EER), is equivalently used for the cooling process. Constant COP parameter is commonly used in MPC approaches [77], since it simplifies the problem while keeping the sufficient accuracy for the aimed purpose. For clarity purposes, within the thesis, the term COP is used for both heating and cooling processes. Thus, if there is no central HVAC level, zone level cumulative thermal energy demand per time step k and the corresponding microgrid electrical load are related through constant COP parameter. Based on the calculated load, microgrid optimizes its behaviour and returns the calculated cost of the thermal energy and a region in which that cost is valid, namely CR, back to the zone level.
- By introducing the central HVAC level into the hierarchy the zone level communicates the required thermal energy for maintaining the comfort in all zones and zones temperatures profiles to the central HVAC level, which then based on the electrical energy price information from the utility grid or microgrid optimizes its behaviour to meet the required thermal demand and based on it calculates the optimized prices for the predicted heating/cooling demand and the defined temperatures from zones. Towards the zone level, the central HVAC level communicates the optimized thermal energy and temperatures prices, the CR in which these prices are valid and predicted profile of supply medium conditions (flow and temperature).

Zone level MPC, defined as (6.4) presents the low hierarchy level (LHL), while high hierarchy level (HHL) MPC optimization problem in both aforementioned cases can be written as:

$$\begin{aligned}
 J^h &= \min_{\mathbf{u}^h} \mathbf{h}^\top \mathbf{u}^h + \mathbf{f}^\top \Theta \\
 \text{s.t.} \quad \mathbf{x}^h &= \mathbf{A}^h x_{k|k}^h + \mathbf{B}^h \mathbf{u}^h \\
 \mathbf{G}^h \begin{bmatrix} \mathbf{x}^h \\ \mathbf{u}^h \end{bmatrix} &\leq \mathbf{w}^h + \mathbf{L}^h \Theta
 \end{aligned} \tag{6.5}$$

where superscript 'h' denotes parameters and variables related to HHL. Parameter Θ is based on a vector of zone level variables which act as disturbance parameters for the HHL.

System states are denoted as \mathbf{x}^h while vector \mathbf{u}^h consists of the controllable HHL inputs stacked over the prediction horizon. Vectors $\mathbf{h} \in \mathbb{R}^{H \cdot n_u^h}$ and $\mathbf{f} \in \mathbb{R}^{H \cdot n_u}$ represent the cost of the energy in the accompanying HHL optimization problems, matrices $\mathbf{A}^h \in \mathbb{R}^{H \cdot n_x^h \times n_x^h}$ and $\mathbf{B}^h \in \mathbb{R}^{H \cdot n_x^h \times H \cdot n_u^h}$ are matrices modelling the dynamics considered on the HHL, while matrices \mathbf{G}^h , \mathbf{L}^h and vector \mathbf{w}^h define all constraints on system states and inputs on the HHL.

6.2.1 Multi-parametric model predictive control and single critical region calculation

Original algorithm for multi-parametric MPC was proposed in [141]. The algorithm is based on direct exploration of the parameter space starting from a single critical region CR_0 formed around the initial parameter value Θ_0 (Fig. 6.2).

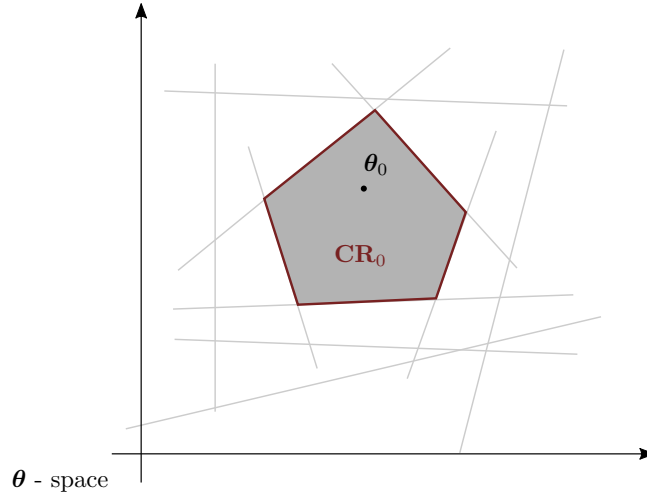


Figure 6.2. Geometric representation of a single critical region.

Important distinction from the multi-parametric MPC approach and the actual algorithm employed here is that only a single CR is determined at one step and no additional partitioning of the parameter space is performed. For convenience, much of the original problem is concisely given in the sequel.

A critical region is a subset of parameters Θ that yield the same set of active constraints, i.e., constraints that are satisfied with equality sign in the optimal solution. Constraints are separated into an active (A) and an inactive (NA) subset for certain CR, with optimal control law \mathbf{u}^{h*} over the prediction horizon H such that:

$$\mathbf{G}_A^h \mathbf{u}^{h*} = \mathbf{w}_A^h + \mathbf{L}_A^h \Theta, \quad (6.6)$$

$$\mathbf{G}_{NA}^h \mathbf{u}^{h*} < \mathbf{w}_{NA}^h + \mathbf{L}_{NA}^h \Theta, \quad (6.7)$$

From (6.6) follows the affine control law with respect to Θ over the CR:

$$\mathbf{u}^{h*}(\Theta) = \underbrace{(\mathbf{G}_A^h)^{-1} \mathbf{L}_A}_{D^h} \Theta + \underbrace{(\mathbf{G}_A^h)^{-1} \mathbf{w}_A^h}_{q^h}, \quad \Theta \in \text{CR}, \quad (6.8)$$

$$\mathbf{u}^{h*}(\Theta) = D^h \Theta + q^h, \quad \Theta \in \text{CR}, \quad (6.9)$$

and the corresponding affine cost function with respect to the parameter Θ , called value function:

$$J^{h*}(\Theta) = \mathbf{h}^\top \mathbf{u}^{h*}(\Theta) + \mathbf{f}^\top \Theta = \underbrace{(\mathbf{h}^\top D^h + \mathbf{f}^\top)}_{c^h} \Theta + \mathbf{h}^\top q^h, \quad (6.10)$$

$$J^{h*}(\Theta) = c^h \Theta + \mathbf{h}^\top q^h. \quad (6.11)$$

The CR, denoted with \mathcal{C}^h , is represented as:

$$G_{\text{CR}} \Theta \leq w_{\text{CR}}, \quad (6.12)$$

following from the inactive constraints subset:

$$\mathbf{G}_{\text{NA}}^h (D^h \Theta + q^h) < \mathbf{w}_{\text{NA}}^h + \mathbf{L}_{\text{NA}}^h \Theta, \quad (6.13)$$

$$\underbrace{(\mathbf{G}_{\text{NA}}^h D^h - \mathbf{L}_{\text{NA}}^h)}_{G_{\text{CR}}} \Theta < \underbrace{\mathbf{w}_{\text{NA}}^h - \mathbf{G}_{\text{NA}}^h q^h}_{w_{\text{CR}}}. \quad (6.14)$$

The closure is obtained by replacing $<$ by \leq in (6.14) [141]. In case of CR degeneracy additional steps are required to obtain a full-dimensional non-degenerate critical region. When a primal degenerate CR is obtained, depending on the primal degeneracy case, either the active constraints subset is reduced using e.g. QR decomposition, or the initial Θ is randomly permuted such that a full-dimensional CR, including the initial Θ , is obtained [141]. For the case of dual degeneracy, a particular optimizer is chosen on a vertex of the feasible solutions set of the HHL [141].

6.2.2 Iterative revisiting between optimization levels

After the CR (6.12) and accompanying cost \mathbf{c}^h (6.11) are calculated, the CR constraints are added as additional set of constraints to the original LHL optimization problem (6.4):

$$\begin{aligned}
 J^* = \min_{\mathbf{u}, \boldsymbol{\sigma}_1, \boldsymbol{\sigma}_2} \quad & J^{h*}(\Theta) + \gamma_e \cdot c_c \cdot \boldsymbol{\delta}^\top |\mathbf{Q}(\mathbf{y}^{\text{ref}} - \mathbf{y})| + g_1 \mathbf{1}^\top \boldsymbol{\sigma}_1 + g_2 \mathbf{1}^\top \boldsymbol{\sigma}_2, \\
 \text{s.t.} \quad & (6.1), (6.2), (6.3), \\
 & \Theta = f^\Theta(\mathbf{u}, \mathbf{y}), \quad \Theta \in \mathcal{C}^h, \\
 & \boldsymbol{\sigma}_1 \geq 0, \quad \boldsymbol{\sigma}_2 \geq 0,
 \end{aligned} \tag{6.15}$$

where $J^{h*}(\cdot)$ is the critical region value function of the HHL level, $f^\Theta(\cdot)$ is a stack of linear functions and c_c is the price of the thermal comfort inside building zones equal to the mean price of the thermal energy along the prediction horizon. The set \mathcal{C}^h represents the constraints of the HHL level CR. If the CR is defined with respect to both thermal energies and zone temperatures as in the case when HHL is central HVAC system, the original LHL optimization problem is additionally modified by introducing the zone temperature cost into the optimization problem as defined in (6.15). After solving the optimization problem on LHL, improved LHL control signals are obtained with respect to HHL objective, denoted with \mathbf{u}^{**} . Initial solution \mathbf{u}^* is shifted along the decreasing value of J^h from (6.11) such that all physical and comfort constraints are satisfied. The hierarchical coordination then continues with respect to the constraints activated by the optimal zone level solution.

Case 1 : If LHL constraints are activated, local optimum is reached and the procedure is concluded. The price optimal HHL solution \mathbf{u}^{h**} within the critical region and the associated cost J^{h**} are obtained from (6.9) and (6.11).

Case 2 : If critical region constraints (6.12) are activated, the LHL solution is transferred to the HHL where new critical region is found by resolving (6.5) with respect to new LHL solution shifted in the direction of the LHL optimizer change between two last iterations:

$$\Theta'_i = \Theta_i + \epsilon \frac{\Delta\Theta}{\|\Delta\Theta\|_2} \tag{6.16}$$

where:

$$\Delta\Theta = \Theta_i - \Theta_{i-1}, \tag{6.17}$$

parameter i is number of current iteration and parameter ϵ is a small value (e.g. solver precision or 1% of $\Delta\mathbf{u}$) chosen to ensure entering into adjacent CR as a starting point for the next iteration where HHL and LHL are respectively solved again. The newly obtained critical region is then passed again to LHL. The procedure is iteratively executed until Case 1 occurs (Fig. 6.3(b)) or HHL level constraints are activated (adjacent CR is non-existent).

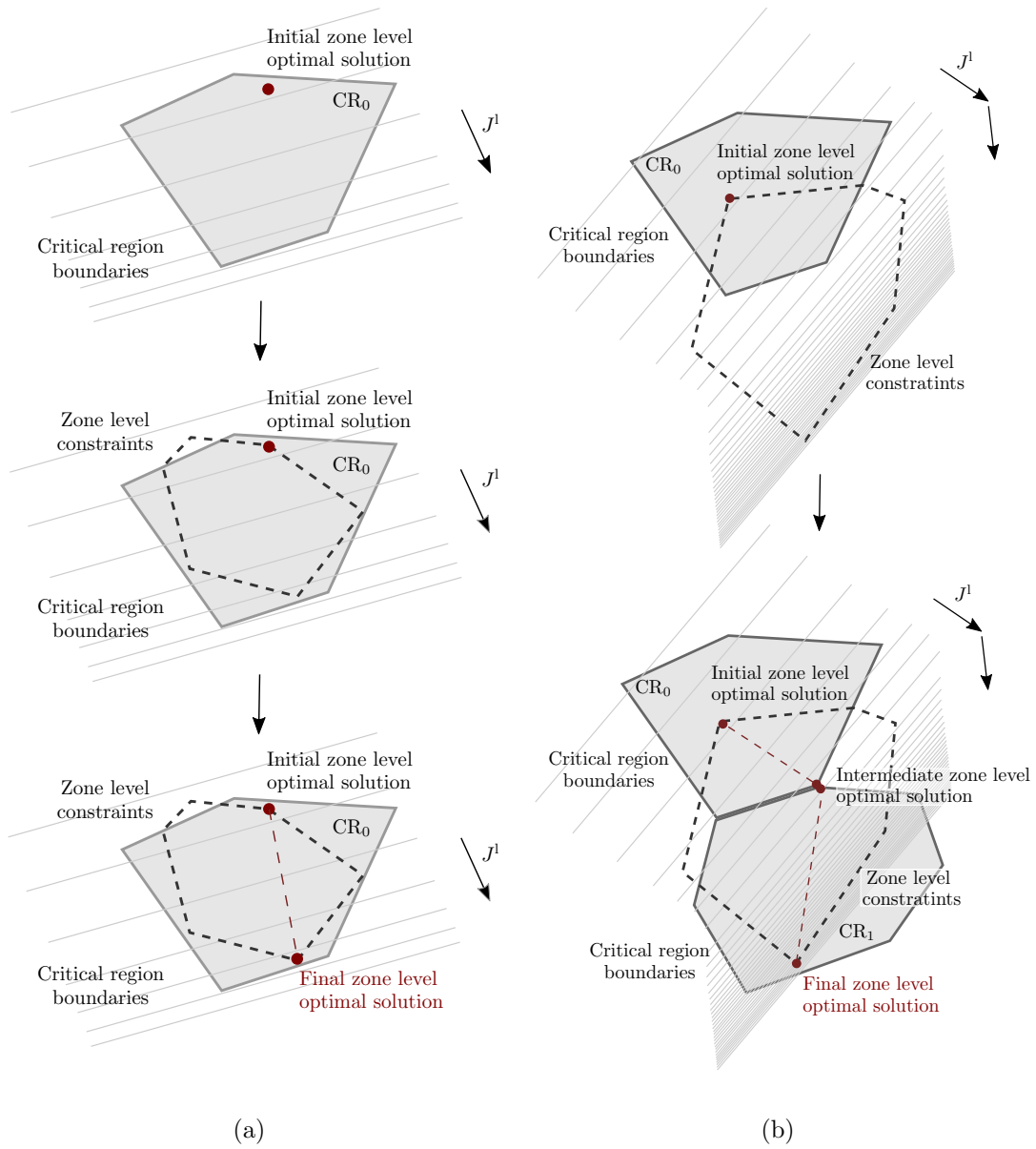


Figure 6.3. Geometric representation of parametric coordination in the space of \mathbf{u} : a) solution is inside the starting CR, b) iteration to a nearby CR. Parallel lines represent the cost function with higher density reflecting a smaller value.

The overall algorithm is presented in Fig. 6.4 as a flowchart.

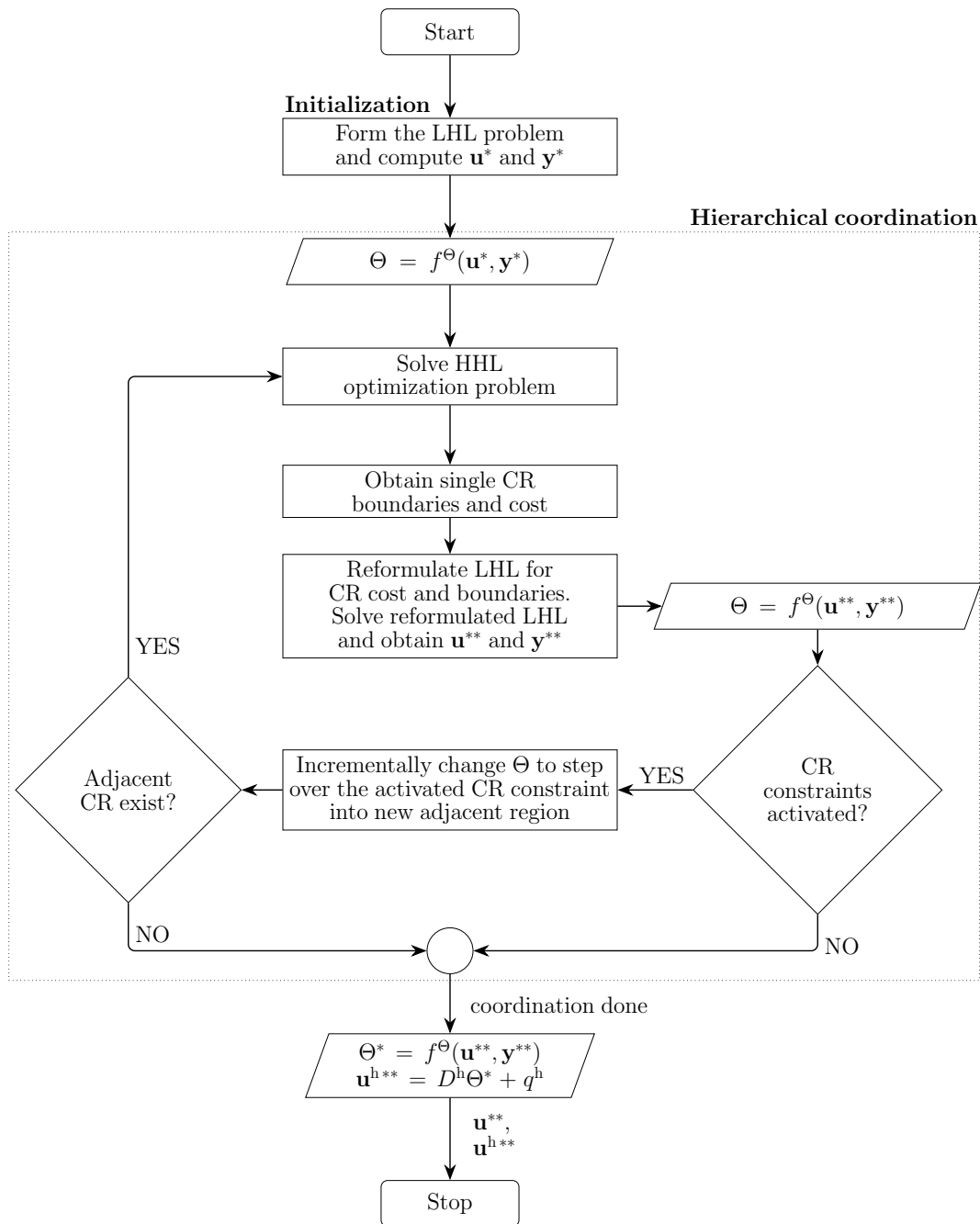


Figure 6.4. Hierarchical coordination algorithm flowchart.

6.3 Simulation results and case-study analysis

The presented hierarchical coordination approach is verified on a simulation case-study of the particular case-study building with controllable thermal energy consumption in building zones, central HVAC system and integrated microgrid. The benefits of the approach are demonstrated by comparing operational costs of the building controlled by conventional control algorithms with the costs arising as a result of energy-optimal hierarchical building control and price-optimal coordinated building control.

The case-study building consists of 248 controllable zones equipped with two-pipe FCUs for seasonal heating or cooling. The cooling energy for the building is supplied from the chiller station with the ability to control the supply temperature of the cooling medium on the central HVAC level. Besides the controllable building zones the chiller also supplies thermal energy towards the adjacent faculty building whose thermal energy consumption is considered non-controllable. The considered microgrid consists of battery storage system with fully controllable power converter and solar power plant. The central HVAC level electrical energy consumption is a controllable load on a microgrid level. It consists of the consumption of the chiller and of the FCUs' fans. The non-controllable electrical energy load on the microgrid level accounts production of the solar power plant and consumption of the office lighting, computers, building elevators as well as electrical air conditioning units in server rooms. More detailed description of the case-study building is given in Appendix A.

6.3.1 Simulation scenario

The considered control strategies are validated for a typical sunny workday in July characterised by external weather conditions shown in Fig. 6.5.

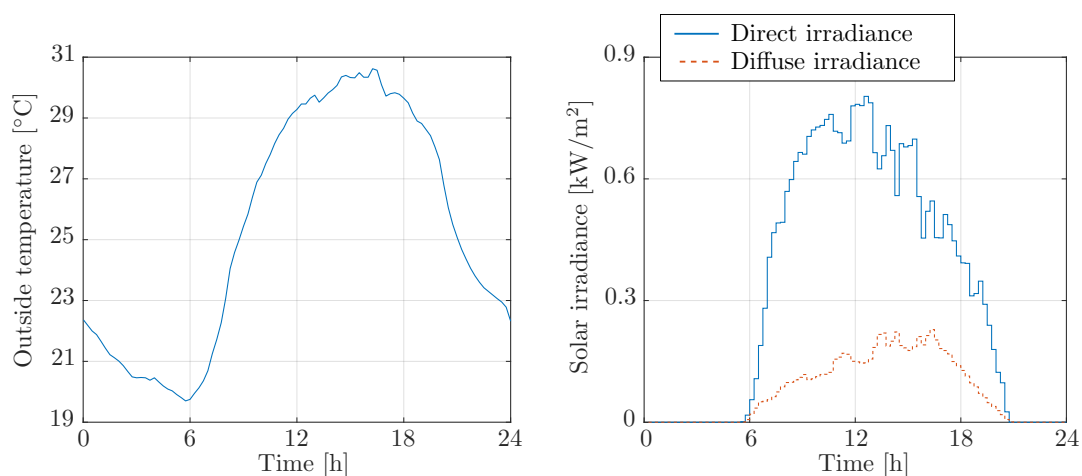


Figure 6.5. Typical weather conditions for a sunny day in July.

The non-controllable consumptions on the central HVAC system level and the microgrid level, estimated based on the historical building data are both shown in Fig. 6.6.

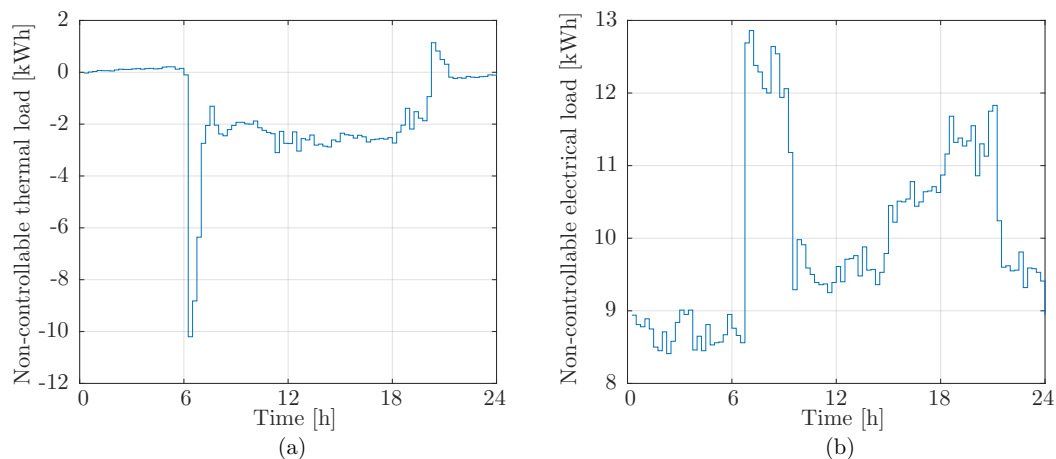


Figure 6.6. Non-controllable consumption of a) thermal energy on the central HVAC level and b) electrical energy on the microgrid level, for a sunny day in July.

Equivalent heat disturbances in all zones are assumed zero-valued. The considered simulation scenario data are obtained from historical measurements as averaged 24-hour profiles of all sunny workdays in July 2018 and 2019. Volatile energy market electricity prices, shown on Fig. 6.7, are taken from European Power Exchange company portal [142] and scaled to match the two-tariff prices comprising grid fees and supplied energy cost in Croatia [143]. The monthly cost of maximum building power consumption is also obtained from [143] and divided by 30 to represent a correct price amount for single day optimization. Battery system degradation costs of 0.226 EUR/kWh both for charging and discharging are calculated based on the battery purchase price and the manufacturer's catalogue [144]. All simulations are performed within Python environment [145, 137].

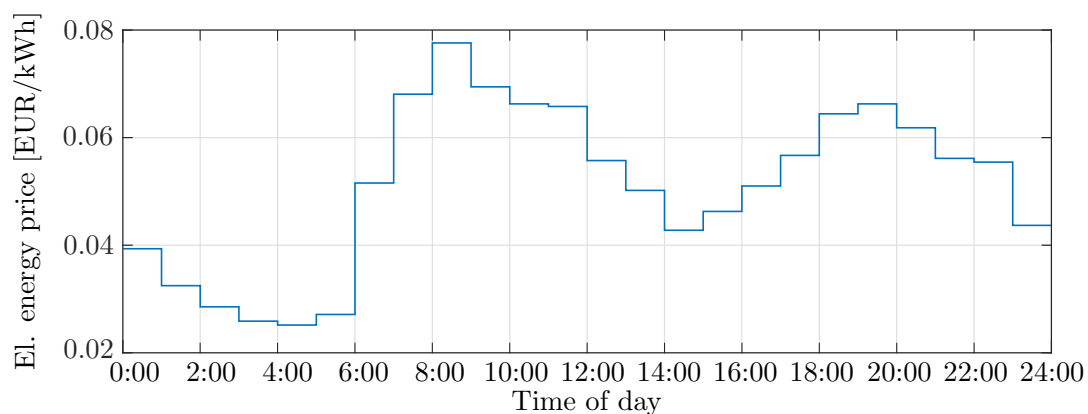


Figure 6.7. Day-ahead electricity price for a sunny workday in July.

The building is assumed to be occupied from 7:00 until 20:00. During the occupancy periods the zone temperature is requested to be within the interval of $24 \pm \Delta^{\text{ref}}$ where $\Delta^{\text{ref}} = 1.5^\circ\text{C}$. Outside that interval the allowed deviation from the temperature reference is set to $\Delta^{\text{ref}} = 8^\circ\text{C}$ to match the building protect limits defined as $24 \pm 8^\circ\text{C}$.

The following control strategies are considered.

1. **Baseline control.** The baseline control on the zone level is based on a simple discrete hysteresis control of zone temperature with sampling time 1 min. The baseline controller switches between available power outputs based on the difference between the temperature reference and the zone temperature, such that the low FCU fan speed is switched on at -0.15°C , medium speed at -0.30°C and high speed at -0.45°C . The maximum attainable thermal power at the highest fan speed is matched with zone level thermal power limitations used in (6.3). For a fair comfort level comparison, the baseline controller starts to operate 1 hour before the start of the occupancy period to meet the comfort requirements in occupancy periods on time. On the central HVAC system level baseline control constantly keeps the medium flow at 23 kg/s and supply temperature at 8°C according to the established practice of the chiller maintenance service. The baseline for the microgrid level control is a simple transactive controller. If the consumed energy is higher than the expected daily average energy consumption, the battery will be discharged with the maximum allowed power. If the consumed energy is lower than the expected daily average consumption, the battery will be charged with the maximum allowed power. Expected daily energy consumption is obtained as the combined baseline central HVAC system level consumption and the microgrid level non-controllable consumption presented in Fig. 6.6.
2. **Energy-optimal control.** In energy-optimal control the BEMS operates in an uncoordinated manner where each building optimization level operates independently (local-wise optimal) with only energy demands exchanged between the levels. During this exchange no feedback is provided from the superior levels regarding the consumption profiles and the corresponding energy prices and no tuning of the initial energy demands is performed. Consequently, the zone level and central HVAC system level optimize their behaviour with respect to the energy consumption only. In such a set-up the zone level consumption is a non-controllable load for the central HVAC system level. Likewise, the consumption of the central HVAC system level adds up in a non-controllable way to the non-controllable load on the microgrid level.
3. **Price-optimal control.** In coordinated control, all considered control levels are joined together by the iterative parametric hierarchical coordination presented in Section 6.2. The building optimization levels exchange information through respective CRs value functions and constraints, and their corresponding parameters. The zone level communicates to the HVAC level the optimized profiles of thermal energy consumptions and temperatures within zones, whereas the HVAC optimizes its behaviour with respect to the obtained zone profiles and communicates the local characterization of the thermal energy cost function to the zone level. Coordination between the microgrid and the HVAC level is achieved by communicating the HVAC

electrical energy consumption profile to the microgrid level and local characterization of the electrical energy cost function from the microgrid to the HVAC level. The procedure is repeated iteratively (see. Fig. 6.4) until the algorithm converges.

The performance of all considered control strategies is verified in a scenario with the enforced repeated behaviour from day to day, i.e. the initial state of the building (at the beginning of the day, at midnight), which is subject to optimization, is equal to the final state of the building (at the next midnight). All control problems mentioned have for this daily planning scenario also the initial state $x_{k|k}$ as the optimization variable. In this way the system does not exploit any initial condition in the building for inducing savings, but leaves the building in the same condition as it was at the beginning of the day – i.e. no energy accumulated in initial conditions is exploited. The repeatability of the baseline controller operation is ensured by simulating the building performance over several days with the same weather conditions as in the considered simulation scenario. The repeatability constraints on the microgrid level assure equal initial and final battery state of charge (SoC) whereas the central HVAC system does not contain any dynamics thus no additional constraints are needed. The additional zone level constraints are:

$$x_{k|k} = x_{k+H|k}, \quad (6.18)$$

where $x_{k|k} \in \mathbb{R}^{n_x}$ is the initial system state at 0:00 and $x_{k+H|k} \in \mathbb{R}^{n_x}$ is the predicted system state at the end of the prediction horizon of length H at 24:00.

Due to the additional state introduced in the zone level optimization problem, the parameter Θ which enables the coordination with the central HVAC system level is defined as:

$$\Theta = \begin{bmatrix} \mathbf{u}^\top & \mathbf{y}_H^\top \end{bmatrix}^\top \quad (6.19)$$

where $\mathbf{y}_H = \left[(y_{k|k})^\top \quad (\mathbf{y})^\top \right]^\top$ and $y_{k|k} \in \mathbb{R}^{n_y}$ is a vector of initial zone air temperatures at time 0:00. After the CR and accompanying cost are calculated, the CR constraints are added as additional set of constraints to the original zone level optimization problem (6.4) such that:

$$\begin{aligned} J^{l*} &= \min_{\mathbf{u}, \boldsymbol{\sigma}_1, \boldsymbol{\sigma}_2} J^{h*}(\Theta) + \gamma_e \cdot \boldsymbol{\delta}^\top \cdot \bar{c}_t \cdot |\mathbf{Q}(\mathbf{y}^{\text{ref}} - \mathbf{y})| + g_1 \mathbf{1}^\top \boldsymbol{\sigma}_1 + g_2 \mathbf{1}^\top \boldsymbol{\sigma}_2, \\ &\text{s.t.} \quad (6.1), (6.2), (6.3), \\ &\quad x_{k|k} = x_{k+H|k}, \\ &\quad \Theta = \begin{bmatrix} \mathbf{u}^\top & \mathbf{y}_H^\top \end{bmatrix}^\top, \quad \Theta \in \mathcal{C}^h, \\ &\quad \boldsymbol{\sigma}_1 \geq 0, \quad \boldsymbol{\sigma}_2 \geq 0, \end{aligned} \quad (6.20)$$

where $\mathcal{C}^h = \left[\mathbf{c}_t^\top \quad \mathbf{c}_y^\top \right]^\top$, $\mathbf{c}_t \in \mathbb{R}^{H \cdot n_u}$ and $\mathbf{c}_y \in \mathbb{R}^{(H+1) \cdot n_y}$. Set \mathcal{C}^h represents the central HVAC level CR constraints.

All the MPC controllers operate with 15-min sampling time and thus $H = 96$ in the considered simulation scenario. For convenience, all the considered simulation scenario parameters are summarized in Table 6.1.

Table 6.1. *Case study parameters.*

Zone temperature reference	24°C
Chiller rated power (electrical)	244.2 kW
Maximum chiller supply temperature	15.6°C
Minimum chiller supply temperature	7°C
Battery capacity	32 kWh
Battery discharge efficiency	90%
Battery charge efficiency	90%
Minimum battery charge state	10%
Maximum battery charge state	90%
Maximum battery energy discharge in 15 min	-2.4 kWh
Maximum battery energy charge in 15 min	2.4 kWh
Maximum grid energy in 15 min (selling)	-90 kWh
Maximum grid energy in 15 min (buying)	90 kWh
Photovoltaic array rated power	10.58 kW
Battery degradation cost	0.226 EUR/kWh
Maximum power cost	0.116 EUR/kW

6.3.2 Results

In order to fully investigate the contributions and savings possibilities of hierarchical coordination between energy flows and consumption levels, the corresponding building operation costs and achieved thermal comfort are investigated for cases with and without battery storage system and for different comfort-savings trade-off parameter values. For the case without battery storage the flexibility is achieved only by modifying the central HVAC system consumption shaped by the thermal comfort demands from the building zones. The savings amount is thus highly influenced by the change of the comfort-savings trade off parameter γ_e and the width of the permissible zone temperature interval Δ^{ref} . The introduction of the battery energy storage system into the building additionally increases the building flexibility and enables additional extensions of the savings margin.

Typical temperature profiles and mean thermal power provided from the FCUs to the zone air in 15-minutes time intervals, presented for four exemplary building zones, all located on the 9th floor of the case-study building, C09-01, C09-16-3, C09-04 and C09-13 are shown in Fig. 6.8, Fig. 6.9, Fig. 6.10 and Fig. 6.11, respectively. The selected building zones are of different sizes and orientations with the description of their physical properties listed in Tab. 6.2.

Table 6.2. *The description of the physical properties of the exemplary building zones.*

Zone	Orientation	Floor area
C09-01	north	48.12 m ²
C09-04	south	35.03 m ²
C09-13	south	7.10 m ²
C09-16-3	north	22.80 m ²

The permissible zone temperature interval during the occupancy periods 7:00-20:00 is denoted with black dashed lines. The control actions of the baseline controller are based only on current measurements resulting with reactive control and significant disruption of the comfort in zones in which the the comfort constraints can not be satisfied without the appropriately applied precooling actions. The deviation of the zone temperature from the reference for price-optimal control and case without batteries in intervals around 14:00 is a clear result of coordination where the microgrid and central HVAC level force the zones to lower the thermal energy demand in intervals in which the peak power demand occurs. For price-optimal control and case with batteries, the peak is already flattened in initial microgrid iteration where in all subsequent iterations the zone level thermal energy consumption is shifted towards the intervals with more beneficial electrical energy prices and HVAC system efficiency.

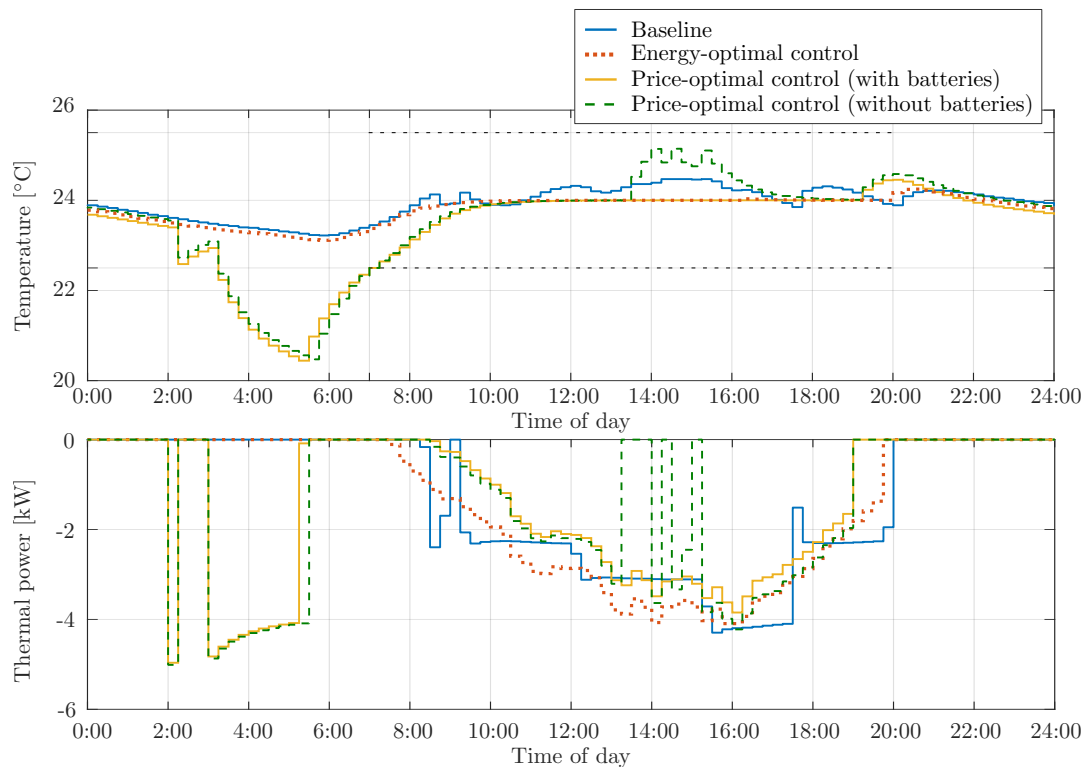


Figure 6.8. The temperature and mean thermal power provided from the FCUs to the zone air in 15-minutes time intervals in zone C09-01 within the analysed day.

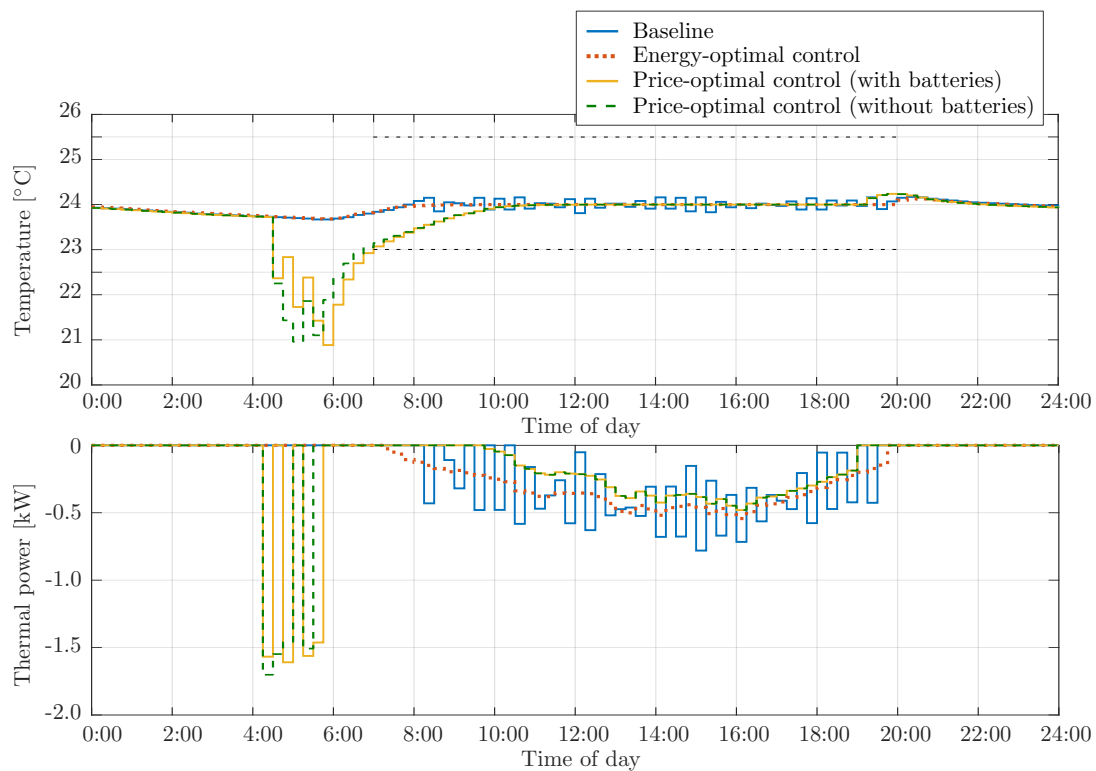


Figure 6.9. The temperature and mean thermal power provided from the FCUs to the zone air in 15-minutes time intervals in zone C09-16-3 within the analysed day.

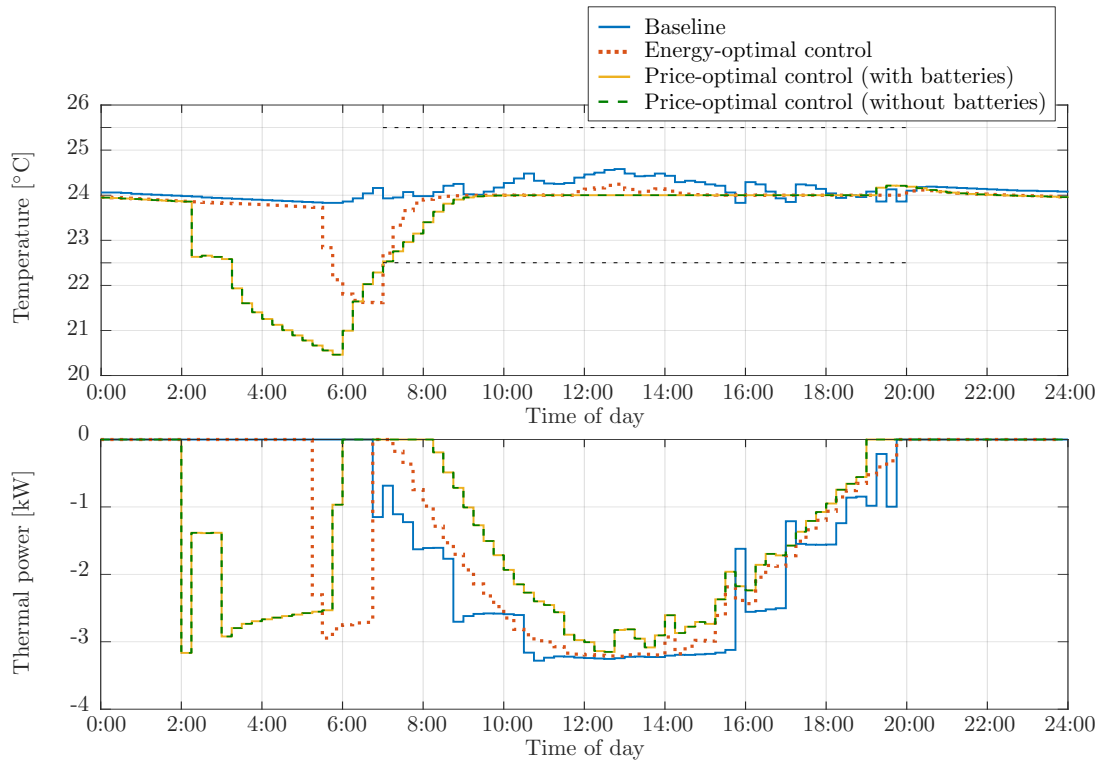


Figure 6.10. The temperature and mean thermal power provided from the FCUs to the zone air in 15-minutes time intervals in zone C09-04 within the analysed day.

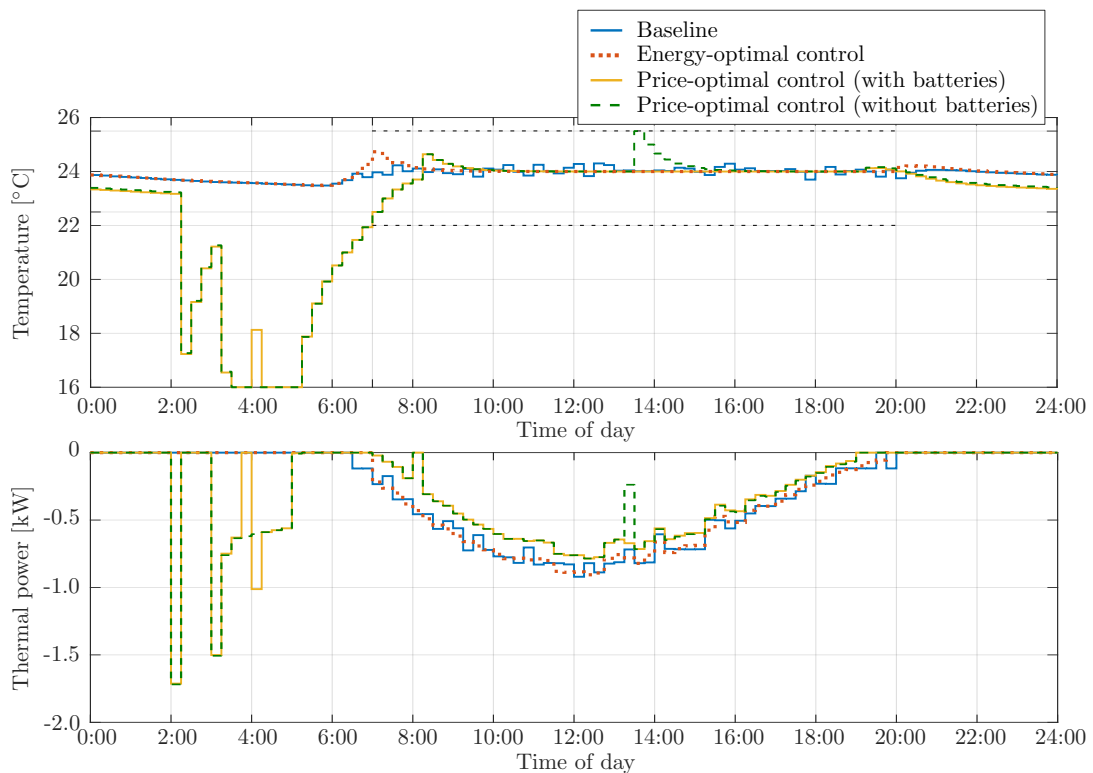


Figure 6.11. The temperature and mean thermal power provided from the FCUs to the zone air in 15-minutes time intervals in zone C09-13 within the analysed day.

The comparison of overall thermal power provided by FCUs to the zone air and averaged on 15-minutes time instants in all 248 controllable zones for different control strategies is shown in Fig. 6.12.

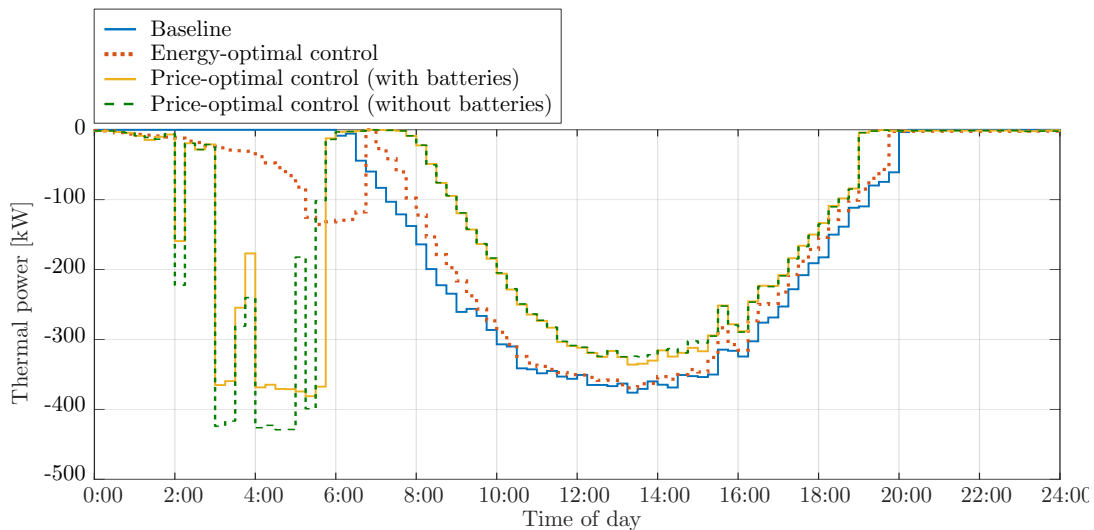


Figure 6.12. Overall cooling energy needs for all the zones (sum of energies that should be provided by FCUs to zones air).

The figure shows the predictive feature of MPC algorithm where cooling is initiated before the start of occupancy period to satisfy comfort demands at the beginning of the occupancy period and to activate the precooling of the building zones in which the temperature constraints can not be respected otherwise. Even though the consumption of the thermal energy on the zone level is increased by up to 1.10% for energy-optimal control and up to 2.76% for price-optimal control when compared to the baseline control, the overall building operational costs presented at the end of the subsection are reduced up to 26.50%.

In the considered case of seasonal cooling, the comfort with baseline controller is significantly disrupted in cases when the available thermal power is insufficient for covering the peak demand. The obtained comfort levels significantly differ for zones with different orientation. Comfort levels, calculated separately for zones oriented towards north and the other oriented towards south are shown in Fig. 6.13 and compared to the resulting thermal energy consumption of the considered zones. The comfort level indicator, measured as average deviation (AD) from the temperature reference is calculated as:

$$AD = \frac{1}{n_s n_y} \sum_{k \in \mathcal{O}} \|\mathbf{y}_k^{\text{ref}} - \mathbf{y}_k\|_1, \quad (6.21)$$

where operator $\|\cdot\|_1$ denotes L_1 norm, \mathcal{O} is the set of all the time-samples within the occupancy periods and n_s is its cardinal number. The comfort level indicator provides information of average expected temperature in each time instant, e.g. for price-optimal control with $\Delta^{\text{ref}} = 1.5^\circ\text{C}$, the expected temperature in south-oriented zones for the

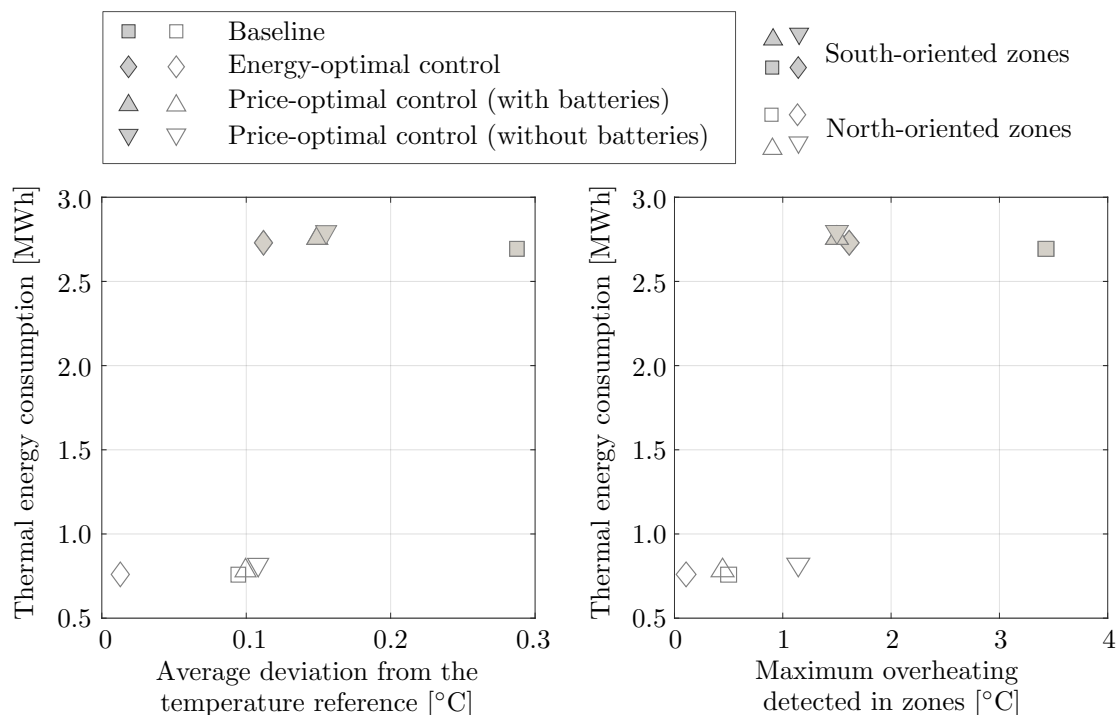


Figure 6.13. Comfort level indicators for different controller strategies.

considered simulation scenario is within the $\pm 0.11^\circ\text{C}$ range around y^{ref} . Besides the average deviation from the temperature reference the performance of different control strategies is also compared with respect to the maximum overheating, i.e. maximum temperature above the reference detected in building during the occupancy periods. The large overheating of south oriented zones when using the baseline control strategy is a clear result of lacking predictive feature. In both MPC based strategies the temperature in all building zones is kept in the permissible temperature range of $y^{\text{ref}} \pm \Delta^{\text{ref}}$, reducing thus the overheating up to 56% and improving the overall comfort in all building zones by at least 57%.

The day-ahead conditioning of the supply medium temperature at the central HVAC level is depicted in Fig. 6.14. The upper and lower limits of the supply temperature are denoted with the black dashed lines. The controller selects the supply medium temperature that will ensure the required amount of thermal energy in the zones given the zone temperature profile stated by the zone level MPC. Additionally, the supply medium temperature value also influences the incurred thermal losses and with it associated cumulative thermal load on the chiller which results with the change of the chiller efficiency. Generally, the decrease of the thermal loads in the zones results with the increase of the supply medium temperature. The reconfiguration of the zone thermal energy consumption allows the cost-optimal central HVAC system controller to keep the supply medium temperature on a higher values in the large part of the prediction horizon, resulting with the lowered thermal energy losses. During the time instants with the increased thermal loads in the zones, the supply medium temperature is kept close to the minimum allowed value.

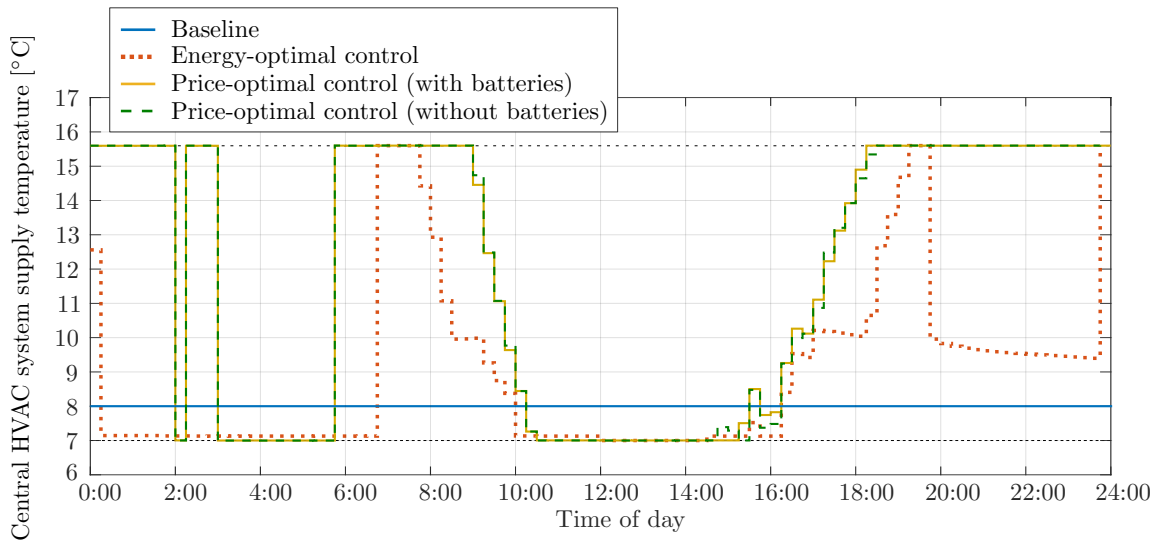


Figure 6.14. Supply medium temperature profiles for different control strategies.

The overall electrical load profile of the central HVAC system, required to cover the controllable thermal energy demand shown in Fig. 6.12 and non-controllable thermal energy demand shown in Fig. 6.6.a), is shown in Fig. 6.15.

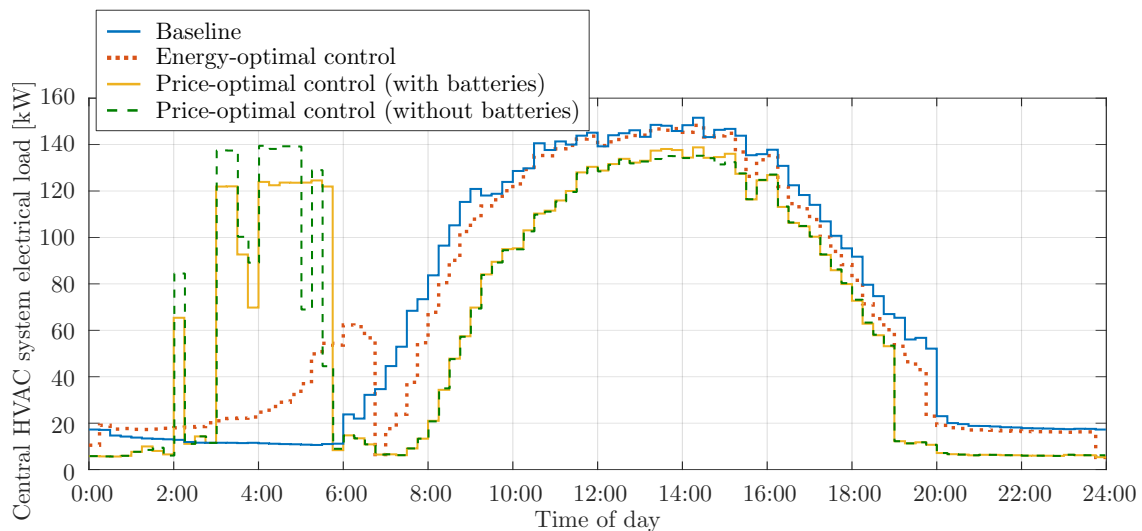


Figure 6.15. Central HVAC system electrical load profile average in 15-minute time instants obtained with different control strategies.

The cost-optimal control minimises the peak power value at time instants with the highest loads at the expense of the increased precooling operation in the morning hours when the considered volatile electrical energy prices are the cheapest, as depicted in Fig. 6.7. With the sudden increase of the electrical energy price around 6:00, the zone level controller and consequently central HVAC controller suddenly reduce the power consumption, which is also indicated by the sudden increase of the supply medium temperature.

Battery storage system energy exchange and SoC levels throughout the day are depicted in Fig. 6.16. In the MPC strategies, the batteries are charged during the lowest electricity prices in the early morning and exploited during the period 11:00-16:00 for peak power reduction. Additional savings are obtained by utilizing the electricity prices difference during the period of 16:00-20:00, where the overall building consumption is lower and peak power reduction is not needed. Figure 6.16 shows that the storage system operational limits as well as operation repeatability are respected.

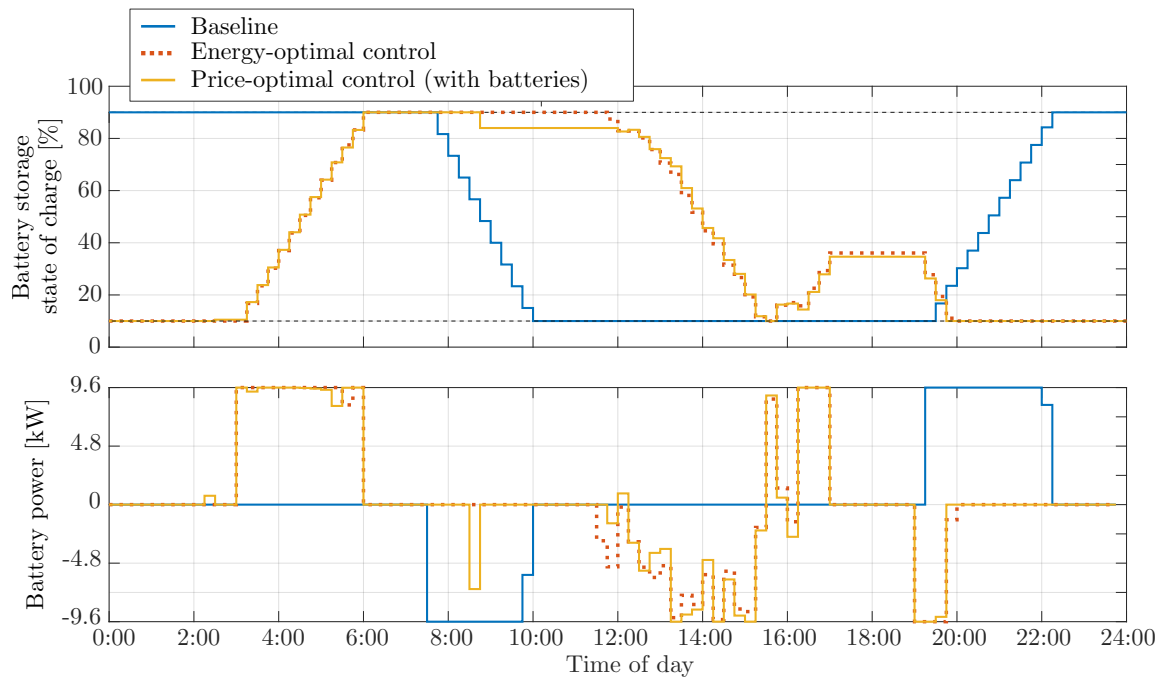


Figure 6.16. Battery storage state of charge and battery storage power exchange profiles averaged in 15-minutes time instants obtained with different control strategies.

Daily energy exchange with the distribution grid is depicted in Fig. 6.17. Lower electricity prices during the early morning from 03.00-06:00 are targeted for increasing the overall building consumption such that the energy consumption during peak prices from 07:00-10:00 is decreased and overall operation costs reduced. Additionally, the building operation costs are further reduced since the peak power consumption is decreased from 189.67 kW in the baseline scenario, to 173.62 kW in the price-optimal scenario without batteries and additionally to 167.32 kW in the price-optimal scenario with batteries. Overall building level operation costs and peak power costs reduction over the iterations is depicted in Fig. 6.18. It is shown that the operation costs are decreasing over iterations until the convergence of the algorithm where additional tuning of the building operation is either not economically viable or is constrained by zones, central HVAC or microgrid level physical limitations.

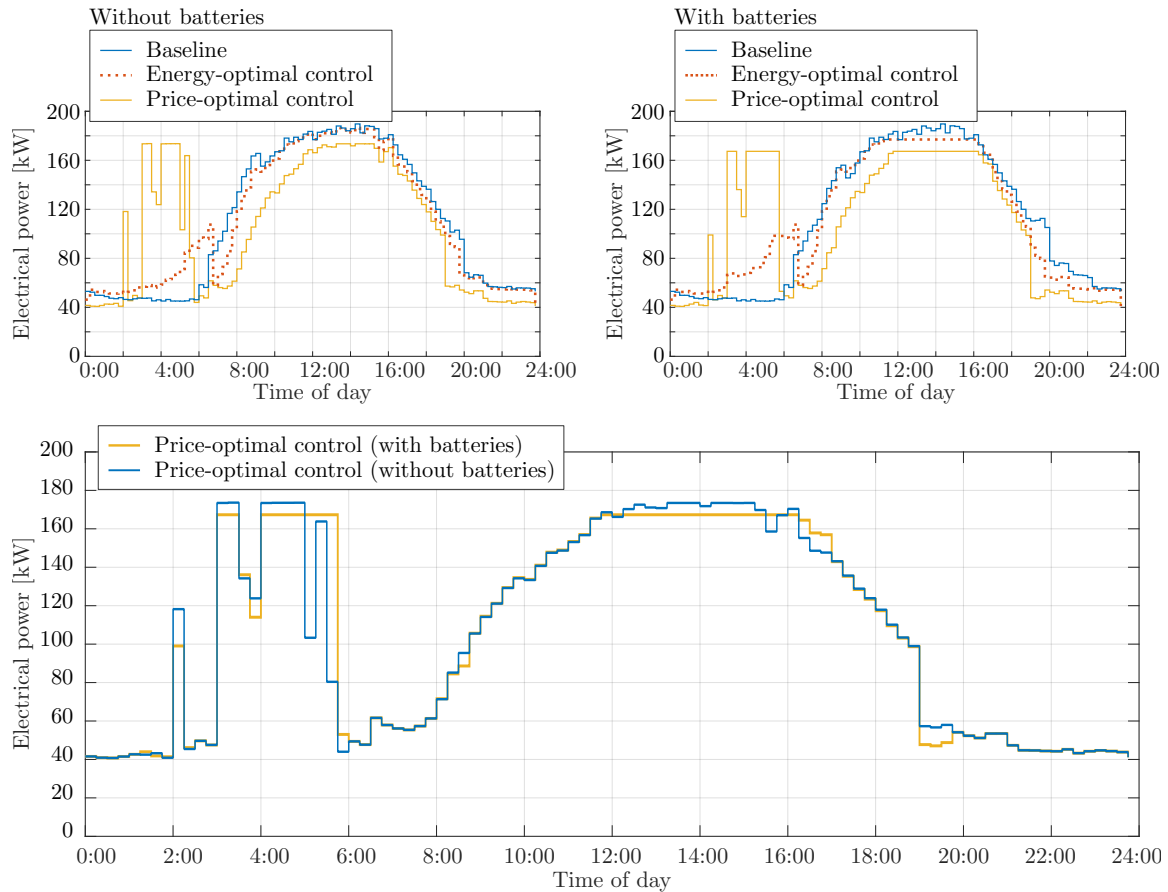


Figure 6.17. The overall day-ahead building energy consumption profile average in 15-minutes time instants obtained with different control strategies.

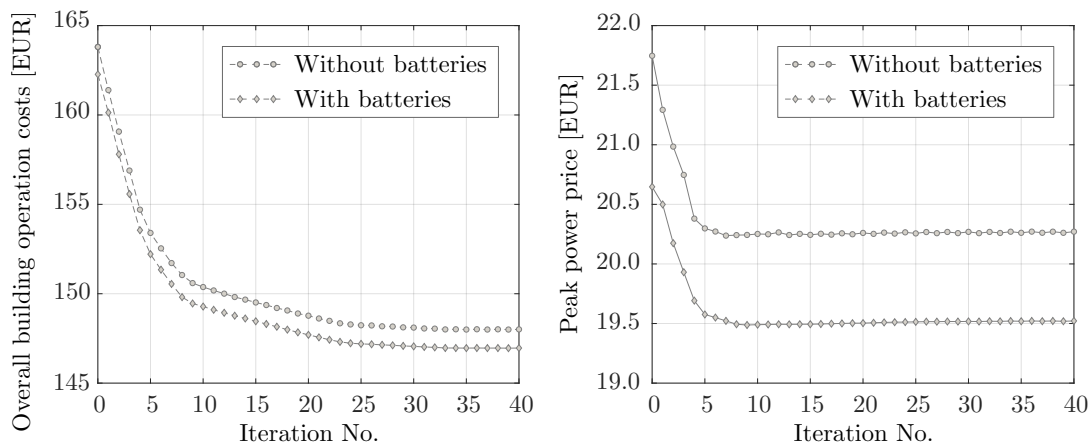


Figure 6.18. Overall building operation (left) and peak power (right) costs over the iterations of the BEMS hierarchical coordination.

In order to fully investigate the contributions and savings possibilities of hierarchical coordination between energy flows and consumption levels, the corresponding building operation costs and achieved thermal comfort in building zones are validated with respect to the comfort-savings trade-off parameter γ_e . The initial comfort focused case-study is extended with the savings focused studies where the parameter γ_e is set to $\gamma_e = 0.5$ and

$\gamma_e = 0$. The comparison of battery storage system energy exchange and state of charge levels throughout the day for different comfort-savings trade-off parameters are shown in Fig. 6.19 and Fig. 6.20.

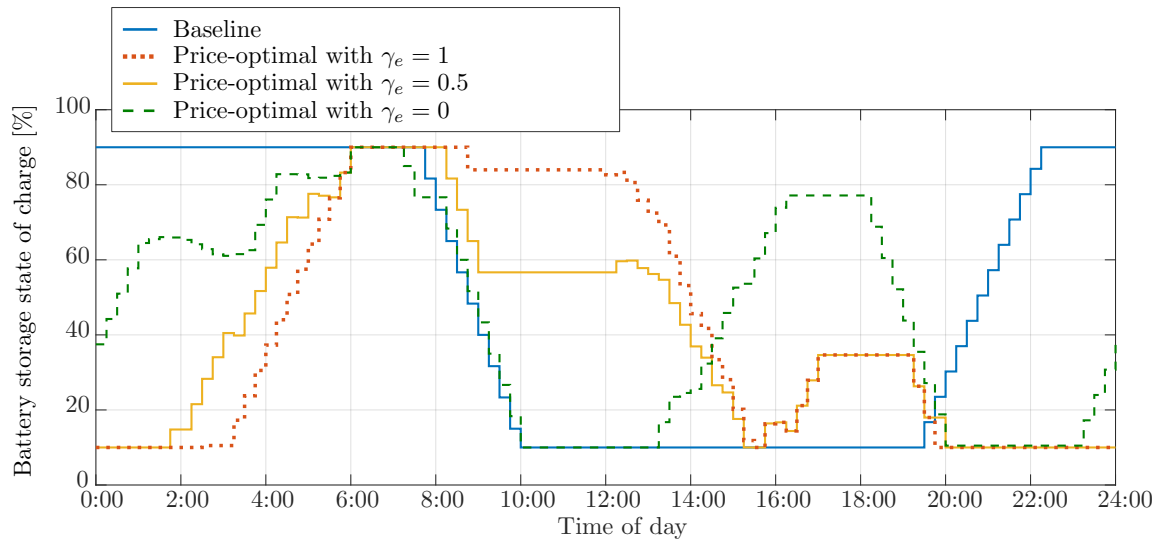


Figure 6.19. Battery state of charge levels for different comfort-saving trade-off parameter γ_e values.

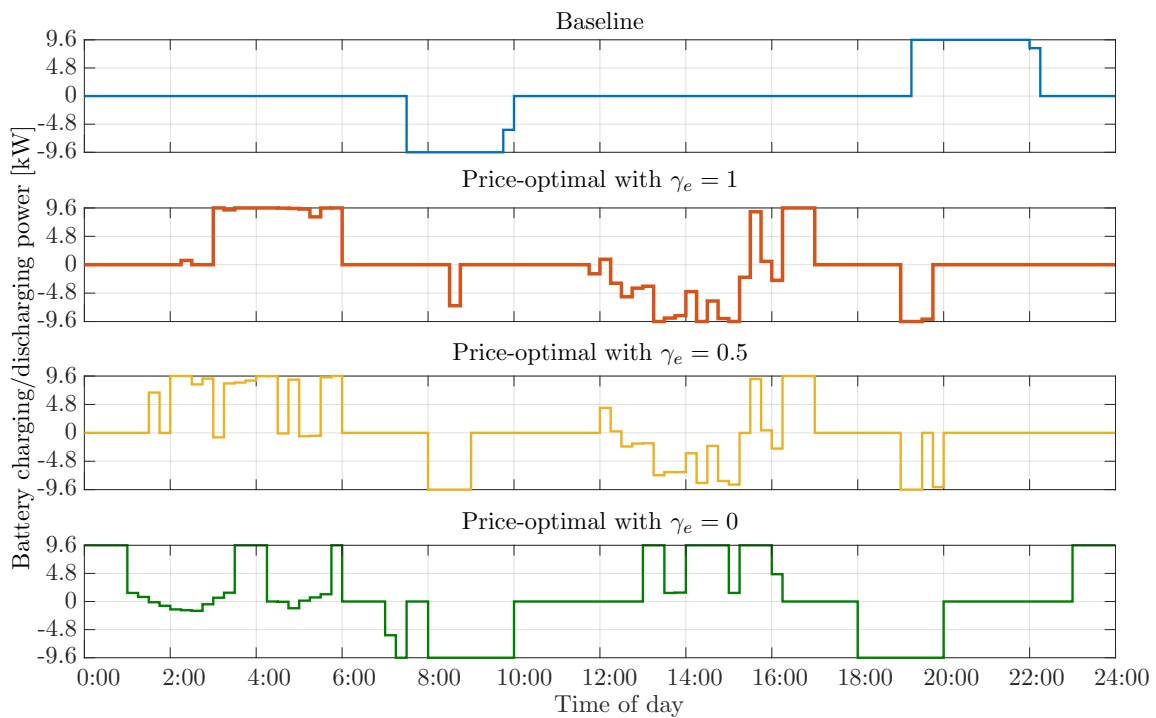


Figure 6.20. Battery storage power exchange profiles averaged in 15-minutes time instants for different comfort-saving trade-off parameter γ_e values.

Based on the flexibility of the zone level, the battery storage system is utilized in different ways and for different purposes. Among the three considered γ_e values the flexibility of the zone level is lowest for the parameter $\gamma_e = 1$ and highest for parameter

$\gamma_e = 0$. For $\gamma_e = 1$ the batteries are fully utilized to lower the peak power demand since the zone level flexibility is too low for flattening the consumption during the peak power periods. In cases with the increased zone level flexibility, the reshaping of the zone level thermal energy demand offers more cost-effective solution for lowering the peak power demands, whereas the batteries are utilized to cover high energy price intervals 7:00-10:00 and 18:00-20:00.

The comparison of overall building operation costs and achieved thermal comfort stemming from baseline operation with the results obtained via energy-optimal control and price-optimal control is shown in Fig. 6.21 and Fig. 6.22 and listed in Tab. 6.3, also supported with the corresponding comfort evaluation metrics. Comfort levels, calculated as the average of all building zones and cases with and without batteries are shown in Fig. 6.23 and compared to the resulting building operation costs.

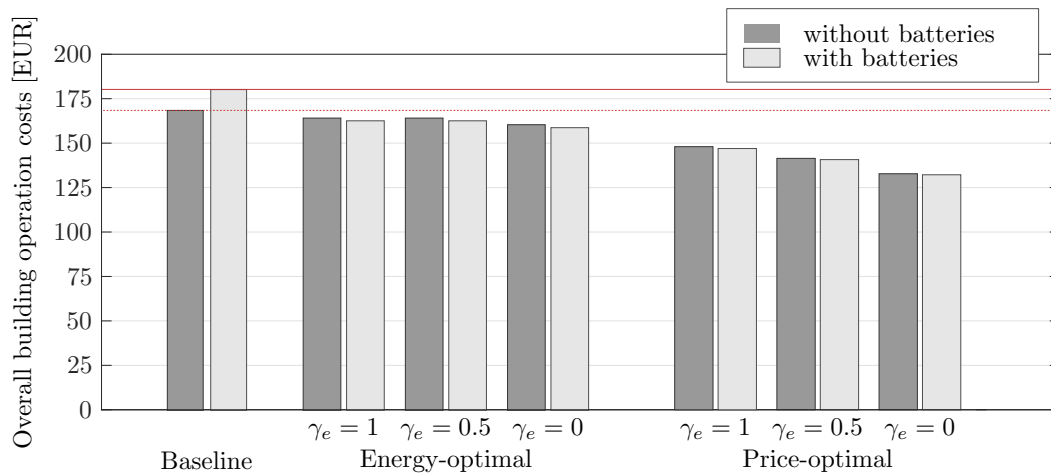


Figure 6.21. Comparison of overall building operation costs for different control strategies.

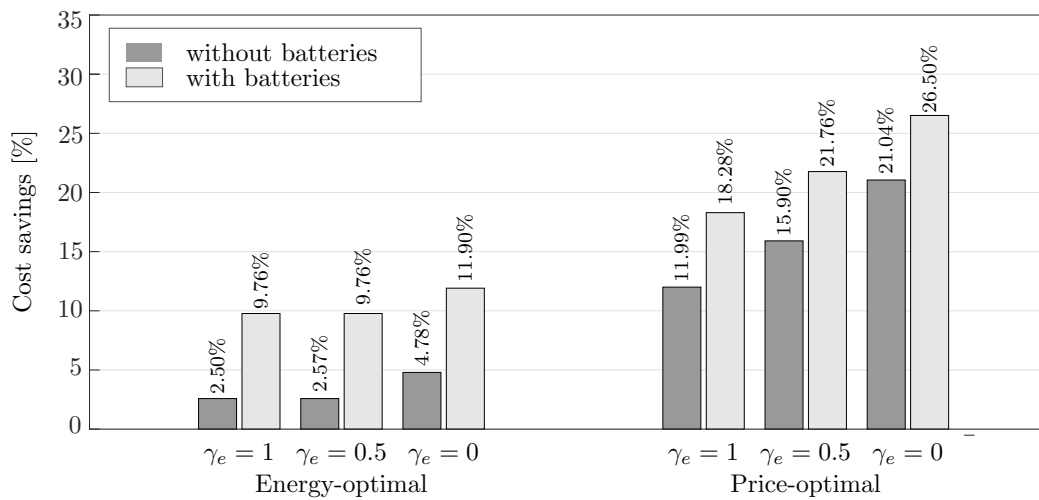
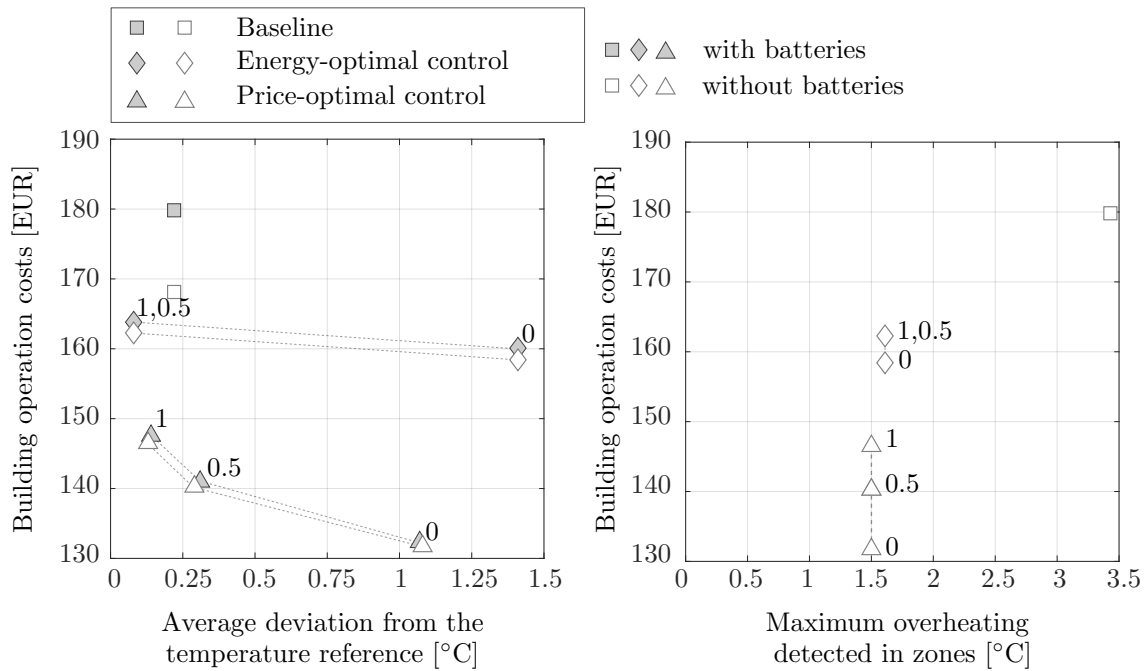


Figure 6.22. Comparison of cost savings for different control strategies.

Table 6.3. Overall building operation costs and achieved thermal comfort in building zones for different control strategies and different comfort-saving trade-off parameter γ_e .

	Operation costs [EUR]	Average deviation from temperature reference [°C]			Maximum overheating [°C]	
		all zones	south-oriented zones	north-oriented zones		
WITHOUT BATTERIES						
$\gamma_e = 1$	Baseline	168.13	0.22	0.29	0.09	3.43
	Energy-optimal	163.81	0.08	0.11	0.01	1.61
	Price-optimal	147.97	0.14	0.16	0.11	1.50
$\gamma_e = 0.5$	Energy-optimal	163.81	0.08	0.12	0.01	1.61
	Price-optimal	141.40	0.31	0.34	0.26	1.50
$\gamma_e = 0$	Energy-optimal	160.09	1.41	1.38	1.47	1.61
	Price-optimal	132.75	1.07	1.12	0.97	1.50
WITH BATTERIES						
$\gamma_e = 1$	Baseline	179.82	0.22	0.29	0.09	3.43
	Energy-optimal	162.27	0.08	0.11	0.01	1.61
	Price-optimal	146.94	0.13	0.15	0.10	1.50
$\gamma_e = 0.5$	Energy-optimal	162.27	0.08	0.12	0.01	1.61
	Price-optimal	140.70	0.29	0.32	0.23	1.50
$\gamma_e = 0$	Energy-optimal	158.42	1.41	1.38	1.47	1.61
	Price-optimal	132.17	1.08	1.14	0.96	1.50

**Figure 6.23.** Comfort level indicators for different controller strategies.

The maximum detected overheating is the same for cases with and without batteries. As expected, with the increased flexibility of the building zone level through the change of the comfort-savings trade-off parameter γ_e the overall building operation costs are reduced at the cost of the decreased thermal comfort in building zones. However, in all considered cases the AD is within the permissible interval and overheating is significantly reduced. Even though the overall thermal energy consumption on the zone level increases in price-optimal control the overall building operations costs are significantly reduced. This is due to the fact that the coordination allows the HVAC level to communicate the localised cost of its electrical energy consumption to the zone controller. Thus, the zone controller reconfigures its operation by including the electrical energy cost of the HVAC level in its objective function together with the comfort objective function. Which results with the decrease in the overall electrical energy cost. Trough the results it has been shown that the software-based coordination between BEMS levels offers the possibility to transform the building energy consumption profile and reduce the building peak power consumption without large financial investments in installation of energy storage systems.

Part II conclusion and future research opportunities

Possible savings of Model Predictive Control (MPC) in building climate control depend largely on the formulation of the MPC optimization problem. The MPC temperature control approach developed within the Chapter 5 allows the individual setting of comfort level with the aim of user satisfaction and increased productivity rather than achieving additional energy savings. The performance of the developed approach is verified with the advanced options like peak shaving or flexible night regime intentionally left out to show that even for a simple case, properly designed MPC outperforms conventional controllers without compromising users' comfort. Moreover, it is shown that the users' comfort is improved. The achieved overall yearly energy consumption gives insight into the expected maximum gains for various commercial buildings and locations. In Chapter 6 a concept of modular building energy management system (BEMS) is presented. It is envisioned as a hierarchical structure that consists of three main levels: zone level, central heating/cooling medium preparation level (referred to as central HVAC) and building microgrid level. The development done within the thesis is focused on zone level only, thus with the Chapter 6 zone level as the lowest level in the proposed hierarchy, is presented independently from the other parts of the system. The MPC as the main underlying technology in the conceptualized BEMS enables to take into account relevant current building conditions and available predictions when deciding how to actuate the building. The modularity of the approach is achieved by a parametric coordination between the levels with exchange of predicted consumption and price of operation. This enables the technology independency, cost-effective implementation and upscaling towards the smart grid and smart city concepts where buildings play active roles. Several control strategies are examined to give a realistic insight into possible cost benefits of imminent or more distant technology utilization in building energy management. Results show large cost-saving opportunities of MPC and highlight the proposed modular approach as a possible integration method.

Part III

Application to a full-scale skyscraper building

Zone model predictive control – real-time implementation

In the last decades, the application of model predictive control (MPC) for building climate control has received considerable attention from research community. Its distinctive advantages over conventional control algorithms make the MPC approach a promising solution for widespread problems of energy management within buildings. Although the earliest applications of MPC date back to early seventies in the chemical industry, the practical implementation of MPC for building climate control is still in its early stages due to its high computational demand followed by the required investment in sensing and information communication technology (ICT) equipment required to collect, store, and analyse the building-related data. Only recently, the decreasing hardware cost and data accessibility, enabled by advances in computational power and ICT technologies started the increased application of MPC to various types of building energy systems (Fig. 8.1¹). Moreover, the growing spread of renewable energy systems combined with the increasing importance of demand response and rising energy prices is evidently changing the paradigm of energy and the role of the buildings in the grid.

Up to date, the practical implementation of MPC for building climate control has been reported on a commercial building in Allschwil [14], a building of the Czech Technical University in Prague [15], one zone in a campus of the University of Almería in Spain [17], two test zones in the Energy Resource Station in Iowa [16], a building used by the Faculty of Sciences and Technology of the University of Algarve [146], a building of Dalhousie University in Halifax [18], the test zone inside Building and Construction Authority SkyLab test facility in Singapore [19], and the laboratory room in the building

¹The statistic is obtained based on the results of SCOPUS (www.scopus.com) search engine. The articles related to MPC in buildings are articles containing the keywords ('model', 'predictive', 'control', 'building') in title, abstract or keywords list. The articles related to experimental validation are articles containing an additional keyword ('experimental') in title, abstract or keywords list.

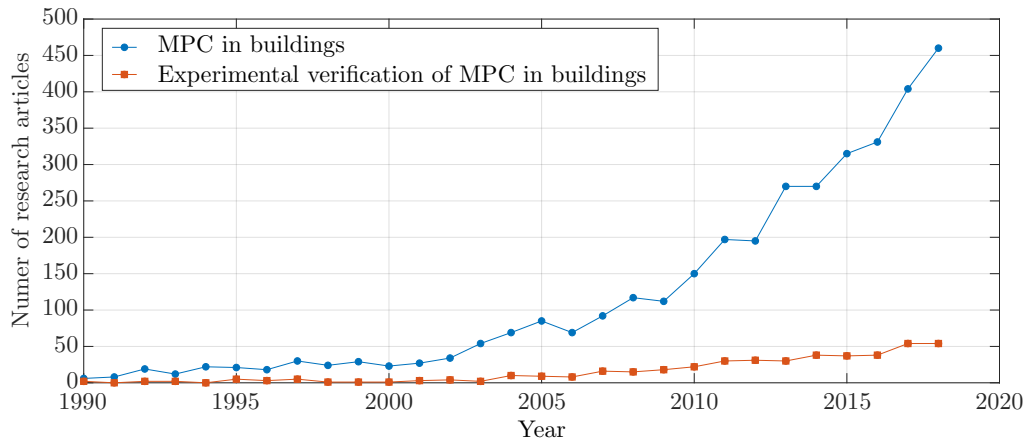


Figure 8.1. Number of research articles related to MPC and experimental verification of MPC in buildings.

of the Royal Institute of Technology campus in Stockholm [20]. The reported experimental studies are listed in Tab. 8 and classified according to the system that is controlled, the heating/cooling elements (HCEs), the total experiment time, and the obtained energy savings.

Table 8.1. Summary and comparison of experimental studies of MPC for zone comfort control.

Study	Controlled system	Heating/cooling elements	Experiment duration	Electric energy savings	Thermal energy savings
[14]	occupied five-floor building	TABS, blinds, AHU	7 months	17%*	-
[15]	occupied eight-floor building	TABS heating	2 months	-	15-28%
[17]	occupied office	FCU	6 hours	53%	-
[16]	two unoccupied test zones	AHU, ice storage, chillers	4 days	17-27%*	-
[146]	four occupied rooms	AHU	3 days	50%	-
[18]	occupied five-floor building	HVAC system, VAV	4 months	29%	63%
[19]	unoccupied test zone	FCU, ACB system	2 days	14-20%	-
[20]	laboratory room	HVAC system	3 days	-	31-33%

* energy savings obtained through simulation

TABS - thermally actuated building structure

ACB - active chilled beams

AC - air conditioner

All addressed studies report a successful operation of MPC and efficiency improvement when compared with a baseline control. The experimentally confirmed energy savings vary significantly from 5% up to 63%, depending on the comprehensiveness of the study, controlled system and baseline used for the comparison. While the optimization criterion and comfort constraints are mostly similarly defined across the studies, the most distinctive feature is the choice of the mathematical model of the building. In the reviewed studies, the used models ranged from building simulation software models [16] and artificial neural networks [146] to more commonly known linear or bilinear state-space models [17, 15, 14, 19]. In all presented studies, the MPC control is implemented as a part

of supervisory (management) level used to optimize the trajectory of internal setpoints whereas the tracking of those setpoints is a task of low-level control. The internal building setpoints are either optimized directly [17, 15, 20, 19, 18] or obtained by post-processing the optimal MPC variables [14].

The zone temperature control approach developed within the thesis differs substantially from the MPC approaches that act by adjusting the optimal temperature setpoint values for local controller and usually neglect the performance of the local HCEs in the zone. Such systems are also practically inapplicable in tight comfort bounds with simple hysteresis controllers used for local temperature control. The distinct advantage of the developed approach is in direct optimization of energy inputs per zone. By doing so, a high level of modularity and flexibility for different actuators, configurations and buildings is gained for fast replication of the method. The unmodelled disturbances, such as occupancy, lighting or electronic equipment, are no longer implicitly compensated, so in order to ensure offset-free comfort control and to be able to compensate such disturbances, an estimator is introduced in the control loop. The realization of the optimal thermal energy inputs is enforced by an interface acting as a link between the optimal thermal inputs and real actuation commands for HCEs (fan coils, radiators, floor heating, etc.) required for those inputs to be realized.

The developed approach relies on the existing building automation system (if such exists), enabling easy switch to standard building operation in case of communication errors or some other system malfunction. This chapter describes the on-line implementation of the zone MPC as a basis for hierarchical energy management, including communication of the optimal control scheme with the building automation system and the component-level feedback loops, as well as the measured energy and indoor comfort performance benefits from the demonstration. On the physical level, the zone level MPC encompasses all building zones, HCEs inside zones and the accompanying sensing and actuation equipment. The interface between control and estimation applications, developed as software modules and the physical world is a two-way real-time database including relevant building data, exterior variables and internal variables for mutual software modules synchronization.

Although the MPC for building temperature control has been broadly discussed in many studies found in the literature, a unique, clear and robust framework summarizing the necessary steps for its deployment does not exist. This chapter focuses on technological prerequisites for the implementation of zone temperature control via MPC as the lowest level among identified hierarchical building subsystems. The rest of the chapter is organized as follows. In Section 8.1 basic principles of the case-study Building Energy Management System (BEMS) infrastructure related to zone temperature control are given. Section 8.2 describes the architecture of the developed zone temperature control system with a detailed description of all software modules required for its deployment. All time units within the chapter are expressed in Coordinated Universal Time (UTC).

8.1 Basic principles of the case-study BEMS infrastructure

The considered case-study building spans over 12 floors of the university skyscraper. The building has east-west orientation with overall 248 controllable zones. Each floor in the building has separate north-side and south-side piping and thus a separate north-side and south-side fan coil unit (FCU) system. The two-pipe system is used for seasonal heating and cooling. All FCUs are equipped with a centrifugal fan with four different fan speeds controlled by a digital controller and sensor for measuring return medium temperature. Each controllable zone includes a separate user interface for temperature reference selection. The existing communication network is enhanced such that the digital controllers are reconfigured to be able to pass the information to a central database (current zone temperature, temperature reference and fan speed) and to be able to receive the commands from the database (fan speed). All FCU control devices are networked with a central monitoring system (SCADA system) based on Siemens DESIGO platform. Thermal consumption in the building is measured with calorimeters installed on every floor supply duct. All mentioned systems are integrated together with a network controller unit employed to enable two-way communication between devices operating on different protocols. The detailed description of case-study building equipment is given in Appendix A.

8.1.1 Temperature control system specifications

Every controllable zone is equipped with a user interface (Fig. 8.2). The interface enables the user to select the temperature reference and current zone operation mode. The three possible operation modes are recorded in the database as a variable *local switch*.

1. **Stand by mode:** The temperature is kept within the building protect limits in the heating season. During the cooling season, in stand by mode temperature is kept within building protect limits in unoccupied mode and within the pre-comfort limits in occupancy mode. Building protect limits are typically set to $[15, 35]^{\circ}\text{C}$ and pre-comfort limits are set to $[19, 28]^{\circ}\text{C}$.
2. **AUTO mode:** The temperature is controlled to follow the temperature reference selected on a wall unit. The permissible range of zone temperature reference during the heating season is $21 \pm 3^{\circ}\text{C}$ and $24 \pm 3^{\circ}\text{C}$ during the cooling season. The switch between zone temperature controlled by a standard digital controller or MPC is done via SCADA system.
3. **Manual mode:** The FCU fan operates continuously in the selected fan speed.

In the heating season, the system automatically switches between stand by and AUTO mode according to the fixed schedule such that during occupancy periods controllers are kept

in AUTO mode while during the unoccupied periods the controllers are kept in stand by mode. During the cooling season, the switch from stand by to AUTO mode is not done by the schedule, instead, if it is required, the transition to AUTO mode is done by preselecting the AUTO mode on the user interface unit. The changes of mode by the user are enabled only during occupancy periods defined as fixed schedules in SCADA system (Tab. 8.2).

Table 8.2. *The case-study building occupancy schedule.*

	occupancy schedule
workday	5:30 - 19:00
Saturday	5:30 - 15:00
Sunday	-

During unoccupied mode, every user selection resets to default after 30 min. Additionally, system operator can enforce constant operation of zone temperature control in the same mode through the SCADA system.

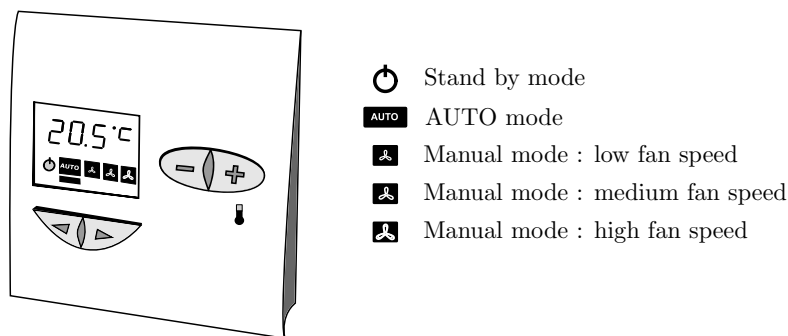


Figure 8.2. *Illustration of zone wall unit for selection of temperature reference and operating mode.*

8.1.2 Information communication infrastructure architecture

The developed MPC temperature control approach is based on minimum intrusiveness on the existing system. In order to achieve it, several basic requirements on the overall ICT architecture need to be followed. These requirements are:

1. **Software switch.** As the control of zone temperature via MPC in principle builds upon some pre-existing automation functions in the building, a possibility for an easy roll-back towards the pre-existing automation system configuration is installed. This functionality is enabled by so-called software switch which enables easy switch between the zone temperature controlled by MPC and zones temperature controlled by standard digital controllers. The selection of the controller is implemented as a part of SCADA system and thus can be influenced only by system operator

or authorized person. Once defined, the selection is recorded to the database as *smart switch* variable. For zones controlled via MPC *smart switch* variable is 'True' while otherwise the variable is defined as 'False'.

2. **Heartbeat signal.** Safety operation for the actuated elements is ensured by introducing the heartbeat signal that the database cyclically sends to the local controllers through the existing BEMS. Given that the heartbeat is running and the *smart switch* is activated, the inputs computed by the software modules are applied to the building actuators. Heartbeat signal on the zone level ensures the resistance of the control via database to the losses of communication between the building and the database caused either by programming errors or communication fallouts. There are 7 different heartbeat groups. The ground floor shares its heartbeat signal with the heat pump and all next floors are grouped by two such that first floor shares its heartbeat with the second, third with the fourth, etc. The heartbeat signal is active only if for every zone in the same group the following holds:

- (a) available measurements from the zone (not older than 2 minutes),
- (b) and one of the following conditions is 'True':
 - i. control via MPC is not enabled, i.e. *smart switch* = 'False',
 - ii. control via MPC is enabled (*smart switch* = 'True') and the selected operating mode is different than AUTO,
 - iii. control via MPC is enabled (*smart switch* = 'True'), user has selected operating mode equal to AUTO and new command is issued towards actuators in the last 2 minutes.

If the conditions do not hold the heartbeat signal changes its state to inactive and zone control is switched automatically back to the local controller until the above-mentioned conditions are satisfied.

3. **Bidirectional data flow between the building and central database.** The central database is a backbone of the developed zone temperature control via MPC. It is implemented using PostgreSQL database management system. All data are sampled with sample time of one minute or less. The data required to be collected to the database are:

- (a) measurements from the building;
- (b) user-selected temperature references;
- (c) actuation commands for the HCEs;
- (d) parameters and mathematical models of the building zones, HCEs and all other installed equipment;
- (e) predictions data;

(f) any other data required for the MPC operation.

For the sake of quick and easy access to current building data (e.g. current zone temperatures), the current data is stored in separate tables containing only one row – the one with the newest data.

Besides the SCADA computer, there is an optimization server that runs software modules implementing the MPC for zone temperature control. Such constellation enables the designed MPC to function as a service which can be selectively and modularly switched on or off. The optimization server is a reliable computer with installed program routines needed to execute the software modules. Currently, two major programmes are required to be run:

1. the application for execution of modules – here Python is preferred due to its easy high-level programming, large number of libraries and compatibility with various optimization tools, and
2. the optimization software – inevitably the modules will include different mathematical optimization programs.

The principal outlook of the ICT part of the automation system is given in Fig. 8.3.

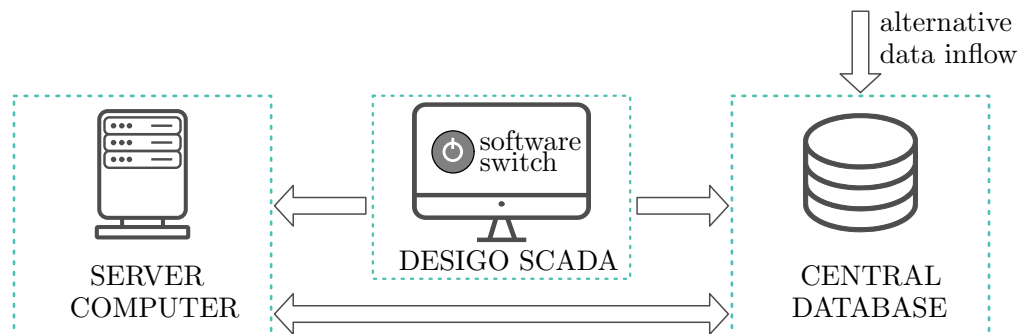


Figure 8.3. The principal outlook of the ICT part of the building automation system.

8.2 Real-time operation of the model predictive control for zone temperature control

The MPC for zone temperature control is composed of three major parts (Fig. 8.4):

1. **Prediction and estimation modules** used for identification of the simplified building model, identification of the mathematical model of HCEs, calculation of thermal power provided by HCEs to the zone, estimation of current states and disturbances of the identified zone thermal model and prediction of the future heat disturbance profiles as well as the temperature setpoints profiles,
2. **MPC module** for zones comfort control employed to calculate optimal thermal energy profiles per zones by taking into account weather forecast, predicted disturbance profiles, current building state, comfort requirements of the end-users (the current and the predicted ones), energy prices, and current and planned supply medium conditions,
3. **Interface modules** which are a link between real actuator commands required to realize optimal thermal energies calculated by MPC and compensate the unmeasurable disturbances affecting the zone temperature. The interface module can also impose coordination between HCEs while delivering the required energies to zones such that the heating/electricity power variance is minimized and peak energy demand suppressed.

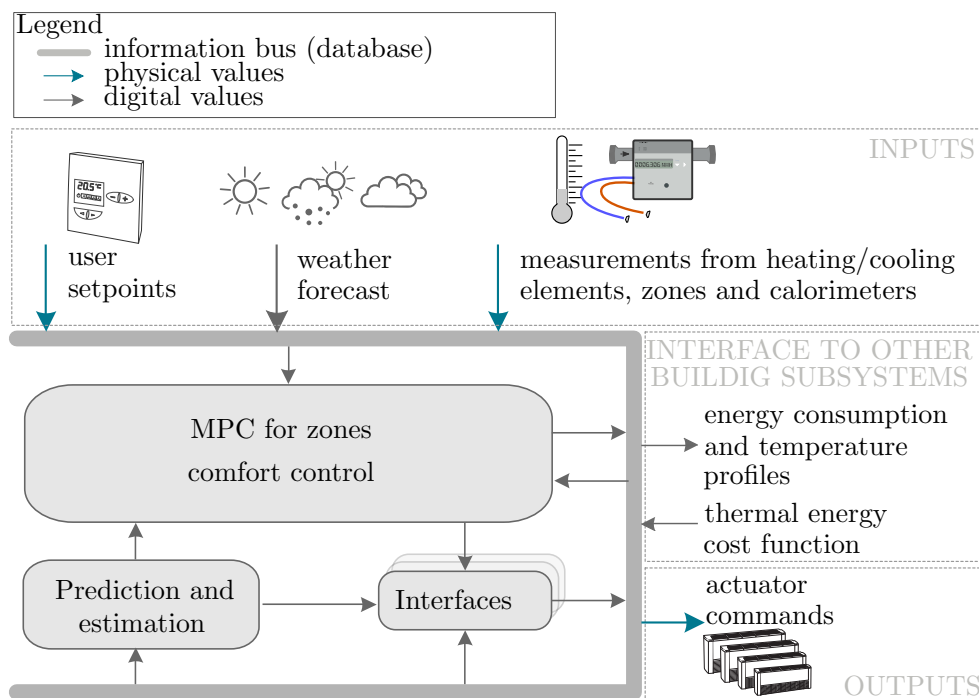


Figure 8.4. Concept of optimal zones temperature control.

The interface between control and estimation applications on the one side, and the physical world on the other, is a two-way real-time database including relevant building and exterior variables. On the physical level, the zone level MPC encompasses all building zones, HCEs inside zones and accompanying sensing and actuation equipment. The interface blocks are executed only when the control via MPC is activated, i.e. *smart switch* is set to 'True'. The software routine of all on-line modules can be divided into three parts:

1. Data fetching: fetching the newest data from the database;
2. Data processing: performing the module related data processing;
3. Data storing: store the results to the database.

All modules are realized in Python environment on the server computer. The sampling time of the modules is in range from 1 min to 15 min for prediction and estimation modules, 15 min for MPC module and 1 min for interface modules.

8.2.1 Prediction and estimation modules

Prediction and estimation modules enabling the implementation of the MPC for zone temperature control are:

- modules for identification of a simple model of zone HCEs, i.e. fan coil units identification module (PE1) for the considered case-study building,
- (PE4) module for identification of the simplified building thermal model,
- (PE5) module for estimation of the states of the simplified building thermal model including also the estimation of heat disturbance in zone,
- (PE6) module for prediction of the heat disturbance evolution per zone,
- (PE7) module for prediction of the comfort setpoint in the zone.

(PE1) Module for identification of fan coil unit model

Fan coil unit identification module is based on a procedure for identification of control-oriented energy model for a system of FCUs described in detail in Chapter 2. The required module inputs are listed in Tab. 8.3. The module consists of two parts:

- *offline part*: used for parameter identification of energy model for a system of FCUs using historical values of the required input parameters;
- *online part*: used for online calculation of current electrical energy consumption of FCU's fan and thermal power provided by the FCU to the zone by the FCU, based on current measurements of required input parameters.

Table 8.3. *Input variables definition of the FCU identification module PE1.*

MODULE INPUTS		Notation	Sampling time
ZONE	Zone temperature [°C]	T_a	1 min
	FCU fan state	x_{fc}	1 min
CALORIMETER	Supply medium temperature [°C]	$T_{w,cal}^{in}$	1 min
	Return medium temperature [°C]	$T_{w,cal}^{out}$	1 min
	Medium flow [kg/s]	$q_{w,cal}$	1 min
	Thermal energy (power) [kWh] ([kW])	$E_{cal}(P_{cal})$	1 min
FCU	Return medium temperature [°C]	T_w^{out}	1 min

The identified energy model for a system of FCUs relates FCU's fan state, zone temperature and medium conditions registered on a calorimeter to thermal energy transmitted to the zone air and electrical energy consumed by FCU's fan. The model

consists of three submodules: hydraulic module of a system of FCUs, thermodynamic model of different FCU types and electrical energy consumption model of FCU's fan for different FCU types (Fig. 8.5). The subscript i denotes measurements related to the i^{th} FCU and n_{fc} is the overall number of considered FCUs. The complete list of the module outputs is given in Tab. 8.4.

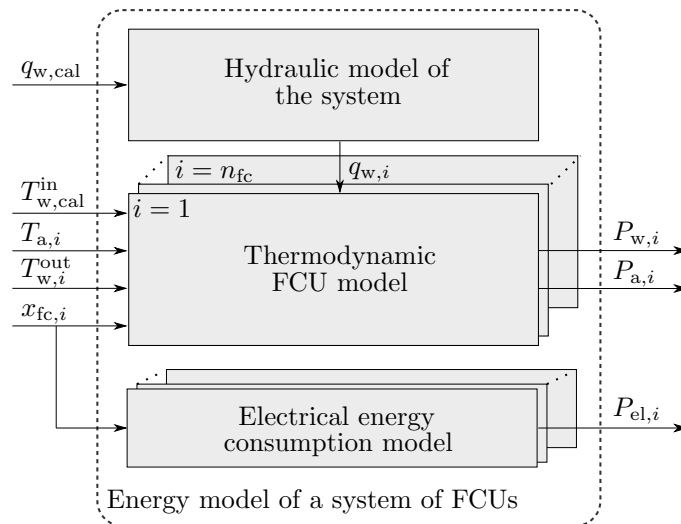


Figure 8.5. Scheme of the control-oriented energy model of a system of FCUs.

Table 8.4. Output variables definition of the FCU identification module PE1.

MODULE OUTPUTS (offline)

Parameters of energy model of a system of FCU		
MODULE OUTPUTS (online)	Notation	Sampling time
Thermal power provided to zone [kW]	P_a	1 min
Water side thermal power [kW]	P_w	1 min
Electrical power of FCU fan [kW]	P_{el}	1 min

The identified energy model parameters are later needed for: *i*) calculation of attainable FCU thermal power limits per building zone for the MPC module, *ii*) the interface module functioning, *iii*) calculation of energy inputs for identification of a simplified building dynamic model and on-line estimation of unmeasurable states and disturbances, and, *iv*) electricity consumption model needed on the higher-level MPC modules. The inputs required for on-line operation of PE1 module and the resulting module outputs for one exemplary FCU on 28 January 2020 are given in Fig. 8.6.

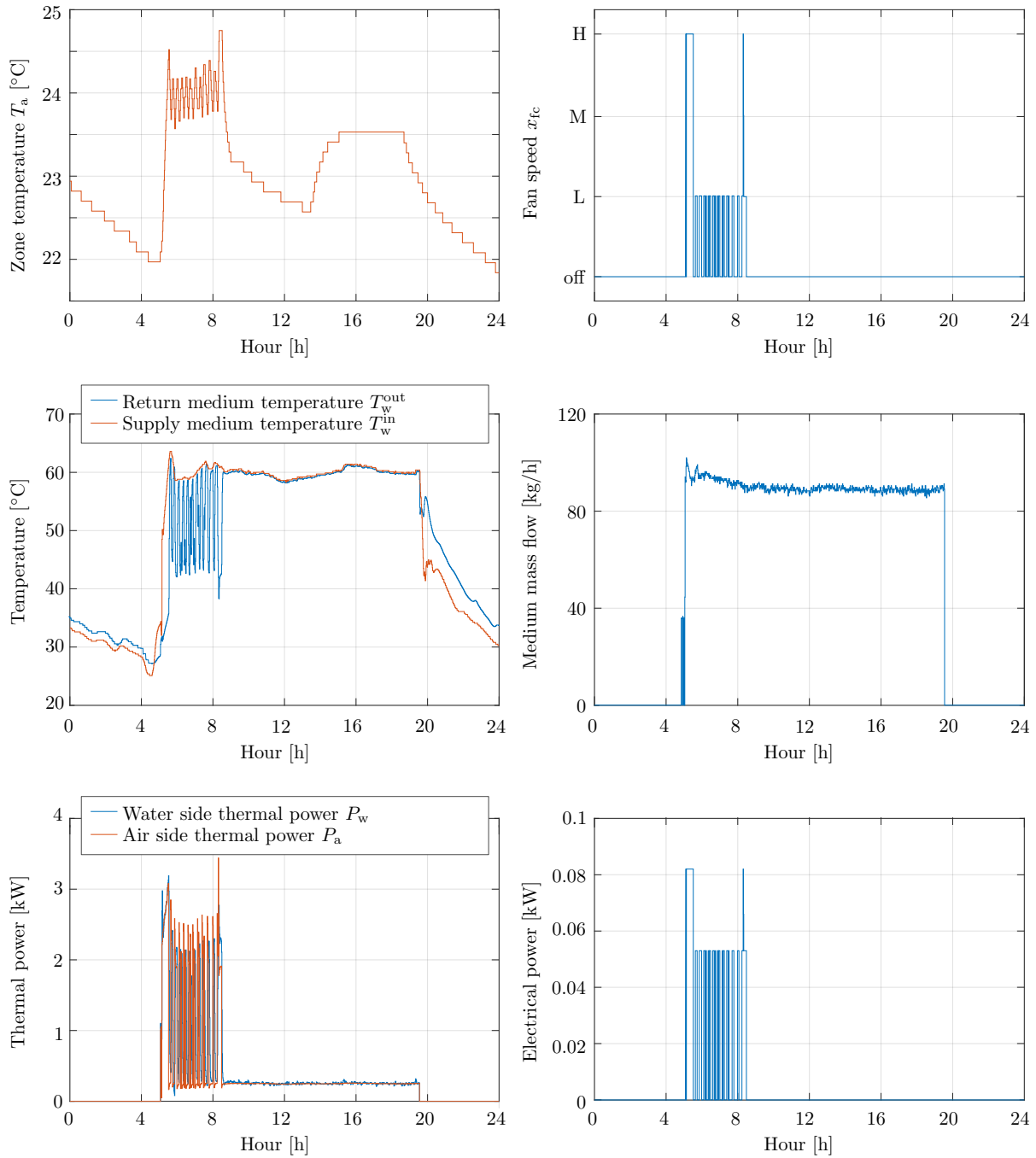


Figure 8.6. On-line operation of PE1 module on 28 January 2020.

The validity of the module operation is confirmed by comparing the sum of calculated thermal energy consumptions of all FCUs connected to one common floor supply duct with the overall thermal energy consumption of the duct measured by the calorimeter. All thermal powers are integrated on 15-min-long time intervals and shown in Fig. 8.7. From the obtained results it is evident that thermal energy calculated via software module shows good agreement with real thermal energy measured by the calorimeter. Overall thermal energy calculated by the PE1 software module, integrated over the selected time interval

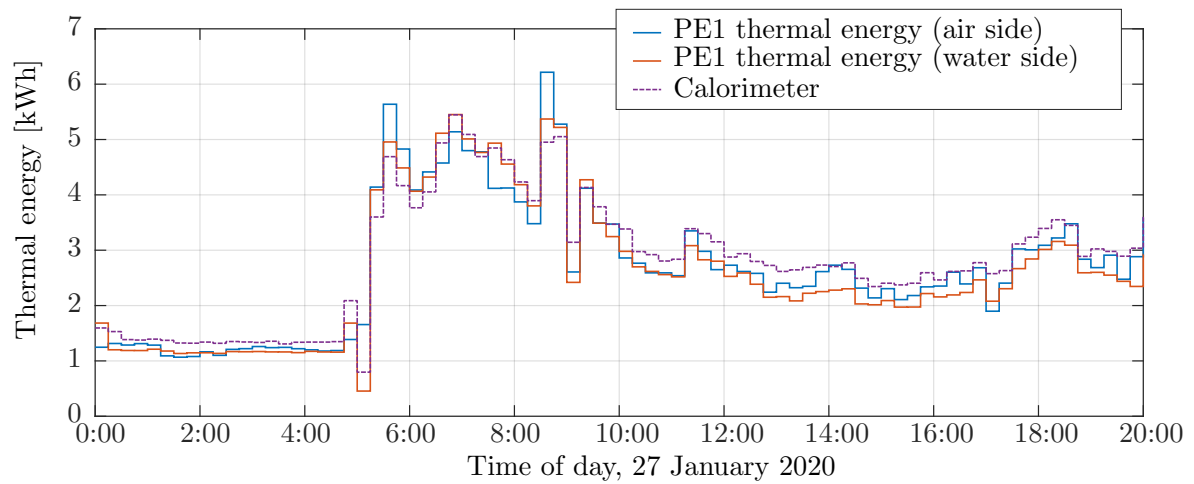


Figure 8.7. Comparison of the overall thermal energy consumption on one specific duct calculated via PE1 software module and measured by the calorimeter on 27 January 2020.

shown in Fig. 8.7, deviates from the thermal energy calculated by the calorimeter for less than 10%, proving thus the validity of the developed software module for calculation of thermal energy consumption of individual FCUs connected to the duct.

(PE4) Module for identification of the simplified building thermal model

The operation of the module for identification of a simplified thermal model is based on the approach developed and verified within the Chapter 3 Section 3.5. The building zone is modelled using two states, one accounting for the dynamics of the air within the zone referred to as temperature fast dynamics, and the other one accounting for the dynamics of the higher thermal capacity elements such as walls or furniture referred to as temperature slow dynamics. The module uses historical data from Tab. 8.5 recorded over periods when building was unoccupied.

Table 8.5. *Input variables definition of the PE4 module.*

MODULE INPUTS		Notation	Sampling time
ZONE	Zone temperature [$^{\circ}\text{C}$]	T_a	1 min
WEATHER STATION	Outside air temperature [$^{\circ}\text{C}$]	T_{out}	1 min
	Direct normal solar irradiance [W/m^2]	I_n^{dir}	1 min
	Diffuse horizontal solar irradiance [W/m^2]	I_h^{diff}	1 min
PE1	Thermal power inserted into zone [kW]	P_a	1 min
DATABASE	Building external walls azimuth and tilt angles	-	-

The module outputs are parameter vectors $\Theta_i = [p_{1,i} \ p_{2,i} \ p_{3,i} \ p_{4,i} \ p_{5,i} \ p_{6,i}]^{\top}$, one for each considered zone, constituting the simplified thermal model of the i^{th} building zone in the following way:

$$\begin{bmatrix} \dot{T}_{a,i} \\ \dot{T}_{z,i} \end{bmatrix} = \underbrace{\begin{bmatrix} -(p_{1,i} + p_{3,i} + p_{7,i}) & p_1 \\ p_{2,i} & -p_{2,i} \end{bmatrix}}_{A_i^c} \begin{bmatrix} T_{a,i} \\ T_{z,i} \end{bmatrix} + \underbrace{\begin{bmatrix} p_{3,i} & p_{4,i} & p_{5,i} & p_{6,i} \\ 0 & 0 & 0 & 0 \end{bmatrix}}_{B_i^c} u_i, \quad (8.1)$$

where $T_{a,i}$ is the temperature of air in the i^{th} zone, $T_{z,i}$ is the temperature of higher thermal capacity mass in the i^{th} zone and input vector u_i is defined as $u_i = [T_{\text{out}} \ I_{\theta}^{\text{diff}} \ I_{\theta}^{\text{dir}} \ P_a]^{\top}$. Solar irradiances I_{θ}^{diff} and I_{θ}^{dir} are diffuse and direct solar irradiances incident on the exterior zone surface calculated with the known direct normal I_n^{dir} and diffuse horizontal I_h^{diff} irradiance, external wall azimuth angle, tilt angle, and solar zenith and azimuth angles (see Appendix B).

(PE5) Module for estimation of the states of the simplified building thermal model including also the estimation of heat disturbance in zone

Heat disturbance in zone implies the sum of additional heat flows in the zone which are not included into the estimated building model or occur due to the changed conditions in the zone compared to the ones used for estimation of the zone model. Typical examples of heat disturbances are window opening, shading position changes, electronic equipment, occupancy, lighting, etc. Slow dynamics temperature, which is a part of the estimated building model represents a substitute variable for all higher thermal capacity element temperatures (e.g. walls and furniture). As such, it is hardly measurable and has to be estimated online. The used approach is described in detail in Chapter 5 Section 5.3. The resulting estimation problem is in a form of a linear estimation problem, so classical linear Kalman filter is utilized. The required module inputs and the outputs of the module are listed in Tab. 8.6.

Table 8.6. *Input/Output variables definition of the PE5 module.*

MODULE INPUTS		Notation	Sampling time
PE4	System and input matrix of identified simplified zone model	A^c, B^c	-
ZONE	Zone temperature [$^{\circ}\text{C}$]	T_a	1 min
WEATHER STATION	Outside air temperature [$^{\circ}\text{C}$]	T_{out}	1 min
	Direct normal solar irradiance [W/m^2]	I_n^{dir}	1 min
	Diffuse horizontal solar irradiance [W/m^2]	I_h^{diff}	1 min
PE1	Thermal power inserted into zone [kW]	P_a	1 min
DATABASE	Building external walls azimuth and tilt angles	-	-
MODULE OUTPUTS		Notation	Sampling time
Fast dynamics temperature estimate (zone temperature) [$^{\circ}\text{C}$]		\hat{T}_a	1 min
Slow dynamics temperature estimate [$^{\circ}\text{C}$]		\hat{T}_z	1 min
Heat disturbance estimate [kW]		\hat{P}_d	1 min

The operation of the module is verified by estimating the additional measurable controllable heat input generated by an electric heater in one selected north-oriented office zone with the overall floor area of 13.33 m^2 . The experiment was conducted during the unoccupied cloudy day such that the estimated heat disturbance is not significantly affected by solar irradiance modelling errors or occupancy. The heater with a nominal thermal power of 1.25 kW was turned on in the interval [12:20 14:30] h. The inputs and outputs of the PE5 module during the experiment are shown in Fig. 8.8.

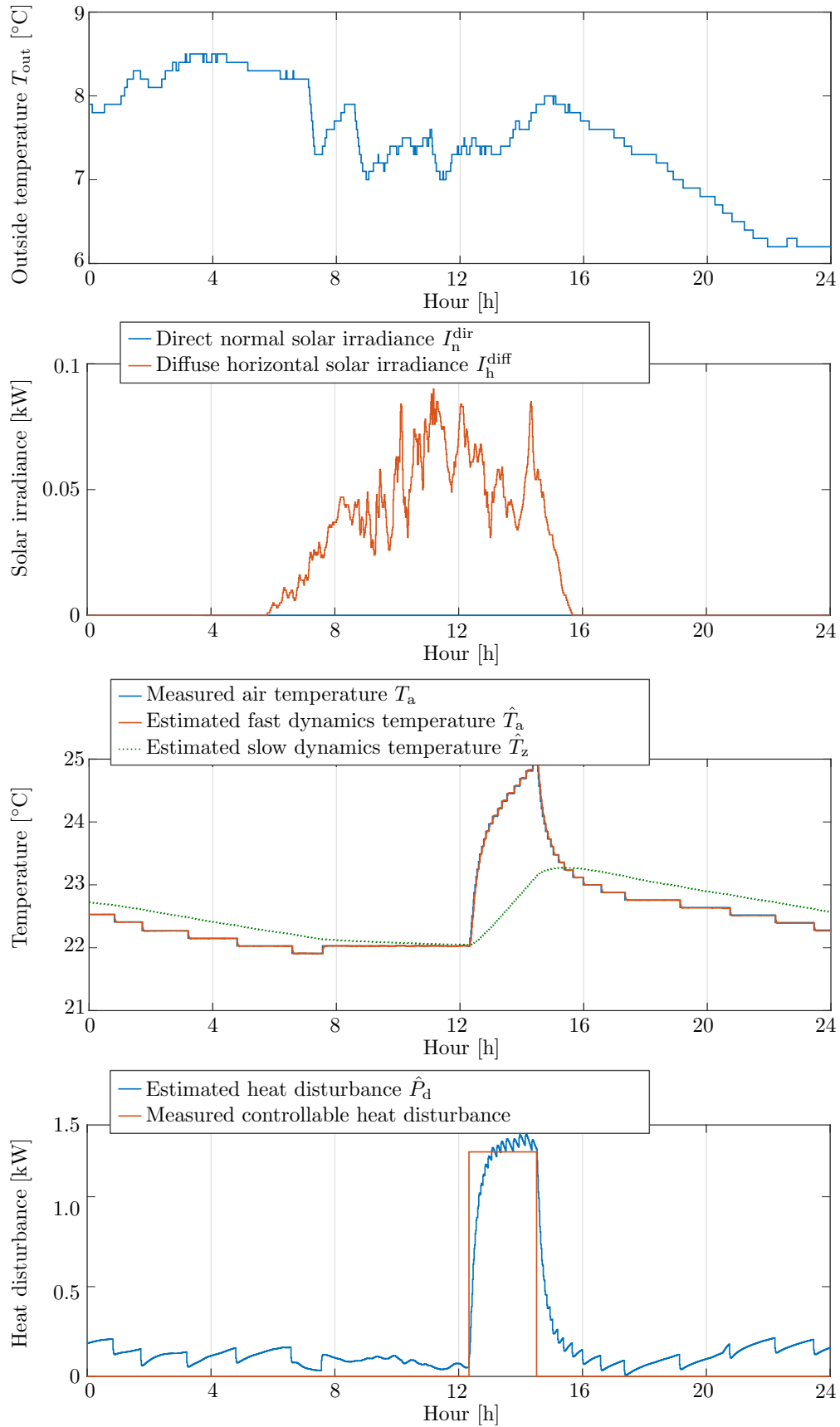


Figure 8.8. On-line operation of PE5 module for in zone C09-10 on 30 October 2019.

Based on available inputs, the PE5 module successfully estimates the introduced heat disturbance. The convergence rate of the algorithm depends on the selected values of the noise covariance matrices corresponding to the process and measurement noise of the system. Based on the system performance, the values are selected to achieve the compromise between the convergence rate and suppression of heat disturbance estimate oscillations which occur due to the quantization of the zone temperature measurements.

The characteristic negative value of the estimated heat disturbance during window opening in the heating season, when the outside temperature is significantly lower than the zone temperature and only heating is available, enables the detection of window opening. Figure 8.9 shows the results of on-line operation of PE5 module in one exemplary north-oriented zone on 29 April 2019. On the selected day, the heating was inactive. The large estimated negative heat flux indicates fully opened window between 7:15 and 8:40 and window only tilted from 8:40 on.

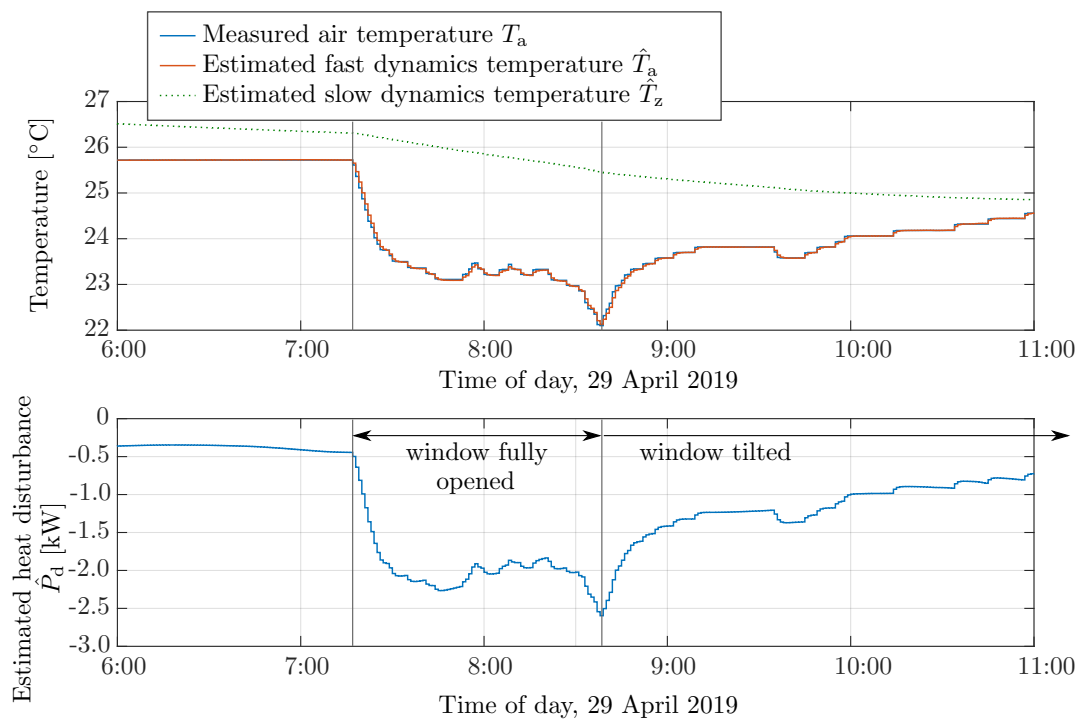


Figure 8.9. On-line operation of PE5 module on one exemplary zone on 29 April 2019.

However, with the window opened for a long time, the specific negative heat disturbance value is often compensated with positive heat fluxes which occur due to the e.g. occupancy, lighting or electronic equipment. The effect is demonstrated in Fig. 8.10 which shows the results of on-line operation of PE5 module in one exemplary south-oriented zone on 18 November 2019. On the selected day, the heating was inactive.

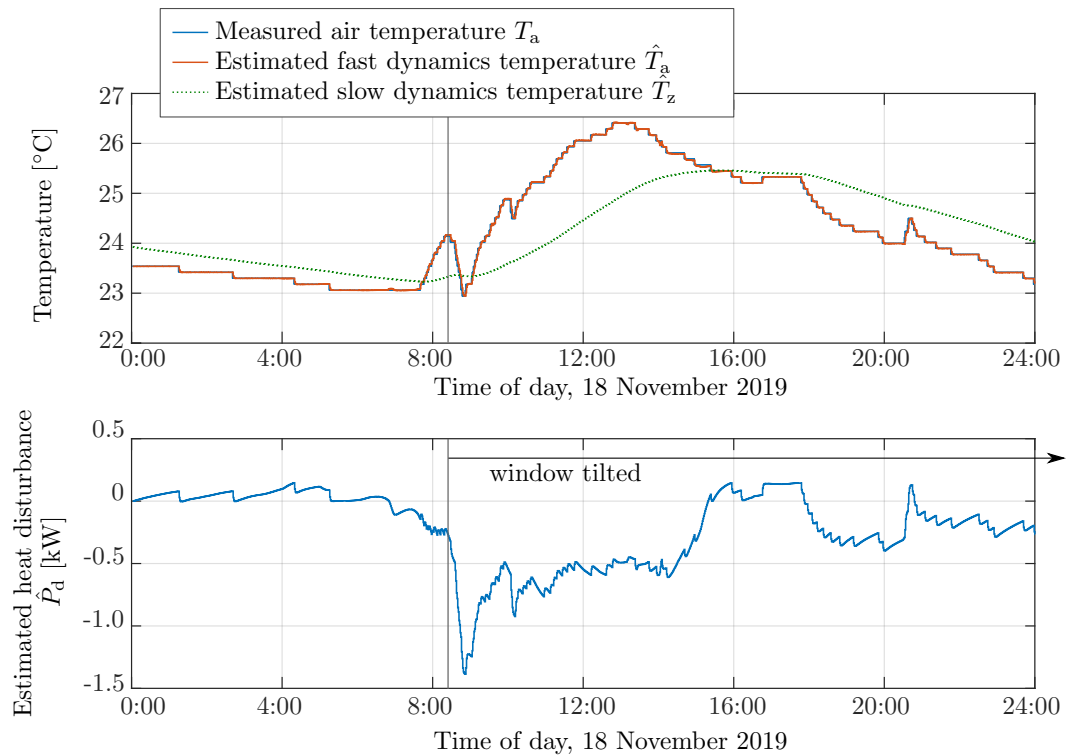


Figure 8.10. On-line operation of PE5 module on one exemplary zone on 18 November 2019.

In the cooling season, the window opening results with positive or negative heat disturbance, depending on the difference between the zone and outside temperature. Thus, it is hard to distinguish its signature among other influences on the overall estimated heat disturbance. Figure 8.11 shows the results of on-line operation of PE5 module on one exemplary south-oriented office zone with 4 working places and overall floor area of 21.15 m² between 30 October 2019 and 4 November 2019. From the figure is clearly evident that the estimated heat disturbance encompasses the occupancy information. The clear regular shape of the disturbance due to the occupancy is the result of inactive heating and cloudy weather on the selected days. The heating power is zero and the discrepancy between the modelled and real solar influence on the zone temperature is low, making the solar irradiance and HCE modelling errors negligible compared to the heat flux generated by occupants, lighting and electronic equipment during the working hours.

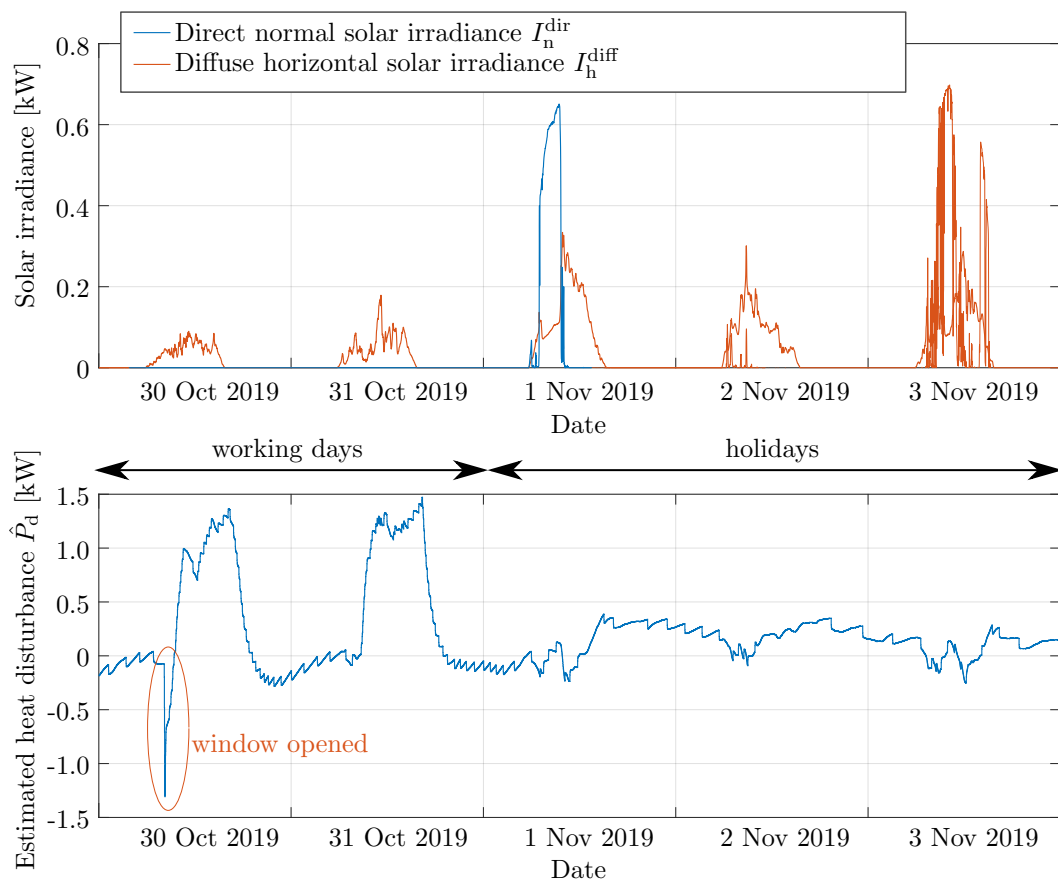


Figure 8.11. On-line operation of PE5 module on one exemplary zone between 30 October 2019 and 4 November 2019.

(PE6) Module for prediction of the heat disturbance evolution per zone

The estimation of the heat disturbance enables possibility to tune models for heat disturbance predictions and exploit them for efficiency gains in predictive zone control. The prediction of the heat disturbance evolution per zone is based on artificial neural networks (ANNs) approach. The system is composed of two parts: off-line and on-line. In the off-line part historical data are used for obtaining the prediction model [147]. The on-line part of the module uses the model developed in the off-line part in order to generate predictions. The inputs of the ANN model are listed in Tab. 8.7. The output of the model is the prediction of the heat disturbance along the defined prediction horizon with 15 min sampling time. The additional inputs used for prediction and learning the model are time indicators representing time of the day, time of the week and day of the year. The frequency of module operation is 15 min, so the input data is either averaged or integrated on 15 min before utilized for learning the prediction model or generating the prediction.

Table 8.7. *Input variables definition of the PE6 module.*

MODULE INPUTS		Notation	Sampling time
PE5	Heat disturbance estimate [kW]	\hat{P}_d	1 min
WEATHER STATION	Outside air temperature [°C]	T_{out}	1 min
	Direct normal solar irradiance [W/m ²]	I_n^{dir}	1 min
	Diffuse horizontal solar irradiance [W/m ²]	I_h^{diff}	1 min

(PE7) Module for prediction of the comfort setpoint in the zone

The prediction of the comfort setpoint in the zone is based on the occupancy schedule defined in the SCADA system. The predictions are generated with respect to the operating mode selected on the wall unit:

- for zones with AUTO mode selected on a wall unit, persistence of the current setpoint is assumed;
- for zones in stand by or manual mode selected on a wall unit, the setpoint prediction is selected to be equal to setpoint realization one week ago.

During unoccupied intervals defined with a fixed schedule (see Tab. 8.2) the setpoint prediction is set to 'NaN' indicating that there are no comfort requests during that interval.

8.2.2 Model predictive control module

The operation of the MPC module is based on the approach developed in Part II of the thesis. The developed approach allows the individual setting of zone comfort level with the aim of user satisfaction and increased productivity rather than achieving additional energy savings. The distinct advantage of the proposed approach is a direct control of thermal energy inputs per zone. For this, the methodology is readily applicable for different HCEs in zones and retains openness for interaction with other building subsystems.

Discrete-time system model

The identified semi-physical model of the case-study building consists of identified second-order models (see Chapter 3 Section 3.4) of all controllable zones in which the conditions for control via MPC are met ($0 \leq n_y \leq 248$) stacked into a compact model form:

$$\begin{aligned} \dot{x} &= A^c x + B_d^c d + B_u^c u, \\ y &= Cx, \end{aligned} \quad (8.2)$$

where $x \in \mathbb{R}^{n_x}$ ($n_x = 2 \cdot n_y$) is a stacked vector of zone fast- and slow-dynamics states $T_{a,i}$ and $T_{z,i}$, respectively, with $i = 1, 2, \dots, n_y$:

$$x = \begin{bmatrix} T_{a,1} & T_{a,2} & \cdots & T_{a,n_y} & T_{z,1} & T_{z,2} & \cdots & T_{z,n_y} \end{bmatrix}^\top, \quad (8.3)$$

$y \in \mathbb{R}^{n_y}$ is the output vector consisted from zone fast-dynamics states which correspond to zone temperatures, $u \in \mathbb{R}^{n_u}$ ($n_u = n_y$) is a vector of thermal energy inputs $P_{a,i} \in \mathbb{R}^1$ into each of n_y controllable zones

$$u = \begin{bmatrix} P_{a,1} & P_{a,2} & \cdots & P_{a,n_y} \end{bmatrix}^\top, \quad (8.4)$$

$d \in \mathbb{R}^{n_d}$ ($n_d = 9 + n_x$) is a vector of disturbances affecting the building zones temperature behaviour:

$$d = \begin{bmatrix} T_{\text{out}} & I_N^{\text{diff}} & I_E^{\text{diff}} & I_S^{\text{diff}} & I_W^{\text{diff}} & I_N^{\text{dir}} & I_E^{\text{dir}} & I_S^{\text{dir}} & I_W^{\text{dir}} & P_{d,1} & P_{d,2} & \cdots & P_{d,n_y} \end{bmatrix}, \quad (8.5)$$

where T_{out} is outside air temperature and I^{diff} and I^{dir} are diffuse and direct solar irradiances incident on the exterior zone surface where the irradiances on the surfaces oriented towards north, east, south and west are denoted with letters N, E, S, W in subscript, respectively. The input parameter $P_{d,i} \in \mathbb{R}^1$ represents the heat disturbance input affecting the i^{th} controllable zone. Continuous-time system matrix $A^c \in \mathbb{R}^{n_x \times n_x}$ and input matrices, $B_u^c \in \mathbb{R}^{n_x \times n_u}$ and $B_d^c \in \mathbb{R}^{n_x \times n_d}$, are constructed from the augmented continuous-time matrices of identified simplified models of the individual zones (5.16).

The resulting discrete-time system is as follows:

$$x_{k+1} = A^d x_k + B_d^d d_k + B_d^{d*} T_{\text{out},k+1} + B_u^d u_k, \quad (8.6)$$

$$y_k = C^d x_k,$$

where A^d , B_u^d , B_d^{d*} and B_d^d are appropriately sized matrices. Influence of outside air temperature T_{out} is discretised by employing first-order hold while the rest of the system is discretised by zero-order hold. The number of zones controlled by the MPC depends on the required conditions. Only zones with *smart switch* variable set to 'True' and selected AUTO mode on the wall unit are controlled via MPC.

Weather forecast

The prototype weather forecasting service for the location of the case-study building is developed by Croatian Meteorological and Hydrological Service and it is active since 2013. Weather forecasts are available for several meteorological variables such as temperature, humidity, air pressure, wind speed, direct and diffuse solar irradiance, etc. Calculation of a new prediction sequence is commenced every day at 00:00, 06:00, 12:00 and 18:00 for the next 72-h period with a 1 h time resolution. The comparison of measured and predicted outside temperature and solar irradiance on the selected time interval between 4 November 2019 and 9 November 2019, with the predictions started at midnight is given in Fig. 8.12 and Fig. 8.13.

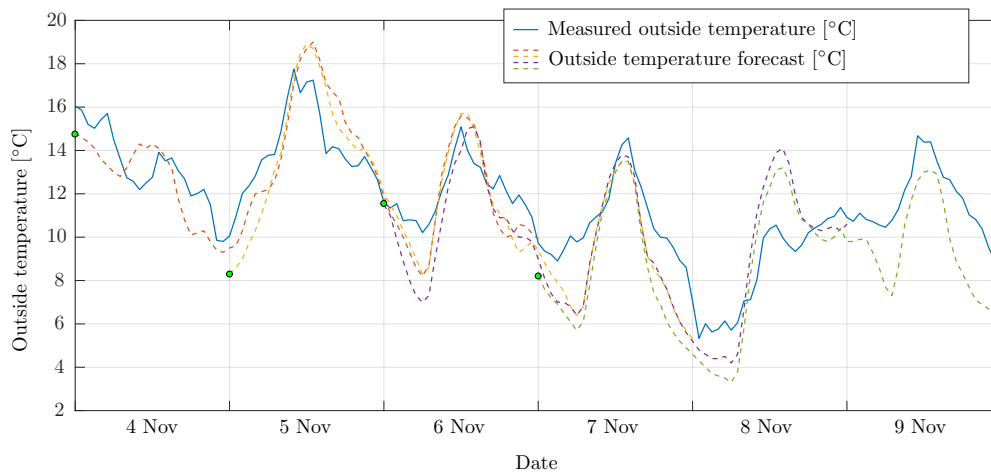


Figure 8.12. Comparison of measured and predicted outside temperature. The predictions start is denoted with circles at midnight of first 4 days.

The irradiances on the exterior building surfaces are recalculated based on the known forecast of the direct normal and diffuse horizontal irradiance and building external walls azimuth angles, tilt angles, and solar zenith and azimuth angles (see Appendix B). The available measurements of current weather conditions are utilized in a way that in the first MPC sampling interval persistence of the currently measured weather conditions is

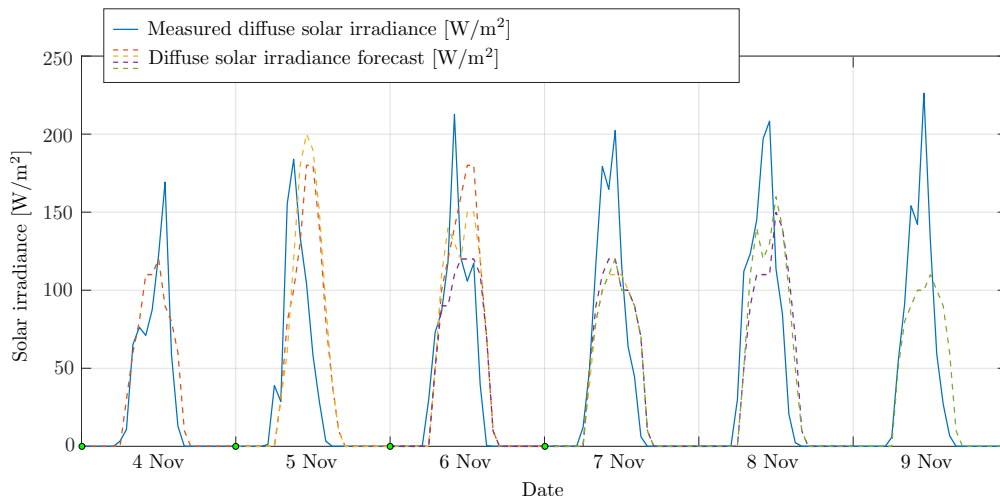


Figure 8.13. Comparison of measured and predicted diffuse solar irradiance. The predictions start is denoted with circles at midnight of first 4 days.

assumed while on the rest of the horizon weather forecast is used. The availability of local weather measurements opens the possibility for additional improvements of the weather forecast with Kalman filter.

Comfort constraints

Smart selection of weighting matrices for penalizing the energy consumption and deviation from the temperature reference enables easy switch between the two often opposing requirements based on the predicted disturbance and energy price profiles. Within such set-up, comfort is defined by temperature reference y^{ref} and permissible zone temperature interval:

$$\mathbf{y}^{\text{ref}} - \mathbf{\Delta}^{\text{ref}} - \boldsymbol{\sigma}_1 \leq \mathbf{y} \leq \mathbf{y}^{\text{ref}} + \mathbf{\Delta}^{\text{ref}} + \boldsymbol{\sigma}_2, \quad (8.7)$$

where bold notation is used to denote variables stacked over the prediction horizon, $\boldsymbol{\sigma}_1$ and $\boldsymbol{\sigma}_2$ are slack variables that allow highly penalized constraints violation and feasible implementation, \mathbf{y}^{ref} is the stack of temperature references along the prediction horizon and $\mathbf{\Delta}^{\text{ref}}$ is the stack of the acceptable deviations from the temperature reference along the prediction horizon. The temperature reference at step k , $y_k^{\text{ref}} \in \mathbb{R}^{n_y}$, is defined as:

$$y_k^{\text{ref}} = [T_{a,1,k}^{\text{ref}} \quad T_{a,2,k}^{\text{ref}} \quad \dots \quad T_{a,n_y,k}^{\text{ref}}]^{\text{T}}, \quad (8.8)$$

where $T_{a,i,k}^{\text{ref}}$ is the temperature reference in the i^{th} zone selected on the zone wall unit. The acceptable deviations along the horizon are defined in the database, separately for every zone.

Limitations of the central HVAC system

The minimum and maximum attainable thermal powers of the HCEs in building zones along the prediction horizon, depend on the current and planned operation of the central HVAC system. If no information on future HVAC operation is available (uncoordinated operation), thermal limits along the horizon are calculated based on the current heating/cooling medium conditions and known nominal operation parameters of the central HVAC system. In standard operation, the central medium mass flow is controlled according to the fixed schedule (Tab. 8.8), where during daily regime the medium mass flow is controlled to the nominal value defined differently for cooling and heating season. In the cooling season the system is turned off during the night regime, while in the heating season the flow is reduced by 50% in the night regime.

Table 8.8. *The case-study building central HVAC schedule.*

	daily regime
workday	5:00 - 19:00
Saturday	5:00 - 15:00
Sunday	-

The medium mass flow through an individual FCU is determined based on the hydraulic model of a system of FCUs for every floor supply duct (PE1) and flow distribution between floor supply ducts. The distribution between floor supply ducts is easily identified due to the available measurements from individual calorimeters mounted on every floor supply duct. Heating/cooling medium supply temperature is controlled with respect to the outside weather temperature such that:

$$T_{w,HVAC}^{in} = a_{HVAC}T_{out} + b_{HVAC}, \quad (8.9)$$

where $T_{w,HVAC}^{in}$ is central HVAC system supply temperature, T_{out} is outside air temperature while a_{HVAC} and b_{HVAC} are coefficients defined in the SCADA system. If the coefficients are not directly reachable from the SCADA system they can be easily estimated from building operation data. The supply temperature of individual FCU is calculated based on the identified temperature drop between central HVAC system and individual floor supply ducts where the drops within the floor ducts are neglected due to the good thermal insulation of the floor supply piping [147]. The prediction of the central supply temperature along the prediction horizon is easily calculated based on (8.9) and known prediction of the outside air temperature.

To utilize the measurements from individual calorimeters, medium conditions until the first switch between the central HVAC operating regimes defined as in Tab. 8.8 are assumed to be equal to the measured values recalculated for every FCU.

FCU thermal power limitations

The FCU thermal power limitations are defined as:

$$\mathbf{u}_{\min} \leq \mathbf{u} \leq \mathbf{u}_{\max}, \quad (8.10)$$

where \mathbf{u}_{\min} and \mathbf{u}_{\max} are minimum and maximum attainable thermal powers along the prediction horizon which are linear functions of the zone temperature as described in the sequel. Positive values of \mathbf{u} represent heating, while negative \mathbf{u} stands for cooling. The FCU system time constants are relatively small compared to the time constants of the building. The highest attainable thermal power of the individual FCU defined over the prediction horizon is thus defined with the following algebraic equation:

$$\mathbf{u}_H = \frac{2\mathbf{q}_w c_w \mathbf{U}_o^H}{2\mathbf{q}_w c_w + \mathbf{U}_o^H} (\mathbf{T}_w^{\text{in}} - \mathbf{T}_a) \quad (8.11)$$

where \mathbf{q}_w is predicted profile of the medium mass flow through the FCU, c_w is heat capacity of the heating/cooling medium, \mathbf{T}_w^{in} is predicted profile of FCU supply temperature, \mathbf{T}_a is air temperature in the zone along the prediction horizon and \mathbf{U}_o^H is the overall heat transfer coefficient for the highest FCU fan speed defined over the prediction horizon. The minimum thermal power of the individual FCU is defined by the natural convection of air around the unit with FCU's fan switched off.

$$\mathbf{u}_{\text{off}} = \frac{2\mathbf{q}_w c_w \mathbf{U}_o^{\text{off}}}{2\mathbf{q}_w c_w + \mathbf{U}_o^{\text{off}}} (\mathbf{T}_w^{\text{in}} - \mathbf{T}_a), \quad (8.12)$$

where $\mathbf{U}_o^{\text{off}}$ is the overall heat transfer coefficient for FCU's fan being switched off along the prediction horizon. Overall heat transfer coefficient changes with different FCU fan speeds x_{fc} such that:

$$\mathbf{U}_o = \begin{cases} \varepsilon_{fc}^{\text{off}} \cdot \frac{a_{fc}^{\text{off}}}{1 + b_{fc}^{\text{off}} \cdot \mathbf{q}_w^{-c_{fc}}}, & \text{for } x_{fc} = \text{off}, \\ \varepsilon_{fc}^L \cdot \frac{a_{fc}^L}{1 + b_{fc}^L \cdot \mathbf{q}_w^{-c_{fc}}}, & \text{for } x_{fc} = L, \\ \varepsilon_{fc}^M \cdot \frac{a_{fc}^M}{1 + b_{fc}^M \cdot \mathbf{q}_w^{-c_{fc}}}, & \text{for } x_{fc} = M, \\ \varepsilon_{fc}^H \cdot \frac{a_{fc}^H}{1 + b_{fc}^H \cdot \mathbf{q}_w^{-c_{fc}}}, & \text{for } x_{fc} = H, \end{cases} \quad (8.13)$$

where $\{\varepsilon_{fc}^{\text{off}}, \varepsilon_{fc}^L, \varepsilon_{fc}^M, \varepsilon_{fc}^H\}$, $\{a_{fc}^{\text{off}}, a_{fc}^L, a_{fc}^M, a_{fc}^H\}$, $\{b_{fc}^{\text{off}}, b_{fc}^L, b_{fc}^M, b_{fc}^H\}$ and c_{fc} are known parameters found through identification as described in Chapter 2. During the cooling season, the thermal power limits are set by replacing \mathbf{u}_{\min} with \mathbf{u}_H and setting \mathbf{u}_{\max} to \mathbf{u}_{off} . In the heating season, the thermal power limits are set by replacing \mathbf{u}_{\max} with \mathbf{u}_H and setting \mathbf{u}_{\min} to \mathbf{u}_{off} . In zones with multiple FCUs thermal power limits are calculated as superposition of individual FCU thermal power limitations.

Optimization problem

The optimization problem for energy-saving and comfortable zone temperature control, written in compact form, is as follows:

$$\begin{aligned}
 \min_{\mathbf{u}, \boldsymbol{\sigma}_1, \boldsymbol{\sigma}_2} \quad & \mathbf{c}_t^\top |\mathbf{u}| + \gamma_e \cdot c_c \cdot \boldsymbol{\delta}^\top |\mathbf{Q}(\mathbf{y}^{\text{ref}} - \mathbf{y})| + g_1 \mathbf{1}^\top \boldsymbol{\sigma}_1 + g_2 \mathbf{1}^\top \boldsymbol{\sigma}_2 \\
 \text{s.t.} \quad & (8.6), (8.7), (8.10), \\
 & \boldsymbol{\sigma}_1 \geq 0, \boldsymbol{\sigma}_2 \geq 0
 \end{aligned} \tag{8.14}$$

where operator $|\cdot|$ denotes absolute value which is applied element-wise on the vector, $\mathbf{c}_t \in \mathbb{R}^{H \cdot n_u}$ is the thermal energy cost important for coordination with higher-level modules, $c_c \in \mathbb{R}^1$ is the associated comfort cost and g_1 and g_2 are non-negative weights for tuning the optimization criterion. The vector $\boldsymbol{\delta} \in \mathbb{R}^{H \cdot n_y}$ is zone occupancy vector, consisted of zeros and ones. The vector equals one for moments with defined temperature reference and equals zero for moments when there is no defined temperature reference, i.e. moments in which no comfort requirements are set. Weighting matrix $\mathbf{Q} \in \mathbb{R}^{H \cdot n_y \times H \cdot n_y}$ transforms temperature deviation from the reference to the corresponding thermal energy such that it is comparable to energy consumption [131]. Bold notation for optimizers \mathbf{u} , $\boldsymbol{\sigma}_1$, $\boldsymbol{\sigma}_2$ stands for vectors stacked over the prediction horizon H . The parameter $\gamma_e \in \mathbb{R}^1$ is introduced for trade-off possibility of comfort-savings criterion. The trade-off parameter is defined in the database separately for every zone. Initially the parameter is set to one for all zones.

Coordination with higher-level modules

If thermal energy cost \mathbf{c}_t is not known, i.e. there is no coordination between building levels, thermal energy price is assumed to be constant. The modifications of the original optimization problem required to enable coordination are described in detail in Part II of the thesis while here only basic principles are presented. In coordinated operation the zone level communicates the required thermal energy for maintaining the comfort in all zones and zone temperatures to the higher-level, i.e. to the central HVAC level for the case of the considered case-study building. Thermal energy requests of other zones which are not controlled via MPC are estimated in one of the following ways:

- if zone operates in stand by or manual mode it is assumed the energy request on the prediction horizon is equal to zero and the temperature along the horizon is predicted using known predictions of weather and heat disturbance profile along the horizon;
- if zone operates in AUTO mode, the thermal energy request on the prediction horizon is predicted by simulating the hysteresis control (see Chapter 5 Section 5.4) with respect to the temperature reference prediction and known predictions of weather and heat disturbance profile along the horizon.

Based on the required thermal energy demand and the electrical energy price information from the utility grid or microgrid, central HVAC MPC calculates the optimized prices for the predicted heating/cooling demand from zones and for zones temperatures which are then communicated back to the zone level MPC together with the critical region describing space of thermal energies and zone temperatures for which that prices are valid and predicted profile of supply medium conditions (flow and temperature of the medium). The hierarchical coordination then continues with respect to the constraints activated by the optimal zone level solution (for more details see Chapter 6).

Input/Output interface of the MPC module

The list of all inputs required for operation of the zones level MPC module is given in Tab. 8.9. The outputs of the MPC module are optimized profiles of thermal energy and temperature along the prediction horizon for zones which are selected to be controlled via MPC and the predicted profile of thermal energy and temperature for all other zones.

Module implementation

The MPC module is realized in Python environment and as such it is deployed on the server computer. The module is executed every 15 min considering new system measurements, predictions and possible changes of *smart switch* and *local switch* variables. The optimization problem (8.14) is solved by using CPLEX [137].

Table 8.9. *Input variables definition required for operation of MPC module.*

	Required input data	Notation
ZONES	Zone temperature reference [°C]	y^{ref}
CALORIMETER	Supply medium temperature [°C]	$T_{\text{w,cal}}^{\text{in}}$
	Medium flow [kg/s]	$q_{\text{w,cal}}$
WEATHER STATION	Outside air temperature [°C]	T_{out}
	Direct normal solar irradiance [W/m ²]	$I_{\text{n}}^{\text{dir}}$
	Diffuse horizontal solar irradiance [W/m ²]	$I_{\text{h}}^{\text{diff}}$
WEATHER FORECAST	Prediction of outside air temperature [°C]	\mathbf{T}_{out}
	Prediction of direct normal solar irradiance [W/m ²]	$\mathbf{I}_{\text{n}}^{\text{dir}}$
	Prediction of diffuse horizontal solar irradiance [W/m ²]	$\mathbf{I}_{\text{h}}^{\text{diff}}$
ZPE1	Identified energy model for a system of FCUs	-
ZPE4	Identified simplified building thermal model	-
ZPE5	Unmeasurable heat disturbance estimate [kW]	E_{d}
	Fast dynamics building states estimates [°C]	\hat{T}_{a}
	Slow dynamics building states estimates [°C]	\hat{T}_{z}
ZPE6	Predicted heat disturbance profile [kW]	\mathbf{E}_{d}
ZPE7	Predicted temperature reference profile [°C]	\mathbf{y}^{ref}
central HVAC MPC	Predicted profile of central mass flow [kg/s]	$\mathbf{q}_{\text{w,HVAC}}$
	Predicted profile of central supply temperature [kg/s]	$\mathbf{T}_{\text{w,HVAC}}^{\text{in}}$
	Thermal energy price [EUR/kWh]	\mathbf{c}_{t}
	Critical region	CR
DATABASE	Acceptable deviations from the temperature reference [°C]	Δ^{ref}
	The energy-comfort trade-of variable	γ_e
	Building external walls azimuth and tilt angles	-
	HVAC operating schedule and nominal operation values	-
	Identified temperature drop model and flow share model between central HVAC and floor supply ducts	-

Operation results

On-line operation of the zone MPC module in two exemplary south-oriented zones on 30 January 2020 and 7 February 2020 are shown in Fig. 8.14 and Fig. 8.15, respectively.

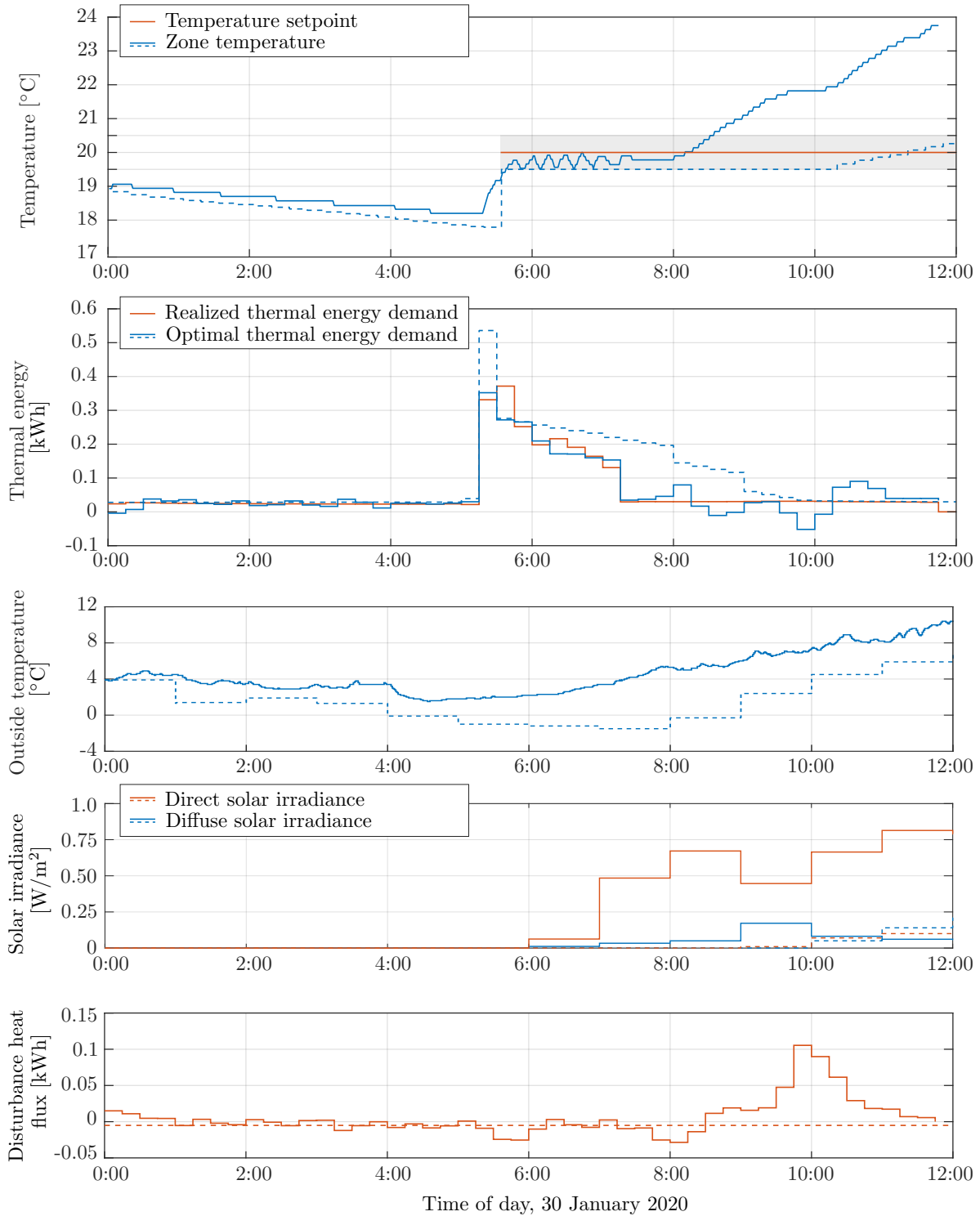


Figure 8.14. On-line operation of the zone MPC module in zone C09-15-1 zone on 30 January 2020.

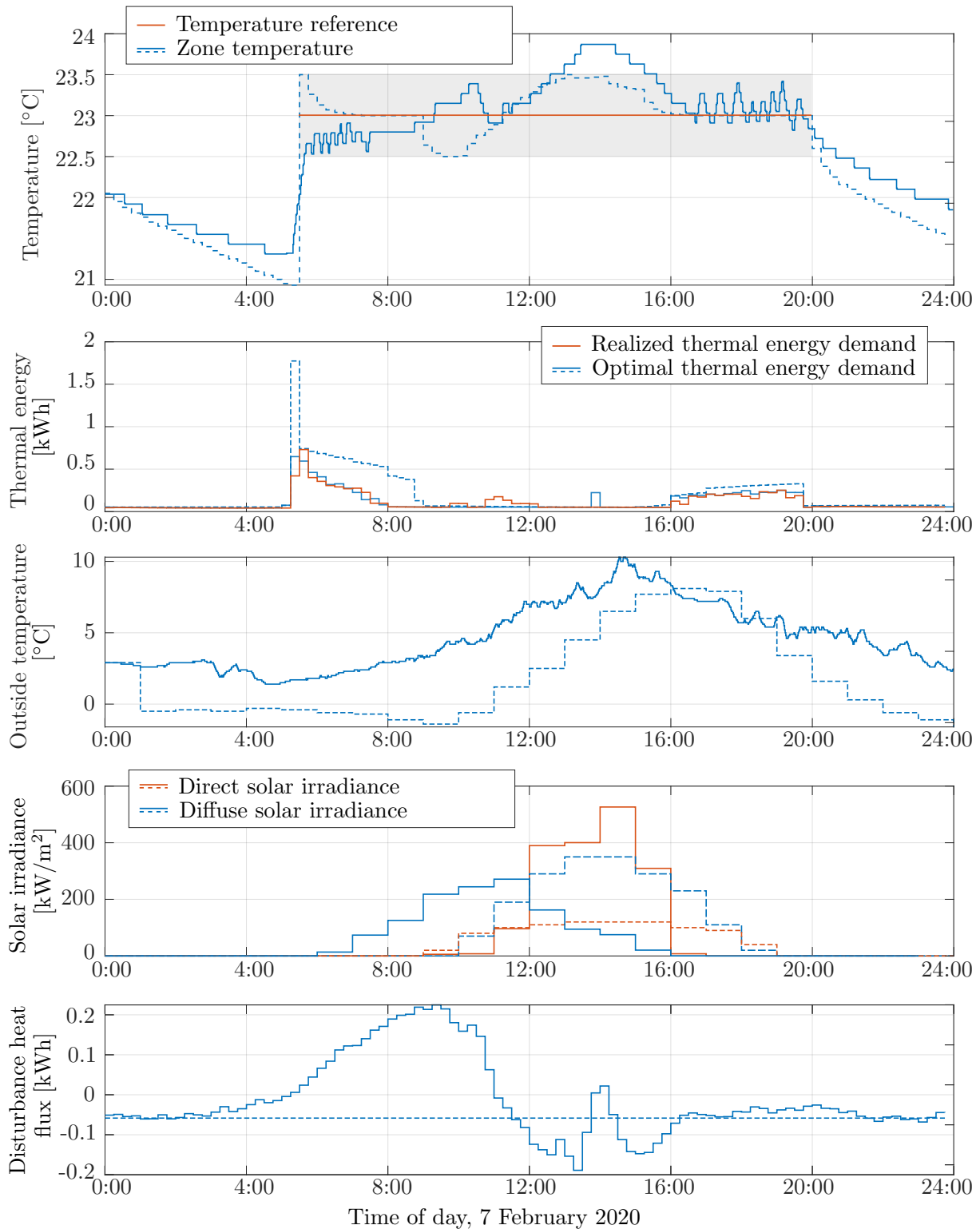


Figure 8.15. On-line operation of the zone MPC module in zone C09-04 on 7 February 2020.

The results of the on-line operation of the zone MPC module on one exemplary north-oriented zone between 24 February 2020 22:00 and 25 February 2020 22:00 is shown in Fig. 8.16.

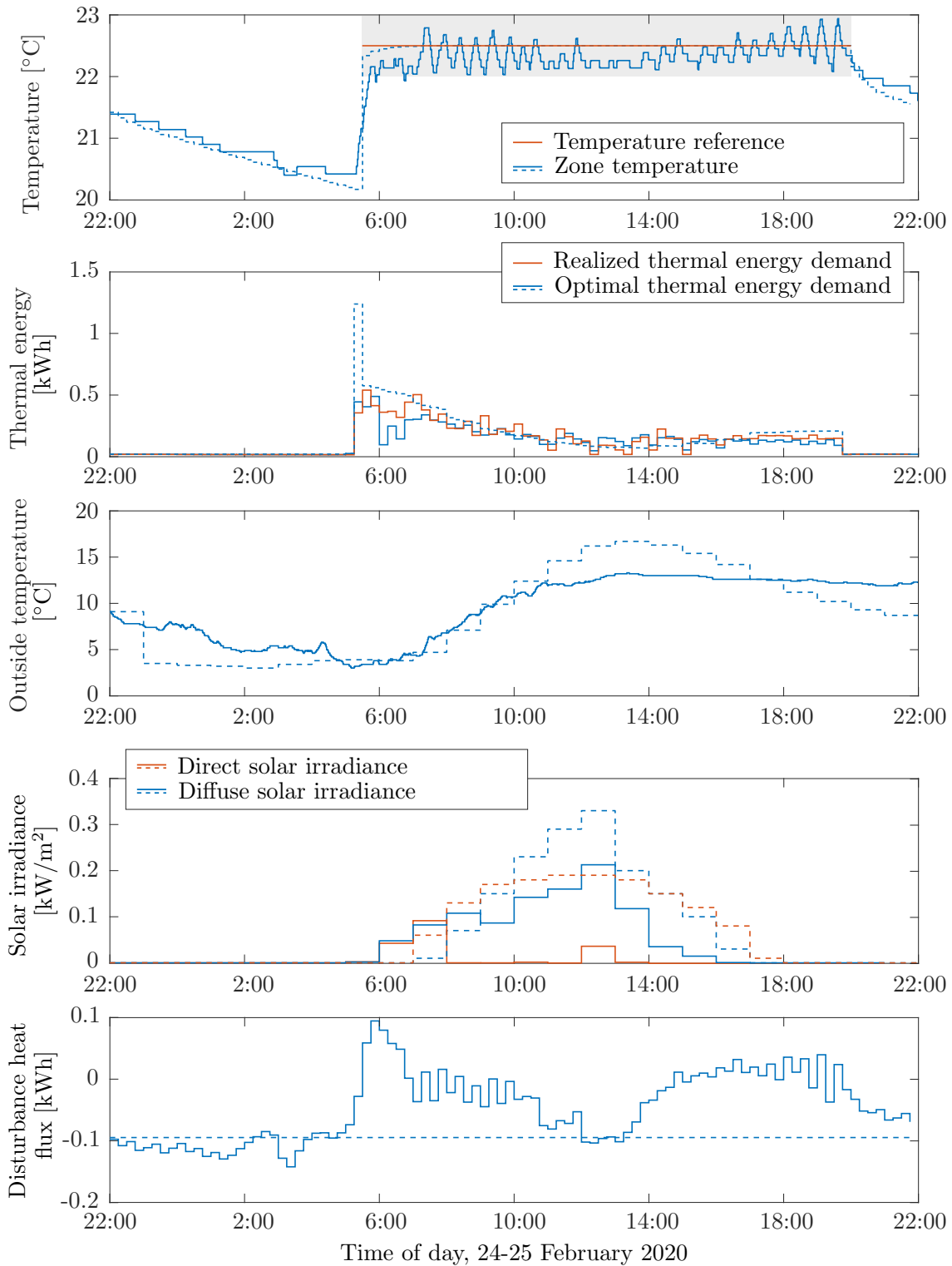


Figure 8.16. On-line operation of the zone MPC module in zone C09-17 between 24 February 2020 22:00 and 25 February 2020 22:00.

The MPC parameters are $\gamma_e = 1$ and $\Delta^{\text{ref}} = 0.5^\circ\text{C}$. Dashed lines represent predictions and optimized profiles calculated at 30 January 2020 0:00 and 24 February 2020 22:00. Solar irradiance is presented as average solar irradiance within 1-hour time intervals. The mismatch between the optimal thermal energy profile predicted at 0:00 and optimal thermal energy demand calculated in receding fashion (solid blue line) is due to the prediction error of the disturbances affecting the zone temperature dynamics and other changes in the building environment handled through the receding horizon principle. Figure 8.17 shows the comparison of the optimized thermal energy profile of 13 south-oriented zones controlled via MPC and realized thermal energy consumption measured by the calorimeter. The considered south-oriented zones are connected to the same floor supply duct. The optimized thermal energy profile is obtained as a sum of optimal thermal energy profiles for the individual zones calculated at 22:00 4 February 2020.

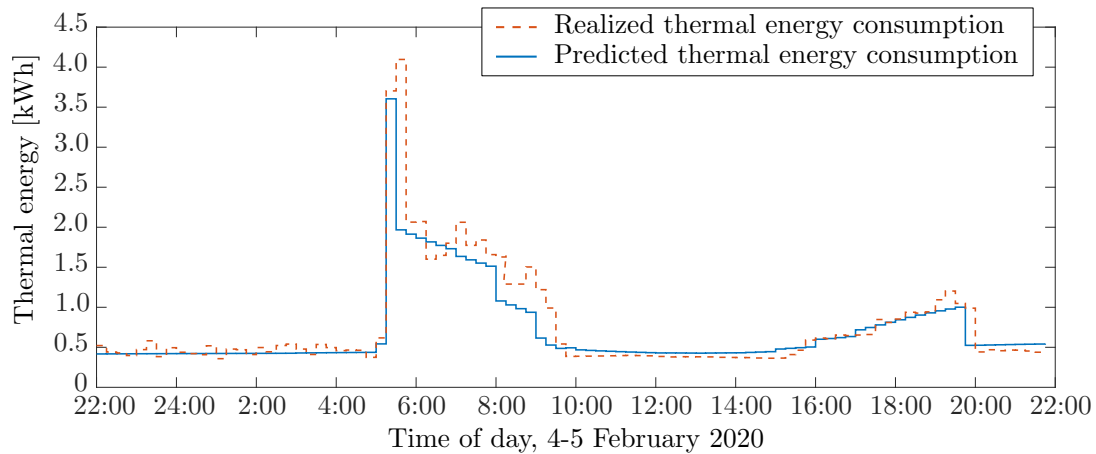


Figure 8.17. Comparison of the thermal energy consumption profile of 13 south-oriented zones controlled via MPC predicted at 22:00 4 February 2020 by MPC and realized thermal energy consumption measured by the calorimeter.

The comparison of the predicted and realized thermal energy consumption in 10 north-oriented zones controlled via conventional digital zone controllers is shown in Fig. 8.18. The considered north-oriented zones are connected to the same supply duct. Since the zones are not controlled via MPC, the thermal energy consumption is predicted by simulating the hysteresis control in an open-loop simulation. The prediction start times are selected to fit the times at which the new 72-hours-long weather prediction was obtained. The mismatch between the predicted and realized thermal energy consumption is due to difference in hysteresis width between the case-study building conventional zone digital controller and hysteresis controller used in simulation. The comparison of the thermal energy consumption of all 248 controllable zones measured by the calorimeter and predicted thermal energy consumption at 22:00 29 January 2020 by simulating the hysteresis control in 231 zones and optimizing the zone temperature via MPC in 17 zones is shown in Fig. 8.19.

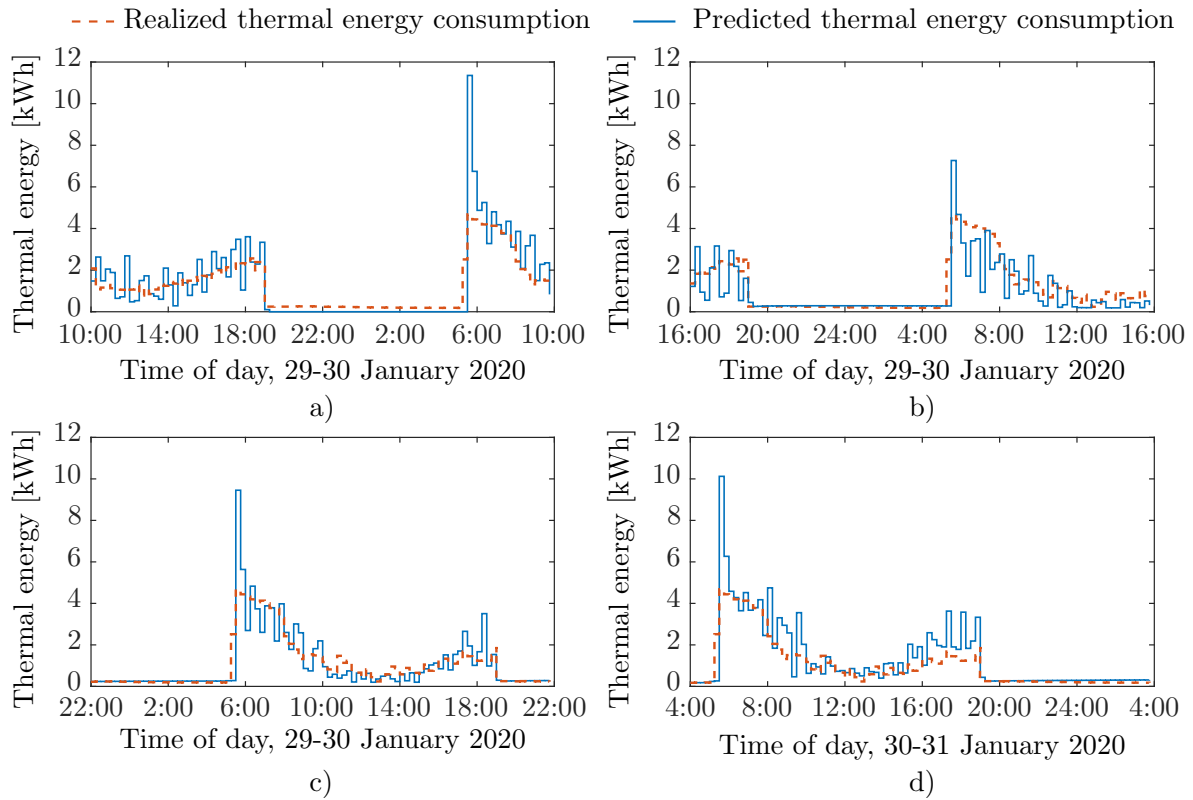


Figure 8.18. Comparison of the thermal energy consumption in 10 north-oriented zones connected to the same supply duct predicted at a) 10:00 29 January 2020, b) 16:00 29 January 2020, c) 22:00 29 January 2020 and d) 4:00 30 January 2020 by simulating the hysteresis control and realized thermal energy consumption measured by the calorimeter.

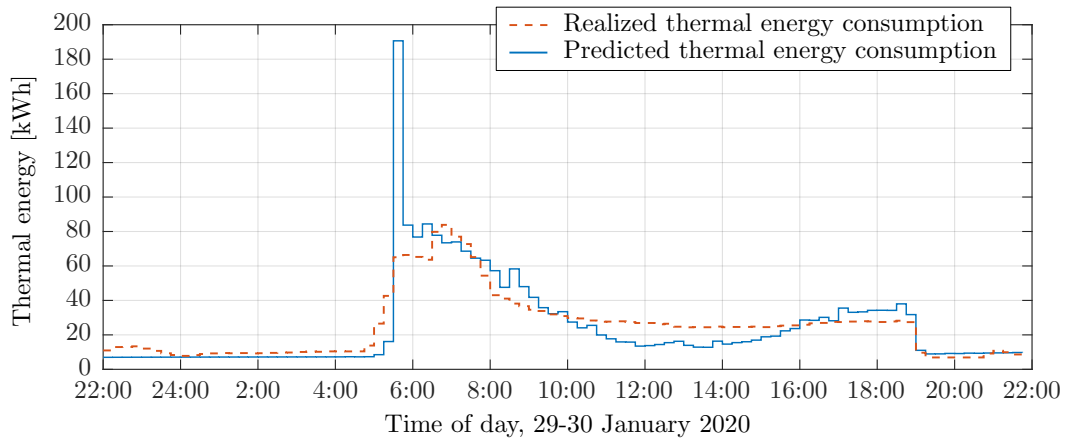


Figure 8.19. Comparison of the thermal energy consumption of all 248 controllable zones predicted at 22:00 29 January 2020 and realized thermal energy consumption measured by the calorimeter.

The operation results show a good agreement between the predicted and the realized thermal energy consumption in building zones and as such prove the applicability of the obtained predictions to be utilized within the hierarchical coordination approach to plan the operation of the central HVAC system.

8.2.3 Fan coil unit interface module

The operation of the FCU interface module is based on the approach developed within Chapter 5 Section 5.5. The module controls the FCU in adherence to the required thermal energy input in zone defined as an output of the MPC module and the difference between the disturbance value predicted for the current 15-min-long time interval by the higher-level MPC and realized heat disturbance estimated by PE5 module every 1 min. The module operates with time resolution of 1 min. The list of all inputs required for operation of the FCU interface module is given in Tab. 8.10.

Table 8.10. *Input variables definition required for operation of the FCU interface module.*

	Required input data	Notation
ZONES	Zone temperature reference [°C]	T_a^{ref}
	Zone temperature [°C]	T_a
FCU	Return medium temperature [°C]	T_w^{out}
CALORIMETER	Supply medium temperature [°C]	T_w^{in}
	Medium flow [kg/s]	$q_{w,\text{cal}}$
WEATHER STATION	Outside air temperature [°C]	T_{out}
	Direct normal solar irradiance [W/m ²]	I_n^{dir}
	Diffuse horizontal solar irradiance [W/m ²]	I_h^{diff}
PE1	Identified energy model for a system of FCUs	-
	Thermal power inserted into zone [kW]	P_a
PE4	Identified simplified building thermal model	-
PE5	Unmeasurable heat disturbance estimate [kW]	\hat{P}_d
	Fast dynamics building states estimates [°C]	\hat{T}_a
	Slow dynamics building states estimates [°C]	\hat{T}_z
zone MPC	Optimal thermal power input on current MPC interval	$u_{k k}^*$
	Predicted heat disturbance on current MPC interval	$P_{d,k k}^*$
	Predicted temperature reference on current MPC interval	$T_a^{\text{ref},*}$
DATABASE	Acceptable deviations from the temperature reference [°C]	Δ^{ref}
	Building external walls azimuth and tilt angles	-

The output of the module is the optimal fan speed trajectory $\mathbf{x}_{\text{fc},t}^*$. Only the first element $x_{\text{fc},t|t}^*$ is applied to the system and the module starts new calculation at the next sampling time instant.

Integral behaviour

Integral behaviour, which ensures the offset-free control, is emulated via iterative update and correction of thermal energy reference calculated by zone MPC with respect to the difference between the predicted and realized heat disturbance and possible plant and model mismatch. The correction amount, denoted here as ΔE_a^{ref} , consists of several parts:

- mismatch between the realized and requested energy within the current 15-min-long time interval,
- difference between the predicted and realized disturbance within the current 15-min-long time interval, and
- predicted disturbance mismatch on the rest of the current 15-min-long time interval.

The detailed analysis of individual correction amounts is given in Chapter 5 Section 5.5. The requested thermal energy within the current 15-min-long interval is recalculated every FCU interface sampling interval as:

$$E_a^{\text{ref}} = E_a^{\text{ref}*} \frac{H_{\text{fc}}}{T_s^c/T_s} + \Delta E_a^{\text{ref}}, \quad (8.15)$$

where E_a^{MPC} is optimal thermal energy input defined as:

$$E_a^{\text{ref}*} = u_{k|k}^* \cdot T_s^c, \quad (8.16)$$

$u_{k|k}^*$ is optimal thermal power calculated by zone MPC, H_{fc} is prediction horizon of the FCU interface and T_s^c and T_s are sampling times of the zone MPC and FCU interface, respectively.

FCU fan speed preselection

The background optimization problem of the control algorithm developed in Chapter 5 Section 5.5 is of Mixed Integer Linear Program (MILP) type. Such programs are computationally extensive when applied for control of large number of zones. To reduce the computational complexity of the algorithm the number of the optimization variables is reduced by preselecting the two of four possible FCU fan speeds (fan off, low, medium and high speed denoted respectively as off, L, M, H). The fan speeds are preselected based on the known thermal energy request and physical thermal energy limits of FCU operation in certain fan speed calculated based on a known FCU energy model (PE1) and assumption of constant zone air temperature. The approach is illustrated in Fig. 8.20.

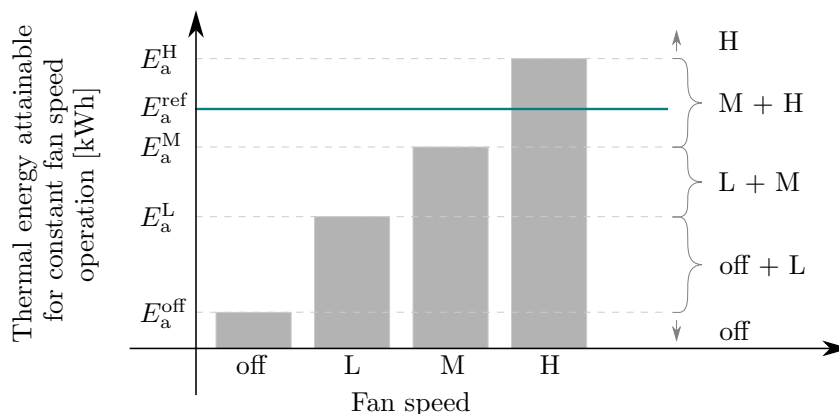


Figure 8.20. Relaxation of computational complexity by preselecting fan speeds required to fulfil the requested energy request.

Thermal energies attainable by constant operation in off, low, medium or high fan speed along the optimization horizon are denoted respectively as E_a^{off} , E_a^L , E_a^M and E_a^H . Based on the requested energy amount, preferred operation in lower fan speeds and minimal number of fan speed changes along the horizon, the number of the required fan speeds for the realization of the requested energy is lowered to only two speeds. Exceptionally, in cases when the E_a^{ref} is higher than the thermal energy attainable in constant high speed operation and lower than the thermal energy attainable with fan constantly switched off, the FCU states on the horizon are fixed to the high speed and fan switched off, respectively. In order not to compromise the comfort, the preselection of fan speeds is allowed only when the temperature reference used by the MPC module corresponds to the temperature reference selected on the wall thermostat, i.e. the temperature reference did not change within the current MPC sampling interval.

Sudden changes of temperature reference within the MPC sampling time

To keep the user comfort, at every FCU interface sampling interval current zone temperature reference T_a^{ref} , read from the wall unit, is compared with the temperature at the beginning of the current 15-min-long time interval and the one assumed in zone MPC module for the current time interval. If those temperatures differ, the interface focuses only on keeping the temperature within the permissible temperature interval defined with the new temperature reference selected by the user and acceptable deviations from the temperature reference Δ^{ref} . By doing so, the users comfort is ensured even if sudden changes of temperature reference occur within the MPC sampling time interval.

FCU interface algorithm

The FCU interface logic, presented in a form of flowchart is shown in Fig. 8.21. In unoccupied mode temperature constraints are matched with the building protect limits to enable the preheating/precooling.

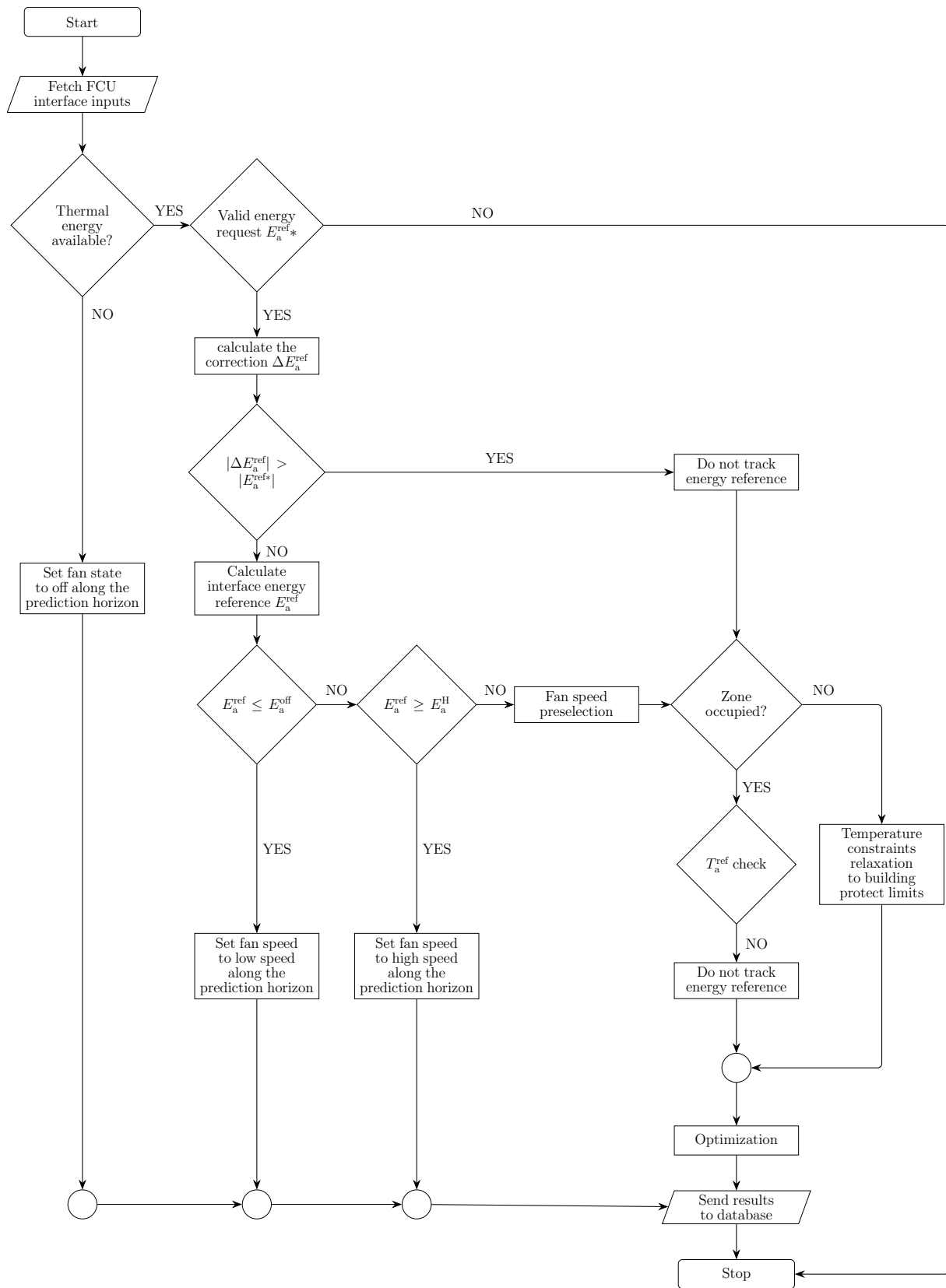


Figure 8.21. FCU interface flowchart.

Operation results

The allowed temperature deviation from the reference Δ^{ref} and comfort-savings trade-off parameter γ_e are set to $\Delta^{\text{ref}} = 0.5^\circ\text{C}$ and $\gamma_e = 1$ in all controllable building zones. The fan speed preselection option was not enabled. The operation results showing the following of the optimal thermal energy input generated by central zone MPC are shown in Fig. 8.22. The energy reference for the interface module is obtained by modifying optimal thermal energy input calculated by the central zone MPC with respect to the correction amount ΔE_a^{ref} .

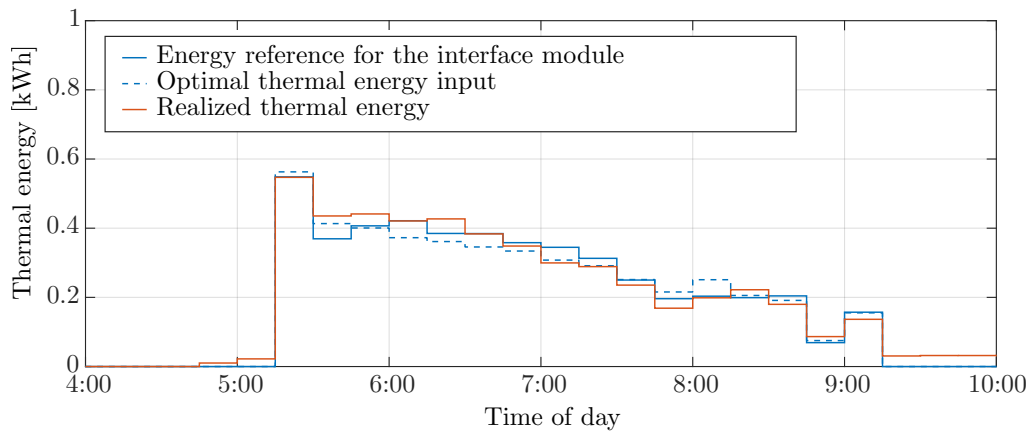


Figure 8.22. Thermal energy reference following in one exemplary south-oriented zone on 15 January 2020.

The average deviation from the energy reference, due to the limited set of available power inputs, during intervals with energy reference larger than 0.1 kWh is $\pm 5\%$. The zone temperature on the selected day is shown in Fig. 8.23.

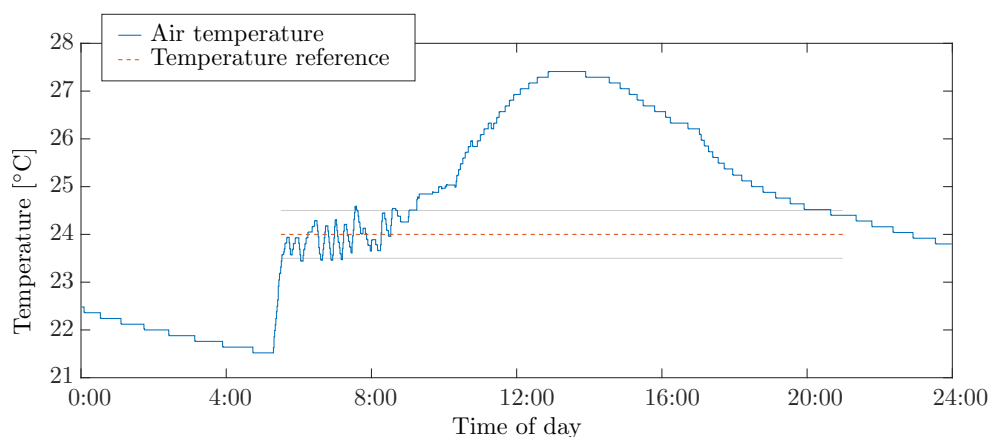


Figure 8.23. Zone temperature in one exemplary south-oriented zone on 15 January 2020.

In intervals in which no comfort constraints are set the temperature reference is not plotted.

The operational results in two exemplary north-oriented zones on 5 February 2020 and 11 February 2020 are shown in Fig. 8.24 and Fig. 8.25.

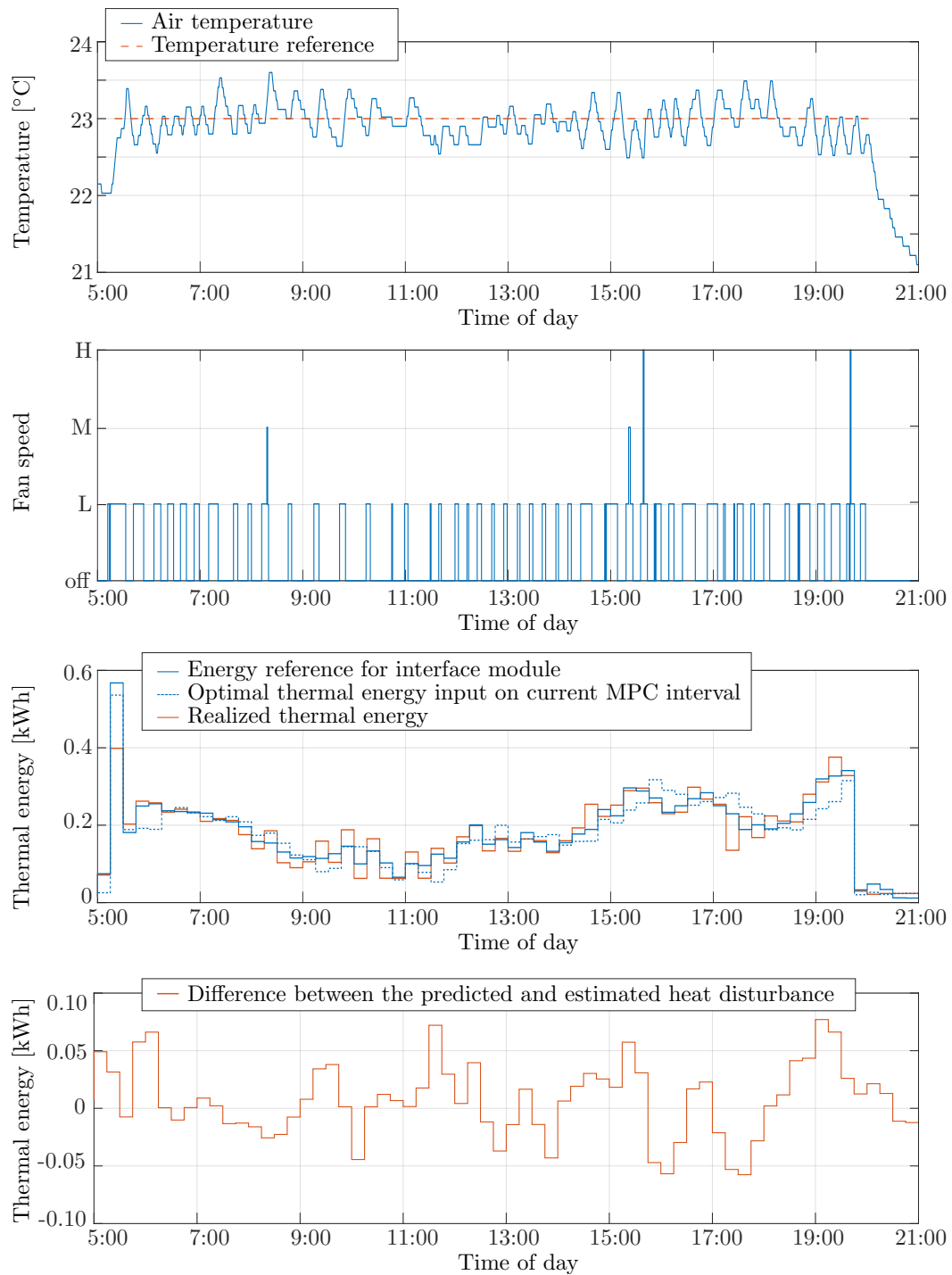


Figure 8.24. Operational results in one exemplary north-oriented zone on 5 February 2020.

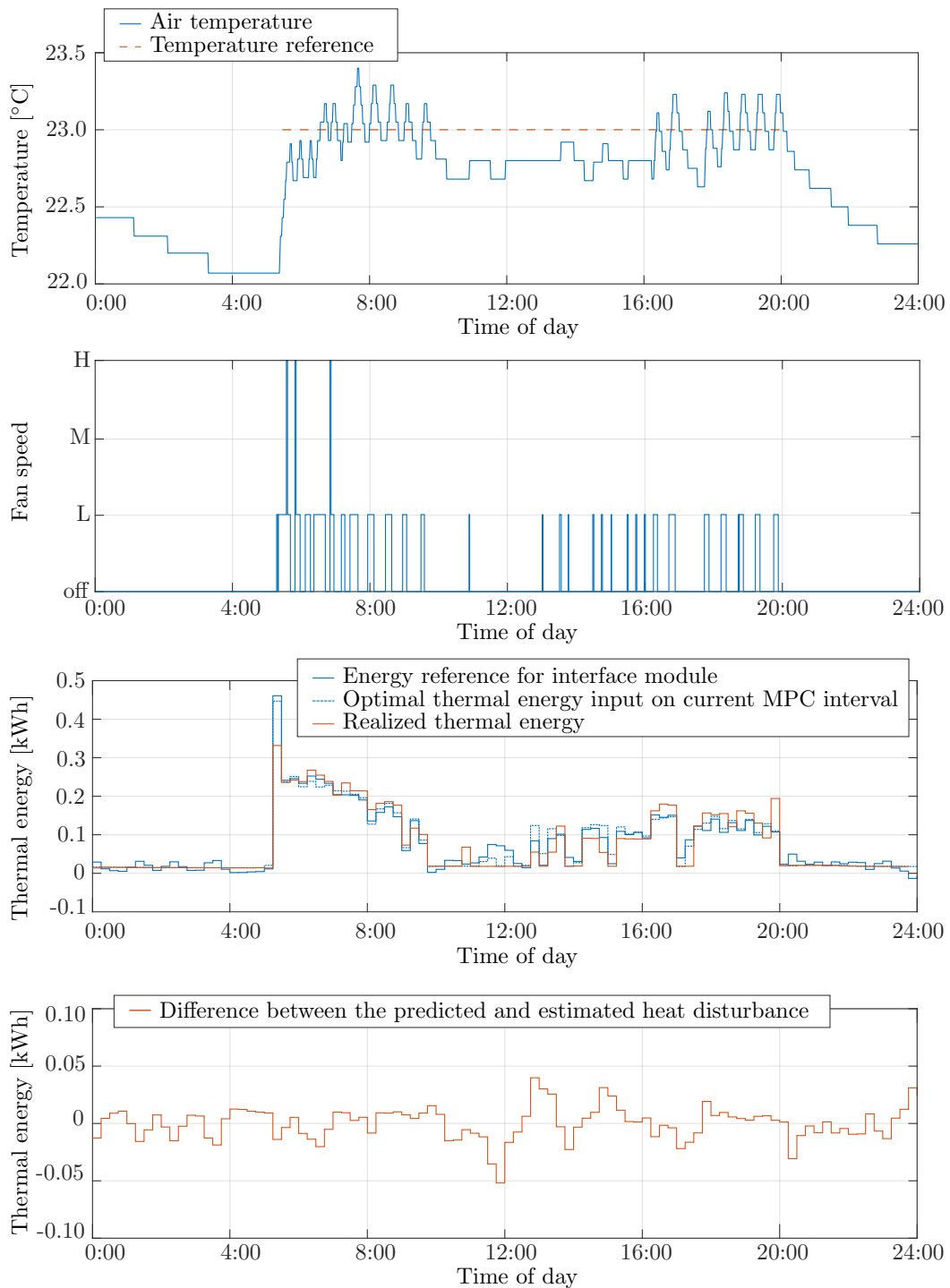


Figure 8.25. Operational results in one exemplary north-oriented zone on 11 February 2020.

Figure 8.26 shows the operational results from one exemplary south-oriented zone. Despite sudden change of the temperature reference at 8:21 and central zone MPC anticipating that change only from 8:45 on, the developed interface algorithm ensured comfort during the transition period by detecting the change and focusing only on keeping the zone temperature within the permissible range until the appropriately computed energy reference was available.

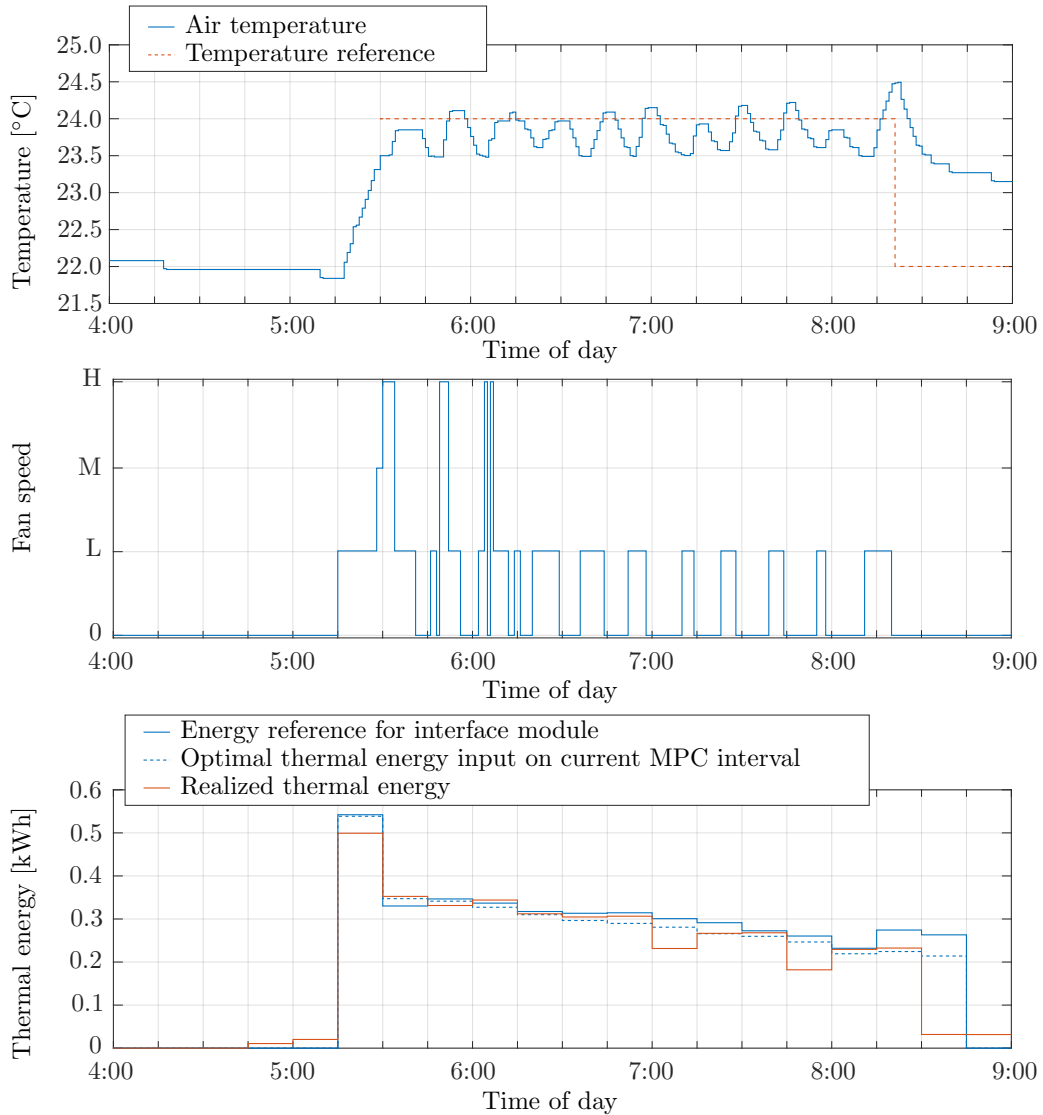


Figure 8.26. Operational results in one exemplary south-oriented zone on 17 January 2020.

Despite complexity, the developed FCU interface module for energy management in building zones based on adherence to the commanded thermal energies shows good performance regarding energy tracking and keeping the zone temperature within the defined temperature range.

Fault detection in a system of fan coil units

Besides playing a vital role in development of advanced model based control algorithms, the mathematical models of the building systems developed in Part I of the thesis proved to be the key for the improvement of reliability and safety of building operation. In [65] the model-based FCU fault detection tool, based on the analysis of discrepancy between the system and nominal simulation model, is developed. The variables used for comparison are valve position, flow rate and zone air temperature. The fault detection approach developed within the thesis is based on the performance monitoring of a return medium temperature measurement which encodes the information on FCU behaviour. One of the most common faults in a system of FCUs is a restriction of, or complete stoppage of heating/cooling medium flow, caused by air trapped inside the system. The air usually enters the system during the interventions on piping and seasonal switch between building thermal energy source. The standard maintenance of the system demands visits to all FCUs in the building after every intervention on the system. Such approach is not only time-consuming but also requires a lot of personnel. Thus, typically only FCUs in zones which are most critical or the users are complaining on the heating/cooling performance are inspected. To remove the air lock, every FCU is equipped with a small manual valve which is then used to release the air from the system. The air lock in the system is detected in one of the two following ways.

1. The air lock is detected when the measured return medium temperature with fan switched off is significantly lower than the supply temperature. This approach relies only on the measurements and can be used only for detection of air lock in FCUs in which the flow is completely obstructed.
2. The air lock detection is performed by comparing the monitored performance of the FCU with the nominal FCU performance calculated via on-line simulation of dynamic FCU return medium temperature model identified in Chapter 2. In such a

set-up, the known nominal performance of the FCU enables also the detection of a level of the performance deterioration.

While the second approach is applicable over the entire FCUs' operating range the first approach is applicable only in situations in which the medium supply temperature is larger than the highest expected zone temperature during the heating season (e.g. 30°C) and smaller than lowest expected zone temperature during the cooling season (e.g. 20°C).

The calculation of the nominal return medium temperature is implemented as part of an additional prediction and estimation software module (PE0) operating in an open loop fashion, i.e. the information on return medium temperature measured by temperature sensor is not used. The on-line operation of ZP0 module ensures the redundancy of the return medium temperature measurements for cases of fault free system operation during which the simulated and measured return medium temperature coincide. For a fixed medium mass flow through the FCU $q_{w,i}$, where subscript i denotes the i^{th} FCU, the thermodynamic model of a single FCU identified in Chapter 2 is in a form of a switched-linear model:

$$\begin{aligned} \dot{T}_{w,i}^{\text{out}} = & \left[-\frac{q_{w,i}}{m_{w,i}} - \frac{U_o(x_{fc,i}, q_{w,i})}{2m_{w,i}c_w} \right] T_{w,i}^{\text{out}} \\ & + \left[\frac{q_{w,i}}{m_{w,i}} - \frac{U_o(x_{fc,i}, q_{w,i})}{2m_{w,i}c_w} \quad \frac{U_o(x_{fc,i}, q_{w,i})}{2m_{w,i}c_w} \right] \begin{bmatrix} T_{w,i}^{\text{in}} \\ T_{a,i}^{\text{in}} \end{bmatrix}, \end{aligned} \quad (9.1)$$

where the fan speed $x_{fc,i}$ is used for switching, $T_{a,i}^{\text{in}}$ is the air temperature inside the i^{th} zone, $T_{w,i}^{\text{in}}$ and $T_{w,i}^{\text{out}}$ are water inlet and outlet temperatures, respectively, c_w is the specific heat capacity of the medium, considered either constant or estimated from the experiments, and parameter $m_{w,i}$ is the mass of water inside the FCU, available from the manufacturer's catalogue. The overall heat transfer coefficient $U_o(x_{fc,i}, q_{w,i})$ is defined as: with constituting model parameters a_{fc} , b_{fc} and c_{fc} determined based on physical system properties or through identification.

$$U_o(x_{fc,i}, q_{w,i}) = \begin{cases} \varepsilon_{fc}^{\text{off}} \cdot \frac{a_{fc}^{\text{off}}}{1 + b_{fc}^{\text{off}} \cdot q_{w,i}^{-c_{fc}}}, & \text{for } x_{fc} = \text{off}, \\ \varepsilon_{fc}^{\text{L}} \cdot \frac{a_{fc}^{\text{L}}}{1 + b_{fc}^{\text{L}} \cdot q_{w,i}^{-c_{fc}}}, & \text{for } x_{fc} = \text{L}, \\ \varepsilon_{fc}^{\text{M}} \cdot \frac{a_{fc}^{\text{M}}}{1 + b_{fc}^{\text{M}} \cdot q_{w,i}^{-c_{fc}}}, & \text{for } x_{fc} = \text{M}, \\ \varepsilon_{fc}^{\text{H}} \cdot \frac{a_{fc}^{\text{H}}}{1 + b_{fc}^{\text{H}} \cdot q_{w,i}^{-c_{fc}}}, & \text{for } x_{fc} = \text{H}. \end{cases} \quad (9.2)$$

The parameters $\{\varepsilon_{fc}^{\text{off}}, \varepsilon_{fc}^{\text{L}}, \varepsilon_{fc}^{\text{M}}, \varepsilon_{fc}^{\text{H}}\}$, $\{a_{fc}^{\text{off}}, a_{fc}^{\text{L}}, a_{fc}^{\text{M}}, a_{fc}^{\text{H}}\}$, $\{b_{fc}^{\text{off}}, b_{fc}^{\text{L}}, b_{fc}^{\text{M}}, b_{fc}^{\text{H}}\}$ and c_{fc} are known parameters found through identification as described in Chapter 2. Four possible FCU fan speeds: off, Low, Medium and High are denoted respectively as off, L, M, H.

Based on (9.1) the dynamics of the return medium temperature is written in general discrete-time model form:

$$T_{w,i}^{\text{out}}(k+1) = f_{\text{fc}}(m_{w,i}, c_{w,i}, u_{\text{fc},i}^{\text{m}}(k), T_{w,i}^{\text{out}}(k)) \quad (9.3)$$

where function $f_{\text{fc}}(\cdot)$ results from integration of the continuous-time model function (9.1) over the selected sampling time interval. Vector u_{fc}^{m} comprises the model inputs and it is defined as:

$$u_{\text{fc},i}^{\text{m}}(k) = \begin{bmatrix} q_{w,i}(k) & x_{\text{fc},i}(k) & T_{a,i}^{\text{in}}(k) & T_{w,i}^{\text{in}}(k) \end{bmatrix}. \quad (9.4)$$

Model inputs are measured directly or indirectly based on the energy model of a system of FCUs identified in Chapter 2.

To verify the approach, the operation of the PE0 module is tested on historical building data. The comparison of the off-line simulation results with the fault-free experimental data in one exemplary zone is shown in Fig. 9.1. The information on nominal model performance is used only in intervals with medium mass flow larger than zero. In intervals in which this condition is not satisfied the simulated return medium temperature is not plotted. From the results it is evident that the nominal FCU model successfully reproduces the dynamics of a FCU under fault-free conditions.

The on-line performance of the developed PE0 software module under the fault-free conditions in one exemplary zone is shown in Fig. 9.2. In on-line operation the time delays are inevitable, thus the fault detection should be performed on stationary data only. The operation under faulty conditions is verified by monitoring performance of one FCU on 9th floor of the case-study building. The FCUs on the selected floor are equipped with three-way valves, which are in normal building operation constantly closed (total flow goes through the FCU). To verify the approach, the air lock in one selected FCU is emulated by opening its associated valve on 23 January 2020 preventing thus the medium to enter the FCU. The valve was opened from 9:45 until 17:20. The medium flow blockage resulted with the discrepancy between simulated and measured return medium temperature.

Overall, the PE0 module successfully reproduces the dynamics of a FCU under fault-free conditions. This allows for a reduced cost of replication of the whole system for optimal temperature management in the building zones, since the initial investment cost can be significantly reduced by estimating the temperature at the outlet of FCUs using the proposed software module instead of having temperature sensors installed on all FCUs. If both measured and simulated outlet temperatures are available, the discrepancy between the two can be used to detect the faults in the system.

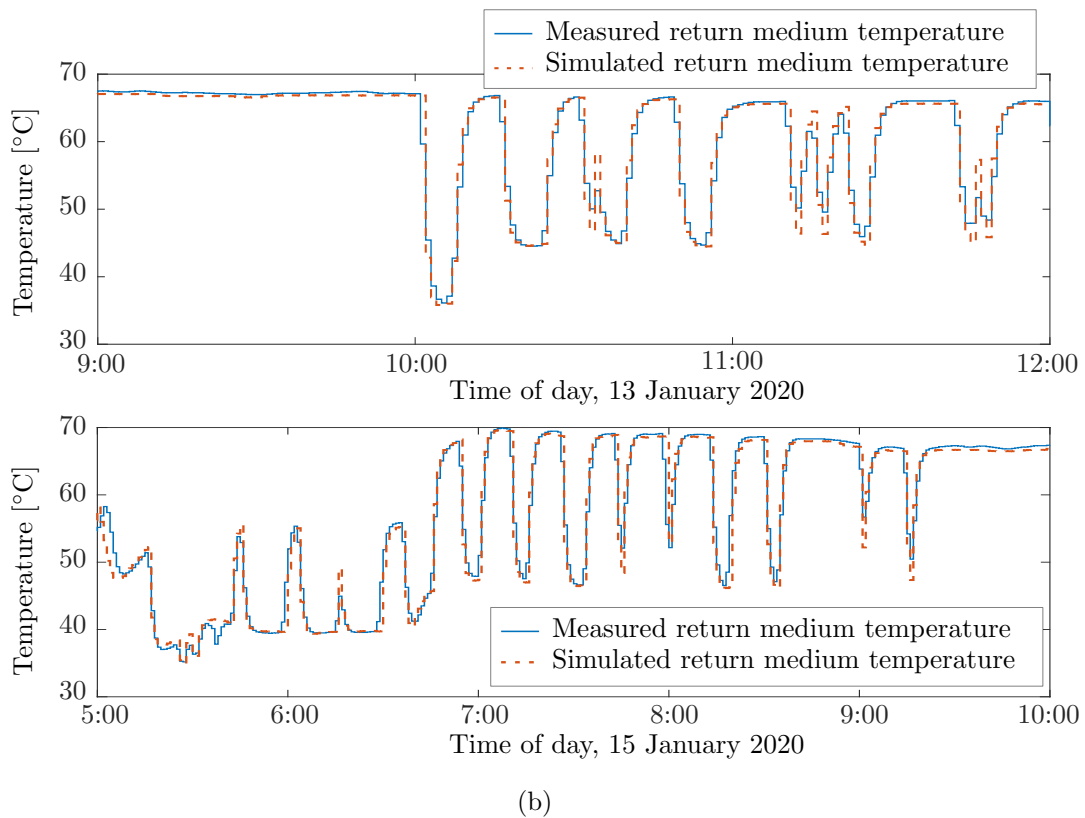
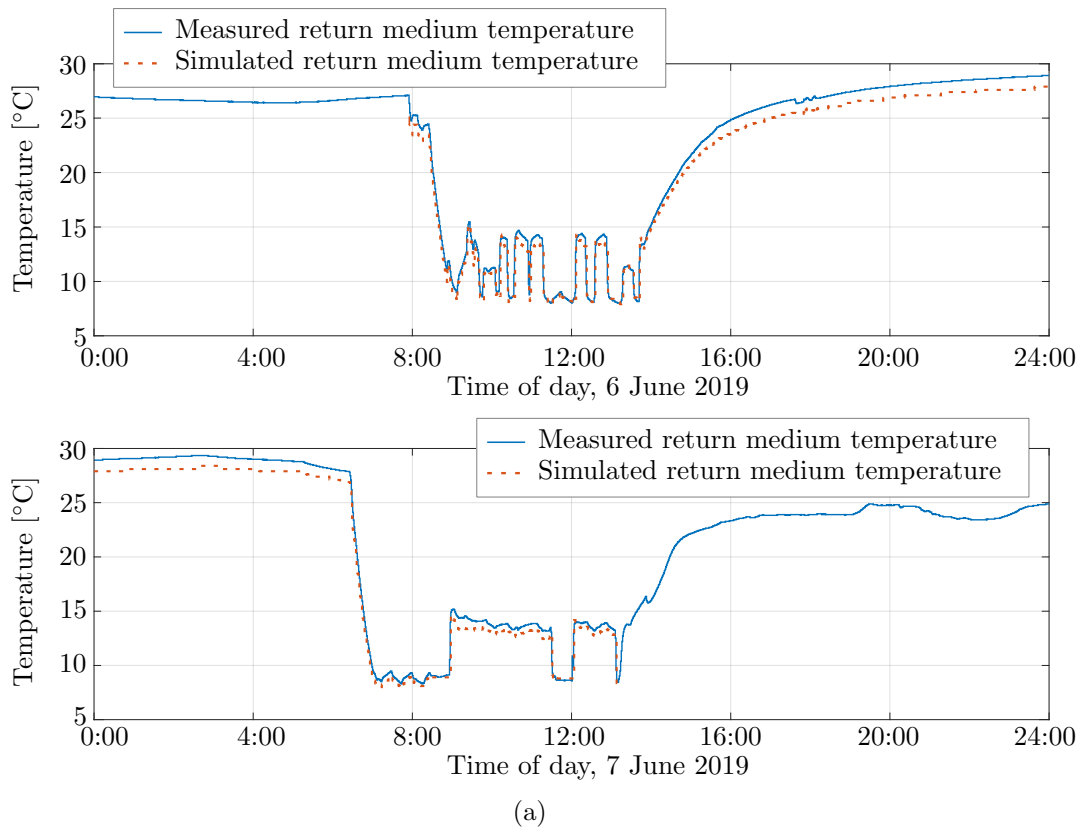


Figure 9.1. The comparison of simulation results with the fault-free experimental data in one exemplary zone in the a) cooling season, b) heating season.

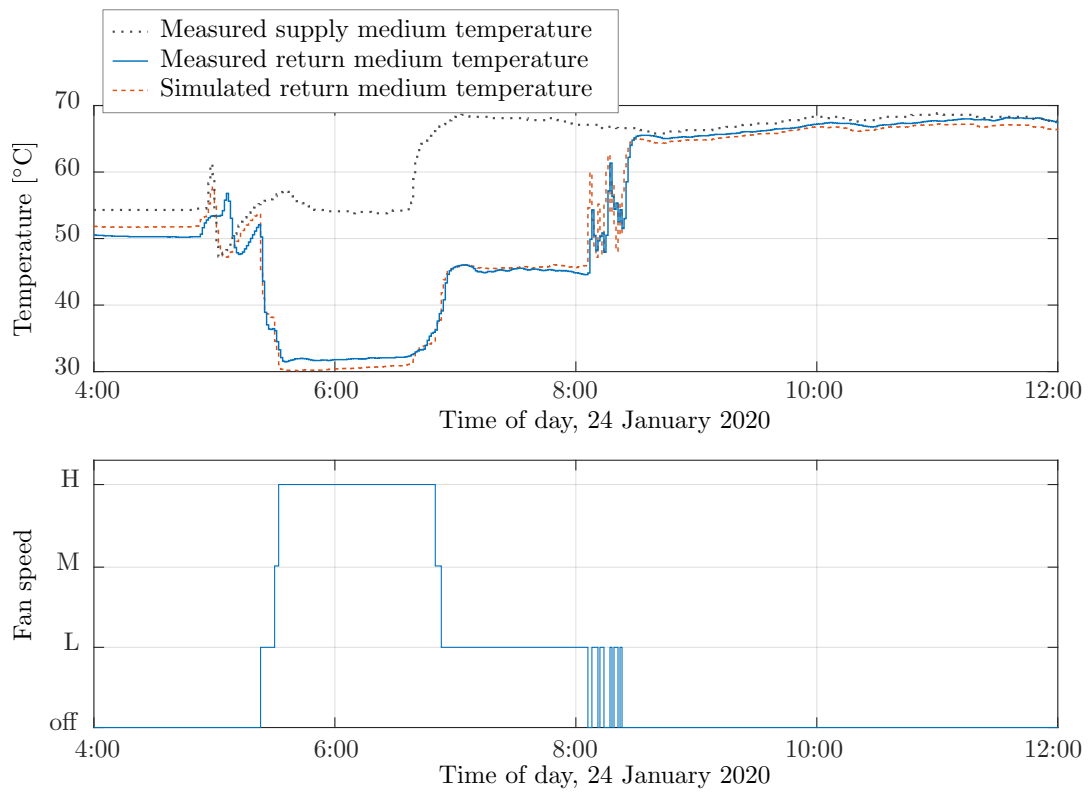


Figure 9.2. *Fault-exclusive on-line operational results in one exemplary zone during the heating season.*

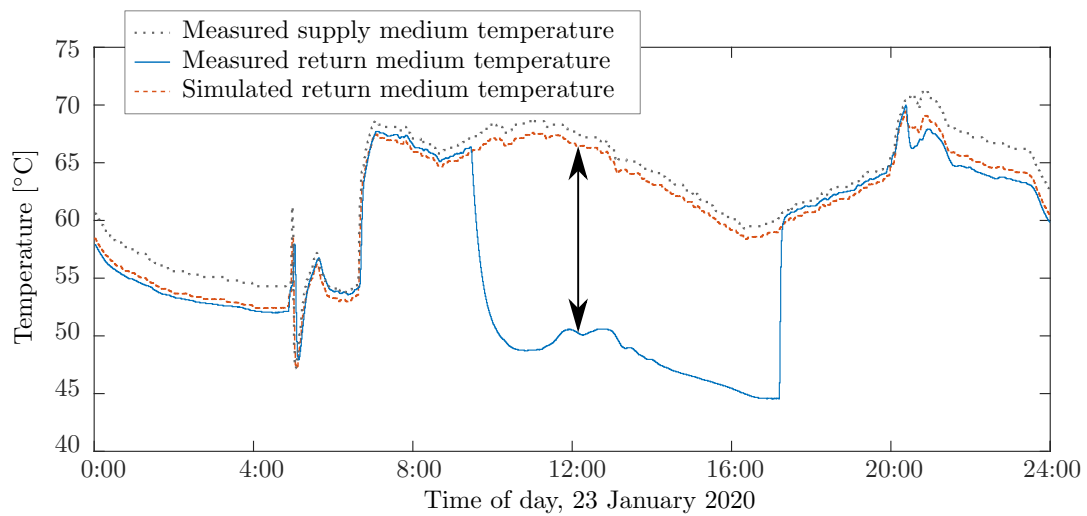


Figure 9.3. *Fault-inclusive on-line operation data in one exemplary zone during the heating season.*

Part III conclusion and future research opportunities

From the results of on-line operation it is evident that the developed MPC strategy successfully controls the temperature in building zones. Contrary to the conventional control algorithms, the MPC allows more advanced and specific system design, especially in terms of accounted hour-to-hour variable energy prices and coordination with central heating/cooling medium conditioning system which is yet to be tested for the case-study building. Although, the real building application results are very encouraging, the achieved energy savings are yet to be calculated. Besides the weather forecast, a second important influence on buildings dynamics are the buildings' occupants, both in terms of the estimated unmeasured heat disturbances and in terms of the thermal comfort demands. The potential benefits of the MPC used for zone temperature control are expected to be significantly increased with the:

- occupancy prediction interconnected with the business system such that the informations on business trips, scheduled lectures, sick leaves, etc. are fully exploited,
- window openness detection and reaction to the system by shutting down the heating/cooling if unnecessary window openness is detected simultaneous with the heating/cooling being active.

The existence of the local building weather station enables the opportunity for improvement of the weather forecast for a specific building location. The local meteorological measurements could be used to eliminate the systematic error due to the fact that the building is not situated directly at the meteorological station site as well as due to the environment of the building itself [29].

General conclusion

In recent years, application of advanced control, fault detection and diagnosis algorithms for building heating and cooling systems has been intensively investigated with the aim to improve their energy efficiency and bring the buildings sector into the smart city arena. The challenging task of the building control is to achieve interior building environment comfort with high energy-efficiency. The inherent complexity of building systems with uncertain and time-varying dynamics, as well as the presence of unmeasurable disturbances, present serious challenges for the development of corresponding efficient control, fault detection and diagnosis algorithms. The goal of the thesis is to present a general methodology of minimizing energy consumption using current energy sources and minimal retrofitting, but instead making use of advanced control techniques. The thesis focuses on model predictive control (MPC) approach that is based on the formulation of the building control as an optimization problem. A detailed summary of the presented results is given at the end of each of the three thesis parts. In the following, a brief overview of the work that was presented in this thesis, as well as an outlook to possible directions for future research on these topics is given.

In *Part I* of the thesis the robust and easily replicable methodologies for identification of the mathematical model of the building and energy model of the system of fan coil units is presented. The developed methodologies are inevitable for a fast deployment of model-based energy management strategies in buildings. The focus of *Part II* of the thesis is the development of real-time MPC method for zone temperature control that guarantees the essential properties of closed-loop feasibility and stability as well as offset-free control. The developed zone temperature control is envisioned as the lowest level in the hierarchical decomposition of building subsystems, thus a special focus is put on developing the possibility for interaction and coordination with the higher-level modules in order to achieve the near-optimal behaviour of the building as a whole. Finally, the developed zone temperature approach is validated by deploying it on full scale in a skyscraper building in *Part III* of the thesis. The following features of the proposed zone

temperature control approach, that do not exist in the current, off-the-shelf, building management products are:

- openness to integration with versatile building automation networks and heating/cooling elements types in zones, independent of the vendors of low-level controllers, as long as they can be networked and re-configured from local controls to sensors/actuators data coupling to the network, and back;
- non-invasive adding upon the existing equipment in zones which means none or small hardware interventions;
- lowering the cost of building operation with respect to current building conditions;
- estimation of heat disturbances on the zone level that indicate any additional heat input or sink compared to the current building model used for control (occupants, equipment, window blinds), with possibility to tune models for heat disturbance predictions as well as comfort requirements predictions and exploit them for efficiency gains in predictive zone control.
- possibility of full anticipation of weather forecast and occupancy schedules;
- possibility of coordination with higher-level modules in building hierarchy such as central heating/cooling medium conditioning system, building microgrid or smart grid in operation with which the building becomes a responsive subject within the smart distribution grid and smart city;

The studies performed within the thesis prove that MPC implementation represents an excellent opportunity to reduce buildings carbon footprint and achieve substantial cost benefits. Furthermore, the established effectiveness of MPC algorithms able to deal with peak shaving and demand-side management allow this technology to be considered as one of the most suitable for integration of buildings in smart grids. This fact represents a crucial perspective for the energy market, which continuously requires further flexible loads to mitigate the renewable energy sources supply fluctuation. The scientific contributions obtained in the thesis are:

- a method for identification of an energy model of a system of fan coil units, which gives a direct relation between the thermal energy provided to a zone, actuation commands, heating/cooling medium conditions and the zone temperature,
- a method for identification of a thermodynamic building model suitable for predictive control design and disturbance estimation,
- predictive control strategy for zone temperature control and hierarchical coordination with the central heating/cooling medium conditioning system, building microgrid, smart grid or some other building subsystem sharing a common energy link with zones,

- validation of the developed hierarchical predictive control system within a living-lab environment in terms of achieved thermal comfort and energy cost reduction,
- validation of the developed zone temperature control via on-line implementation on a skyscraper building in a full scale.

Future research is oriented towards the automation of the procedures required for deployment of the developed approach on different building configurations with the aim to increase their robustness and reproducibility. The future research opportunities related to individual parts of the thesis are addressed at the end of each part.

Appendices

Case-study skyscraper building

This chapter gives a detailed description of University of Zagreb Faculty of Electrical Engineering and Computing (UNIZGFER) skyscraper building located at Unska 3, Zagreb (Fig. A.1). The building is fully equipped with required hardware and information technology infrastructure for testing and validating a wide range of control and estimation algorithms in buildings which are crucial parts of a Building Energy Management System (BEMS). The building itself is a living-lab on model predictive control algorithms. Within the thesis, all experiments and case studies are performed on the UNIZGFER building.



Figure A.1. *UNIZGFER skyscraper building.*

The building's top view longer axis is almost aligned with east-west direction with a slight deviation from the true east-west direction for 5° (normal of the south-oriented façade surface points 5° out of south towards east). The building consists of 13 floors, a ground-floor, a basement and a flat roof. Detailed description of building physics, construction details and used materials, is given in Appendix A.2. The heating/cooling is based on two-pipe system using Fan Coil Units (FCU) in laboratory and office spaces and

radiators in smaller service rooms. All FCU control devices are networked with a central monitoring system (SCADA system) based on Siemens DESIGO platform. The building has in total 248 controllable zones with altogether 368¹ FCUs used both for heating and cooling, more than 70 non-controllable zones equipped with radiators and manual valves used only for heating, and more than 16 non-controllable zones in which heating/cooling is unavailable. All controllable zones are equipped with digital zone units and additional sensors for measuring the temperature of the FCU return medium temperature on every controllable FCU. Digital zone units are equipped with temperature sensor and display unit for selection of temperature reference and operation mode of the local FCU controller. The heating energy for the system is supplied from the district heat distribution system via a heat exchanger in the heating substation of type Kompakt 1000. The cooling energy for the building is supplied from UNIZGFER's own chiller station RTAC 200 HE produced by Trane manufacturer. To track the consumed thermal energy and monitor the conditions of the heating/cooling medium, calorimeters are installed on central and floor supply ducts. The building also comprises 32 kWh battery storage system with fully controllable power converter and the solar power plant (22.5 kWp). The meteorological conditions influencing the building performance are monitored on a small meteorological station placed on the building rooftop. The overview of the installed equipment is given in Fig. A.2.

All building subsystem are integrated together with developed possibility of a simple and modular changeover between *i*) mode of the building operation in which climate control is performed on a classical decentralized way using local control loops, and *ii*) Smart Operation Mode (SOM) in which commands are issued by software modules through a central database. The SOM enables coordinated control of different energy-relevant building subsystems which finally in a coordinated action shape an optimal energy exchange profile between the building and the grid. The information technology support systems, enabling the SOM, have two important functions - one is to make data exchange between the software modules and the building automation system equipment in the field smooth and reliable, and the other is to enable easy and safe transition from the standard operation to the SOM and back to standard if there is a problem in the execution of software routines. Reliable two-way communication between building automation in the field and software modules is implemented through the central database utilized to collect and consolidate the data from the building, weather service and energy utilities. The variables which are controllable in SOM are: *i*) FCU fan speeds in all zones, *ii*) starting temperature of the medium from the heating substation towards the building, *iii*) pressure difference on the circulation pump of the heating substation secondary circuit (building circuit), *iv*) starting temperature of the medium from the chiller towards the building *v*) battery system reference charging/discharging AC power or reference DC current for charging/discharging the battery system stack.

¹Some zones have more than one FCU depending on their size.

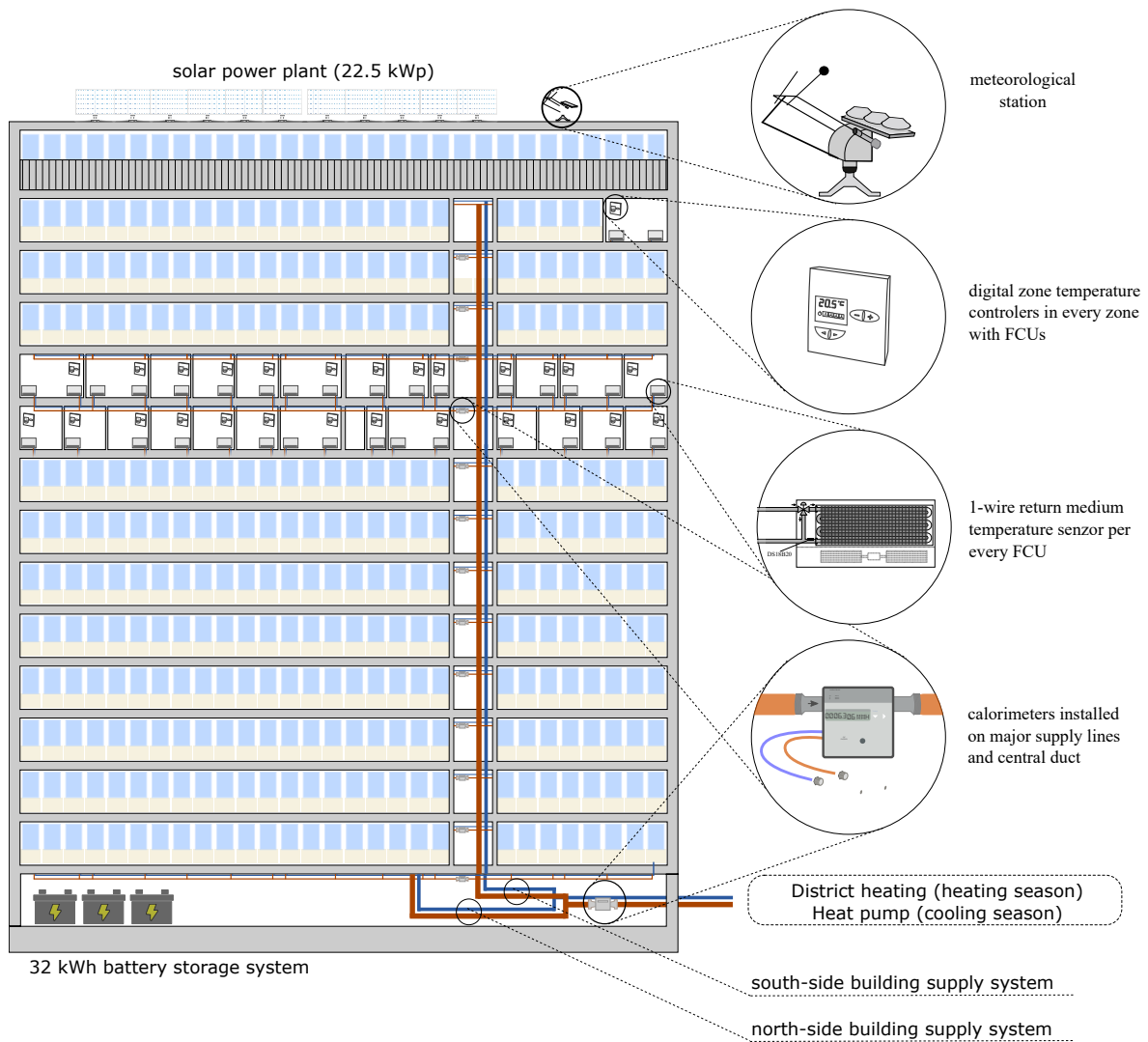


Figure A.2. *Equipment installed in UNIZGFER building.*

A.1 Living-lab on predictive building zones control

The level of digitalization in the building enables testing of various control and estimation algorithms, making the building living-lab on predictive building zones control. Enable/disable (on/off) switches for control of different parts of the building automation system via database are included in the DESIGO SCADA system such that the building operator has under its control where the control is performed via database and where not. For each zone a separate on/off signal is introduced (248 of them), and two additional ones are introduced to switch the controls of the heating station and chiller from current way of operation to operation via database and back. Also a watchdog timer functionality (or, the so-called heartbeat) is introduced such that the system goes back to normal operation if for sufficiently long interval of time no new command from the database is issued. The central part of the living lab is a PostgreSQL database. Table A.1 contains a detailed list of data collected from the zone level to the database. The configuration of the equipment in the living-lab on predictive building zones control is given in Fig. A.3.

Table A.1. *Measurements collected in the central database from the zone level.*

ZONES		
a.1	Zone temperature	[°C]
a.2	Zone temperature setpoint	[°C]
a.3	Zone temperature control mode	(stand by, auto, manual low/medium/high)
a.4	Smart switch	(true, false)
FCUs		
b.1	Fan speed	(off, low, medium, high)
b.2	Return medium temperature	[°C]
b.3	Air intake temperature*	[°C]
b.4	Air exhaust temperature*	[°C]
CALORIMETER		
c.1	Supply medium temperature	[°C]
c.2	Return medium temperature	[°C]
c.3	Mass flow	[kg/s]
c.4	Thermal power	[kW]
c.5	Thermal energy	[kWh]
WEATHER STATION		
d.1	Outside temperature	[°C]
d.2	Direct normal solar irradiance	[W/m ²]
d.3	Diffuse horizontal solar irradiance	[W/m ²]

* available only on two FCUs

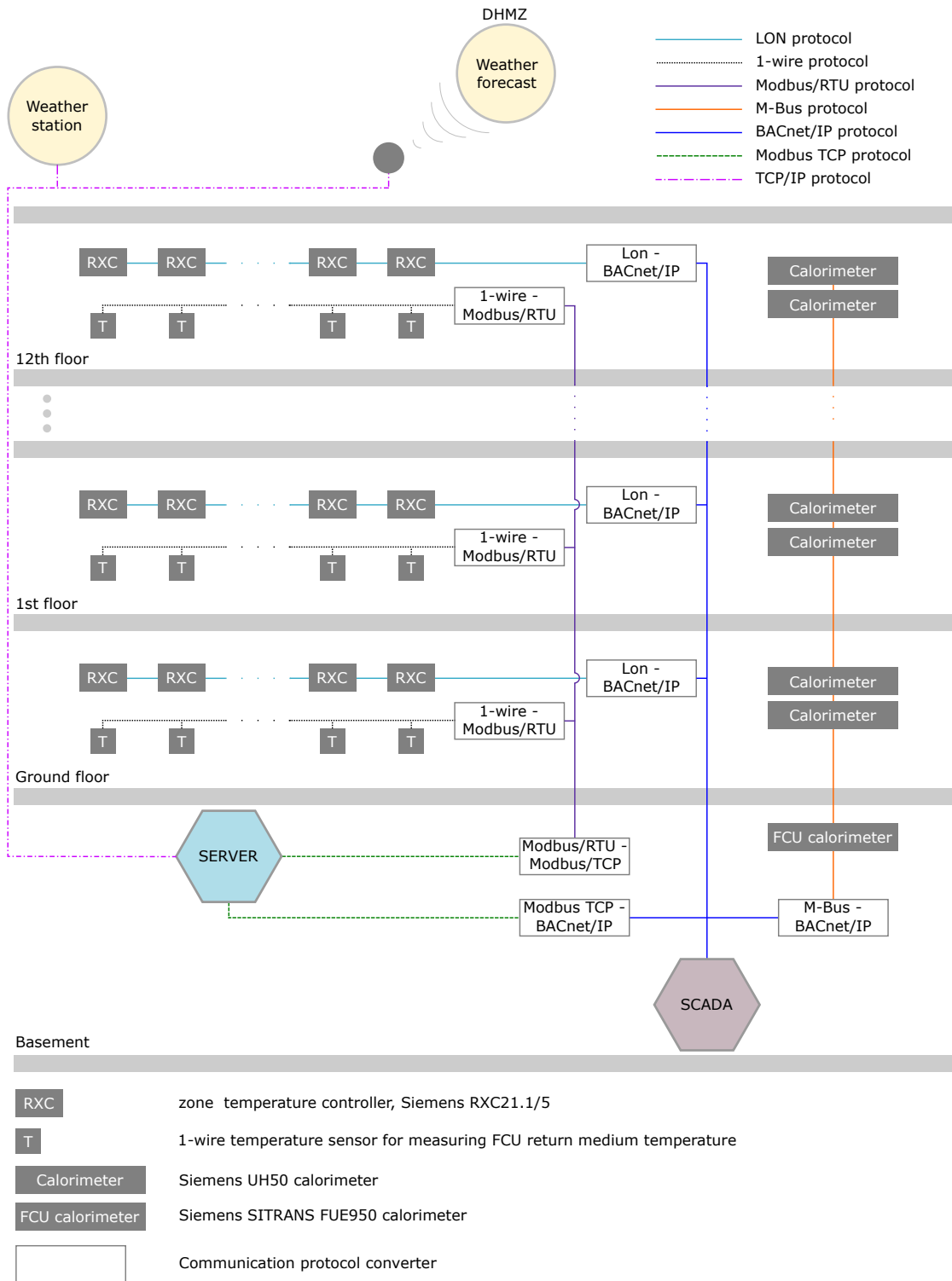


Figure A.3. Configuration of equipment installed within the Living-lab on predictive building zones control.

The FCUs, manufactured by Trane [72] (models FCC06 and FCC04), are equipped with a centrifugal fan with four different fan speeds (off, low, medium and high speed) and digital 1-wire temperature sensor DS18B20 on the return pipe (Fig. A.4(a)). On two selected FCUs, the same temperature sensors are installed to monitor incoming and

outgoing air temperatures (Fig. A.4(b)). Additionally, FCUs on the 9th and 10th floor are equipped with a three-way valve (on-off type) (Fig. A.4(a)). The return medium temperature sensors are connected via 1-wire communication to floor concentrators which communicate via MODBUS RTU to the building concentrator, and the building concentrator can be accessed from the server via MODBUS TCP/IP. The FCUs control for maintaining the zone temperature is implemented on the level of every zone by using Siemens control device RXC21.1 or RXC21.5 and accompanying display units QAX34.1 or QAX34.3 which enable the user to control the mode of FCUs local operation and to set the required temperature for the zone. The RXC21.1/5 controllers are connected via LON to floor concentrators. These concentrators are connected via BACNET/IP communication with the SCADA computer whereas DESIGO is used as the software for SCADA implementation. The RXC21.1/5 are loaded with standard FNC02 application which is changed so as to enable direct control of the FCU control variables (fan speeds and valves control variables), while keeping all the data from the QAX34.1/3 intact and accessible via LON. Also, an additional software switch is implemented for switching between the standard RXC21.1/5 operation and control of the FCUs via database in SOM. The modification related to FNC02 application was performed by Siemens Building Technologies headquarters in Zug, Switzerland.

The zones on the north side and on the south side of the building are supplied via separate supply lines. Supply of the heating or cooling medium to the building floor is performed by one vertical to horizontal transition on the north building side and by one on the south building side (Fig. A.2). As there are 13 floors operated by the RXC controllers in zones, there are overall 26 vertical-horizontal transitions. Each supply of the heating/cooling medium on floors (north and south supply duct) is equipped with calorimeter (Siemens UH50-A50-00 operating on M-Bus protocol). The performance of the overall building FCUs system is monitored via separate calorimeter (Siemens SITRANS FUE950 noted as *FCU calorimeter* on Fig Fig. A.3). The installed calorimeters are used to measure supply and return medium temperature, temperature difference, medium flow, thermal power and consumed thermal energy with one minute time resolution.

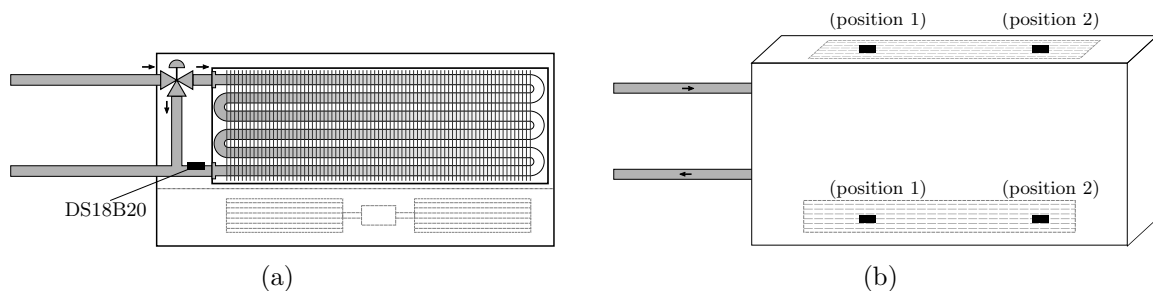


Figure A.4. a) FCU installation with three-way valve and 1-wire return medium temperature sensor DS18B20 mounted on the return pipe, b) placement of additional 1-wire DS18B20 sensors for monitoring incoming and outgoing air temperatures.

All calorimeters are connected to a concentrator connected via BACNET/IP communication with the SCADA computer and central server. The weather station is located on the building rooftop. It is equipped with an outdoor temperature sensor and units for measuring direct normal and diffuse horizontal solar irradiance (Kipp&Zonnen CMP11, Kipp&Zonnen CHP1). The solar irradiance measurements are recorded with a 1 s time-step using a real-time embedded industrial controller (NI cRIO-9066). Raw sensor measurements are later integrated and averaged on 1-min long intervals and uploaded to an FTP server from where the data is transferred to the database. The prototype weather forecasting service for the location of the UNIZGFER skyscraper building, developed by Croatian Meteorological and Hydrological Service (DHMZ), is active since 2013. Weather forecasts are created with a numerical weather prediction ALADIN (state-of-the-art weather prediction model for the region of Croatia, simultaneously used in over 20 other countries) for several meteorological variables such as temperature, humidity, air pressure, wind speed etc. Calculation of a new prediction sequence is commenced every day at 00:00, 06:00, 12:00 and 18:00 for the next 72-h period with a 1 h time resolution, for a spatial grid of 2×2 km. Due to the complexity of the numerical weather prediction model in terms of the computational effort, a prediction sequence of meteorological variables is available with a nearly 4-h lag, e.g. a prediction sequence commenced at 00:00 becomes available at 03:55 on the DHMZ's server from where the data is transferred to local database.

A.2 Building construction and materials

The case-study building is designed as reinforced concrete skeleton buildings with external shear walls on the east and west side of the building and 58 uniformly distributed columns on the north and south face of the building. The walls between columns are typical brick walls covered with asbestos-cement boards. The internal walls are made of brick or drywall.

External building walls

East- and west-facing parts of building envelope are made of reinforced concrete. The basement walls are made solely from 40 cm thick reinforced concrete (Fig. A.5) while in the rest of the building the reinforced concrete is combined with reed and bricks (Fig. A.6).

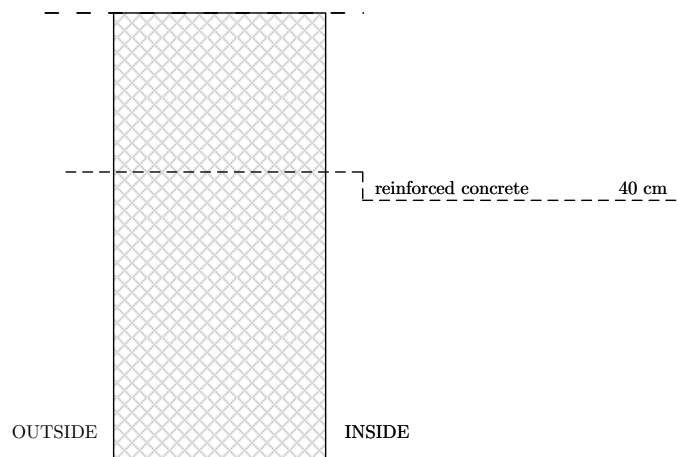


Figure A.5. East- and west-facing external walls in the basement (EW1).

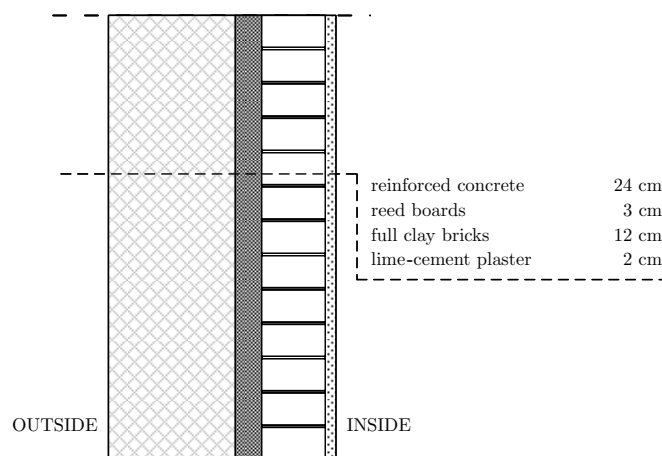


Figure A.6. East- and west-facing external walls from the ground floor to 13th floor (EW2).

South- and north-facing building envelope consists of 58 uniformly distributed reinforced concrete columns with 1 cm of lime-cement plaster insulation on inner sides. The columns have a width of 25 cm and a depth of 45 cm (Fig. A.7).

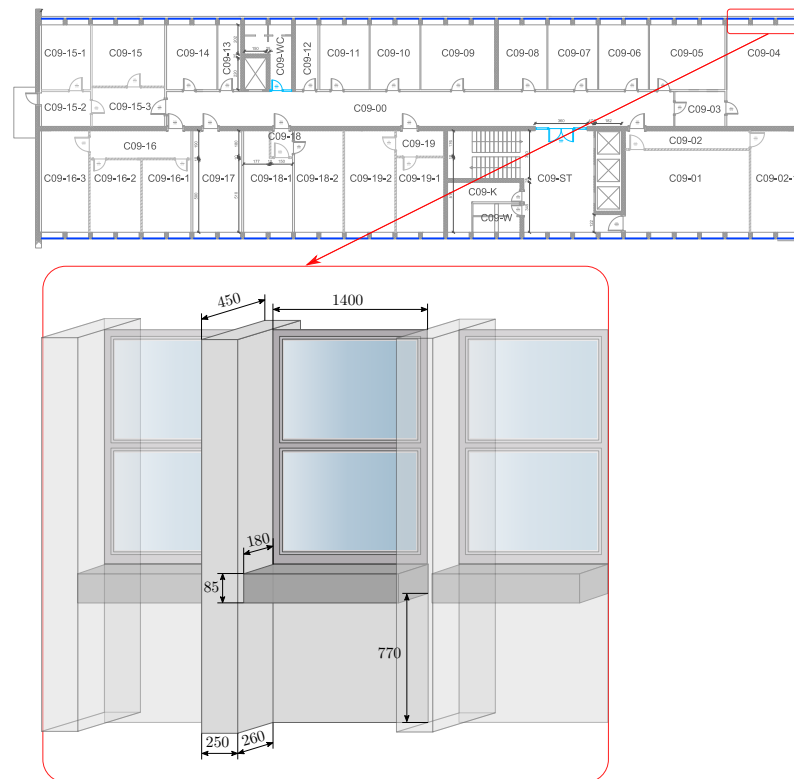


Figure A.7. Reinforced concrete columns on south- and north-facing sides of the building.

The space between the columns is filled with 40 cm reinforced concrete in the basement and brick walls (EW3) in the rest of the building (Fig. A.8).

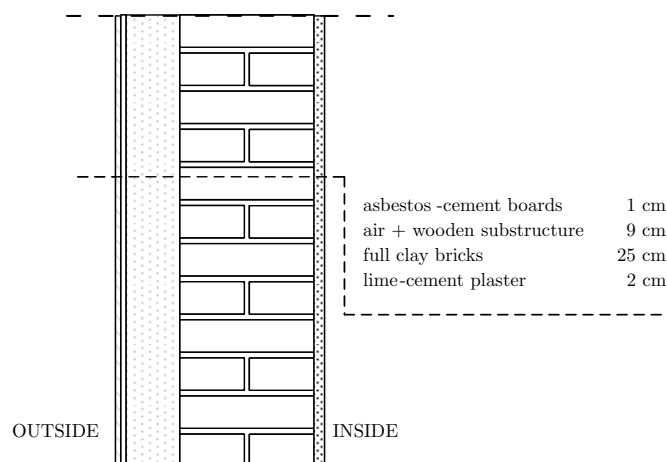


Figure A.8. South- and north-facing external walls from ground-floor to 12th floor (EW3).

The detailed cross section view of a south- and north-facing external wall can be found in [148]. The south- and north-facing external walls on 13th floor are made of bricks and insulated with lime-cement plaster and Styrofoam (Fig. A.9).

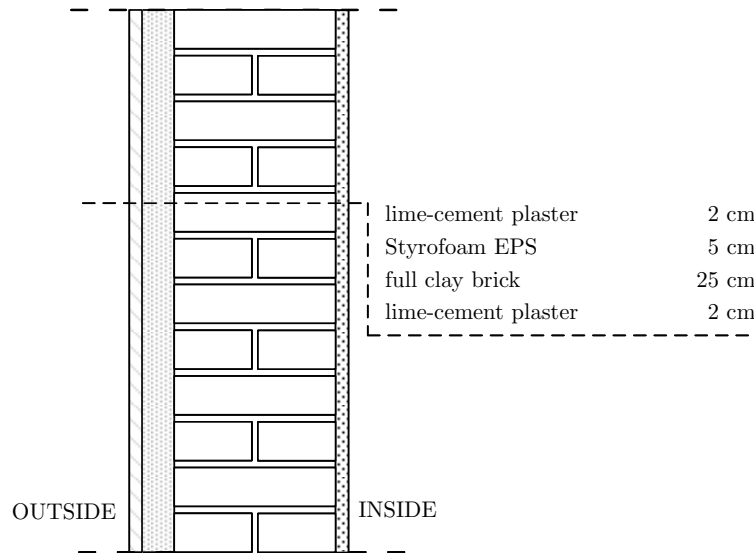


Figure A.9. South- and north-facing external walls on the 13th floor (EW4).

Internal walls

There are two types of internal walls, shear concrete walls and partition walls made of bricks or drywall. Shear walls are made as 25 cm, 30 cm and 50 cm thick reinforced concrete with 1 cm lime-cement plaster insulation on each side (SW1, SW2, SW3) (Fig. A.10).

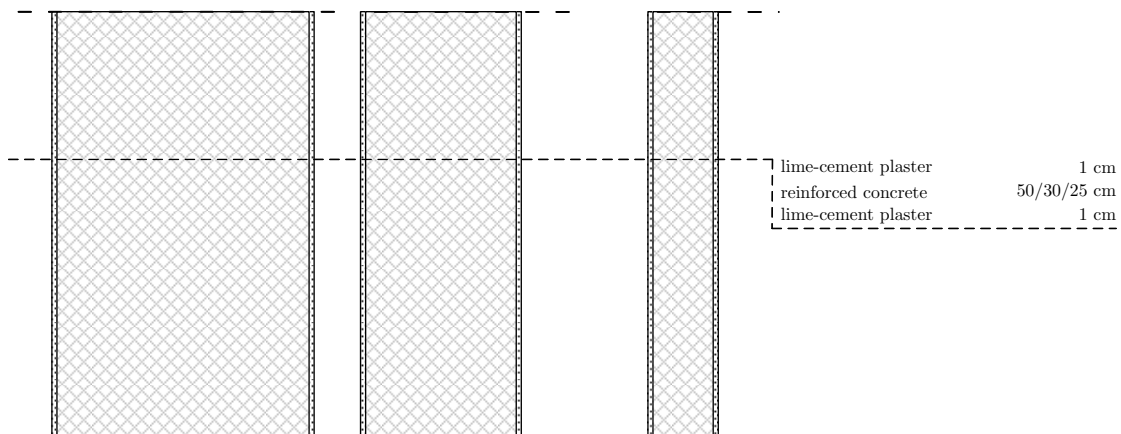


Figure A.10. Internal bearing walls (SW1-SW3).

Brick walls are made in two standard variations, as 7 cm thick walls (PW1) (Fig. A.11) and as 13 cm thick walls (PW2) (Fig. A.12).

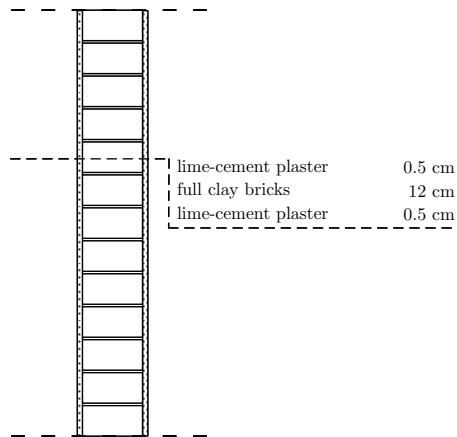


Figure A.11. *Internal brick wall (PW1).*

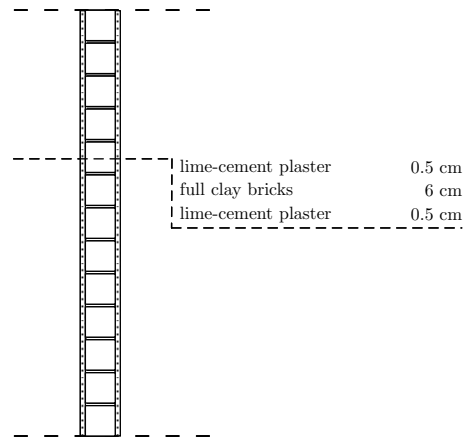


Figure A.12. *Internal brick wall (PW2).*

Drywalls are made in two standard variations, as 10 cm thick walls with single gypsum board on each side and 7 cm mineral wool insulation (PW3) (Fig. A.13) or as 15 cm thick walls with double gypsum boards on each side and 10 cm mineral wool insulation (PW4) (Fig. A.14).

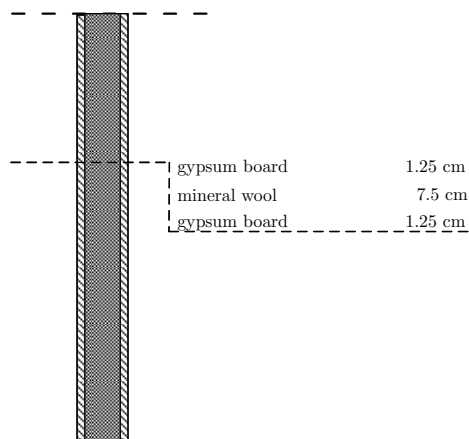


Figure A.13. *Internal gypsum wall (PW3).*

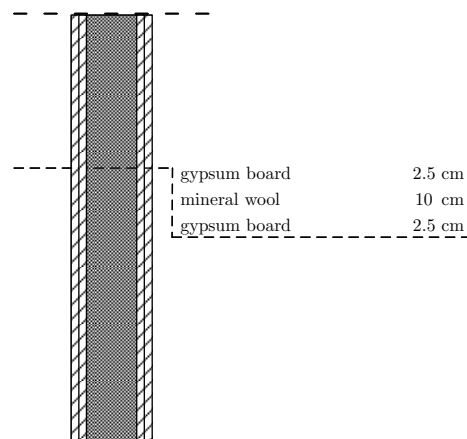


Figure A.14. *Internal gypsum wall (PW4).*

Floors and ceilings

Typical floors/ceilings in the building are made of 5 cm thick reinforced concrete positioned on 13 cm thick and 35 cm high reinforced concrete beams. There are 2 main types of floor covering, wooden oak parquet (FC1) and terazzo (FC2), both 6 cm thick. Ceilings are the same across the building, made of 5 cm reed and cement plaster. The cross section of FC1 and FC2 are shown in Fig. A.15 and Fig. A.16, respectively.

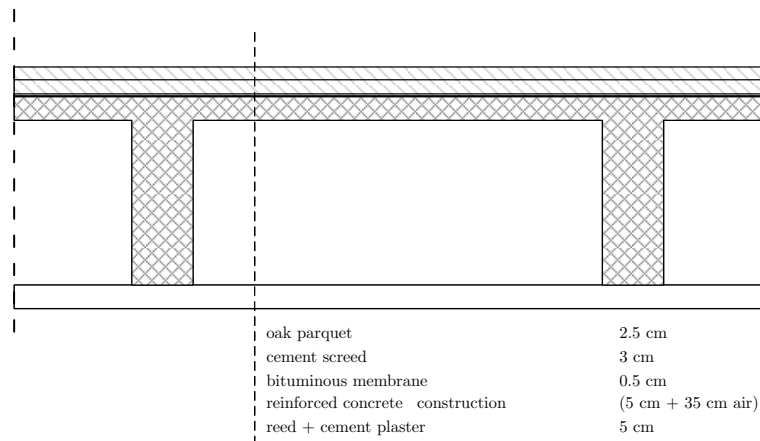


Figure A.15. Definition of FC1 floors/ceilings across the building.

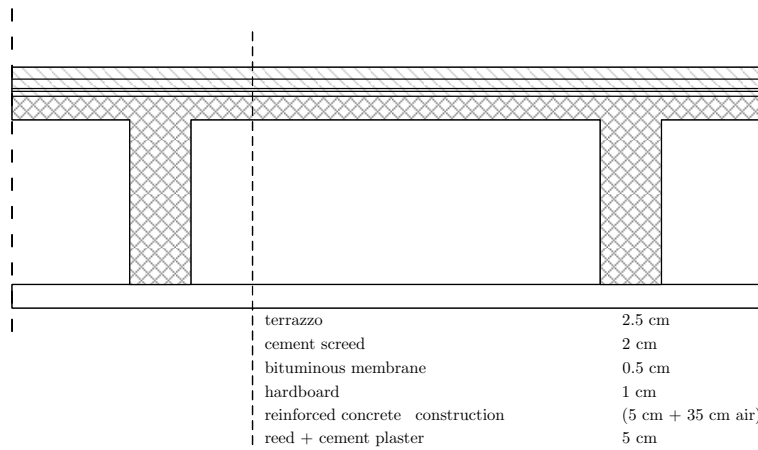


Figure A.16. Definition of FC2 floors/ceilings across the building.

The basement floor is made of 80 cm thick reinforced concrete covered with bituminous membrane to assure hydro-isolation, 3 cm thick cement screed and oak parquet (FC3) (Fig. A.17).

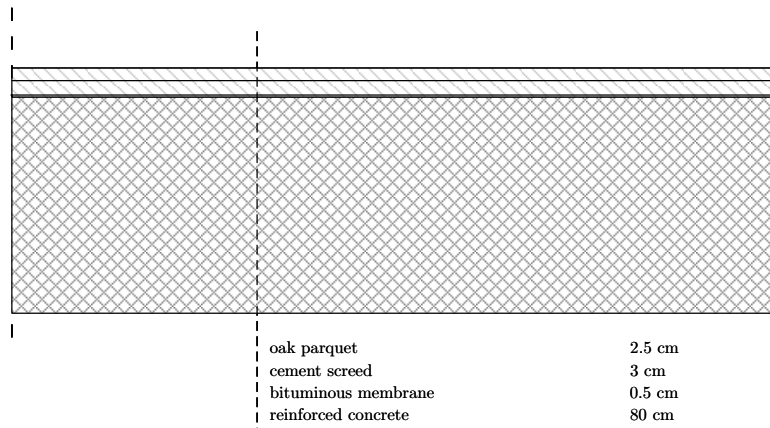


Figure A.17. *Basement floor (FC3).*

The 13th floor has an enclosed terrace so the ceiling of the 12th floor is additionally insulated (FC4) (Fig. A.18). The terrace floors are made of 4 cm concrete tiles, insulated with 1 cm bituminous membrane, 1 cm cement screed, 6 cm concrete, additional 0.5 cm bituminous membrane and 1.5 cm hardboard (FC5) (Fig. A.19).

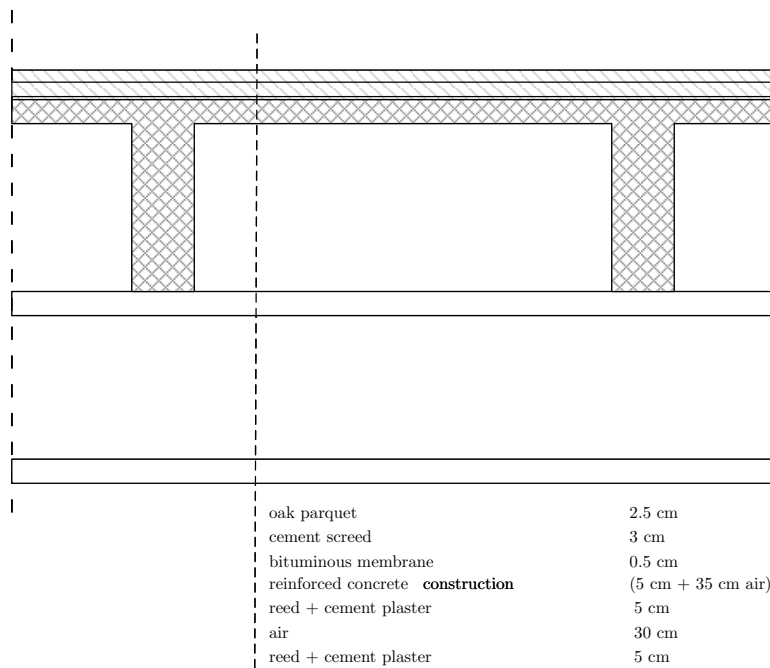


Figure A.18. *Ceiling on the 12th floor (FC4).*

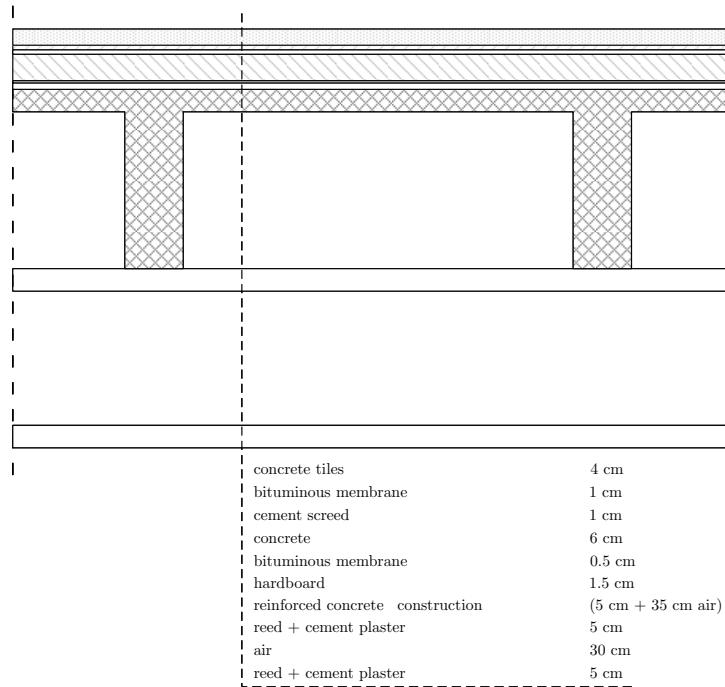


Figure A.19. Ceiling on the 12th floor (FC5).

Roof

The building roof (FC6) is made as a flat roof, with ceiling made of gypsum board placed on typical ceiling reinforced concrete composition insulated with 1 cm cement screed, 2 cm bituminous membrane, 10 cm extruded polystyrene foam (XPS), 1.5 cm thick geotextile fabric and covered with 5-7 cm gravel (Fig. A.20).

Windows and doors (openings)

All windows are double glazing aluminium frame windows 6/12/5 (6 mm of clear float glass from outside, 12 mm of air, 5 mm of clear float glass from inside). North- and south-faced envelope walls from ground floor up to 12th floor have the same windows with total area of each window equal 3.04 m² (WT1) (Fig. A.21). Approximately 30% of the total window area goes to the frame. Total glazing area is 2.1 m² and the total frame area is 0.935 m². Upper part of the window has the ability to twist while the bottom has ability to twist and tilt. Frame is made of the FEAL profiles, TERMO 65 series. The dimension of windows on the 13th floor and basement differ only slightly from the WT1 window type. Thermal properties of the WT1 windows, waterproofing, wind resistance and soundproofing were tested at Civil Engineering Institute of Croatia. The obtained thermal properties are shown in Tab. A.2, while other properties can be found in [149].

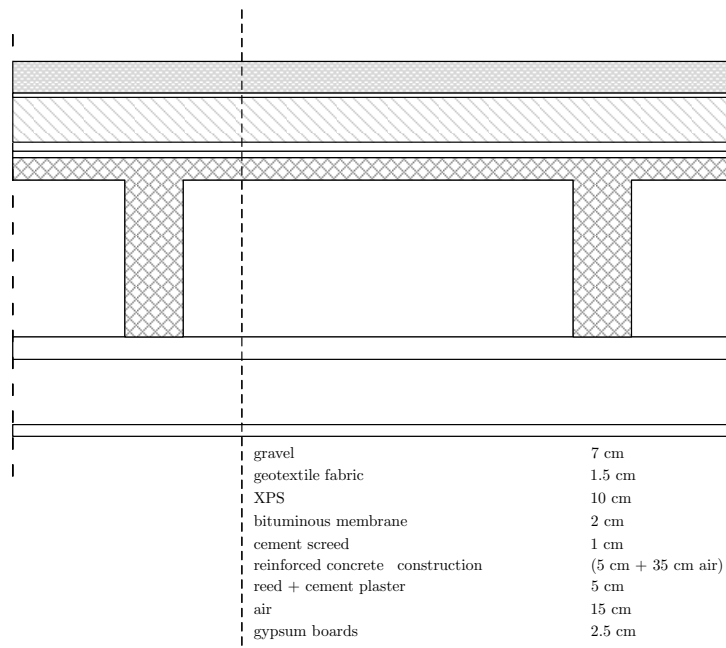


Figure A.20. Flat building roof (FC6).

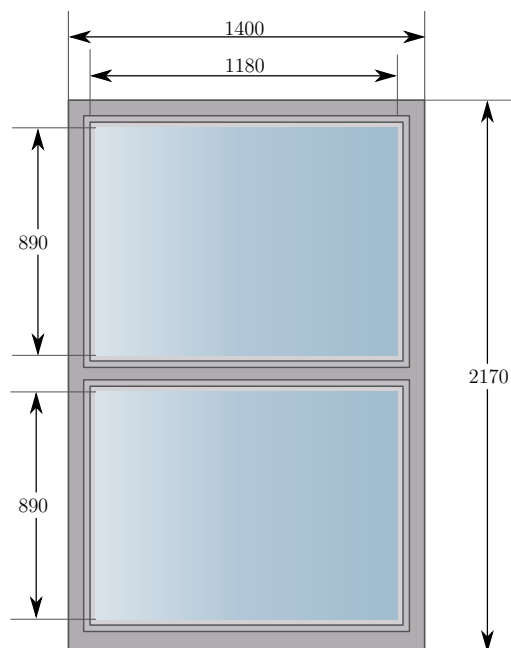


Figure A.21. Window dimensions (WT1).

Table A.2. Heat transfer coefficients of the window characteristic parts.

	Glazing	Frame	Jamb
Total area [m ²]	2.100	0.332	0.603
Heat transfer coefficient [W·(m ² K) ⁻¹]	2.850	2.210	2.130

Overall heat transfer coefficient of the window is calculated as:

$$U_{\text{window}} = \frac{2.100 \cdot 2.850 + 0.332 \cdot 2.210 + 0.603 \cdot 2.130}{2.850 + 2.210 + 2.130} = 2.630 \text{ W} \cdot (\text{m}^2\text{K})^{-1} \quad (\text{A.1})$$

The Solar Heat Gain Coefficient (SHGC) dependence in relation to the Sun inclination angle calculated for the WT1 windows with Window software [96] is shown in Tab. A.3.

Table A.3. *The SHGC valued dependence on the incidence angle.*

Incidence angle [°]	0	10	20	30	40	50	60	70	80	90
SHGC [W/(m ² K)]	0.723	0.723	0.720	0.714	0.700	0.671	0.605	0.471	0.244	0

Hemispherical averaged solar heat gain coefficient is $\overline{\text{SHGC}}=0.626 \text{ W}/(\text{m}^2\text{K})$.

Doors through the building are standard size wooden doors made of oak. Three most typical door dimensions are 82/205 cm, 90/205 cm and 102/205 cm. Entrance doors to the individual floors are made of glass with iron frames. Restroom doors are made of glass with wooden door frame. Detailed specifications of door dimensions can be found in [148]. In the hallways and other rooms without external windows, transparent glass or polycarbonate partitions are installed [148].

Thermal bridges

For thermal bridges empirical values from [150] are adopted.

Table A.4. *Thermal bridges.*

Thermal bridge	W/K/(m joint)
external wall/internal slab	0.65
external wall/internal wall	0.50
external walls inner corner	-0.15
external wall shear columns	0.90
external windows/door perimeter	0.05

Detailed properties of construction materials

Detailed thermal properties of the building construction materials are given in Tab. A.5.

Table A.5. Detailed properties of construction material used in the building.

Material	Thermal conductivity [W·(m·K) ⁻¹]	Density [kg·m ⁻³]	Specific heat capacity [J·(kg·K) ⁻¹]
reinforced concrete	2.60	2500	1000
concrete	1.4	2300	880
reed boards	0.055	155	2000
full clay bricks	0.721	1922	837
lime-cement plaster	0.50	1300	1000
asbestos-cement board	0.58	1900	1000
air	0.23	1.2	1006
expanded polystyrene (EPS)	0.035	29	1213
gypsum	0.16	950	840
mineral wool	0.035	30	1000
oak parquet	0.19	700	2390
cement screed	0.41	1200	840
plaster ceiling tiles	0.380	1120	840
bituminous membrane	0.023	1100	2600
concrete tiles	1.100	2100	837
terrazzo flooring	1.802	2243	837
hardboard	0.130	2000	9
roof gravel	1.442	1674	881
geotextile	-	0.2	-
extruded polystyrene (XPS)	0.040	35	1500
aluminium	160	2800	896
clear float glass	1.45	2500	910
iron	80.2	447	7870
polycarbonate board	0.20	1200	1200

A.3 List of controllable building zones

The description of the physical properties of the controllable UNIZGFER building zones is given in Tab. A.6.

Table A.6. *The description of the physical properties of the controllable case-study building zones.*

Zone No.	Zone name	Floor	Orientation	Floor area	FCU type	Number of FCUs
1	C00-02-5	0	N	42.30	FCC06	3
2	C00-02-7	0	N	18.07	FCC06	1
3	C00-02-6	0	N	23.55	FCC06	1
4	C00-02-4	0	S	23.45	FCC06	2
5	C00-02-3	0	S	16.16	FCC06	1
6	C00-02-2	0	S	17.70	FCC06	1
7	C00-02-1	0	S	17.80	FCC06	1
8	C00-03	0	S	7.48	FCC06	1
9	C00-04	0	S	23.04	FCC06	3
10	C00-05	0	S	38.39	FCC06	3
11	C00-06	0	S	22.89	FCC06	2
12	C00-07	0	S	7.59	FCC04	1
13	C00-08	0	S	35.88	FCC06	2
14	C00-09	0	N	71.72	FCC06	3
15	C00-12	0	N	15.91	FCC06	1
16	C00-13	0	N	16.53	FCC06	1
17	C00-14	0	N	72.17	FCC06	3
18	C01-01	1	N	84.00	FCC04	4
19	C01-02	1	S	84.00	FCC06	4
20	C01-03	1	S	23.30	FCC04	2
21	C01-04	1	S	14.89	FCC06	1
22	C01-05	1	S	22.66	FCC04	2
23	C01-06	1	S	15.33	FCC06	1
24	C01-07	1	S	15.33	FCC06	1
25	C01-07-1	1	S	7.11	FCC04	1
26	C01-08	1	S	14.80	FCC06	1
27	C01-09	1	S	22.60	FCC04	2
28	C01-10	1	S	35.84	FCC04	2
29	C01-10-1	1	N	71.47	FCC04	3
30	C01-11	1	N	24.50	FCC06	1
31	C01-12	1	N	47.97	FCC04	2
32	C01-13	1	N	47.67	FCC04	2
33	C02-01	2	N	35.00	FCC04	2
34	C02-01-1	2	N	24.43	FCC04	1
35	C02-01-2	2	N	22.83	FCC04	1
36	C02-02	2	S	14.71	FCC06	1
37	C02-02-1	2	S	15.23	FCC06	1
38	C02-02-2	2	S	14.89	FCC06	1
39	C02-04	2	S	23.04	FCC06	2
40	C02-05	2	S	22.70	FCC04	2

Zone No.	Zone name	Floor	Orientation	Floor area	FCU type	Number of FCUs
41	C02-06	2	S	22.66	FCC04	2
42	C02-07	2	S	15.33	FCC06	1
43	C02-08	2	S	22.75	FCC04	2
44	C02-09	2	S	14.80	FCC06	1
45	C02-10	2	S	15.11	FCC06	1
46	C02-11	2	S	15.33	FCC06	1
47	C02-12	2	S	14.93	FCC06	1
48	C02-13	2	N	23.17	FCC04	1
49	C02-14	2	N	23.59	FCC04	1
50	C02-15	2	N	23.66	FCC04	1
51	C02-16	2	N	23.59	FCC04	1
52	C02-17	2	N	23.59	FCC04	1
53	C02-18	2	N	23.52	FCC04	1
54	C02-19	2	N	23.59	FCC04	1
55	C02-20	2	N	23.17	FCC04	1
56	C03-01	3	N	84.08	FCC04	4
57	C03-02	3	S	84.00	FCC06	4
58	C03-03	3	S	23.30	FCC04	2
59	C03-04	3	S	14.92	FCC06	1
60	C03-05	3	S	22.66	FCC04	2
61	C03-06	3	S	15.33	FCC06	1
62	C03-07	3	S	15.26	FCC06	1
63	C03-08	3	S	7.11	FCC04	1
64	C03-09	3	S	14.80	FCC06	1
65	C03-10	3	S	22.60	FCC04	2
66	C03-11	3	S	35.84	FCC04	2
67	C03-12	3	N	28.05	FCC04	1
68	C03-12-1	3	N	14.88	FCC04	1
69	C03-13	3	N	23.66	FCC06	1
70	C03-14	3	N	24.40	FCC04	1
71	C03-14-1	3	N	24.04	FCC06	1
72	C03-15	3	N	60.34	FCC04	3
73	C03-16	3	N	10.92	FCC04	1
74	C04-01-1	4	N	22.83	FCC04	1
75	C04-02	4	N	60.34	FCC04	3
76	C04-03	4	S	22.75	FCC06	1
77	C04-04	4	S	15.46	FCC06	1
78	C04-05	4	S	15.31	FCC06	1
79	C04-06	4	S	15.41	FCC06	1
80	C04-07	4	S	14.51	FCC06	1
81	C04-07-1	4	S	15.83	FCC06	1
82	C04-08	4	S	14.96	FCC06	1
83	C04-09	4	S	15.33	FCC06	1
84	C04-10	4	S	15.33	FCC06	1
85	C04-11	4	S	14.93	FCC06	1
86	C04-12	4	S	14.80	FCC06	1
87	C04-13	4	S	15.24	FCC06	1
88	C04-14	4	S	15.33	FCC06	1
89	C04-15	4	S	14.93	FCC06	1
90	C04-16	4	N	47.67	FCC04	2

Zone No.	Zone name	Floor	Orientation	Floor area	FCU type	Number of FCUs
91	C04-17	4	N	72.17	FCC04	3
92	C04-18	4	N	48.03	FCC04	2
93	C04-20	4	N	23.59	FCC04	1
94	C05-01	5	N	84.08	FCC04	4
95	C05-02	5	S	84.00	FCC06	4
96	C05-03	5	S	15.50	FCC06	1
97	C05-04	5	S	22.71	FCC04	2
98	C05-05	5	S	22.78	FCC04	2
99	C05-06	5	S	15.33	FCC06	1
100	C05-07	5	S	15.26	FCC06	1
101	C05-08	5	S	7.11	FCC04	1
102	C05-09	5	S	14.93	FCC06	1
103	C05-10	5	S	15.33	FCC06	1
104	C05-11	5	S	15.33	FCC06	1
105	C05-12	5	S	14.89	FCC06	1
106	C05-13	5	N	47.67	FCC04	2
107	C05-14	5	N	48.09	FCC04	2
108	C05-15	5	N	35.84	FCC04	2
109	C05-16	5	N	23.59	FCC04	1
110	C05-17	5	N	35.64	FCC04	2
111	C06-02	6	N	84.02	FCC04	4
112	C06-03	6	S	71.75	FCC06	3
113	C06-04	6	S	15.34	FCC06	1
114	C06-05	6	S	15.34	FCC06	1
115	C06-06	6	S	14.83	FCC06	1
116	C06-07	6	S	22.78	FCC04	2
117	C06-08	6	S	15.33	FCC06	1
118	C06-09	6	S	15.26	FCC06	1
119	C06-10	6	S	7.11	FCC04	1
120	C06-11	6	S	14.97	FCC06	1
121	C06-12	6	S	14.91	FCC06	1
122	C06-13	6	S	15.33	FCC06	1
123	C06-14	6	S	14.93	FCC06	1
124	C06-15	6	N	23.15	FCC04	1
125	C06-16	6	N	23.59	FCC04	1
126	C06-17	6	N	23.07	FCC04	1
127	C06-18	6	N	23.59	FCC04	1
128	C06-19	6	N	35.24	FCC04	2
129	C06-20	6	N	23.52	FCC04	1
130	C06-21	6	N	35.64	FCC04	2
131	C07-01	7	N	83.94	FCC04	4
132	C07-02	7	S	35.17	FCC06	2
133	C07-03-1	7	S	26.74	FCC06	2
134	C07-03-2	7	S	17.94	FCC06	1
135	C07-04	7	S	14.56	FCC06	1
136	C07-05	7	S	14.97	FCC06	1
137	C07-06	7	S	22.69	FCC06	2
138	C07-07	7	S	15.33	FCC04	1
139	C07-08	7	S	15.26	FCC06	1
140	C07-09	7	S	7.08	FCC06	1

Zone No.	Zone name	Floor	Orientation	Floor area	FCU type	Number of FCUs
150	C08-02	8	N	35.39	FCC04	2
151	C08-03	8	N	23.29	FCC04	1
152	C08-04	8	N	23.15	FCC04	1
153	C08-05	8	S	14.87	FCC06	1
154	C08-06	8	S	15.23	FCC06	1
155	C08-07	8	S	14.93	FCC06	1
156	C08-08	8	S	14.98	FCC06	1
157	C08-09	8	S	15.66	FCC06	1
158	C08-10	8	S	14.48	FCC06	1
159	C08-11	8	S	22.61	FCC04	2
160	C08-12	8	S	15.20	FCC04	2
161	C08-13	8	S	22.75	FCC04	2
162	C08-14	8	S	14.51	FCC06	1
163	C08-15	8	S	15.72	FCC06	1
164	C08-16	8	S	14.93	FCC06	1
165	C08-17	8	S	14.93	FCC06	1
166	C08-18	8	N	35.53	FCC04	2
167	C08-19	8	N	23.45	FCC04	1
168	C08-20	8	N	35.56	FCC04	2
169	C08-21	8	N	23.57	FCC04	1
170	C08-22	8	N	72.35	FCC04	3
171	C09-01	9	N	48.12	FCC04	3
172	C09-02-1	9	N	23.57	FCC04	1
173	C09-04	9	S	35.03	FCC06	2
174	C09-05	9	S	23.26	FCC06	2
175	C09-06	9	S	15.16	FCC06	1
176	C09-07	9	S	15.34	FCC06	1
177	C09-08	9	S	15.04	FCC06	1
178	C09-09	9	S	22.80	FCC04	2
179	C09-10	9	S	15.33	FCC06	1
180	C09-11	9	S	15.20	FCC06	1
181	C09-12	9	S	6.97	FCC04	1
182	C09-13	9	S	7.10	FCC06	1
183	C09-14	9	S	15.47	FCC06	1
184	C09-15	9	S	21.15	FCC04	2
185	C09-15-1	9	S	15.32	FCC06	1
186	C09-16-1	9	N	16.85	FCC04	1
187	C09-16-2	9	N	17.25	FCC04	1
188	C09-16-3	9	N	22.80	FCC04	1
189	C09-17	9	N	23.38	FCC04	1
190	C09-18-1	9	N	20.56	FCC04	1
191	C09-18-2	9	N	23.30	FCC04	1
192	C09-19-1	9	N	16.86	FCC04	1
193	C09-19-2	9	N	24.36	FCC04	1
194	C10-01	10	N	83.80	FCC04	4
195	C10-02	10	S	35.22	FCC06	2
196	C10-03	10	S	23.13	FCC06	2
197	C10-04	10	S	15.34	FCC06	1
198	C10-05	10	S	15.10	FCC06	1
199	C10-06	10	S	14.77	FCC06	1
200	C10-07	10	S	14.83	FCC06	1

Zone No.	Zone name	Floor	Orientation	Floor area	FCU type	Number of FCUs
201	C10-08	10	S	14.95	FCC06	1
202	C10-09	10	S	14.93	FCC06	1
203	C10-09-1	10	S	15.20	FCC06	1
204	C10-10	10	S	30.17	FCC06	2
205	C10-11	10	S	15.53	FCC06	1
206	C10-12	10	S	14.96	FCC06	1
207	C10-13	10	N	71.87	FCC04	3
208	C10-14	10	N	47.57	FCC04	2
209	C10-15	10	N	47.25	FCC04	2
210	C11-01	11	N	36.01	FCC04	2
211	C11-02	11	N	47.15	FCC04	2
212	C11-03	11	S	47.18	FCC06	2
213	C11-04	11	S	15.20	FCC06	1
214	C11-05	11	S	15.25	FCC06	1
215	C11-06	11	S	15.10	FCC06	1
216	C11-07	11	S	14.84	FCC06	1
217	C11-08	11	S	22.65	FCC04	2
218	C11-09	11	S	15.06	FCC06	1
219	C11-10	11	S	15.40	FCC06	1
220	C11-11	11	S	6.71	FCC04	1
221	C11-12	11	S	14.89	FCC06	1
222	C11-13	11	S	15.18	FCC06	1
223	C11-14	11	S	14.93	FCC06	1
224	C11-15	11	S	23.38	FCC06	1
225	C11-16	11	N	47.76	FCC04	2
226	C11-17	11	N	48.15	FCC04	2
227	C11-18	11	N	23.59	FCC04	1
228	C11-19	11	N	23.52	FCC04	1
229	C11-20	11	N	47.71	FCC04	2
230	C12-02	12	N	84.04	FCC04	4
231	C12-03	12	S	22.68	FCC06	1
232	C12-04	12	S	15.42	FCC06	1
233	C12-05	12	S	14.95	FCC06	1
234	C12-06	12	S	15.08	FCC06	1
235	C12-07	12	S	15.22	FCC06	1
236	C12-08	12	S	14.77	FCC06	1
237	C12-09	12	S	22.65	FCC04	2
238	C12-10	12	S	15.65	FCC06	1
239	C12-11	12	S	15.09	FCC06	1
240	C12-11-1	12	S	6.71	FCC04	1
241	C12-12	12	S	14.81	FCC06	1
242	C12-13	12	S	15.04	FCC06	1
243	C12-14	12	S	15.20	FCC06	1
244	C12-15	12	S	14.96	FCC06	1
245	C12-16	12	N	72.50	FCC04	3
246	C12-17-1	12	N	35.21	FCC04	2
247	C12-17-2	12	N	19.04	FCC04	1
248	C12-18	12	N	59.53	FCC04	3

Solar irradiance incident on a tilted surface

Typically, only measurements of direct normal I_n^{dir} and diffuse horizontal I_h^{diff} solar irradiance are available. The direct solar irradiance incident on a tilted surface I_θ^{dir} , e.g. wall or window, is easily calculated with the known surface azimuth angle, tilt angle, and solar zenith and azimuth angle. The solar incidence angle θ is the angle between direct solar ray and a line normal to the irradiated surface. To calculate θ first the position of the Sun relative to the considered surface has to be determined. Position of the Sun is described with solar zenith angle θ_z and solar azimuth angle ϕ_s (Fig. B.1).

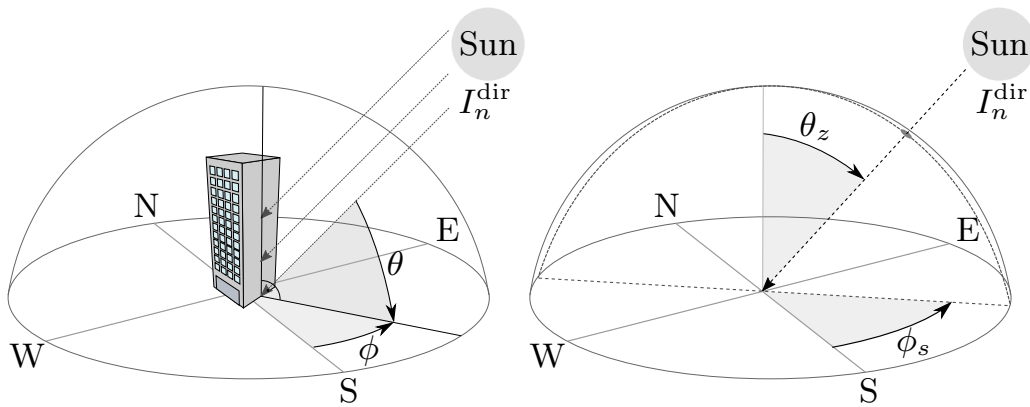


Figure B.1. Surface azimuth angle and solar incidence angle (left) and solar zenith and azimuth angles (right).

Solar azimuth angle ϕ_s defines in which direction the Sun is, whereas the solar zenith angle θ_z defines how high the Sun is. In conventional time keeping, regions of the Earth are divided into certain time zones. However, in these time zones, noon does not necessarily correspond to the time when the Sun is highest in the sky, so called solar noon. The equation of time (ET) describes the discrepancy between these two times.

$$\text{ET} = 9.87 \sin(2X) - 7.53 \cos(X) - 1.5 \sin(X), \quad X = \frac{360}{365}(D - 81), \quad (\text{B.1})$$

where D is the number of the days since the start of the year¹. Local solar time t_{LST} is defined as when the Sun is highest in the sky. Local time t_{LT} usually varies from t_{LST} due to the eccentricity of the Earth's orbit and human adjustments such as time zones and daylight saving². The Local Solar Time is defined as:

$$t_{\text{LST}} = t_{\text{LT}} + \frac{\text{ET}}{60} + \frac{(15^\circ \cdot t_{\Delta} - \text{LON})}{15}, \quad (\text{B.2})$$

where LON is local longitude and t_{Δ} is the difference of the local time from Greenwich Mean Time (GMT) in hours (for Zagreb $t_{\Delta} = +1$). Solar declination angle δ_s varies seasonally due to the tilt of the Earth on its axis of rotation and the rotation of the Earth around the Sun and it is defined as:

$$\delta_s = 23.45^\circ \sin \left(\frac{360}{365} (D + 284.5) \right). \quad (\text{B.3})$$

Observing the Sun from earth, the solar hour angle H_s is an expression of time, expressed in angular measurement, usually degrees, from solar noon. At solar noon the hour angle is 0.0° , with the time before solar noon expressed as negative degrees, and the local time after solar noon expressed as positive degrees.

$$H_s = 15^\circ \cdot (t_{\text{LST}} - 12). \quad (\text{B.4})$$

The solar elevation angle is the altitude of the Sun, the angle between the horizon and the centre of the Sun's disc defined as $\theta_e = 90^\circ - \theta_z$. The approximate value of the solar elevation angle is calculated using the following formula:

$$\sin(\theta_e) = \cos(H_s) \cos(\text{LAT}) \cos(\delta_s) + \sin(\text{LAT}) \sin(\delta_s), \quad (\text{B.5})$$

where LAT is local latitude. The solar azimuth angle ϕ_s is then defined as:

$$\cos(\phi_s) = \frac{\sin(\delta_s) - \cos(\theta_z) \sin(\text{LAT})}{\sin(\theta_z) \cos(\text{LAT})}. \quad (\text{B.6})$$

Angle of incidence θ is the angle a ray of direct solar radiation makes with a line perpendicular to an observed surface. For a vertical building surface (tilt angle= 90°) it is defined as [151]:

$$\cos(\theta) = \cos(\theta_z) \cos(\phi - \phi_s), \quad (\text{B.7})$$

where ϕ is the surface azimuth, i.e. the angle between true south and the projection on a horizontal plane of the normal to the surface. The direct solar irradiance incident on a

¹Floating point number, e.g. at 0:00 on January 1st $D = 1.00$.

²Local time is expressed as floating point number of hour in a day, e.g. at 6:30 $t_{\text{LT}} = 6.50$.

tilted surface I_{θ}^{dir} is then defined as:

$$I_{\theta}^{\text{dir}} = \begin{cases} \cos(\theta)I_{\text{n}}^{\text{dir}} & \text{for } \theta \leq 90^{\circ}, \\ 0 & \text{otherwise,} \end{cases} \quad (\text{B.8})$$

In general, the diffuse solar irradiance component affecting the vertical building surface is calculated as:

$$I_{\theta}^{\text{diff}} = \epsilon I_{\text{h}}^{\text{diff}}, \quad (\text{B.9})$$

where ϵ is the diffuse irradiance transposition factor defined differently for each model in literature. Across the thesis, $\epsilon = 0.5$ proposed by Kondratev [152] is used. More general approach for tilt angles different than 90° can be found in [151].

BIBLIOGRAPHY

- [1] International Energy Agency. World energy outlook 2016. 2016.
- [2] *Europe's buildings under the microscope*. Buildings Performance Institute Europe, 2011.
- [3] J. Cigler, S. Prívvara, Z. Váňa, E. Žáčková, and L. Ferkl. Optimization of predicted mean vote index within model predictive control framework: Computationally tractable solution. *Energy and Buildings*, 52:39 – 49, 2012.
- [4] I. Lymeropoulos, F. A. Qureshi, T. Nghiem, A. A. Khatir, and C. N. Jones. Providing ancillary service with commercial buildings: the swiss perspective. *IFAC-PapersOnLine*, 48(8):6 – 13, 2015. 9th IFAC Symposium on Advanced Control of Chemical Processes ADCHEM 2015.
- [5] F. Tahersima, J. Stoustrup, H. Rasmussen, and S. A. Meybodi. Economic COP optimization of a heat pump with hierarchical model predictive control. In *2012 IEEE 51st IEEE Conference on Decision and Control (CDC)*, pages 7583–7588, Dec 2012.
- [6] D. Setlhaolo, S. Sichilalu, and J. Zhang. Residential load management in an energy hub with heat pump water heater. *Applied Energy*, 208:551–560, 2017.
- [7] F. Oldewurtel, D. Sturzenegger, G. Andersson, M. Morari, and R. S. Smith. Towards a standardized building assessment for demand response. In *52nd IEEE Conference on Decision and Control*, pages 7083–7088, 2013.
- [8] K. Klein, S. Herkel, H. M. Henning, and C. Felsmann. Load shifting using the heating and cooling system of an office building: Quantitative potential evaluation for different flexibility and storage options. *Applied Energy*, 203:917 – 937, 2017.
- [9] M. Gruber, A. Trüschel, and J.-O. Dalenbäck. Model-based controllers for indoor climate control in office buildings - Complexity and performance evaluation. *Energy and Buildings*, 68:213 – 222, 2014.

- [10] T. T. Gorecki, L. Fabietti, F. A. Qureshi, and C. N. Jones. Experimental demonstration of buildings providing frequency regulation services in the swiss market. *Energy and Buildings*, 144:229–240, 2017.
- [11] M. Razmara, G. R. Bharati, D. Hanover, M. Shahbakhti, S. Paudyal, and R.D. Robinett. Building-to-grid predictive power flow control for demand response and demand flexibility programs. *Applied Energy*, 203:128 – 141, 2017.
- [12] D. T. Nguyen and L. B. Le. Optimal bidding strategy for microgrids considering renewable energy and building thermal dynamics. *IEEE Transactions on Smart Grid*, 5(4):1608–1620, July 2014.
- [13] V. Lešić, A. Martinčević, and M. Vašak. Modular energy cost optimization for buildings with integrated microgrid. *Applied Energy*, 197:14 – 28, 2017.
- [14] D. Sturzenegger, D. Gyalistras, M. Morari, and R. S. Smith. Model predictive climate control of a Swiss office building: Implementation, results, and cost-benefit analysis. *IEEE Transactions on Control Systems Technology*, 24(1):1–12, Jan 2016.
- [15] J. Široký, F. Oldewurtel, J. Cigler, and S. Prívará. Experimental analysis of model predictive control for an energy efficient building heating system. *Applied Energy*, 88(9):3079–3087, 2011.
- [16] G. P. Henze, D. E. Kalz, S. Liu, and C. Felsmann. Experimental analysis of model-based predictive optimal control for active and passive building thermal storage inventory. *HVAC&R Research*, 11(2):189–213, 2005.
- [17] M. Castilla, J. D. Álvarez, J. E. Normey-Rico, and F. Rodríguez. Thermal comfort control using a non-linear MPC strategy: A real case of study in a bioclimatic building. *Journal of Process Control*, 24(6):703–713, 2014.
- [18] T. Hilliard, L. Swan, and Z. Qin. Experimental implementation of whole building mpc with zone based thermal comfort adjustments. *Building and Environment*, 125:326 – 338, 2017.
- [19] S. Yang, M. P. Wan, B. F. Ng, S. Dubey, G. P. Henze, S. K. Rai, and K. Baskaran. Experimental study of a model predictive control system for active chilled beam (ACB) air-conditioning system. *Energy and Buildings*, 203:109451, 2019.
- [20] A. Parisio, E. Rikos, and L. Glielmo. A model predictive control approach to microgrid operation optimization. *IEEE Transactions on Control Systems Technology*, 22(5):1813–1827, Sep. 2014.
- [21] S. Prívará, J. Cigler, Z. Váňa, F. Oldewurtel, and E. Žáčková. Use of partial least squares within the control relevant identification for buildings. *Control Engineering Practice*, 21(1):113 – 121, 2013.

- [22] M. Schmelas, T. Feldmann, and E. Bollin. Savings through the use of adaptive predictive control of thermo-active building systems (TABS): A case study. *Applied Energy*, 199:294 – 309, 2017.
- [23] W. Liang, R. Quinte, X. Jia, and J.Q. Sun. MPC control for improving energy efficiency of a building air handler for multi-zone VAVs. *Building and Environment*, 92:256 – 268, 2015.
- [24] G. P. Henze. Model predictive control for buildings: a quantum leap? *Journal of Building Performance Simulation*, 6(3):157–158, 2013.
- [25] EQUA Simulation AB. *IDA Indoor Climate and Energy*. Sweden.
- [26] D. B. Crawley, C. O. Pedersen, L. K. Lawrie, and F. C. Winkelmann. Energyplus: Energy simulation program. *ASHRAE Journal*, 42:49–56, 2000.
- [27] S. A. Klein et al. *TRNSYS 17: A Transient System Simulation Program*. Solar Energy Laboratory, University of Wisconsin, Madison, USA, 2010.
- [28] J. E. Seem. *Modeling of Heat Transfer in Buildings*. University of Wisconsin–Madison, 1987.
- [29] F. Oldewurtel, A. Parisio, C. N. Jones, D. Gyalistras, M. Gwerder, V. Stauch, B. Lehmann, and M. Morari. Use of model predictive control and weather forecasts for energy efficient building climate control. *Energy and Buildings*, 45:15–27, 2012.
- [30] M. A. Fayazbakhsh, F. Bagheri, and M. Bahrami. A resistance–capacitance model for real-time calculation of cooling load in hvac-r systems. *Journal of Thermal Science and Engineering Applications*, 7, 12 2015.
- [31] S. Li, J. Joe, J. Hu, and P. Karava. System identification and model-predictive control of office buildings with integrated photovoltaic-thermal collectors, radiant floor heating and active thermal storage. *Solar Energy*, 113:139–157, 2015.
- [32] G. Mustafaraj, J. Chen, and G. Lowry. Development of room temperature and relative humidity linear parametric models for an open office using BMS data. *Energy and Buildings*, 42(3):348–356, 2010.
- [33] S. Wu and J.-Q. Sun. A physics-based linear parametric model of room temperature in office buildings. *Building and Environment*, 50:1–9, 2012.
- [34] N. L. Kristensen, H. Madsen, and S. B. Jørgensen. Parameter estimation in stochastic grey-box models. *Automatica*, 40(2):225–237, 2004.
- [35] P. Radecki and B. Hencsey. Online building thermal parameter estimation via unscented Kalman filtering. *Proceedings of the American Control Conference*, pages 3056–3062, 2012.

- [36] M. Maasoumy, B. Moridian, M. Razmara, M. Shahbakhti, and A. Sangiovanni-Vincentelli. Online simultaneous state estimation and parameter adaptation for building predictive control. *ASME 2013 Dynamic Systems and Control Conference, DSCC 2013*, 2, 2013.
- [37] A. Martinčević, A. Starčić, and M. Vašak. Parameter estimation for low-order models of complex buildings. In *IEEE PES Innovative Smart Grid Technologies, Europe*, pages 1–6, Oct 2014.
- [38] N. Hure, A. Martinčević, and M. Vašak. Model predictive control of building hvac system employing zone thermal energy requests. In M. Fikar and M. Kvasnica, editors, *Proceedings of the 2019 22nd International Conference on Process Control (PC19)*, pages 13–18, Štrbské Pleso, Slovakia, 2019.
- [39] A. Starčić, V. Lešić, and M. Vašak. Predictive control for heating power variance and peak reduction in buildings. In *IECON 2016 - 42nd Annual Conference of the IEEE Industrial Electronics Society*, pages 7089–7094, Oct 2016.
- [40] Renewable Energy Policy Network for the 21st Century (REN21). *Renewables 2016, Global Status Report*, 2016.
- [41] B. Bueno, M. Street, T. Pflug, and C. Braesch. A co-simulation modelling approach for the assessment of a ventilated double-skin complex fenestration system coupled with a compact fan-coil unit. *Energy and Buildings*, 151:18 – 27, 2017.
- [42] Y. Chen and S. Treado. Development of a simulation platform based on dynamic models for HVAC control analysis. *Energy and Buildings*, 68:376 – 386, 2014.
- [43] L. Ratna Raju and T. K. Nandi. Effective NTU of a counterflow heat exchanger with unbalanced flow and longitudinal heat conduction through fluid separating and outer walls. *Applied Thermal Engineering*, 112:1172–1177, 2017.
- [44] D. Rodríguez, G. Bejarano, J.A. Alfaya, M.G. Ortega, and F. Castaño. Parameter identification of a multi-stage, multi-load-demand experimental refrigeration plant. *Control Engineering Practice*, 60:133 – 147, 2017.
- [45] A. Zavala-Río, C.M. Astorga-Zaragoza, and O. Hernández-González. Bounded positive control for double-pipe heat exchangers. *Control Engineering Practice*, 17(1):136 – 145, 2009.
- [46] S. Wongwises and Y. Chokeman. Effect of fin pitch and number of tube rows on the air side performance of herringbone wavy fin and tube heat exchangers. *Energy Conversion and Management*, 46(13-14):2216–2231, 2005.

- [47] D. Junqi, C. Jiangping, C. Zhijiu, Z. Yimin, and Z. Wenfeng. Heat transfer and pressure drop correlations for the wavy fin and flat tube heat exchangers. *Applied Thermal Engineering*, 27(11):2066 – 2073, 2007.
- [48] Y. L. He, P. Chu, W. Q. Tao, Y. W. Zhang, and T. Xie. Analysis of heat transfer and pressure drop for fin-and-tube heat exchangers with rectangular winglet-type vortex generators. *Applied Thermal Engineering*, 61(2):770–783, 2013.
- [49] M. Jagirdar and P. S. Lee. Mathematical modeling and performance evaluation of a desiccant coated fin-tube heat exchanger. *Applied Energy*, 212:401–415, 2018.
- [50] M. D’Antoni, D. Romeli, and R. Fedrizzi. A model for the performance assessment of hybrid coolers by means of transient numerical simulation. *Applied Energy*, 181:477–494, 2016.
- [51] J. D. Álvarez, J. L. Redondo, E. Camponogara, J. Normey-Rico, M. Berenguel, and P. M. Ortigosa. Optimizing building comfort temperature regulation via model predictive control. *Energy and Buildings*, 57:361 – 372, 2013.
- [52] H. Maddah and N. Ghasemi. Experimental evaluation of heat transfer efficiency of nanofluid in a double pipe heat exchanger and prediction of experimental results using artificial neural networks. *Heat and Mass Transfer*, 53(12):3459–3472, 2017.
- [53] M. Mohanraj, S. Jayaraj, and C. Muraleedharan. Applications of artificial neural networks for thermal analysis of heat exchangers - A review. *International Journal of Thermal Sciences*, 90:150–172, 2015.
- [54] K. S. Yigit and H. M. Ertunc. Prediction of the air temperature and humidity at the outlet of a cooling coil using neural networks. *International Communications in Heat and Mass Transfer*, 33(7):898–907, 2006.
- [55] C. K. Tan, J. Ward, S. J. Wilcox, and R. Payne. Artificial neural network modelling of the thermal performance of a compact heat exchanger. *Applied Thermal Engineering*, 29(17):3609 – 3617, 2009.
- [56] C. R. Ruivo and G. Angrisani. Empirical component model to predict the overall performance of heating coils: Calibrations and tests based on manufacturer catalogue data. *Energy Conversion and Management*, 89:749–763, 2015.
- [57] Y. Shin, Y. Soo Chang, and Y. Kim. Controller design for a real-time air handling unit. *Control Engineering Practice*, 10(5):511 – 518, 2002.
- [58] C. Ghiaus, A. Chicinas, and C. Inard. Grey-box identification of air-handling unit elements. *Control Engineering Practice*, 15(4):421 – 433, 2007.

- [59] J. Fernández-Seara, R. Diz, F. J. Uhía, and J. A. Dopazo. Experimental analysis on pressure drop and heat transfer of a terminal fan-coil unit with ice slurry as cooling medium. *International Journal of Refrigeration*, 33(6):1095–1104, 2010.
- [60] Y. W. Wang, W. J. Cai, Y. C. Soh, S. J. Li, L. Lu, and L. Xie. A simplified modeling of cooling coils for control and optimization of HVAC systems. *Energy Conversion and Management*, 45(18–19):2915 – 2930, 2004.
- [61] L. E. Ormsbee and D. J. Wood. Explicit pipe network calibration. *Journal of Water Resources Planning and Management*, 112(2):166–182, 1986.
- [62] M. Picón-Núñez, L. Canizalez-Dávalos, and G. T. Polley. Modelling the thermo-hydraulic performance of cooling networks and its implications on design, operation and retrofit. In Amimul Ahsan, editor, *Evaporation, Condensation and Heat Transfer*, pages 189–206. InTech, Boston, 2011.
- [63] X. Wang, W. Cai, and X. Yin. A global optimized operation strategy for energy savings in liquid desiccant air conditioning using self-adaptive differential evolutionary algorithm. *Applied Energy*, 187:410–423, 2017.
- [64] A. Martinčević, F. Rukavina, V. Lešić, and M. Vašak. Comfort control in buildings with adherence to the required thermal energy input in zones. In *IEEE International Symposium on Industrial Electronics*, pages 1477–1482, 2017.
- [65] S. Pourarian, J. Wen, D. Veronica, A. Pertzborn, X. Zhou, and R. Liu. A tool for evaluating fault detection and diagnostic methods for fan coil units. *Energy and Buildings*, 136:151 – 160, 2017.
- [66] F. Delmotte, M. Dambrine, S. Delrot, and S. Lalot. Fouling detection in a heat exchanger: A polynomial fuzzy observer approach. *Control Engineering Practice*, 21(10):1386 – 1395, 2013.
- [67] E. Weyer, G. Szederkényi, and K. Hangos. Grey box fault detection of heat exchangers. *Control Engineering Practice*, 8(2):121 – 131, 2000.
- [68] A. D. Kraus, J. R. Welty, and A. Aziz. Flow in pipes and pipe networks. In *Introduction to Thermal and Fluid Engineering*, chapter 17, pages 523–562. Taylor & Francis, New York, 2011.
- [69] E. S. Menon and P. S. Menon. Pressure loss through piping systems. In *Working Guide to Pumps and Pumping Stations*, pages 69–112. Gulf Professional Publishing, Boston, 2010.
- [70] MATLAB. *version 9.4.0 (R2018a)*. The MathWorks Inc., 2018.

- [71] G. Y. Jin, W. J. Cai, Y. W. Wang, and Y. Yao. A simple dynamic model of cooling coil unit. *Energy Conversion and Management*, 47(15–16):2659 – 2672, 2006.
- [72] TRANE, Cooling and Heating Systems and Services. Unitrane fan coil units (unt-prc006-e4), 2010.
- [73] J. Joe and P. Karava. Agent-based system identification for control-oriented building models. *Journal of Building Performance Simulation*, 10(2):183–204, 2017.
- [74] E. Asadi, M. Gameiro da Silva, C. Henggeler Antunes, and L. Dias. A multi-objective optimization model for building retrofit strategies using trnsys simulations, genopt and matlab. *Building and Environment*, 56:370 – 378, 2012.
- [75] P. Sankelo, J. Jokisalo, J. Nyman, J. Vinha, and K. Sirén. Cost-optimal energy performance measures in a new daycare building in cold climate. *International Journal of Sustainable Energy*, 38(2):104–122, 2019.
- [76] A.L.S. Chan. Effect of adjacent shading on the thermal performance of residential buildings in a subtropical region. *Applied Energy*, 92:516 – 522, 2012.
- [77] T. Žakula, P.R. Armstrong, and L. Norford. Modeling environment for model predictive control of buildings. *Energy and Buildings*, 85:549 – 559, 2014.
- [78] K. Deng, P. Barooah, P. G. Mehta, and S. P. Meyn. Building thermal model reduction via aggregation of states. In *Proceedings of the 2010 American Control Conference, ACC 2010*, pages 5118–5123, 2010.
- [79] M. M. Gouda, S. Danaher, and C. P. Underwood. Building thermal model reduction using nonlinear constrained optimization. *Building and Environment*, 37(12):1255–1265, 2002.
- [80] D. Sturzenegger, D. Gyalistras, M. Morari, and R. S. Smith. Semi-automated modular modeling of buildings for model predictive control. In *Proceedings of the Fourth ACM Workshop on Embedded Sensing Systems for Energy-Efficiency in Buildings*, BuildSys '12, pages 99–106, New York, NY, USA, 2012. ACM.
- [81] T. R. Nielsen. Simple tool to evaluate energy demand and indoor environment in the early stages of building design. *Solar Energy*, 78(1):73–83, 2005.
- [82] P. Radecki and B. Hency. Online model estimation for predictive thermal control of buildings. *IEEE Transactions on Control Systems Technology*, 25(4):1414–1422, 2017.
- [83] H. Harb, N. Boyanov, L. Hernandez, R. Streblow, and D. Müller. Development and validation of grey-box models for forecasting the thermal response of occupied buildings. *Energy and Buildings*, 117:199–207, 2016.

- [84] E. Žáčková, Z. Váňa, and J. Cigler. Towards the real-life implementation of MPC for an office building: Identification issues. *Applied Energy*, 135:53–62, 2014.
- [85] S. Baldi, S. Yuan, P. Endel, and O. Holub. Dual estimation: Constructing building energy models from data sampled at low rate. *Applied Energy*, 169:81–92, 2016.
- [86] S. F. Fux, A. Ashouri, M. J. Benz, and L. Guzzella. EKF based self-adaptive thermal model for a passive house. *Energy and Buildings*, 68:811 – 817, 2014.
- [87] S. Wang and X. Xu. Parameter estimation of internal thermal mass of building dynamic models using genetic algorithm. *Energy Conversion and Management*, 47(13-14):1927–1941, 2006.
- [88] Z. Liao and A. L. Dexter. A simplified physical model for estimating the average air temperature in multi-zone heating systems. *Building and Environment*, 39(9):1013 – 1022, 2004.
- [89] K. K. Andersen, H. Madsen, and L. H. Hansen. Modelling the heat dynamics of a building using stochastic differential equations. *Energy and Buildings*, 31(1):13 – 24, 2000.
- [90] T. Y. Chen and A. K. Athienitis. Investigation of practical issues in building thermal parameter estimation. *Building and Environment*, 38(8):1027 – 1038, 2003.
- [91] C. Lombard and E.H. Mathews. Efficient, steady state solution of a time variable RC network, for building thermal analysis. *Building and Environment*, 27(3):279–287, 1992.
- [92] T. Dewson, B. Day, and A. D. Irving. Least squares parameter estimation of a reduced order thermal model of an experimental building. *Building and Environment*, 28(2):127–137, 1993.
- [93] R. Kramer, J. van Schijndel, and H. Schellen. Simplified thermal and hygric building models: A literature review. *Frontiers of Architectural Research*, 1(4):318–325, 2012.
- [94] M. Maasoumy, A. Pinto, and A. Sangiovanni-Vincentelli. Model-based hierarchical optimal control design for HVAC systems. In *ASME 2011 Dynamic Systems and Control Conference and Bath/ASME Symposium on Fluid Power and Motion Control, DSCC 2011*, volume 1, pages 271–278, 2011.
- [95] American Society of Heating Refrigerating and Air-Conditioning Engineers. 2009 ASHRAE HANDBOOK, fundamentals. 2009.
- [96] Lawrence Berkeley National Laboratory. *WINDOW*. University of California.

- [97] M. M. Gouda, S. Danaher, and C. P. Underwood. Low-order model for the simulation of a building and its heating system. *Building Services Engineering Research and Technology*, 21(3):199–208, 2000.
- [98] Equa Simulation Technical Group. *Validation of IDA Indoor Climate and Energy 4.0 build 4 with respect to ANSI/ASHRAE Standard 140-2004*. Solna, Sweden, 2010.
- [99] Equa Simulation AB. *Validation of IDA Indoor Climate and Energy 4.0 with respect to CEN Standard EN 15255-2007 and EN 15265-2007*.
- [100] S. J. Julier, J. K. Uhlmann, and H. F. Durrant-Whyte. A new approach for filtering nonlinear systems. In *American Control Conference, Proceedings of the 1995*, volume 3, pages 1628–1632, Jun 1995.
- [101] R. Van Der Merwe and E. A. Wan. The square-root unscented Kalman filter for state and parameter-estimation. *ICASSP, IEEE International Conference on Acoustics, Speech and Signal Processing - Proceedings*, 6:3461–3464, 2001.
- [102] S. J. Julier, J. K. Uhlmann, and H. F. Durrant-Whyte. A new method for the nonlinear transformation of means and covariances in filters and estimators. *IEEE Transactions on Automatic Control*, 45(3):477–482, Mar 2000.
- [103] S. J. Julier and J. K. Uhlmann. New extension of the Kalman filter to nonlinear systems. *Proceedings of SPIE - The International Society for Optical Engineering*, 3068:182–193, 1997.
- [104] C. V. Rao, J. B. Rawlings, and J. H. Lee. Constrained linear state estimation - a moving horizon approach. *Automatica*, 37(10):1619–1628, 2001.
- [105] C. V. Rao, J. B. Rawlings, and D. Q. Mayne. Constrained state estimation for nonlinear discrete-time systems: Stability and moving horizon approximations. *IEEE Transactions on Automatic Control*, 48(2):246–258, 2003.
- [106] S. J. Julier. The scaled unscented transformation. In *Proceedings of the 2002 American Control Conference (IEEE Cat. No.CH37301)*, volume 6, pages 4555–4559 vol.6, May 2002.
- [107] S. Kolås, B. A. Foss, and T. S. Schei. Constrained nonlinear state estimation based on the UKF approach. *Computers and Chemical Engineering*, 33(8):1386–1401, 2009.
- [108] R. Kandepu, B. Foss, and L. Imsland. Applying the unscented Kalman filter for nonlinear state estimation. *Journal of Process Control*, 18(7-8):753–768, 2008.

- [109] S. Murtuza Baker, C. H. Poskar, F. Schreiber, and B. H. Junker. An improved constraint filtering technique for inferring hidden states and parameters of a biological model. *Bioinformatics*, 29(8):1052–1059, 2013.
- [110] B. O. S. Teixeira, L. A. B. Tôrres, Luis A. Aguirre, and D. S. Bernstein. On unscented Kalman filtering with state interval constraints. *Journal of Process Control*, 20(1):45 – 57, 2010.
- [111] A. Calabrese, S. Strano, and M. Terzo. Adaptive constrained unscented Kalman filtering for real-time nonlinear structural system identification. *Structural Control and Health Monitoring*, 25(2), 2018.
- [112] S. J. Julier and J. J. LaViolar Jr. On Kalman filtering with nonlinear equality constraints. *IEEE Transactions on Signal Processing*, 55(6 II):2774–2784, 2007.
- [113] D. Simon. Kalman filtering with state constraints: a survey of linear and nonlinear algorithms. *IET Control Theory Applications*, 4(8):1303–1318, 2010.
- [114] F. Yang, Y. Xing, D. Wang, and K. Tsui. A comparative study of three model-based algorithms for estimating state-of-charge of lithium-ion batteries under a new combined dynamic loading profile. *Applied Energy*, 164:387–399, 2016.
- [115] M. Partovibakhsh and G. Liu. An adaptive unscented Kalman filtering approach for online estimation of model parameters and state-of-charge of lithium-ion batteries for autonomous mobile robots. *IEEE Transactions on Control Systems Technology*, 23(1):357–363, 2015.
- [116] M. Maasoumy, M. Razmara, M. Shahbakhti, and A. Sangiovanni Vincentelli. Handling model uncertainty in model predictive control for energy efficient buildings. *Energy and Buildings*, 77:377 – 392, 2014.
- [117] E. A. Wan and R. Van Der Merwe. The unscented Kalman filter. In *Kalman Filtering and Neural Networks*, pages 221–280. Wiley, 2001.
- [118] S. A. Billings and L. A. Aguirre. Effects of the sampling time on the dynamics and identification of nonlinear models. *International Journal of Bifurcation and Chaos*, 05(06):1541–1556, 1995.
- [119] H. D. I. Abarbanel, R. Brown, and J. B. Kadtke. Prediction in chaotic nonlinear systems: Methods for time series with broadband fourier spectra. *Phys. Rev. A*, 41:1782–1807, Feb 1990.
- [120] R. E. Kalman. A new approach to linear filtering and prediction problems. *Journal of Basic Engineering*, 81:35–45, 1960.

- [121] N. J. Higham. Computing a nearest symmetric positive semidefinite matrix. *Linear Algebra and its Applications*, 103:103 – 118, 1988.
- [122] M. Razmara, M. Maasoumy, M. Shahbakhti, and R.D. Robinett. Optimal exergy control of building HVAC system. *Applied Energy*, 156:555 – 565, 2015.
- [123] A. Afram and F. Janabi-Sharifi. Theory and applications of HVAC control systems - A review of model predictive control (MPC). *Building and Environment*, 72:343 – 355, 2014.
- [124] B. Dong and K. P. Lam. A real-time model predictive control for building heating and cooling systems based on the occupancy behavior pattern detection and local weather forecasting. *Building Simulation*, 7(1):89–106, Feb 2014.
- [125] P.-D. Moroşan, R. Bourdais, D. Dumur, and J. Buisson. Building temperature regulation using a distributed model predictive control. *Energy and Buildings*, 42(9):1445 – 1452, 2010.
- [126] A. Alessio and A. Bemporad. Decentralized model predictive control of constrained linear systems. In *2007 European Control Conference (ECC)*, pages 2813–2818, July 2007.
- [127] J. Lofberg. Approximations of closed-loop minimax MPC. In *42nd IEEE International Conference on Decision and Control (IEEE Cat. No.03CH37475)*, volume 2, pages 1438–1442 Vol.2, Dec 2003.
- [128] F. Oldewurtel, C. N. Jones, A. Parisio, and M. Morari. Stochastic model predictive control for building climate control. *IEEE Transactions on Control Systems Technology*, 22(3):1198–1205, 2014.
- [129] M. Vařak, A. Starčić, and A. Martinčević. Model predictive control of heating and cooling in a family house. In *MIPRO 2011 - 34th International Convention on Information and Communication Technology, Electronics and Microelectronics - Proceedings*, pages 739–743, 2011.
- [130] A. S. O. Ogunjuyigbe, T. R. Ayodele, and O. A. Akinola. User satisfaction-induced demand side load management in residential buildings with user budget constraint. *Applied Energy*, 187:352 – 366, 2017.
- [131] A. Martinčević, M. Vařak, and V. Lešić. Model predictive control for energy-saving and comfortable temperature control in buildings. In *2016 24th Mediterranean Conference on Control and Automation (MED)*, pages 298–303, June 2016.
- [132] U. Maeder, F. Borrelli, and M. Morari. Linear offset-free model predictive control. *Automatica*, 45(10):2214 – 2222, 2009.

- [133] K. R. Muske and T. A. Badgwell. Disturbance modeling for offset-free linear model predictive control. *Journal of Process Control*, 12(5):617 – 632, 2002.
- [134] T. I. Salsbury. A survey of control technologies in the building automation industry. *IFAC Proceedings Volumes*, 38(1):90 – 100, 2005. 16th IFAC World Congress.
- [135] Indoor environmental input parameters for design and assessment of energy performance of buildings addressing indoor air quality, thermal environment, lighting and acoustics. *EN 15251:2007*, 2007.
- [136] European Committee for Standardization. Ergonomics of the thermal environment - analytical determination and interpretation of thermal comfort using calculation of the pmv and ppd indices and local thermal comfort criteria. *EN ISO 7730:2005*, 2005.
- [137] ILOG, Inc. Ilog cplex: High-performance software for mathematical programming and optimization, 2018.
- [138] Y. Li, J. Bian, N. Zhang, and J. Li. Experimental study on intelligent control scheme for fan coil air-conditioning system. *Advances in Mechanical Engineering*, 2013, 2013.
- [139] C.-M. Chu, T.-L. Jong, and Y.-W. Huang. Thermal comfort control on multi-room fan coil unit system using lee-based fuzzy logic. *Energy Conversion and Management*, 46(9-10):1579–1593, 2005.
- [140] *Smart Building – Smart Grid – Smart City*. Danube Transnational Programme, grant DTP1-502-3.2- 3Smart, <http://www.interreg-danube.eu/3smart>.
- [141] F. Borrelli, A. Bemporad, and M. Morari. Geometric algorithm for multiparametric linear programming. *Journal of Optimization Theory and Applications*, 118(3):515–540, Sep 2003.
- [142] EPEX SPOT. European Power Exchange Electricity Index.
- [143] HEP ODS. HEP distribution system operator. Available: <http://www.hep.hr/ods/>.
- [144] GWL Power Group CA100AHA Lithium Cell batteries. Available: <https://www.gwl.eu/>.
- [145] Python Software Foundation. *Python: A dynamic, open source programming language*. version 3.5.4, 2020.
- [146] P. M. Ferreira, A. E. Ruano, S. Silva, and E. Z. E. Conceição. Neural networks based predictive control for thermal comfort and energy savings in public buildings.

- Energy and Buildings*, 55:238 – 251, 2012. Cool Roofs, Cool Pavements, Cool Cities, and Cool World.
- [147] A. Martinčević, H. Novak, V. Lešić, M. Vašak, I. Bevanda, P. Marić, G. Lješić, and B. Crnokić. Open software module for zone consumption management – Estimation and prediction submodules. Technical report, University of Zagreb Faculty of Electrical Engineering and Computing, 11 2017.
- [148] A. Martinčević and M. Vašak. Dynamic building model for building simulation in a professional tool - UNIZGFER skyscraper building. Technical report, University of Zagreb Faculty of Electrical Engineering and Computing, 11 2017.
- [149] Zavod za zgradarstvo, Laboratorij građevinske fizike. Izvještaj o ispitivanju br. 2900-1023/03. Technical report, Institut građevinarstva hrvatske d.d., 2003.
- [150] N. Vezlić Strmo, D. Užarević, S. Mudrinić, and D. Sumina. Sadržaj izvješća o provedenom energetske pregledu građevine: Fakultet elektrotehnike i računarstva Sveučilišta u Zagrebu - Zgrada C. Technical report, Fakultet strojarstva i brodogradnje, 2014.
- [151] J. Twidell and A.D. Weir. *Renewable Energy Resources*. Taylor & Francis, 2006.
- [152] K.Y. Kondratev. *Radiation in the atmosphere*. Academic Press New York, 1969.

Symbols

α	UKF tuning parameter
α_h	exponent of pressure drop characteristics of hydraulic network element
β	UKF tuning parameter
α	linear system matrix stacked over the prediction horizon
β	linear system input matrix stacked over the prediction horizon
δ	sequence of zone occupancy vectors, $\delta = [\delta_{k+1 k}^T, \delta_{k+2 k}^T, \dots, \delta_{k+H k}^T]^T$
γ	linear system disturbance input matrix stacked over the prediction horizon
\mathbf{G}^h	HHL optimization problem constraint matrix
\mathbf{G}_{CR}	critical region constraints matrix
\mathbf{L}^h	HHL optimization problem constraint matrix
\mathbf{w}^h	HHL optimization problem constraint vector
χ	UKF sigma points
ΔE	energy mismatch [Ws]
Δh	change in pipe elevation [m]
Δp	pressure drop [Pa]
Δp_f	frictional pressure drop [Pa]
Δp_h	hydrostatic pressure drop [Pa]
Δx_{fc}	penalization of fan speed switching, $\Delta x_{\text{fc}} \in \{0, 1\}$

Δ	ICUT sigma point step (equal to γ for standard UT)
δ	zone occupancy, $\delta \in \mathbb{R}^{n_y}$
Δ^{ref}	permissible deviation from temperature reference vector y^{ref} , $\Delta^{\text{ref}} \in \mathbb{R}^{n_y}$
δ_s	solar declination angle [$^\circ$]
$\Delta_{k,i}$	UKF step in k^{th} iteration for i^{th} sigma point
ϵ	diffuse irradiance transposition factor
η	flow share through an individual FCU
η_d	share of the transmitted diffuse solar irradiance absorbed by the internal wall
η_t	share of the transmitted solar irradiance absorbed by the zone air
γ	UKF scaling parameter
γ_e	weighting factor for trade-off between the comfort and energy savings
κ	UKF tuning parameter
Re	Reynolds number
μ	dynamic viscosity [Pa·s]
ω	absolute air humidity [$\text{kg}_{\text{vapour}} \cdot \text{kg}_a^{-1}$]
ϕ	surface azimuth angle
Φ_{yy}	autocorrelation function
ψ_{fc}	heat transfer coefficient [K^{-1}]
ρ	density [$\text{kg} \cdot \text{m}^{-3}$]
σ	Stefan-Boltzmann constant unit
σ_k	slack variable, $\sigma_k \in \mathbb{R}^{n_y}$
τ	transport delay [s]
τ_y	time of the first minimum of the autocorrelation function Φ_{yy} [s]
$\mathbf{0}$	zero matrix of appropriate dimension
$\mathbf{1}_n$	n -dimensional row vector of ones, $\mathbf{1} \triangleq [1, \dots, 1]$

\mathbf{c}_h	HHL cost function parameter
\mathbf{c}_t	sequence of thermal energy price vectors [EUR/kW], $\mathbf{c}_t = [c_{t,k k}^T, c_{t,k+1 k}^T, \dots, c_{t,k+H-1 k}^T]^T$,
\mathbf{d}	sequence of disturbance vectors, $\mathbf{d} = [d_{k k}^T, d_{k+1 k}^T, \dots, d_{k+H-1 k}^T]^T$,
\mathbf{I}	identity matrix of appropriate dimension
\mathbf{I}_n	identity matrix of dimension n
\mathbf{Q}	weighting matrix, $\mathbf{Q} \in \mathbb{R}^{H \cdot n_y \times H \cdot n_y}$
\mathbf{q}	sequence of weight parameters, $\mathbf{q} = [q_{k+1 k}^T, q_{k+2 k}^T, \dots, q_{k+H k}^T]^T$,
\mathbf{r}	sequence of weight parameters, $\mathbf{r} = [r_{k k}^T, r_{k+1 k}^T, \dots, r_{k+H-1 k}^T]^T$,
\mathbf{u}	sequence of input vectors, $\mathbf{u} = [u_{k k}^T, u_{k+1 k}^T, \dots, u_{k+H-1 k}^T]^T$
\mathbf{y}	sequence of output vectors, $\mathbf{y} = [y_{k+1 k}^T, y_{k+2 k}^T, \dots, y_{k+H k}^T]^T$
Θ	parameter vector
θ	angle of incidence [°]
θ_e	solar elevation angle [°]
θ_z	solar zenith angle [°]
Υ	ICUT algorithm auxiliary matrix
ε	emissivity of the surface
A	area [m ²]
a	absorptivity
A^c	continuous-time system matrix, $A^c \in \mathbb{R}^{n_x \times n_x}$
A^d	discrete-time system matrix, $A^d \in \mathbb{R}^{n_x \times n_x}$
a_{fc}	coefficient of a FCU model
a_k	ICUT sigma point step variation parameter in k^{th} iteration
B^c	continuous-time system input matrix
B^d	discrete-time system input matrix
b_{fc}	coefficient of a FCU model

C	capacitance
c	specific heat capacity [$\text{J}\cdot(\text{kg}\cdot\text{K})^{-1}$]
c_{fc}	coefficient of a FCU model
c_c	thermal comfort price [EUR/kW], $c_c \in \mathbb{R}^1$
$c_{t,k}$	thermal energy price [EUR/kW], $c_{t,k} \in \mathbb{R}^{n_u}$
D	day in a year, $D \in \mathbb{R}$
d	diameter [m]
D^{h}	HHL affine control law matrix
E	energy [kWh]
$E[\cdot]$	mathematical expectation
$f(\cdot)$	system input function
f_D	friction coefficient
g	weighting parameter, $g \in \mathbb{R}^1$
H	prediction horizon length, $H \in \mathbb{N}$
h	convective heat transfer coefficient [$\text{W}\cdot(\text{m}^2\cdot\text{K})^{-1}$]
$h(\cdot)$	system output function
H_s	solar hour angle, $H_s \in \mathbb{R} [^\circ]$
I	solar irradiance [W/m^2]
$I_{\text{h}}^{\text{diff}}$	diffuse horizontal solar irradiance [W/m^2]
$I_{\text{n}}^{\text{dir}}$	direct normal solar irradiance [W/m^2]
J	optimization criterion value, $J \in \mathbb{R}^1$
$J^{\text{h}*}(\Theta)$	HHL affine cost function with respect to the parameter Θ
K	Kalman gain
k	thermal conductivity [$\text{W}\cdot(\text{m}\cdot\text{K})^{-1}$]
L	thickness [m]
l	length [m]

l_{eq}	equivalent length of a straight pipe [m]
L_k	lower system state bound at time instant k , i.e. $x_k \geq L_k$
m	mass [kg]
N	number of zones supplied through the considered duct
n_{fc}	number of FCUs connected to the same duct, $n_{\text{fc}} \in \mathbb{N}$
n_v	number of observation noise variables, $n_v \in \mathbb{N}$
n_w	number of process noise variables, $n_w \in \mathbb{N}$
n_d	number of disturbance inputs, $n_d \in \mathbb{N}$
n_l	number of layers, $n_l \in \mathbb{N}$
n_u	number of system inputs, $n_u \in \mathbb{N}$
n_x	number of system states, $n_x \in \mathbb{N}$
n_y	number of system outputs, $n_y \in \mathbb{N}$
P	power [W]
p_i	i^{th} parameter of the simplified building model, $i \in \mathbb{N}$
p_t^{diff}	diffuse solar irradiance parameter [m ²]
p_t^{dir}	direct solar irradiance parameter [m ²]
$P_{x_k y_k}$	cross covariance matrix
P_{x_k}	covariance matrix
Q	heat transfer rate [W]
q	mass flow [kg·s ⁻¹]
q^{h}	HHL affine control law vector
Q_k	process noise covariance matrix
q_k	weighting parameter, $q_k \in \mathbb{R}^{n_y}$
R	resistance
R_h	hydraulic resistance
R_k	observation noise covariance matrix

r_k	weighting parameter, $r_k \in \mathbb{R}^{n_u}$
S_{x_k}	square root of covariance matrix
T	temperature [$^{\circ}\text{C}$]
t_{Δ}	time difference of the local time from Greenwich Mean Time (GMT), $t_{\Delta} \in \mathbb{N}$
T_a^{ref}	temperature reference
t_{LST}	local solar time, $t_{\text{LST}} \in \mathbb{R}$
t_{LT}	local time, $t_{\text{LT}} \in \mathbb{R}$
T_{out}	external temperature [$^{\circ}\text{C}$]
T_{sur}	surface temperature [$^{\circ}\text{C}$]
T_s	sampling time [s]
T_a	zone air temperature [$^{\circ}\text{C}$]
T_a^{RC}	zone air temperature simulated by using RC model [$^{\circ}\text{C}$]
T_a^{SS}	zone air temperature simulated by using building simulation software [$^{\circ}\text{C}$]
T_w	water temperature [$^{\circ}\text{C}$]
T_z	equivalent temperature of solid zone parts (slow-dynamics temperature) [$^{\circ}\text{C}$]
u	system inputs
U_o	Overall heat transfer coefficient [$\text{W}^{\circ}\text{C}^{-1}$]
U_k	upper system state bound at time instant k , i.e. $x_k \leq U_k$
V	volume [m^3]
v	observation noise
w	process noise
$W^{(\cdot)}$	UKF sigma point related weights
w_{CR}	critical region constraints vector
x	system states
x^n	system states normalized to interval $[0,1]$
x_{fc}	fan speed $x_{\text{fc}} \in \{\text{off}, \text{L}, \text{M}, \text{H}\}$

x_v	valve position, $x_v \in \mathbb{R}^1$
y	system outputs
y^{ref}	temperature reference vector, $y^{\text{ref}} \in \mathbb{R}^{n_y}$

Sets, spaces and distributions

\mathcal{V}	set of all adjacent zones
\mathbb{N}	set of natural numbers
\mathbb{R}	set of real numbers
$\mathbb{R}^{n \times m}$	set of n by m matrices with real entries
\mathbb{R}^n	set of n -dimensional (column) vectors with real entries
$\mathcal{N}(0, Q)$	multivariate normal (Gaussian) distribution with mean 0 and covariance Q
$\boldsymbol{\varepsilon}_{\text{fc}}$	set of unknown scalar ε_{fc} coefficients for every fan speed x_{fc} , $\boldsymbol{\varepsilon}_{\text{fc}} := \{\varepsilon_{\text{fc}}^{\text{off}}, \varepsilon_{\text{fc}}^{\text{L}}, \varepsilon_{\text{fc}}^{\text{M}}, \varepsilon_{\text{fc}}^{\text{H}}\}$
\mathbf{a}_{fc}	set of unknown scalar a_{fc} coefficients for every fan speed x_{fc} , $\mathbf{a}_{\text{fc}} := \{a_{\text{fc}}^{\text{off}}, a_{\text{fc}}^{\text{L}}, a_{\text{fc}}^{\text{M}}, a_{\text{fc}}^{\text{H}}\}$
\mathbf{b}_{fc}	set of unknown scalar b_{fc} coefficients for every fan speed x_{fc} , $\mathbf{b}_{\text{fc}} := \{b_{\text{fc}}^{\text{off}}, b_{\text{fc}}^{\text{L}}, b_{\text{fc}}^{\text{M}}, b_{\text{fc}}^{\text{H}}\}$
\mathbf{U}_o	set of scalar values of U_o for every fan speed x_{fc} , $\mathbf{U}_o := \{U_o^{\text{off}}, U_o^{\text{L}}, U_o^{\text{M}}, U_o^{\text{H}}\}$
E_k	set of ordered pairs, $E_k = \{e_k \times e_k\}$
e_k	set of indices of excited states x_k
N_k	set of ordered pairs, $N_k = \{n_k \times n_k\} \cup \{e_k \times n_k\}$
n_k	set of indices of all unexcited states x_k

Algebraic operations

\cup	set union
$\dot{\square}$	time derivation, $\dot{T} = dT/dt$.
$\text{blkdiag}(\cdot)$	block-diagonal concentration of matrices listed as arguments
$\text{col}_i(\cdot)$	i^{th} column of matrix
\times	cartesian product

$|\cdot|$ element-wise absolute value

$\|\cdot\|_1$ L_1 norm

Superscripts

*

energy-optimal solution

**

price-optimal solution obtained through the hierarchical coordination

a

a priori

c

calibrated measurement

cd

manufacturer's catalogue data

diff

diffuse

dir

direct

H

associated with high FCU fan speed

h

related to higher hierarchy level

in

input/inside

L

associated with low FCU fan speed

M

associated with medium FCU fan speed

m

measured value

off

associated with switched-off FCU fan

out

output/outside

r

return

raw

raw measurement

ref

referent value

s

supply

x

associated with a certain fan speed x_{fs}

Subscripts

θ

incident on external surface

a

absorbed

k	time instant, $k \in \mathbb{N}$
$k + t k$	predicted variable at time k for a time instant $k + t$, $t \in \mathbb{N}$
A	active constraints subset
a	air
cal	calorimeter
cond	conductive
conv	convective
el	electrical
fc	fan coil unit
max	upper bound
min	lower bound
NA	inactive constraints subset
p	pipe
rad	radiant
s	solar
t	thermal
w	water

Abbreviations

ANN	Artificial Neural Network
BEMS	Building Energy Management System
COP	Coefficient Of Performance
CR	Critical Region
EER	Energy Efficiency Ratio
EKF	Extended Kalman Filter
ET	Equation of Time
FCU	Fan Coil Unit

GMT	Greenwich Mean Time
H	High fan speed
HHL	Higher Hierarchical Level
HVAC	Heating, Ventilation, and Air Conditioning
L	Low fan speed
LAT	Geographic Latitude
LHL	Lower Hierarchical Level
LON	Geographic Longitude
LP	Linear Program
M	Medium fan speed
MILP	Mixed Integer Linear Program
MPC	Model Predictive Control
NLP	Nonlinear Problem
NRMSE	Normalised Root Mean Squared Error
off	Fan switched off
QP	Quadratic Program
RC	Resistance-Capacitance
RMSE	Root Mean Squared Error
SHGC	Solar Heat Gain Coefficient
SoC	State of Charge
SOM	Smart Operation Mode
TMY	Typical Meteorological Year
UKF	Unscented Kalman Filter
UNIZGFER	University of Zagreb Faculty of Electrical Engineering and Computing
UT	Unscented Transformation
UTC	Coordinated Universal Time

CURRICULUM VITAE

Anita Martinčević was born in 1990 in Varaždin, Croatia. In 2008 she enrolled in Engineering and Information Technology study programme at University of Zagreb Faculty of Electrical Engineering and Computing (UNIZGFER). She finished her bachelor's degree in Control Engineering and Automation in 2011. In 2013 she obtained master's degree in the same field under the supervision of Prof. Mario Vašak. The same year she starts to work at UNIZGFER as a research assistant within the Department of Control and Computer Engineering and starts her PhD studies.

From April 2013 she was employed on a research project *Enhancement of Research, Development and Technology Transfer Capacities in Energy Management Systems for Buildings* (ENHEMS-Buildings). Within this project research and development infrastructure for comprehensive and energy-efficient control of comfort in buildings was established on UNIZGFER through the implementation of energy-efficient optimal control on two floors of UNIZGFER skyscraper. Her work was oriented on the development of advanced estimation and control algorithms for optimal comfort control in buildings. From January 2017 she was working on international project *Smart Building – Smart Grid – Smart City* (3Smart) which follows the main idea of ENHEMS-Buildings by integrating the building comfort control into a general system for building energy management. The operation of the developed building energy management system, able to coordinate all the building subsystems including thermal energy production, microgrid, distribution grid or any other consumer, has been tested on 5 pilot locations in Danube region. Currently, she is a part of Innovation Centre Nikola Tesla team working on the project *Development of a System for Predictive Control and Autonomous Trading of Energy in Buildings* (PC-ATE Buildings) focused on production and commercialization of services for predictive control of energy in buildings connected to energy grids and subject to dynamic energy market conditions.

She is a member of the Laboratory for Renewable Energy Systems (LARES). She has more than 5 years of research and development experience in the building energy management via advanced control which resulted in more than 10 research articles in international scientific journals and on international scientific conferences.

Anita Martinčević rođena je 1990. godine u Varaždinu, Hrvatska. Studij Elektrotehnike i informacijske tehnologije upisala je 2008. godine na Sveučilištu u Zagrebu Fakultet elektrotehnike i računarstva (FER). Preddiplomski studij završila je 2011. godine na profilu Automatika. Na istom profilu završila je i diplomski studij 2013. godine pod mentorstvom prof. dr. sc. Marija Vašaka. Iste godine zapošljava se na Zavodu za automatiku i računalno inženjerstvo FERa te upisuje doktorski studij.

Tijekom rada na FERu sudjelovala je na istraživačkom projektu *Unapređenje kapaciteta istraživanja, razvoja i transfera tehnologije vezanih uz sustave gospodarenja energijom u zgradama* (ENHEMS-Buildings) u sklopu kojeg se na FERu uspostavila razvojna infrastruktura za napredno upravljanje potrošnjom energije u zgradama te omogućila implementacija naprednog upravljanja na dva kata neboderske zgrade FERa. Na projektu se bavila razvojem estimacijskih algoritama za identifikaciju termodinamičkih modela zgrada i estimaciju poremećajnih toplinskih tokova u zgradama kao i razvojem naprednih algoritama upravljanja energijom po zonama zgrade i algoritama optimalnog upravljanja ventilokonvektorima. Od siječnja 2017. godine radila je na međunarodnom istraživačkom projektu *Smart Building – Smart Grid – Smart City* (3Smart) koji je nastavak istraživanja provedenih u sklopu projekta ENHEMS-Buildings projekta s ciljem integracije zgrade s proizvodnjom toplinske energije i naprednom elektroenergetskom mrežom u cjelovit sustav za gospodarenje energijom. Razvijeni sustav validiran je na 5 pilotskih lokacija u dunavskoj regiji. Trenutno je dio tima Inovacijskog centra Nikola Tesla koji radi na projektu *Razvoj sustava prediktivnog upravljanja i autonomnog trgovanja energijom u zgradi*.

Članica je Laboratorija za sustave obnovljivih izvora energije (LARES). Kroz rad na projektima ostvarila je iskustvo u istraživanju i razvoju na području gospodarenja energijom u zgradama temeljeno na naprednim algoritmima upravljanja i estimacije što je rezultiralo s više od 10 članaka u međunarodnim znanstvenim časopisima te na međunarodnim znanstvenim skupovima.

Patent

1. A. Martinčević, M. Vašak, D. Marušić, B. Kovačević. Sustav za detekciju začepjenja zrakom izmjenjivača topline ventilokonvektora. Patent No. P20181196A 2020.

Journal papers

1. A. Martinčević, M. Vašak. Constrained Kalman Filter for Identification of Semiphysical Building Thermal Models. *IEEE Transactions on Control Systems Technology*, 2019, doi: 10.1109/TCST.2019.2942808.
2. A. Martinčević, V. Lešić and M. Vašak. Identification of a control-oriented energy model for a system of fan coil units. *Control Engineering Practice*, vol. 91, 104100, 2019, doi: 10.1016/j.conengprac.2019.07.018
3. V. Lešić, A. Martinčević, M. Vašak. Modular energy cost optimization for buildings with integrated microgrid. *Applied Energy*, vol. 197, 14-28, 2017, doi: 10.1016/j.apenergy.2017.03.087

Conference papers

1. N. Hure, A. Martinčević, M. Vašak. Model predictive control of building HVAC system employing zone thermal energy requests. *Proceedings of the 22nd International Conference on Process Control*, 13-18, 2019.
2. V. Lešić, M. Vašak, A. Martinčević, H. Novak. Nonlinear hierarchical building zone and microgrid control based on sensitivity analysis. *Proceedings of the 21st International Conference on Process Control*, 321-326, 2017.

3. A. Martinčević, F. Rukavina, V. Lešić, M. Vašak. Comfort Control in Buildings with Adherence to the required thermal energy input in zones. *Proceedings of the 2017 IEEE International Symposium on Industrial Electronics*, Edinburgh, Scotland, United Kingdom, 1477-1482, 2017.
4. M. Vašak, A. Starčić, V. Lešić, A. Martinčević. Upgrade of a typical office building automation system for enabling open energy management services. *Proceedings of the International Conference on Smart Systems and Technologies 2017*, 309-314, 2017.
5. A. Martinčević, M. Vašak, V. Lešić. Model Predictive Control for Energy-saving and Comfortable Temperature Control in Buildings. *Proceedings of the 24th Mediterranean Conference on Control and Automation*, Athens, Greece, 298-303, 2016.
6. M. Gulin, A. Martinčević, V. Lešić, M. Vašak. Multi-level Optimal Control of a Microgrid-supplied Cooling System in a Building. *Proceedings of the IEEE PES Innovative Smart Grid Technologies Conference Europe*, ISGT Europe 2016, Ljubljana, Slovenija, 2016.
7. V. Lešić, M. Vašak, A. Martinčević, M. Gulin, A. Starčić, H. Novak. Computer-assisted Management of Building Climate and Microgrid with Model Predictive Control. *Proceedings of the 17th International Conference on Civil and Building Engineering*, 2276-2287, ICCBE 2015.
8. A. Starčić, A. Martinčević, M. Vašak, Estimation of disturbance heat flux in buildings. *IEEE Sensors Applications Symposium (SAS) Proceedings*, 272-275, 2015.
9. A. Martinčević, A. Starčić, M. Vašak. Parameter estimation for low-order models of complex buildings. *Proceedings of the Innovative Smart Grid Technologies Conference Europe (ISGT Europe)*, 2014.
10. M. Vašak, A. Martinčević. Optimal Control of a Family House Heating System. *Proceedings of the 36th International Convention on Information and Communication Technology, Electronics and Microelectronics, Computers in Technical Systems*, 1145-1150, 2013.
11. M. Vašak, A. Starčić, A. Martinčević. Model predictive control of heating and cooling in a family house. *Proceedings of the 34th International Convention on Information and Communication Technology, Electronics and Microelectronics*, 99-103, 2011.